University of Southampton

High-precision isotope ratio measurements of uranium and plutonium in the environment

January 2002

A thesis submitted for the degree of Doctor of Philosophy

Thorsten Warneke *Dipl. Phys.* (Heidelberg)

Faculty of Science

School of Ocean and Earth Science

Southampton Oceanography Centre

ABSTRACT

A high-precision mass spectrometry method has been developed to measure $^{240}Pu/^{239}Pu$ at low concentrations in environmental samples. A reproducibility of <1% for sample sizes of > 0.5pg has been achieved using a highly sensitive and precise multi-collector ICP-mass spectrometer (Micromass IsoProbe). The research has involved applying the developed methods to a number of environmental studies.

Application I: A chronology for $^{240}Pu/^{239}Pu$ is presented. This chronology over the period 1945-1980 is derived from grass samples from the IACR Rothamsted Archive at Harpenden (Hertfordshire, UK) and an Alpine ice core from Dome du Gouter, Mont Blanc, French Alps. Activity concentrations for ^{137}Cs and $^{239,240}Pu$ and the $^{238}U/^{235}U$ atomic ratio were also determined in the same samples. The activity concentrations clearly reflect the yearly yields of atmospheric testing. A higher abundance of ^{235}U can be linked to nuclear testing between 1950-1963. A higher abundance of ^{238}U is found in the period 1970-80 in the grass, but not in the ice. The $^{240}Pu/^{239}Pu$ ratio is compared with Polar ice core and stratospheric data that have appeared in the literature. It is particularly notable that the UK herbage samples clearly identify fallout from the early U.S. tests in the Nevada desert (1952 and 1953) and that 1954-68 samples show isotope ratios reflecting stratospheric fallout. Ratios for the 1970s cannot be uniquely attributed to a single source. Complementary measurements of the $^{240}Pu/^{239}Pu$ have been carried out on stratospheric air filters from Sweden and ground-level air filters from Germany.

Application IIA: Plutonium isotopes have been measured in a sediment core from the Wyre saltmarsh. Radionuclide contamination in this area is much higher than in many other UK sites because of its incorporation of discharges from the BNFL Sellafield. A model for the transport of radiolabelled sediment from the Sellafield area is also presented.

Application IIB: Plutonium isotopic ratios in a mudflat core from Poole Harbour reflect the pattern that is expected from weapons fallout in the pre-1970 period. The post-1970 sediment shows an additional source that is considered to be the discharges from AEA Winfrith.

Application III: Radioactive contamination of the environment by Pu and U as a result of operations at the AWE sites at Aldermaston and Burghfield has been investigated. Isotope ratio results show that contamination of the environment around the sites is patchy and its concentration very small. It is interesting to note that measurable contamination is not expected from the annual discharge records when a dispersion model is applied.

ACKNOWLEDGMENTS

I would like to gratefully acknowledge my supervisors Drs Ian Croudace, Rex Taylor and Phillip Warwick. I especially thank them for continuing to support my PhD studies even though I had to return to Germany in my final 18 months to fulfil my paternal duties. During the research Ian, as the main supervisor, was always available for questions and advice. Rex provided much analytical input and expertise in connection with setting up the plutonium isotope ratio measurements and Phil was always on hand to assist with many chemistry questions. I would also like to thank Jung-Suk Oh, who worked with me on the Aldermaston samples. Whenever I made a mistake or forgot something he corrected it without mentioning it - apart from this he was a great person to work with. Last, but not least I wish to thank Andy Milton, Andy Cundy, Fran Dyer, Frank Wigley and Wink Janes who have provided me with help whenever I needed it. All the people mentioned above contributed to my experience and enjoyment whilst working at SOC.

Contents

LIST OF FIGURES

List of Tables

PhD Proposal (1998)
Graduate School of Ocean & Earth Science

Characterisation and differentiation of Pu and U isotopes in the environment

Supervisors: Dr IW Croudace, Dr PE Warwick & Dr R Taylor

The recent radiometric survey of Greenham Common, Newbury District and surrounding areas (Croudace, Warwick, Taylor and Dee, 1997)* was specifically tasked with studying the alleged nuclear incident at the Greenham Common airbase. Despite using mass spectrometric techniques no evidence for any such incident was found at or around the airbase. Sampling around AWE (Aldermaston) was also carried out and small amounts of anomalous U (and Pu to a lesser extent) were detected in the vicinity of the site.

Specific measurements for ^{235}U, ^{238}U, ^{239}Pu, ^{240}Pu and ^{241}Pu should allow apportionment to be made between the two main source terms (*viz*. AWE discharges and weapons fallout). Thermal ionisation mass spectrometry (TIMS) will be used to determine the ratio of $^{239}Pu/^{240}Pu$ and $^{238}U/^{235}U$ in samples (soils and other environmental materials) collected at various distances from AWE to study the lateral and vertical (historical) distribution of anomalous U and Pu. Although a general $^{239}Pu/^{240}Pu$ ratio of 5 (compared with *ca*. 10-15 for weapons material) is known from weapons' fallout more detailed temporal variations for the southern UK are not known. It is also proposed to determine a unique time-series dataset using a national herbage archive. This archive consists of grass, cut and stored annually since 1830, which should preserve a reliable record of weapons' fallout. Promising preliminary measurements on samples from 1930 (pre-fallout), 1958 and 1963 (peak fallout) and 1995 (post Chernobyl) grass have already been made.

Pu behaviour in the environment

Most thermonuclear weapons use Pu in the core (>90% ^{239}Pu with the rest mostly ^{240}Pu) but have U (mostly ^{238}U) in the tamper. Any Pu in the weapon that is not fissioned will form chemically resistant (refractory) PuO_2 that will eventually return to the ground as fallout. ^{239}Pu and ^{240}Pu are also formed during the nuclear detonation by neutron capture reactions on ^{238}U. It has been suggested that fallout-Pu formed on irradiation of ^{238}U during a nuclear weapon detonation is chemically more available than the Pu derived in the weapon core. Approximately 66% of the Pu released to the stratosphere during atmospheric weapons' testing would be formed through neutron capture during the fusion-fission lifetime of the detonated device (relatively short). The irradiation of ^{238}U will produce ^{239}U and ^{240}U which then decay to ^{239}Pu and ^{240}Pu over a period of days (i.e. much longer than the lifetime of the thermonuclear reactions). This Pu, which is not high-fired, will be more labile in the environment than the original Pu used in the weapon construction. The study will investigate whether the two forms of Pu (labile and non-labile) have different isotopic composition. If a variation in composition is confirmed then Pu isotopic measurements using TIMS will be used to investigate whether there is any evidence for the variation of chemical behaviour in the environmental samples.

***Croudace, I, Warwick, P., Taylor, R. and Dee, S.** (1997) An investigation of radioactive contamination at Greenham Common, Newbury District and surroounding areas Final Report

Presentations given

Geoscience 2000, Manchester, UK

Poster: $^{240}Pu/^{239}Pu$ isotopic ratio measurements by IsoProbe MC-ICP-MS

Coger 2000, Southampton, UK

Talk: $^{240}Pu/^{239}Pu$ isotopic ratio measurements in environmental samples using MC-ICP-MS

AGU 2001, San Francisco, USA

Talk: Environmental applications of $^{240}Pu/\ ^{239}Pu$ measurements using the IsoProbe MC-ICP-MS

Papers and reports

Croudace I., Warwick P., Taylor R., Bradshaw K. and Warneke T. (1999) An assessment of radioactive contamination in the environment as a result of operations at the AWE sites in Berkshire Report No.1

Croudace I., Warwick P., Cundy A., Warneke T., Oh J.S. and Taylor R.N. (2000) An assessment of radioactive contamination in the environment as a result of operations at the AWE sites in Berkshire Report No.2

Croudace I., Warwick P., Warneke T., Cundy A., Oh J.S. and Taylor R.N. (2001) An assessment of radioactive contamination in the environment as a result of operations at the AWE sites in Berkshire Report No.3

Taylor R.N., Warneke T., Milton J.A., Croudace I.W., Warwick P.E. and Nesbitt R.W. (2001) Plutonium isotope ratio analysis at femtogram to nanogram levels by multicollector ICP-MS, *J. Anal. At. Spectrom*. 16, 279-284

Declaration

The work presented in this thesis was predominantly carried out by myself. Some data have resulted from collaboration with individuals within the School, in which case this is indicated in the text, or in the list of authors on the papers.

CHAPTER 1

1. Introduction

1.1. Aims of the research

The project is concerned with the detection of uranium and plutonium pollution in the environment. Isotope ratio data are used to characterise the sources of plutonium and uranium. In most measurements, the uranium background is dominated by natural uranium. The isotopic ratios in natural uranium are well known and constant over the time periods of interest. In contrast to uranium plutonium does not occur naturally only in trace amounts. A background of plutonium was introduced into the environment by nuclear weapon testing. The plutonium isotopic ratios vary over the time periods of interest and its variation is not well known.

The following goals have been achieved during the PhD research:

- Investigation of the $^{240}Pu/^{239}Pu$ atomic ratio measurement using TIMS and MC-ICPMS. Several filament loading techniques for TIMS were investigated at an early stage in the project. However, the IsoProbe MC-ICPMS proved to be superior for the determination of the $^{240}Pu/^{239}Pu$ at low concentrations (~0.5pg). The development of the plutonium measurement on the IsoProbe MC-ICPMS has been published in Taylor *et al.*, 2001.
- **Application I:** A chronology of plutonium and uranium isotopic ratios in grass samples from the IACR Rothamsted Archive at Harpenden (Hertfordshire, UK) and in an ice core from the Mont Blanc, French Alps, is presented for the time period 1945-1990. The ^{137}Cs concentration in the grass agrees well with surface air concentrations and deposition data measured in Canada and the UK. The plutonium ratio data are compared with plutonium isotopic ratios in Arctic and Antarctic ice cores (Koide *et al*, 1985) and stratospheric data from the U.S. Environmental Measurement Laboratory (EML, 1997). For the time period 1955 onwards the $^{240}Pu/^{239}Pu$ can be attributed to stratospheric fallout from nuclear tests. In the early 1950s tropospheric fallout from the Nevada test site has been detected in the grass. Uranium isotopic ratios are also investigated and are seen to vary by up to 0.5% from the natural ratio in the grass and up to 7% in the Alpine ice. In the 1950s and 1960s the deviations can be linked to atmospheric weapons testing. This is the

first time that a chronology based on ground-level deposition of the $^{240}Pu/^{239}Pu$ and the $^{238}U/^{235}U$ has been presented for northern temperate latitudes.

- **Application II A:** Plutonium isotopes have been measured in a sediment core from the Wyre saltmarsh. Anthropogenic radionuclide contamination in this area is much higher than in many other areas because of the relatively close proximity to BNFL Sellafield. A model for the transport of the discharges and a $^{240}Pu/^{239}Pu$ history of Sellafield discharge is presented.
- **Application II B:** Plutonium concentrations and isotopic ratios have been investigated in a sediment core from Poole Harbour. In the pre-1970 period the plutonium isotopic ratios show the same pattern as was expected from weapons fallout. Post-1970 an additional source could be identified. The ratios suggest an origin from material that had been in the nuclear-fuel cycle and the assumed source is AEA Winfrith, which is approximately 20 km west of Poole Harbour.
- **Application III:** Radioactive contamination as a result of operations at the Berkshire AWE sites at Aldermaston and Burghfield has been investigated by the Geosciences Advisory Unit at the Southampton Oceanography Centre over the period 1998-2001. The results are published in 3 reports (Croudace *et al*., 1999, 2000, 2001). This 3-year contract funded this PhD project and part of the PhD was the involvement in the project. In Chapter 6 the contamination of uranium and plutonium is modelled from airborne discharge records and compared with the results from the survey.

1.2. The elements U and Pu and their characteristic ratios from different sources

Uranium:

Uranium is a naturally occurring element. It occurs at approximately 2 ppm in the earth's crust. Natural uranium consists essentially of the three isotopes ^{234}U, ^{235}U and ^{238}U. A further 3 artificial uranium isotopes (^{232}U, ^{233}U, ^{236}U) have half-lives greater than 1 year. The half-life and the natural abundance of the U isotopes of interest are given in Table 1.1 and all these isotopes decay via alpha emission. To capitalise on the fission properties of ^{235}U, it is necessary to enrich the isotope from natural uranium and the amount of enrichment required depends on the application. Fuel for nuclear reactors typically contains between 3-5% ^{235}U, depending on the reactor type whereas weapon material contains more than 90% ^{235}U (Lieser, 1991). The enrichment process leads to the production of large quantities of depleted uranium, which contains about 0.2-0.3% ^{235}U. Depleted uranium is used in the outer shell in warheads.

Isotope	Half life (years)	Natural U atomic abundance
^{233}U	1.59×10^5	
^{234}U	2.45×10^5	<0.055 %
^{235}U	7.04×10^8	0.7200 %
^{236}U	2.34×10^7	
^{238}U	4.46×10^9	99.2745 %

Table 1.1 Half lives and abundance of U isotopes of interest

Due to the natural variation of U concentrations, it is not straightforward to detect anthropogenic uranium contamination using concentration data alone. A more reliable approach is to measure the $^{238}U/^{235}U$ ratio, which is constant in nature. The current isotopic abundances of the two primordial isotopes are 0.72% and 99.2745% respectively and the atomic ratio of $^{238}U/^{235}U$ is 137.88 (Chen and Wasserburg 1980). This ratio is very well known and is possibly uncertain to only ±0.1% (2 s.d.). No significant variation exists for this ratio in nature except in very special circumstances, e.g. in the case of the fossil nuclear reactor at Oklo, West Africa (Cowan, 1976). The neutron irradiation history of uranium can

be indicated by the presence of ^{236}U. It is difficult to use the $^{238}U/^{234}U$ because of its natural variability. The $^{238}U/^{235}U$ for the cases discussed above are given in Table 1.2. In this research the $^{238}U/^{235}U$ was used to characterise the contamination in soils around the AWE site at Aldermaston and Burghfield. There are two problems in using the $^{238}U/^{235}U$ when investigating soils:

1. The high natural level of uranium in the environment dilutes the anthropogenic source term. Hence high precision measurements are required to detect slight changes in the $^{238}U/^{235}U$.

2. In many cases both depleted and enriched uranium are discharged together and therefore there are three effective components (natural, depleted and enriched). The relative proportion of each will therefore determine the measured ratio and an apparent natural ratio may include anthropogenic components.

Type of uranium	**$^{238}U/^{235}U$**
Natural	137.88
Reactor	15 – 32 before burn-up
Weapon grade	<0.1
Depleted	250-500

Table 1.2 $^{238}U/^{235}U$ for different sources

Plutonium:

Trace amounts of plutonium occur naturally in uranium ores due to neutron capture. However, in environmental studies those traces can be neglected compared with the anthropogenic plutonium injected into the environment during the post-World War II period. Deposition densities up to approximately 80 Bq/m^2 (25 ng/m^2 assuming $^{240}Pu/^{239}Pu$ = 0.18; Kelley *et al*, 1999) can be present in temperate latitudes soils due mostly to atmospheric nuclear weapon tests in the period 1950-1963 (Hardy et al, 1973). Assuming that all the plutonium stays in the top 5 cm and a soil density of 1000 kg/m^3 (typical for samples collected around Aldermaston) the concentration in the soil is 1.6 Bq/kg (0.5 ppt (pg/g), assuming $^{240}Pu/^{239}Pu$ = 0.18), which is much lower than the uranium background. The half-lives and the decay mode of the Pu isotopes of interest are given in Table 1.3.

Isotope	Half life in years	Decay mode
^{238}Pu	87.7	alpha
^{239}Pu	2.41×10^4	alpha
^{240}Pu	6537	alpha
^{241}Pu	14.4	Beta-(99+), alpha(0.002)
^{242}Pu	3.76×10^5	alpha
^{244}Pu	8.20×10^7	Alpha(99.9), S.F.(0.1)

Table 1.3 Half lives and decay mode of plutonium isotopes of interest

Plutonium is produced by the ^{238}U capture of neutrons. This capture produces neutron rich uranium, which decays then by two beta- decays to plutonium. The quantities of the produced isotopes depend on the neutron flux and the time of the neutron bombardment. In a nuclear reactor the neutrons are produced by the fission of ^{235}U. Since one-neutron-capture dominates amongst other nuclides mainly ^{239}Pu is produced. Once established ^{239}Pu also fissions or transmutes to ^{240}Pu. The interplay between the uranium and plutonium isotopes changes the ^{239}Pu content relative to heavier Pu isotopes with time. The highest ^{239}Pu content is obtained at low burn-up. In civil use it is not economically efficient to refuel the reactor at low burn-up, but for nuclear weapons a high ^{239}Pu and a low ^{240}Pu content are required. The ^{240}Pu content is chosen to grade plutonium. The plutonium grades are listed in Table 1.4. Since the plutonium isotopes ^{239}Pu and ^{240}Pu are particularly important for the potential usage, ^{240}Pu/^{239}Pu is an important tool for source characterisation, especially to differentiate between civil and military use. In Table 1.5 Pu isotopic ratios are listed for different sources. Since the reactor ratios depend on the design of the reactor, the ratios for different reactor types are listed separately in Table 1.6.

Grade	^{240}Pu	Remarks
Super	≤3%	Sub-category of weapon grade
Weapon	≤7%	
Fuel	7-19%	Produced in tritium production reactors
Reactor	>19%	Power reactors

Table 1.4 Plutonium Grades

	$^{238}Pu/^{239,240}Pu$ activity	$^{240}Pu/^{239}Pu$	$^{241}Pu/^{239}Pu$	$^{242}Pu/^{239}Pu$	Reference
Weapon Pre 1960 (LANL)		0.01			Rokop *et al*, (1995)
Weapon Modern (LANL)		0.055-0.065			Rokop *et al*, (1995)
Weapon grade		<0.075	0.005-0.007		Rokop *et al*, (1995)
Chernobyl calculated [measured]	0.38 [0.42]	0.42 [0.33]	0.11 [0.07]	0.03 [0.02]	Bondarenko and Sobotovich, (1998); Boulyga *et al*, (1997)
Integrated weapons test ratios	0.024	0.18	0.014		Harley, (1980)
Reactor		0.23-0.67	0.04-0.23	0.006-0.1	See Table 1.6

Table 1.5 Plutonium ratios for different sources

Reactor type	Fuel burn-up from normal operation [GWd/t]	$^{240}Pu/^{239}Pu$	$^{238}Pu/^{239,240}Pu$ activity	$^{241}Pu/^{239}Pu$	$^{242}Pu/^{239}Pu$
GCR	3.6	0.23	40.6	0.045	0.006
PHWR	7.5	0.41	51.7	0.077	0.023
AGR	18	0.57	99.4	0.184	0.093
RBMK	20	0.67	98.1	0.203	0.108
BWR	27.5	0.40	121	0.177	0.055
PWR	33	0.43	148.3	0.228	0.096

Table 1.6 Plutonium ratios for different reactor types (Carlson *et al*., 1988)

MAGNOX Reactor (GCR), Pressurised Heavy Water Reactor (PHWR), Advanced Gas-cooled Reactor (AGR), Pressure Tube Boiling Water Reactor (RBMK), Boiling Water Reactor (BWR), Pressurised Water Reactor (PWR)

1.3. Nuclear tests and satellite accidents as global sources of Pu and U in the environment

The main source of Pu in the environment is fallout from **atmospheric nuclear weapon tests**, which were conducted between 1945 and 1980. Yearly test yields are shown in Figure 1.1 and the locations of the tests in Figure 1.2. Tests with yields of less then 500 ktonnes are not taken into account. Details of these tests can be found in Carter and Moghissi (1977) and Lawson (1998). Approximately 15000 TBq ^{239,240}Pu were produced in the tests. About 2500 TBq Pu are deposited as local fallout and about 12500 TBq were globally distributed (Harley, 1980) via the stratosphere. The stratospheric inventories of ^{239,240}Pu are shown in Figure 1.3. Other radioactive isotopes in nuclear tests are produced by neutron induced fission of ^{235}U, ^{238}U and ^{239}Pu. These three nuclei have fairly similar fission yield curves with two peaks at masses 100 and 140. Therefore, in contrast to plutonium, the composition of these isotopes does not vary much with the type of the nuclear device. The formed nuclei are mostly unstable and pass through a variety of decay chains before becoming stable.

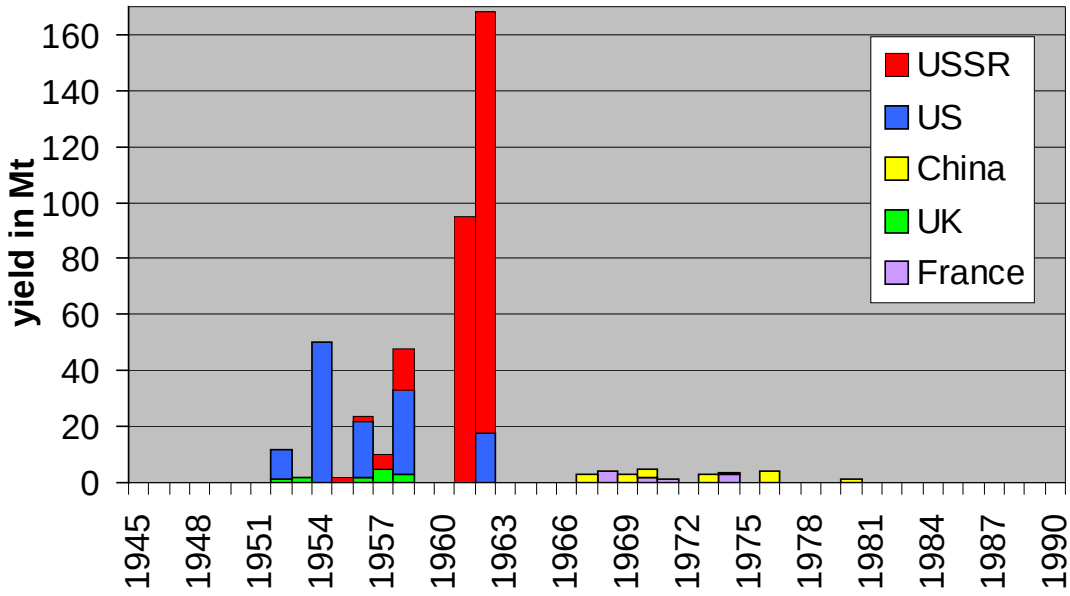

Figure 1.1 Yearly test yields of atmospheric nuclear tests

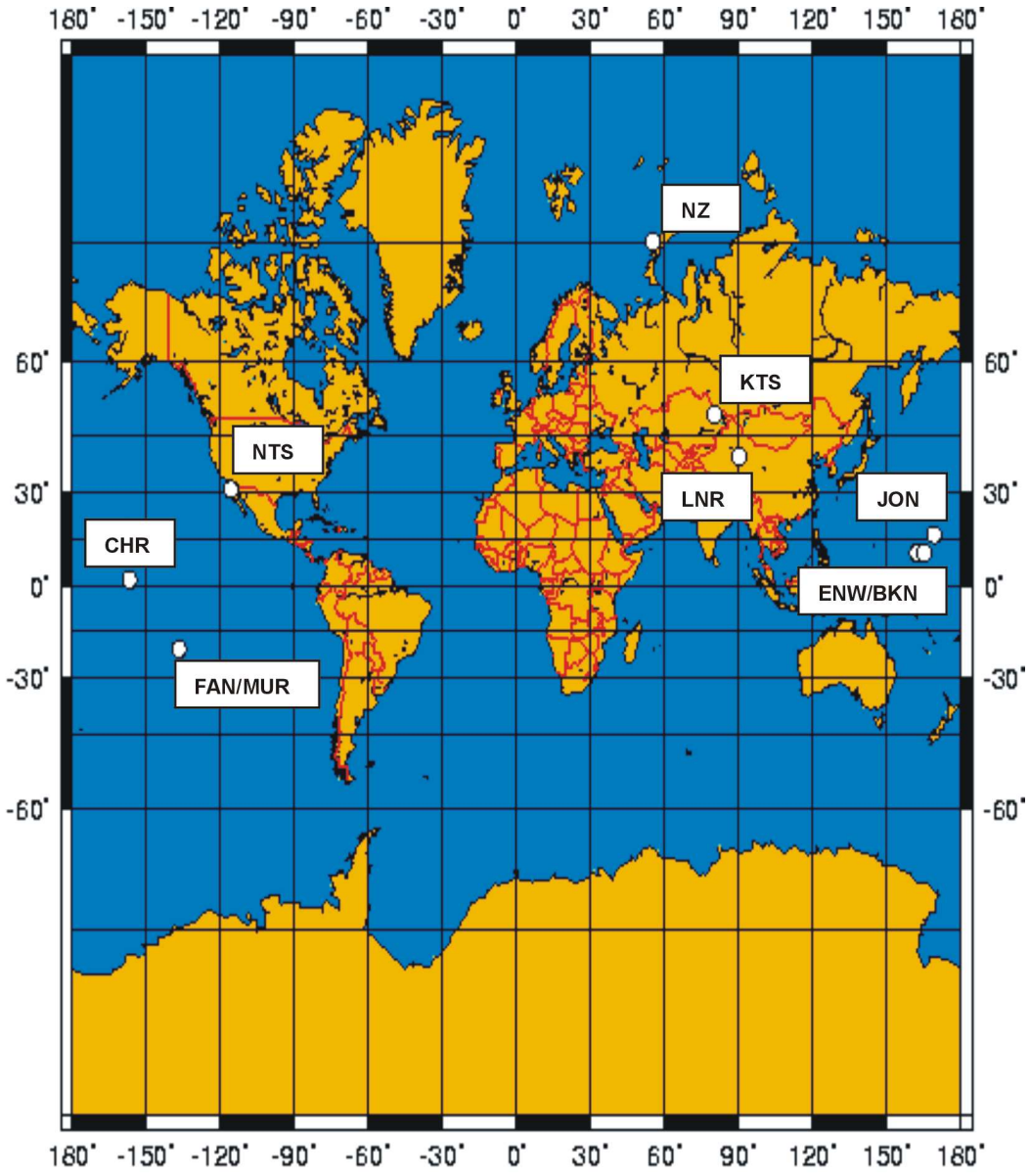

Figure 1.2 Locations of major atmospheric nuclear tests

NTS: Nevada Test Site, Nevada (US), BKN: Bikini (US), ENW : Enwetak (US), JON: Johnston Island (US), CHR: Christmas Island (UK and US), NZ: Novaya Zemlya (USSR), KTS: Eastern Kazakh or Semipalitinsk test site (USSR), LNR: Lop Nor (China), MUR: Muruora Is. (France), FAN: Fangataufa Is. (France)

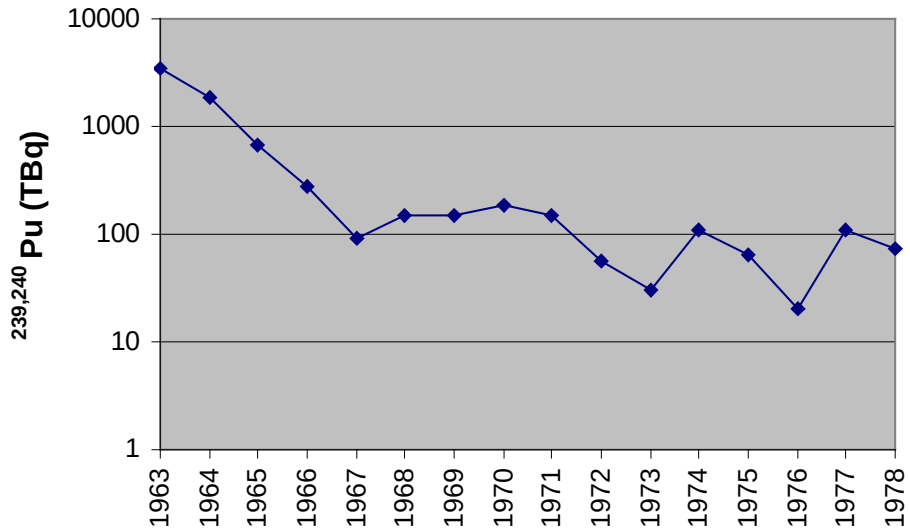

Figure 1.3 Stratospheric ^{239,240}Pu inventories due to Harley (1980)

There are different ways of producing/modifying plutonium in a nuclear explosion. One part of the weapons fallout plutonium originates from neutron irradiation of ^{238}U during the explosion by the following reactions:

$$^{238}\text{U}\ (1n,\gamma)\ ^{239}\text{U}\ (\beta\text{-})\ ^{239}\text{Np}\ (\beta\text{-})\ ^{239}\text{Pu}$$
$$^{238}\text{U}\ (2n,\gamma)\ ^{240}\text{U}\ (\beta\text{-})\ ^{240}\text{Np}\ (\beta\text{-})\ ^{240}\text{Pu}$$
$$^{238}\text{U}\ (3n,\gamma)\ ^{241}\text{U}\ (\beta\text{-})\ ^{241}\text{Np}\ (\beta\text{-})\ ^{241}\text{Pu}$$
$$^{238}\text{U}\ (4n,\gamma)\ ^{242}\text{U}\ (\beta\text{-})\ ^{242}\text{Np}\ (\beta\text{-})\ ^{242}\text{Pu}$$
$$^{238}\text{U}\ (6n,\gamma)\ ^{244}\text{U}\ (\beta\text{-})\ ^{244}\text{Np}\ (\beta\text{-})\ ^{244}\text{Pu}$$

The duration of the neutron flux in a thermonuclear explosion is of the order of microseconds and the half-life of the neutron rich uranium isotopes of the order minutes or hours. Therefore the plutonium isotopes produced do not undergo further neutron capture. The second part of the plutonium comes from the plutonium that was present in the weapon before the detonation. This plutonium consists of non-irradiated plutonium and neutron irradiated, but not fissioned plutonium. In the first mode of production, the uranium is exposed to the high temperatures of the thermonuclear explosion and the plutonium is produced after the particles have been cooled down. In the second mode of production the plutonium is exposed to the high temperatures. This might result in differences of produced metal phases with different chemical behaviour. Chemical and/or physical differences exist

between stratospheric and tropospheric fallout. Plutonium fallout from the stratosphere consists of small plutonium metal oxide particles attached to aerosols (Harley, 1980). Tropospheric fallout consists of larger particles that result from partial or completely vaporised ground material. Differences in chemical behaviour of Pu are reported for sediments from the North Atlantic (Noshkin and Gatrousis, 1974, Buessler and Sholkovitz, 1987), the Gulf of Mexico (Scott *et al.*, 1983) and the North Pacific (Buessler, 1997). All studies suggest that the tropospheric fallout is quickly removed from the water column, whereas stratospherically-derived plutonium remains in solution with a residence time greater than 10-100 years. The source of the tropospheric fallout in the North Atlantic and the Gulf of Mexico is the Nevada Test Site and in the North Pacific it is the Pacific Proving Grounds (Marshall Islands).

The second source of environmental contamination with a global impact is from accidents involving satellites and their power packs. A major source of plutonium in the stratosphere was the SNAP-9A accident in April 1964 over the Indian Ocean. It introduced about 630 TBq ^{238}Pu into the atmosphere at about 50 km altitude (Harley, 1980). Since the plutonium from atmospheric weapons tests consists mainly of ^{239}Pu and ^{240}Pu (^{238}Pu/ ^{239,240}Pu activity ratio = 0.024, see Table 1.5) the SNAP-9A accident was the main source of ^{238}Pu in the stratosphere (see Figure 1.4). Other satellite accidents introduced uranium in the atmosphere. The satellite Cosmos-954 re-entered the atmosphere over northern Canada in January 1978 and the Cosmos-1402 satellite desintegrated over the South Atlantic Ocean in February 1983. Both satellites contained about 50kg enriched uranium. The assumed isotopic composition of the uranium is 1% ^{234}U, 90% ^{235}U, 0.5% ^{236}U and 8.5% ^{238}U (Krey *et al*, 1979, Leifer *et al*, 1987).

The **latitudinal distribution** of ^{239,240}Pu and ^{238}Pu was investigated by Hardy et.al. (1973) in soils taken from 65 sites between October 1970 and January 1971 (Figure 1.4). The average values of 10-degree latitude bands and their standard deviations are shown in Figures 1.4a and 1.4b. The ^{238}Pu is differentiated between plutonium from weapons testing and the one from the SNAP-9A accident. The weapons plutonium shows the heaviest deposition in the Northern Hemisphere temperate latitudes and a minimum in the equatorial region. In contrast the plutonium from the SNAP-9A accident is mostly deposited in the Southern Hemisphere. This shows that the inter-hemispheric exchange is small and the deposition takes place mainly in the hemisphere where the Pu was injected into the stratosphere. According to

Reiter (1975) about 15% of the stratospheric mass is exchanged with the other hemisphere per year. The plutonium isotopic ratios depend on the design of the weapon and the parameters of the test. Therefore the ratio is not constant over time. The integrated $^{240}Pu/^{239}Pu$ in soils is 0.18 and does not vary greatly with latitude (Kelley *et al*, 1999). The only exceptions are lower ratios around 35°N due to the Nevada Test Site.

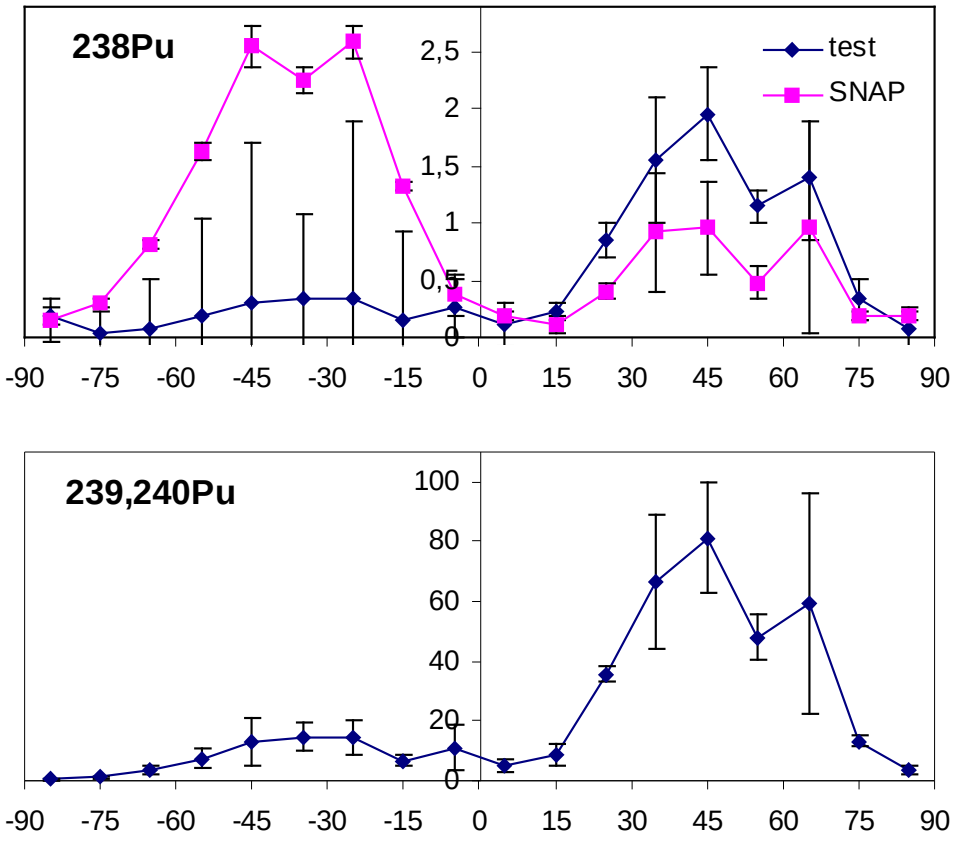

Figure 1.4 Latitudinal distribution of (a) ^{238}Pu and (b) $^{239,240}Pu$ in Bq/m^2 in 1971 due to Hardy *et al*. (1973)

1.4 Local sources with impact to the UK environment

Local sources of Pu are authorised discharges from plants that process Pu or accidental releases of plutonium. In the following sections any local sources that could have an impact on the environment in the UK are discussed. Besides their impact on the environment some information about selected sites is given. All the listed facilities could potentially be sources of radionuclides to the UK environment. In 1.4.2 –1.4.6 the sources that are thought to be relevant for this research are discussed in more detail. This discussion includes two sources outside the UK which are the La Hague reprocessing plant and the Chernobyl accident.

1.4.1 British nuclear activities and facilities

During World War II Britain collaborated with the US on the Manhattan Project. In 1946, the atomic partnership with the US was ended by the US Atomic Energy Act and Britain decided to start its own nuclear weapons program. From 1946 to 1954 the U.K. Ministry of Supply was responsible for nuclear activities. The Ministry's Division of Atomic Energy oversaw the construction of the Atomic Energy Research Establishment at Harwell, reactors at Calder Hall and Chapelcross, uranium factories at Springfield and Capenhurst and a reactor and a reprocessing plant at Windscale. On 1 April 1950 the building of the weapons factory at Aldermaston was started and at nearby Burghfield a nuclear weapons assembly factory was built. The main buildings in Aldermaston were finished in April 1952. The first British nuclear test was conducted on 3 October 1952. In 1958, the Royal Ordnance factory at Llanishen near Cardiff was converted to produce uranium shells and beryllium tampers for nuclear warheads. Of the eight key plants for Britain's bomb production (Springfields, Capenhurst, Sellafield, Chapelcross, Cardiff, Aldermaston, Burghfield and Harwell) only the Atomic Weapon Establishments at Cardiff, Aldermaston and Burghfield had purely military functions. The other ones served also civilian purposes from the 1960s onwards. Since regulations in Canada and Australia prohibit using their uranium for military purposes, Britain's main source for the military uranium supply were South Africa and Namibia. Springfields converted the imported uranium ore concentrates directly into fuel for the Magnox reactors or into uranium hexafluoride, which was then sent to Capenhurst for enrichment. Capenhurst returned enriched uranium hexafluoride to Springfields, which fabricated it into fuel. After a low burnup in one of the reactors at Windscale, Calder Hall or Chapelcross the plutonium was separated from the fuel in the Sellafield reprocessing plant.

The separated plutonium was then transported to Aldermaston for the weapons construction. The quantities of plutonium produced for military purposes were 0.4 metric tons at Windscale during 1951-1957 and 3.2 metric tons at Sellafield/Calder Hall and Chapelcross during 1957-1964 (Makhijani, 1995). The locations of all nuclear facilities in the UK can be seen in Figure 1.5 and details about the facilities are given in Table 1.7 and Table 1.8.

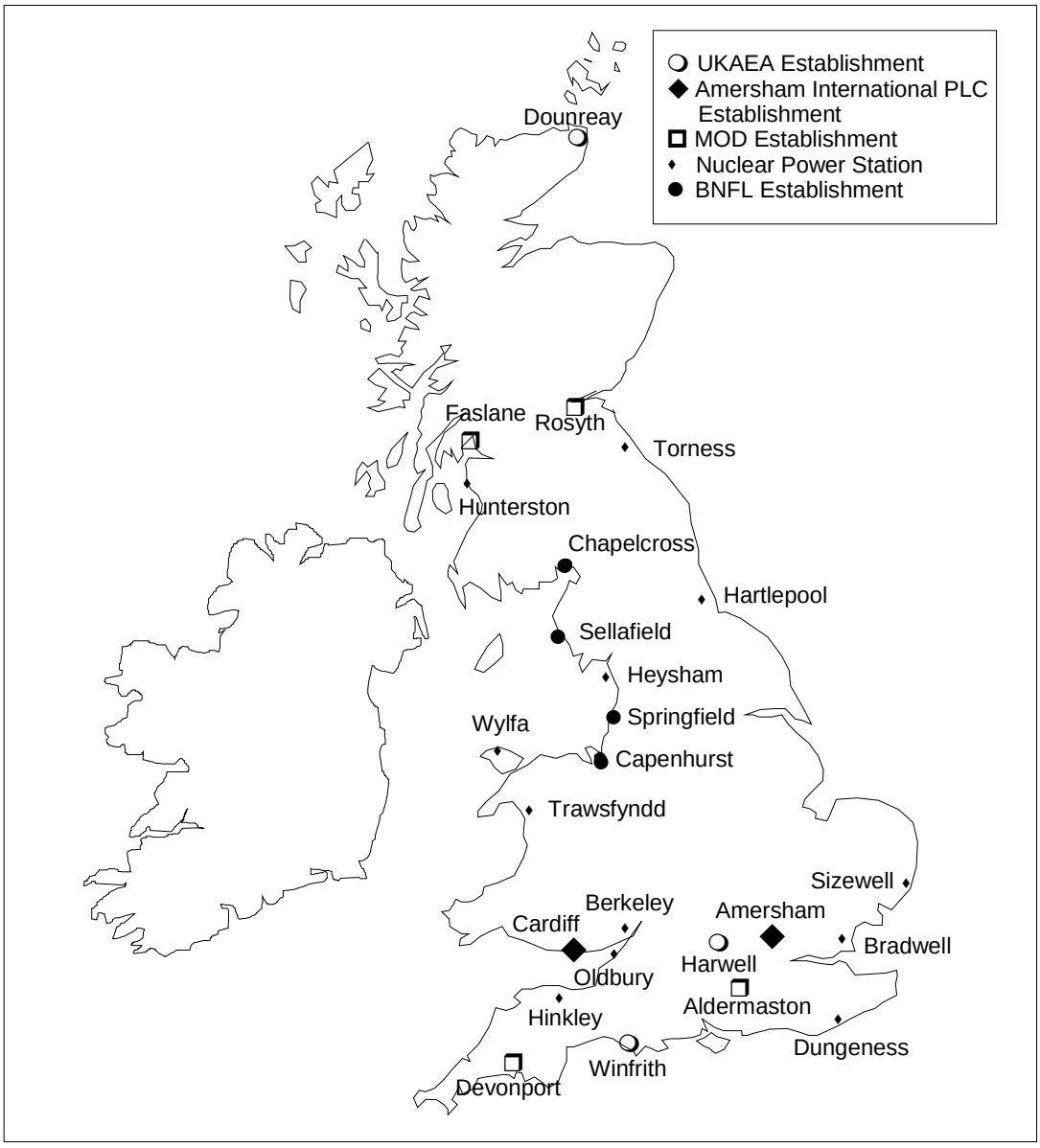

Figure 1.5 Nuclear facilities in the UK

Name	Type	Start	End	Capacity (MWe)
Berkeley A	GCR	06/62	03/89	166
Berkeley B	GCR	10/62	10/88	166
Bradwell Unit A	GCR	07/62		146
Bradwell Unit B	GCR	11/62		146
Calder Hall Unit A	GCR	10/56		60
Calder Hall Unit B	GCR	02/57		60
Calder Hall Unit C	GCR	05/58		60
Calder Hall Unit D	GCR	04/59		60
Chapel Cross Unit A	GCR	03/59		60
Chapel Cross Unit B	GCR	08/59		60
Chapel Cross Unit C	GCR	12/59		60
Chapel Cross Unit D	GCR	03/60		60
Dounreay DFR	Fast reactor R&D	10/62	03/77	15
Dounreay PFR	Fast reactor R&D	07/76	03/94	250
Dungeness Unit A	GCR	10/65		230
Dungeness Unit B	GCR	12/65		230
Dungeness-B1	AGR	04/85		610
Dungeness-B2	AGR	04/89		610
Hartlepool-A1	AGR	04/89		650
Hartlepool -A2	AGR	04/89		650
Heysham -1 Unit A	AGR	04/89		620
Heysham -1 Unit B	AGR	04/89		620
Heysham -2 Unit A	AGR	04/89		680
Heysham -2 Unit B	AGR	04/89		680
Hinkley Point-A Unit A	GCR	03/65		267
Hinkley Point -A Unit B	GCR	05/65		267
Hinkley Point -B Unit A	AGR	10/78		660
Hinkley Point -B Unit B	AGR	09/76		660
Hunterston -A1	GCR	03/64	03/90	634
Hunterston -A2	GCR	09/64	12/89	634
Hunterston -B1	AGR	02/76		634
Hunterston -B2	AGR	03/77		634
Oldbury -A Unit A	GCR	12/67		230
Oldbury -A Unit B	GCR	09/68		230
Sizewell-A Unit A	GCR	03/66		245
Sizewell -A Unit B	GCR	09/66		245
Sizewell -B	PWR	09/95		1258
Torness Unit A	AGR	05/88		682
Torness Unit B	AGR	02/89		682
Trawsfynydd 1	GCR	03/65	02/91	235
Trawsfynydd 2	GCR	03/65	02/91	235
Windscale	AGR	03/63	04/81	41
Winfrith	SGHWR, Reactor R&D	01/68	09/90	100
Wylfa Unit A	GCR	11/71		540
Wylfa Unit B	GCR	01/72		540

Table 1.7 Power Reactors in the UK (from Makhijani, 1995, AMNA, 1999 and FAS, 2000)

Magnox Reactor (GCR), Advanced Gas-cooled Reactor (AGR), Pressurised Water Reactor (PWR), Steam-Generating Heavy Water Reactor (SGHWR)

Site	Type	Origin	Closure
AWE Aldermaston	R&D Weapons Laboratory (since 1950s), fissile material storage and recycle, component manufacture	1952 (begun in 1950)	
AWE Burghfield	Weapons Assembly and Disassembly, non-fissile component manufacture	1954 (constructed 1941)	
AWE Cardiff	Depleted uranium and beryllium component manufacture	1958 (engineering establishment since 1939)	1997
Capenhurst	Enrichment	1953	
Chapelcross	Military Production Reactors (Pu) Tritium production (since 1980)	1958	today civilian
Dounreay	Reprocessing	1955	1998
Foulness Island	High- Explosives testing		1997
Harwell Site	R&D Weapons Laboratory (pre mid 1950s)	1946	
Sellafield	Reprocessing	1951 (existed since 1939 as a munitions factory)	
Sellafield/ Windscale	Military Production Reactors (Pu)	1951	1957
Sellafield/ Calder Hall	Military Production Reactors (Pu)	1956	
Springfields	Conversion	1948	

Table 1.8 Weapons-related sites in the UK (from Makhijani, 1995, AMNA, 1999 and FAS, 2000)

1.4.2 BNFL Sellafield

The Sellafield Site is located on the coast 20 km south of Whitehaven in West Cumbria. During the Second World War Sellafield was established as a conventional munition factory. In 1946 work began to build two reactors, the Windscale Piles, to produce plutonium for the UK weapons program. Pile No. 1 began operating in October 1950, Pile No. 2 started up 8 months later. A spent fuel reprocessing plant started operation in 1952. The Windscale Piles were closed after a serious fire in Pile No.1 on 10 October 1957. Besides the Windscale Piles four Magnox reactors at Calder Hall entered service between October 1956 and May 1959. These reactors, identical to those at Chapelcross, produced both weapons-grade plutonium and electricity and are still in operation. Since these early days many other facilities have

been brought into operation on site. Currently the main activity at Sellafield is recycling of used fuel from nuclear power stations worldwide. Large stocks of military plutonium are held in special vaults at the site, though no plutonium for use in nuclear weapons is produced nowadays. Sellafield began under the Ministry of Supply in 1947 and responsibility was transferred to the United Kingdom Energy Authority (UKAEA) in 1954. In 1971 British Nuclear Fuels Limited (BNFL) took over.

Liquid waste is discharged via pipelines which extend 2.5 km from the high water mark out into the Irish Sea. Discharges started in 1952. An annual discharge record is given in Appendix A6 and further details are given in Gray *et al*, 1995. Atmospheric discharges occur from many separate points on the Sellafield site and a complete set of annual records is not available. A further problem is that significant atmospheric discharges have arisen from accidents or abnormal plant operation. Sellafield is one of two major European sources of plutonium into the environment and concentrations of up to 15800Bq/kg ^{239,240}Pu are found in sediments close to the plant (Oh, 1999). The ^{240}Pu/^{239}Pu found in the Esk estuary sediment ranges from 0.16-0.26 (McCarthy and Nicholls, 1990; Sampson *et al.*,1991; Momoshima *et al.*, 1997; Erfurd, 1995 due to Rokop *et al.*, 1995). Soil samples within 10km of the plant, collected between 1976-1986 (McCarthy and Nicholls, 1990), have ^{240}Pu/^{239}Pu ratios that depend on the sampling location but no correlation with sampling time can be made. The ^{240}Pu/^{239}Pu in the soil ranges from 0.057 to 0.126. The concentration was between 0.64-30 Bq/kg ^{239,240}Pu. The low ^{240}Pu/^{239}Pu ratios suggest that the plutonium is mostly due to aerial discharges in the early years of operation. Compared with Sellafield the other nuclear installations in the UK are only minor sources of plutonium. In the fourth report of the Committee on Medical Aspects of Radiation in the Environment (COMARE, 1996) it was concluded that there is a significantly elevated level of all malignancies in young people (0-24) in Seascale for the period between 1963-1992. However, it was also concluded that the calculated radiation dose from both routine and accidential discharges was too low to explain the observed cancer rates.

1.4.3 AWE Aldermaston and Burghfield

The Atomic Weapons Establishment (AWE) Aldermaston, Berkshire, is the facility which designs, produces and maintains components for British nuclear warheads. This main centre for warhead research and manufacture is located 10 miles from the town of Newbury, 8

miles from Basingstoke, and 12 miles from the town of Reading. The first building was completed in spring 1951 and the main warhead fabrication plant in April 1952. Six months later Britain had carried out its first nuclear test. Nowadays AWE's prime purpose is still the support of the UK nuclear deterrent, but it is also an important research and development centre. Aldermaston started off under the control of the Ministry of Supply, then by the United Kingdom Atomic Energy Authority. In 1973 it was taken over by the Ministry of Defence. Ten years later the MoD Procurement Executive Directorate of Research and Development Establishment took over control. In 1987 the two Royal Ordnance Factories, Burghfield and Llanishen (Cardiff), were renamed Atomic Weapons Establishment (AWE) and combined with Aldermaston to create the AWE group. On 1 April 1993 AWE was contractorised and managed on behalf of the MoD by Hunting BRAE Ltd, a consortium comprising Hunting Engineering (51%), Brown & Root (31%) and AEA Technology (18%). In April 2000 a new consortium AWE plc comprising BNFL, Lockheed Martin and Serco took over. Until 31 March 1999 Aldermaston received a total of 17.12 tonnes plutonium with 3.51 tonnes still held at the site at 31March 1999 (MOD, 2000).

According to the Ministry of Defence (MoD), radionuclides have been discharged from the site since 1952. Annual records of discharges are given in Appendix A3. Accidental discharges are included in these discharge data. The majority of discharges are supposed to derive from work on warheads for nuclear weapons and a minority from a research reactor at the site. Atmospheric discharges are released from 73 of 81 ventilation stacks and consist mainly of U and Pu. The discharges are discussed in more detail in Chapter 6. Liquid discharges are pumped through a 11-km twin pipeline into the River Thames near Pangbourne. In December 1987 a sampling valve of the pipe was left open which resulted in discharge of low level radiation into public land. The amounts were less than the required amount to be notified. In addition very low-level radioactive waste is released to the local sewageworks at Silchester after which it is discharged into the River Kennet. Airborne levels around the AWE sites have been monitored since 1972 by the Ministry of Agriculture, Fishery and Food (MAFF), but responsibility has now been transferred to the UK Environment Agency. Passive and active deposition collectors are used around the site at fixed positions. AWE records claim that the main variations in general radioactivity level are due to weapon testing fallout (COMARE, 1989). The MoD environmental monitoring programme sampled soil, vegetation, surface water, fish and the rabbit population after 1978. They found no significant increase above natural background level. For 33 years the DoE,

MAFF and now the EA have inspected areas associated with discharge twice a year. In the third report of the Committee on Medical Aspects of Radiation in the Environment (COMARE, 1989) it was stated that there is a small but statistically significant increase in registration rates of childhood cancers within 10km of AWE Aldermaston and AWE Burghfield, compared with both national rates and regional rates for Oxford and Wessex. However, it was also concluded that the discharges (data supplied by the MoD) are too low to explain this increase. It was pointed out that the distribution of childhood cancer around nuclear installations cannot be seen in a proper context due to a lack of information about national geographical pattern of the distribution of childhood cancer.

AWE Burghfield covers 265 acres and is located 5 miles north-east of Aldermaston near Reading in Berkshire. Established in 1954 as Royal Ordnance Factory (ROF), the facility is used for the final assembly for British nuclear weapons and the decommissioning and re-commissioning of older weapons. According to the MoD atmospheric discharges started in 1970 and consisted purely of tritium until 1987 ($4x10^3$ - $6x10^4$ MBq/yr). Since 1987 ^{85}Kr has also been discharged. Liquid discharges began in 1962 and are of low activity similar to the AWE Aldermaston trade waste. They are discharged via the sewage works at the same point as the AWE trade waste.

The impact of both AWE facilities is investigated in Chapter 6.

1.4.4 AEA Winfrith

The Winfrith site in Dorset was developed by UKAEA in the mid 1950s. The main facility at Winfrith was the prototype Steam Generating Heavy Water Reactor (SGHWR) which was closed in 1991 and is now being decommissioned. Besides that several different kinds of low power (and zero power) reactors were operated but are all now closed and are being decommissioned. The discharge records are given in the Appendix A4.

1.4.5 COGEMA La Hague

The La Hague reprocessing plant site is located about 20Km west of Cherbourg on the tip of the Cotentin peninsula. It is operated by the **Co**mpanie **Ge**nerale des **Ma**tieres Nucleaires (COGEMA), 89% of which is owned by the government-controlled Commissariat a

l'Energie Atomique (CEA) - which has conducted France's nuclear weapons testing and production program - and 11% of which is owned by the French national petroleum company Total. COGEMA is therefore wholly owned and operated by the French government. In 1966 the UP2 reprocessing plant started operation. This plant reprocessed metallic fuel until 1987. Oxide-fuel reprocessing began at UP2 in 1976. In 1994 new plant components increased the nominal capacity from 400 tonnes of fuel per year to 800 tonnes of fuel per year. In 1989 a new reprocessing plant known as UP3 was commissioned. It is designed to reprocess oxide fuel and has a nominal capacity 800 tonnes of fuel per year. A small scale reprocessing plant, the AT1 facility operated at La Hague between 1969 and 1984 to reprocess fast-reactor fuel. Some fast reactor fuel was also reprocessed at UP2 between 1979 and 1984. Mixed-oxide (MOX) fuel was reprocessed at UP2 in 1992 and 1998. The upgrade of the UP2 and the opening of the UP3 can be seen in an increase in the discharge between 1989 and 1995.

The discharge records are given in the Appendix A5.

1.4.6 The Chernobyl accident

Another source of environmental radionuclide contamination in the UK is from the accident which occurred in the Chernobyl RBMK reactor on 26th April 1986. The released radioactivity initially contained a large number of different fission products and actinides. The radioactive plume was tracked as it moved over the European part of the Soviet Union and Europe (Figure 1.6). Initially the wind was blowing in a northwesterly direction and was responsible for much of the deposition in Scandinavia, the Netherlands and Belgium and Great Britain. It can be seen that the cloud reached Great Britain at the 2nd May 1986. Later the plume shifted to the south and much of Central Europe, the Northern Mediterranean and the Balkans received some deposition. The plume was detectable in the Northern hemisphere as far away as Japan and North America (EML, 2000). However, no deposition was detected in the Southern Hemisphere. Actinides were primarily contained in the larger and heavier particulates and were therefore deposited close to the accident site. The most radiologically important radionuclides detected outside the Soviet Union were iodine-131, tellurium/iodine-132, caesium-137 and caesium-134. Though the actinides had no significant radiological impact outside the Soviet Union, the low plutonium background allowed the determination of isotopic ratios in surface air during the passage of the plume. In Berlin (Germany) a

$^{238}Pu/^{239,240}Pu$ activity ratio of 0.4 was measured which is about ten times higher than the average value in 1985 (Arnold, 1999). Aerosol samples from different locations in Austria show a $^{238}Pu/^{239,240}Pu$ between 0.33-0.76 and a $^{241}Pu/^{239,240}Pu$ between 31.6-74.6 at times shortly after the accident (Irlweck and Wicke, 1998). No actinides attributed to Chernobyl have been measured in Britain. The deposition of ^{137}Cs was closly related to rainfall intercepting the plume. The deposition densities of ^{137}Cs on grass are between 4 Bq/m^2 and 25 Bq/m^2 in predominantly dry areas and reach values of 2300 Bq/m^2 in areas with high rainfall (Clark and Smith,1988).

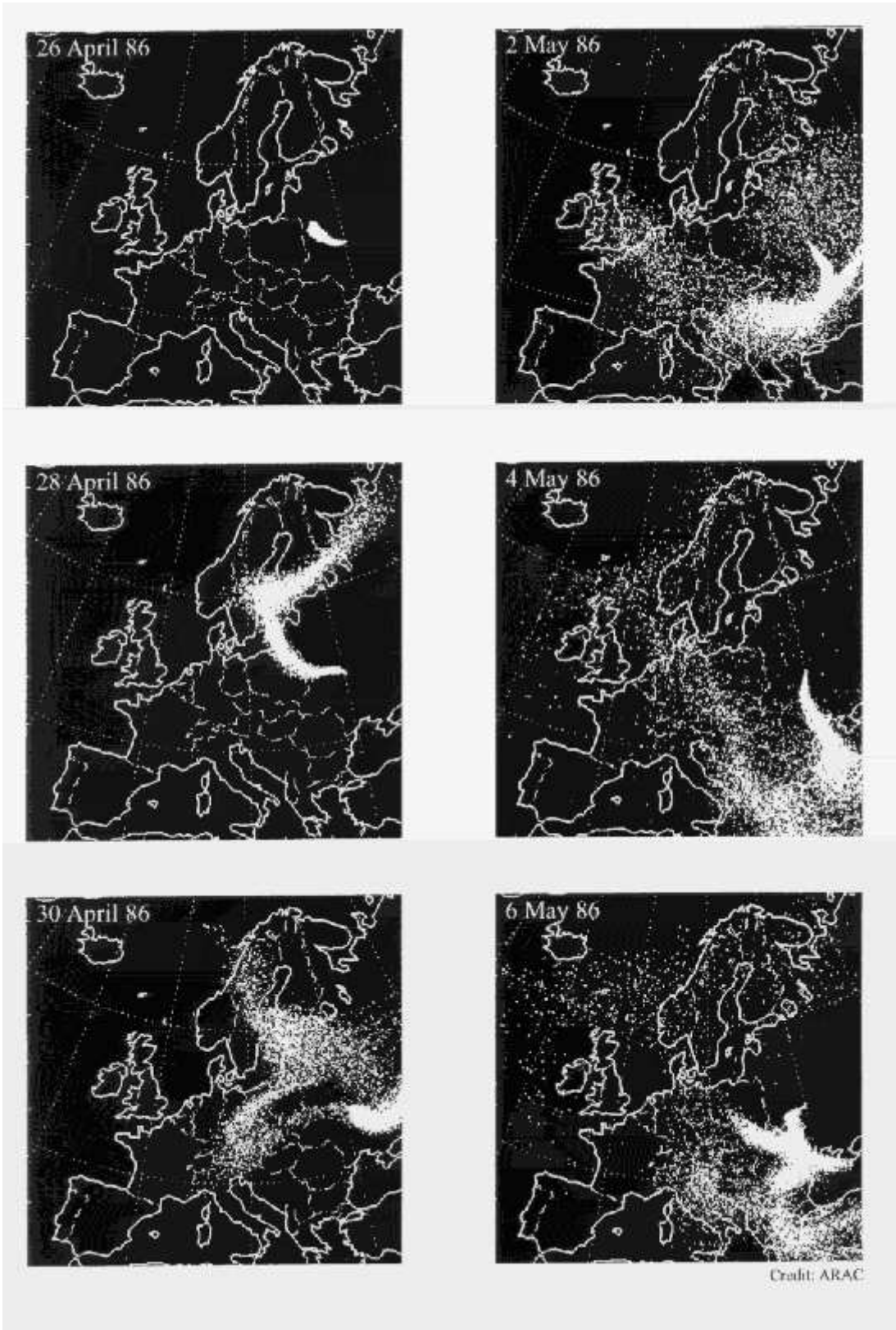

Figure 1.6 The passage of the Chernobyl plume (from NEA, 1995)

CHAPTER 2

2. Methods used for the research

2.1. Separation of U and Pu from environmental samples

2.1.1 Dissolution methods

Complete dissolution (Option 1)

The soil sample was dried at 100°C and the weight was recorded. After grinding the sample was transferred into a furnace. The temperature was slowly increased to 600°C and then ignited for approximately 24 hours. 5g of ignited sample was combined with 7g of eutectic lithium borate flux (80% lithium metaborate, 20% lithium tetraborate; ICPH, France) along with tracers (^{233}U - ^{236}U double spike and/or ^{242}Pu). The mixture was dried, mixed and transferred either to a grain-stabilised platinum-gold dish or a graphite crucible before fusion at 1200°C for approximately 20min. The melt was quenched in 75ml of deionised water in a 250ml beaker. A 4 cm diameter Pt lid was placed at the bottom of the beaker to dissipate heat and prevent the beaker from cracking. The Pt lid was removed after the fused mix had been poured into the beaker. The water was discharged and 30 ml of 8M HNO_3 and 1ml of 0.2M polyethylene glycol was added to each beaker. The samples were transferred to a combined hot plate/magnetic stirrer and left overnight at 40°C under constant stirring to dissolve the glass. The sample was filtered under suction through a Whatman GF/C glass fibre filter mounted on top of a Whatman No. 540 filter funnel. After washing with approximately 10ml of 8M HNO_3 and 10ml of deionised water the residue was discarded. The filtrate was acidified with 10ml concentrated nitric acid and 0.5 ml of concentrated HCl.

***Aqua regia* leaching (Option 2)**

Aqua regia was added to the ignited sample in the weight proportion 10:1. The mixture was transferred to a combined hot plate/magnetic stirrer and left for 24 hours at 100°C under constant stirring. After cooling to room temperature the liquid was separated from the solid phase by centrifugation and poured into a glass beaker. The solid phase was leached again by the same procedure. The separated liquids from the two leaches were combined and dried down on a hotplate. After drying it was re-dissolved in 30 ml 8M HNO_3 and 1drop of concentrated HCl. Before loading this solution onto a column it was filtered by a Whatman GF/C glass fibre filter.

2.1.2 Chemical separation

Basic separation of U and Pu

Two ion-exchange columns were prepared for each sample. The first a 6cm high 0.7 cm internal diameter column with Eichrom anion exchange resin (100-200 mesh, 8% cross-linked), and the second a 2cm high x 0.7 cm internal diameter column containing Eichrom UTEVA™ resin. The UTEVA™ column was placed immediately below the anion exchange column and both columns were pre-conditioned with 10ml 8M HNO_3. The sample was transferred to the anion exchange column and the eluent passed directly onto the UTEVA™ column. The two columns were washed with 20ml 8M HNO_3 followed by 30ml of 3M HNO_3, and then separated. The anion column was washed with 30ml 3M HNO_3 followed by 25ml 9M HCl to remove thorium. Plutonium was then eluted with 50 ml of freshly prepared 1.2M HCl/H_2O_2 (50:1). The UTEVA column was washed with 10ml 3M HNO_3 followed by 10ml 9M HCl. The uranium was eluted with 10ml 0.02M HCl.

Additional Purification of U

If the uranium was to be measured by TIMS the following additional purification was used:
10ml of concentrated HCl (12M) was added to the eluent from the UTEVA™ column to adjust the concentration to 6M. The solution was then loaded onto a 2x0.7cm internal diameter anion exchange column (Eichrom 100-200 mesh 8% cross-linked) pre-conditioned with 10ml 6M HCl and washed with 10ml 6M HCl. The U was eluted with 10ml H_20 and the eluent evaporated to dryness in a PFA beaker.

Additional purification of Pu

The following additional purification is required in the following cases:

- ^{233}U was added and the plutonium is to be measured by alpha spectroscopy. **Reason:** The ^{233}U has a high specific activity and its alpha peak overlaps with the ^{242}Pu tracer peak.
- High amounts of natural uranium are present in the sample and the plutonium is to be measured with MCICPMS. **Reason:** The ^{238}U forms a hydride that interferes with the ^{239}Pu measurement.

Clean-up method: The eluent from the first Pu column was concentrated to 2ml. To the concentrate 5ml 9M HCl, 1 drop H_2O_2 and 7ml concentrated HCl were added before loading it onto an 4x0.7cm internal diameter anion exchange column (Eichrom 100-200 mesh 8% cross-linked) pre-conditioned with 9M HCl. The column was washed with 10ml 9M HCl,

40ml 7.2M HNO_3 and 15ml 9M HCl. Plutonium was then eluted with 25 ml of freshly prepared ammonium iodide reagent (0.1M NH_4I/9M HCl). The eluent was evaporated to dryness and the residue was treated with concentrated HNO_3 to decompose the excess NH_4I.

Electrodeposition of Pu

The EDP (electrodeposition) cell was prepared by placing a new stainless steel disc into the base of the EDP cell, a new insert into the top of the EDP cell and screwing on the top. The cells were checked for any leaks by doing an initial test using distilled water. The dry residue from the purification was dissolved in 1ml of 10% hydrochloric acid. 5ml of 2% ammonium oxalate solution were added to the beaker and the solution was transferred to the electrodeposition cell. The beaker was washed with another 5ml of 2% ammonium oxalate solution that was then added to the electrodeposition cell and the cathode connection was attached. The platinum anode was lowered into the solution, the current was adjusted to 400 mA and electrodeposition was carried out for 100 minutes. The current and sample level in the cell were checked at regular intervals. The current was adjusted accordingly and the cell was topped up with water if the level dropped significantly. After 100 minutes of electrodeposition, a few drops of ammonia solution were added. Deposition was continued for another 30 seconds and then the power supply was disconnected. The cell was rinsed several times with water and the stainless steel disc was removed. The disc was washed with water again and dried on a hot plate. The disc was then counted on a EG&G Octete PC alpha spectrometer.

2.2. Blank values for different acid grades

The chemical separation of U and Pu involves great amounts of nitric and hydrochloric acid. Hence the U and Pu content of these acids is of great importance, especially for low level measurements. The uranium contents of different acid grades were measured by TIMS. 20g of acid were spiked with ^{236}U, evaporated to dryness in a PFA container (Savillex, USA), redissolved in a drop of nitric acid and loaded onto a rhenium filament with Aquadag™. For some of the early measurements, containers that had been previously used for uranium fractions of the AWE samples were used. They were cleaned with *aqua regia* for 24 hours at 100°C and then rinsed with MQ water. The measured uranium levels were in the order of 1ng and did not correlate with the acid grade. This shows that old pots can be a significant source of contamination and should not be used especially if any moderately high U was

found. The same measurement was repeated in brand new PFA containers. This time a correlation between the U content and the acid grade could be seen. The results are shown in Table 2.1.

	Technical grade	Analytical grade	Aristar grade	sub-boiled Aristar	2 times sub-boiled Aristar
HCl	55	0.573	0.567	0.133	
HNO_3	59	0.167	0.373	0.037	0.058

Table 2.1 Uranium content of different acid grades (Merck) measured by TIMS in pg/g

The measurement of the technical grade acids has errors up to 50% because of strongly fluctuating ion signals. This fluctuation is probably due to a high organic content. Analar and Aristar grade acids contain less than 1pg/g Uranium. Analar HCl and Aristar HCl contain the same amount of uranium within the errors of the measurement. Sub-boiling reduced the uranium blank by a factor of about 5 for both HCl and HNO_3. A second sub-boiling does not show any further significant improvement. Besides the acids MQ water was also measured. The uranium value was below the detection limit of the measurement.

2.3. Gamma spectrometry of ^{137}Cs

^{137}Cs decays to ^{137}Ba via beta decay. The excited ^{137}Ba emits gamma rays when decaying to its ground state. These gamma rays are used to detect ^{137}Cs (Figure 2.1). Gamma spectrometry was used to determine ^{137}Cs in the Rothamsted grass samples. The ignited samples were transferred into 22 ml polythene scintillation vials and counted for 24 hours using Canberra well-type HPGe detectors (see Table 2.2). The acquired energy spectra were then analysed and the activity of radionuclides calculated using Fitzpeaks™ software. The gamma spectrometer was previously calibrated for both energy and efficiency against an Amersham QCY-48 mixed radioisotope standard adsorbed onto a sediment matrix.

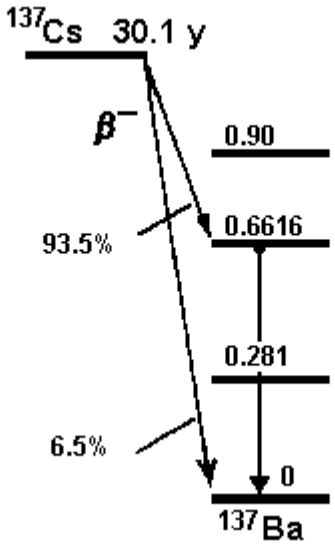

Figure 2.1 Decay scheme of ^{137}Cs

	Details	Note
Model	GCW 4523	Canberra
Type	Coaxial one open end	
Diameter	76 mm	
Active volume	239 cc	
Well depth	45 mm	
Resolution	FWHM (2.25 keV)	^{60}Co (1332 keV)
Peak/Compton	46.5 : 1	"
Efficiency	41.1 %	"

Table 2.2 Typical detector specification and performance data of the gamma detector

2.4. Mass spectrometric measurements

2.4.1 Introduction

The instruments used are Inductively Coupled Plasma Mass Spectrometry (ICP-MS), Thermal Ionisation Mass Spectrometry (TIMS) and the Isoprobe Multi-Collector Inductively Coupled Plasma Mass Spectrometry (MC-ICPMS).

ICPMS has ionisation efficiencies of more than 20%. However, the ions have an energy spread of 20-30eV, which results in broad peaks, and a transmission of less than 2%.

Another disadvantage are beam fluctuations due to instabilities in the plasma. Because of these beam fluctuations and the poor peak shape, ICPMS is not suitable for precise isotopic ratio measurements. Using a MCN6000 nebuliser an overall efficiency of 0.045% can be achieved.

TIMS in contrast to ICPMS has stable beams and is commonly used for plutonium isotopic ratio measurements (e.g. Buesseler and Halverson, 1987). The instrument used is a single-focusing VG (Micromass) Sector 54 thermal ionisation mass spectrometer. The instrument is equipped with seven Faraday collectors and a Secondary Electron Multiplier/Daly detector (SEM) positioned behind the axial Faraday collector. Signals from the SEM are received by an EG&G® Ortec 9302 amplifier/discriminator and EG&G® Ortec 996 ion counter/timer. The main disadvantage in TIMS is a low ionisation efficiency of less than 0.1% and an overall efficiency of 0.002%. The ionisation efficiencies are further reduced by other matrix atoms. Therefore extremely good elemental separations are required. Another disadvantage is the time dependent mass fractionation due to small differences in the quantum states of the different isotopes, which is particularly large for small sample loads. Using ^{236}U-^{233}U double spike, the $^{238}U/^{235}U$ can be measured to a reproducibility of <0.2% (2sd) on nanogram loads of uranium (Croudace *et al*., 1999) Due to the lack of an internal fractionation correction and different ionisation behaviour the reproducibility in $^{240}Pu/^{239}Pu$ measurements is only 3% (2sd).

The **Isoprobe MCICPMS** (Micromass, Ltd, Withenshaw, UK) is the mass spectrometer that proved to be best for the isotope ratio measurements in this research. A schematic of the mass-spectrometer is shown in Figure 2.2. The Isoprobe has a plasma source like the ICPMS thus providing high ionisation efficiencies, but it also suffers from the high energy spread of the ions produced in the plasma. To compensate for this effect, after passing through the sample and skimmer cones, the ions enter a Hexapole collision cell. Argon is continuously introduced to the collision cell at flow rates of about 1ml/min and then pressurised to about 10^{-4} mbar. The ions collide with the argon and reduce their energy to the energy of the gas molecules which is about 1eV. These ions are then concentrated into the centre of the Hexapole by an RF field. After accelerating them to about 5.5 kV they pass through the magnetic sector to the detector system. The collision procedure increases the transmission by a factor 5-10. In addition the collision produces electrons to neutralise ions of high ionisation potential. This results in a reduced argon signal. This process can be enhanced by small

amounts of hydrogen. The detection system consists of Faraday collectors for simultaneous collection of ions and a Daly detector for high sensitivity ion analysis. The Daly detector is positioned behind a WARP (Wide Angle Retarding Potential) filter. This increases the abundance sensitivity by two orders of magnitude. For the WARP to be effective it is essential that the energy spread of the entering ions is reduced because its acceptance is restricted to 5500+/-1V. Such a small energy spread is provided by the TIMS and the Isoprobe but not by normal ICPMS. Using the MCN6000 nebuliser an overall efficiency of 0.8% is achievable. $^{238}U/^{235}U$ can be measured with a reproducibility of <0.2% (2sd) on the Isoprobe (Croudace *et al*, 2000). An advantage of a plasma source MS is that mass fractionation corrections can be carried out using a different element. The reason is that different elements of similar mass tend to have similar levels of ionisation and similar levels of mass fractionation. For example, the uranium fractionation factor can be applied to correct for isotopic fractionation of plutonium (Taylor *et al*, 2001). This element-to-element style of correction is not possible in TIMS because both, the evaporation from the filament, and the ionisation vary significantly between elements.

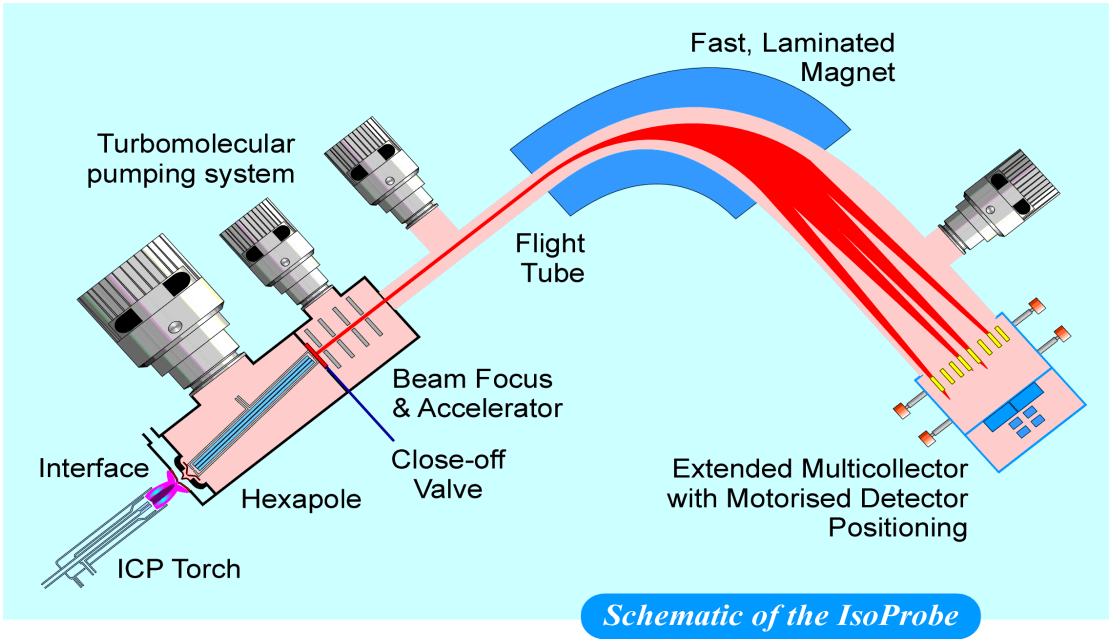

Figure 2.2 Schematic of the Isoprobe from Micromass, Ltd, Withenshaw, UK

2.4.2 Loading techniques for Thermal Ionisation Mass Spectrometry (TIMS)

Thermal ionisation sources are based on the fact that the particles evaporated from a heated metal surface contain ions in addition to the neutral particles. The ratio of the number of evaporated ions n+ to the number of evaporated neutral particles n is called the efficiency. The Saha-equation gives the following proportionality:

$$\frac{n^+}{n} \propto \exp\left[\frac{W-I}{kT}\right]$$

where k is the Boltzmann constant, W the work function of the metal, I the ionisation potential and T the temperature. In our case (W-I) is negative. Hence the temperature has to be high to get a reasonable efficiency. On the other hand the sample will evaporate very quickly when T becomes too high. Therefore a compromise must be made between the efficiency of the ionisation and the length of time for which the sample lasts. Another limit of the temperature is given by the melting point of the filament. Besides the temperature the efficiency can be influenced by the choice of the filament material as one can see from the equation above. The material should be refractory and possess a high work function. The common filament material for U and Pu is carburized rhenium. Carbon acts as a reducing agent, promoting the production of elemental ions at the expense of oxide species (Buesseler and Halverson 1987; Kelley and Robertson 1985). Besides that, carbon can enhance or reduce the work function and change the Pu ion emission characteristics. The work function of pure rhenium is 4.96eV. If the carbon is completely dissolved in the rhenium the work function is 0.25 V higher, but as soon as graphite layers on the filament surface are formed the work function decreases by 0.9 V with respect to pure rhenium (Pallmer *et al*, 1980). Kelley and Robertson (1985) observed a useful ion signal of small Pu quantities only if the carbon saturation temperature of the filament was exceeded. Hence supersaturated rhenium is not suitable as a filament material. The saturation temperature is the temperature at which carbon redissolves into the filament. It can be determined by an irregularity in the filament temperature respond to the current passed through (Gordon, 1983).

Several sample loading methods have been proposed. Solution loaded samples may result in intense but short-lived signals (Kelley and Robertson, 1985). It is suitable if large amounts of sample are available, but not for minute quantity measurements. The method of loading a resin bead has proven to be a suitable method for minute quantities (Smith *et al*., 1980,

Kelley and Robertson, 1985; Buessler and Halverson, 1987). The resin bead has the advantage that quantitative high amounts of Pu can be loaded nearly as a point source. In addition the heated and pyrolysed resin bead serves as a carbon source. The carbon dissolves into the rhenium upon heating. However, the amount of carbon might not be sufficient to enhance the work function and an additional carburization step might be required. Very precise measurements have been made by employing a porous emitter (Smith and Carter, 1981) or by overplating the filament with platinum (Perrin *et al*., 1985). These two methods have been shown to enhance the lifetime of the signal and reduce fractionation.

$^{238}U/^{235}U$ isotopic ratios can be measured in 5g soil with an overall precision of 0.2% at the 99.73% uncertainty level using a solution load onto a carbon coated filament. (Taylor *et al*., 1998). However, Pu concentrations are much smaller and the sample loading technique becomes more important. The different loading techniques have been investigated in this study using approximately 20pg ^{239}Pu and the results are given in Table 2.3. The best method was the overplating by platinum. The measured ratio for Site 112 (an Irish Sea sediment contaminated with Pu isotopes) was $^{240}Pu/^{239}Pu$=0.227 +/-0.6%(SdErr).

Loading technique	^{239}Pu counts/s	Duration of signal	Comments
Solution load with aquadag	7000	<5 min	duration of signal too short for measurement
Resin bead	1000	>30min	potential loss of bead during decomposition
Rhenium sucrose overlayer	500	>30min	no reliable measurement due to strongly fluctuating signal
Overplating with platinum	1000	>30min	best investigated loading technique

Table 2.3 Loading techniques for TIMS- filaments tested in this study

2.4.3 Measurement of plutonium isotopic ratios using Isoprobe-MCICPMS

The measurement of plutonium isotopic ratios using the Isoprobe MC-ICPMS is published in Taylor et al. (2001; see Appendix). In the following some details that might be useful for users of the Isoprobe and some additional results are presented.

Sensitivity/Backgrounds/Blanks

The day before each measurement period the nebuliser, torch and cone were cleaned. The night before each measurement day the Hexapole was baked. On the measurement day the instrument was first tuned for optimum sensitivity using a 250ppt natural uranium solution. The 238-voltage of this solution on the Faraday detector ranges between 0.05V-0.13V for an extract setting of 40%. The strong variation in sensitivity is due to machine performance and variation in solution uptake by the MCN 6000 nebuliser. On some measurement days the exchange of the nebuliser tube increased the sensitivity by a factor 2. Backgrounds are determined using 2% HNO_3. Background signals were found at all masses from 239 through 242. As a typical example the backgrounds from the 25 August 2001 are shown in Table 2.4 for an extract setting of 40%. On this day the voltage of the 250ppt natural uranium solution was 0.1V. Both background and signal decrease by lowering the extract. However the functional relation between background and extract is different from the functional relation between signal and extract. Hence it is sometimes useful to optimise the signal-background-ratio by changing the extract.

n=20	Average signal in µV	Stdev in µV
^{239}Pu	0.81	0.35
^{240}Pu	0.78	0.38
^{242}Pu	0.64	0.30

Table 2.4 Typical backgrounds for an extract setting of 40%. The voltage of the 250ppt natural uranium solution was 0.1V (400V/ppm ^{238}U).

The ^{240}Pu/^{239}Pu could be determined in two ways, either by subtracting a method blank or by subtracting the 2% HNO_3 acid blank. The ^{240}Pu/^{239}Pu measured for the method blank is between 0.4 and 0.8. These high ratios suggest that the measured ^{240}Pu/^{239}Pu is due to interferences and not due to plutonium contamination. In Figure 2.3 the method blank corrected ^{240}Pu/^{239}Pu is plotted versus the sample concentration for 3 different concentrations of the method blank. The assumed acid-blank corrected ratio (true ratio) is 0.2 and the ratio

in the method blank is 0.8. It can be seen that for low concentrations the method blank corrected $^{240}Pu/^{239}Pu$ can be significantly different from the acid-blank-corrected $^{240}Pu/^{239}Pu$. A low method blank (~0.5ppq) was achieved by dissolving the dry residue first in *aqua regia*, taking the sample to dryness again and repeating the same procedure with nitric acid. For some samples this procedure reduced the method blank by a factor of 5, which suggests that organic residues are responsible for high method blanks.

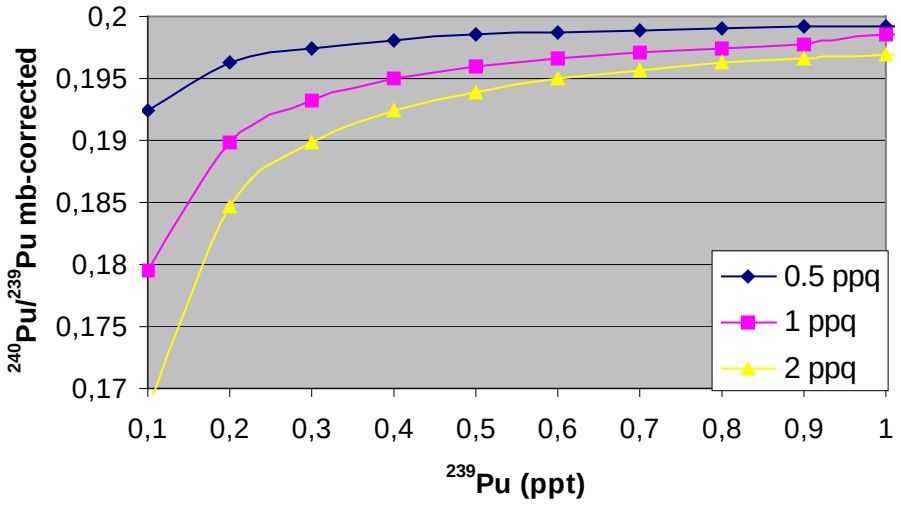

Figure 2.3 Method blank corrected $^{240}Pu/^{239}Pu$ versus sample concentration. The acid blank corrected $^{240}Pu/^{239}Pu$ (true ratio) of the sample is 0.2. The assumed concentrations of the method blank are 0.5ppq, 1ppq and 2ppq. The assumed $^{240}Pu/^{239}Pu$ in the method blank is 0.8.

Standards and $^{242}Pu/^{239}Pu$ measurement

In Taylor *et al.* (2001) the reproducibility of the isotopic ratio measurement is determined from an in-house sediment 'standard', called Site112 (Irish Sea Sediment) and the accuracy is tested on the standard UK-Pu-5 (Table 2.5). In addition to those measurements the U.S. standards NBL122, NBL126 and NBL128 from the Brookhaven National Laboratory are measured (Table 2.6). The $^{240}Pu/^{239}Pu$ measurement of those standards expands the range where the method proves to be accurate. The measurement confirms that $^{240}Pu/^{239}Pu$ ratios between 0.01 and 0.13 can be accurately measured. This range is especially important for the detection of weapons grade plutonium in the environment. The NBL-standards also confirm the accuracy of the $^{242}Pu/^{239}Pu$ measurement for ratios around one, but for the rather extreme NBL122 standard about twice the certified value of 0.002 is measured. The error in the

measurement of the $^{242}Pu/^{239}Pu$ only appears if the ratio was determined using the sequence ^{240}Pu - ^{239}Pu - ^{242}Pu (see Taylor *et al*, 2001). The $^{242}Pu/^{239}Pu$ in the NBL122 was accurately measured, if the ratio was calculated from the first and second cycle of the sequence ^{242}Pu - ^{239}Pu - ^{242}Pu. In this research the only case where $^{242}Pu/^{239}Pu$ ratios of less than 1 were determined is in the Wyre sediment core (see Chapter 4). Some of the samples were re-measured using the sequence ^{242}Pu - ^{239}Pu - ^{242}Pu. Figure 2.4a shows that for $^{242}Pu/^{239}Pu$ below 0.01 the ratios from the two cycles start to deviate. The deviation does not correlate with the voltage (Figure 2.4b). However, the deviation is not random, but seems to follow a simple function.

	Certified $^{240}Pu/^{239}Pu$	**Measured $^{240}Pu/^{239}Pu$**	
		0.5 ppt	**5-10ppt**
Site112	0.2264 +/- 0.0024*	0.2263 +/-0.0021 (n=13)	0.2262 +/-0.0007 (n=22)
UK-Pu-5	0.9662 +/- 0.0011	-	0.9645 +/- 0.0013 (n=7)
	Certified $^{242}Pu/^{239}Pu$	**Measured $^{242}Pu/^{239}Pu$**	
		0.5 ppt	**5-10ppt**
Site112	-	0.0.0095 +/-0.0008 (n=13)	0.0095 +/-0.0002 (n=7)
UK-Pu-5	0.9662 +/- 0.0011	-	1.0252 +/- 0.0034 (n=7)

*not certified, but assumed to be accurate from high concentration measurements by TIMS

Table 2.5 $^{240}Pu/^{239}Pu$ and $^{242}Pu/^{239}Pu$ for the Site112 sediment and UK-Pu-5

	Certified $^{240}Pu/^{239}Pu$	**Measured $^{240}Pu/^{239}Pu$**	
		0.5 ppt	**5ppt**
NBL122	0.1320	0.1318 +/-0.001 (n=4)	0.1321 +/-0.0001 (n=3)
NBL 126	0.0209	0.0211 (n=1)	0.0204 (n=1)
NBL 128	0.0007	-	0.0007 (n=1)
	Certified $^{242}Pu/^{239}Pu$	**Measured $^{242}Pu/^{239}Pu$**	
		0.5 ppt	**5ppt**
NBL122	0.0021	0.0040 +/-0.001 (n=4)	0.0046 +/-0.0004 (n=3)
NBL 126	$<5x10^{-6}$	-	-
NBL 128	1.00106	-	0.9996 (n=1)

Table 2.6 $^{240}Pu/^{239}Pu$ and $^{242}Pu/^{239}Pu$ for the standards NBL122, NBL126 and NBL128

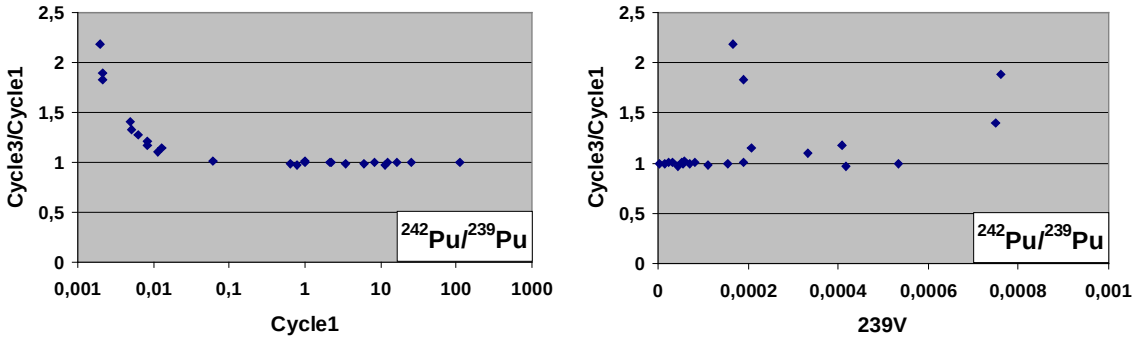

Figure 2.4 Dependance of the $^{242}Pu/^{239}Pu$ on the measurement cycle. Cycle i (i= 1, 2, 3) is defined as the $^{242}Pu/^{239}Pu$ where the ^{242}Pu from the cycle i is used. **(a)** Cycle3/Cycle1 vs Cycle1 **(b)** Cycle3/Cycle1 *vs* voltage of 239

2.4.4 Static measurements of the $^{238}U/^{235}U$ using Faraday collectors (used for Rothamsted grass)

Uranium masses 233, 234, 235, 236 and 238 were measured statically using Faraday detectors. A natural uranium standard extracted and purified from CCRMP-BL1 was run between each sample. All ratios were corrected for low-mass tailing of the other uranium peaks. The factors for the tailing correction are given in Table 2.7 and were determined by normalising the measured ratio for the BL1-standard to the natural $^{238}U/^{235}U$ of 137.88. These factors are lower than those reported by Thirlwall (2001). Both samples and standard were spiked with a ^{233}U-^{236}U double spike to correct for mass fractionation (Croudace *et al*, 1999). In addition measured compositions are corrected for the ^{238}U and ^{235}U in the double spike. ($^{238}U/^{235}U$=4, Taylor *et. al*, 2001) The calculations are shown in Appendix M.2. Finally the ratio of each sample is externally corrected by normalising to the mean of the two adjacent standards. The voltage of the method blanks was between 0.2V and 0.5V on 238 and the $^{238}U/^{235}U$ appears to be natural. However, the samples have been diluted to approximately the same concentration as the BL1-standard. Applying this dilution to the method blank it yields a 238-voltage of 0.02V – 0.05V. That is a factor 40-100 smaller than the lowest measured sample. Since the $^{238}U/^{235}U$ in the method blank is natural, it is likely that the uranium is due to small amounts of contamination in the laboratory. The method blank shows that the contamination in the lab is small and can be neglected for those samples. The $^{238}U/^{235}U$ of all measured samples and standards is plotted versus the signal intensity in Figure 2.5. A correlation between the measured ratio and the signal intensity

could not be observed. The 3 s.d. uncertainty has been determined from all standards that were run during the analysis of the samples. Only samples outside the 3 s.d. limit are considered to deviate from natural uranium.

Mass units (amu)	light peak/heavy peak
1	0.000012
2	0.000009
3	0.000004
4	0.000002
5	0.000001

Table 2.7 Correction factors for peak tailing to the low mass side

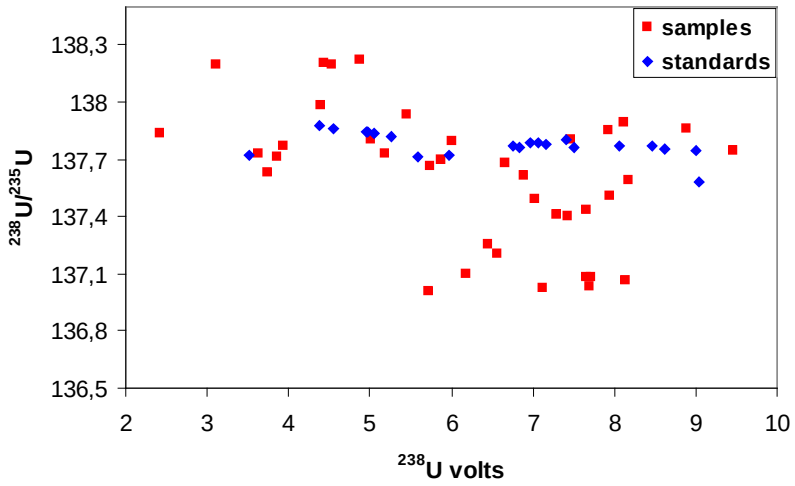

Figure 2.5 $^{238}U/^{235}U$ atomic ratio vs. ^{238}U voltage

2.4.5 Static Faraday-Daly measurement of $^{238}U/^{235}U$ (used for alpine ice samples)

The $^{238}U/^{235}U$ is measured statically with mass 235 on the Daly and 238 on the Faraday detector. The measurement of the samples is made using a natural uranium standard run between two samples. Standard solutions are prepared over the concentration range of the sample solutions and after each sample a standard close to the sample concentration was measured. The measured $^{238}U/^{235}U$ depends on the concentration of the solution. A typical

example for variation of the $^{238}U/^{235}U$ versus concentration is shown in Figure 2.6 for the natural standard. The relationship always appears to be linear. A method blank was prepared using a brand new anion exchange filter. The voltage of the method blanks was 0.2V on 238 which is a factor of 5-15 lower than voltages in the samples. The $^{238}U/^{235}U$ in the method blank is natural and has been subtracted from all measured samples.

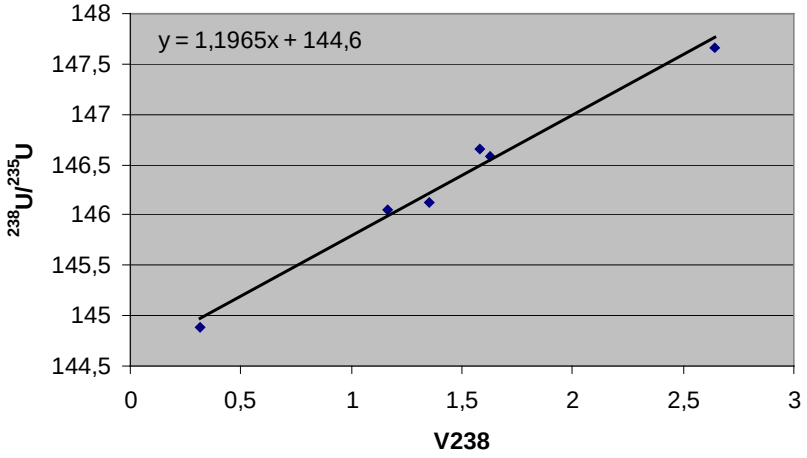

Figure 2.6 $^{238}U/^{235}U$ versus voltage on mass 238. The concentration range is 2.5ppb-15ppb.

1. Concentration correction of the measured $^{238}U/^{235}U$

Each day a linear trendline was fitted through the $^{238}U/^{235}U$ versus voltage of 238 and the equation of the trendline was determined. Both standard and samples are then corrected by

$$R^c = R^m \times \left[137.88/\left(m * V_{238} + b\right)\right]$$

where: R^c=corrected $^{238}U/^{235}U$

R^m=measured $^{238}U/^{235}U$

($m* V_{238}+b$)=linear equation with the voltage of 238 (V_{238}) as the variable

2. Time drift correction of the measured $^{238}U/^{235}U$ for time drift

The $^{238}U/^{235}U$ of the standard at the time of the sample measurement was calculated via

$$R^c_{Std}(t_a) = R^c_{Std}(t_1) + \frac{R^c_{Std}(t_2) - R^c_{Std}(t_1)}{t_2 - t_1}\left(t_a - t_1\right),\ t_2 > t_a > t_1$$

where R^c_{Std} is the concentration corrected $^{238}U/^{235}U$ of the standard, t_1 and t_2 the time of measurement of the two adjacent standards and t_a the time of the sample measurement. The

concentration- and time-corrected $^{238}U/^{235}U$ of the sample $R^c_{Sa}(t_a)$ is calculated by

$$R^c_{Sa}(t_a) = R^c_{Sa}(t_a) \times \left[137.88 / R^c_{Std}(t_a)\right]$$

3. Error calculations:

(a) Error due to time drift

The error in $^{238}U/^{235}U$ of the sample at t_a is called $\Delta R^c_{Sa}(t_a)$ and estimated in the following way. The times of the four standard measurements in the vicinity of t_a are t_0, t_1, t_2 and t_3 with $t_0 < t_1 < t_a < t_2 < t_3$. The sample was corrected to a virtual standard at t_a, calculated via a line determined by the standard measurements at t_1 and t_2. The same line was used to calculate virtual standards at t_0 and t_3. Three times the maximal absolute value of the difference between the calculated and the measured standard is the stated error due to time drift.

The equation used for the error calculation is

$$\Delta R^c_{Sa}(t_a) = 3 \times \max\left\{ \left| R^c_{Std}(t_3) - \left[R^c_{Std}(t_1) + \frac{R^c_{Std}(t_2) - R^c_{Std}(t_1)}{t_2 - t_1}(t_3 - t_1) \right] \right|, \left| R^c_{Std}(t_0) - \left[R^c_{Std}(t_1) + \frac{R^c_{Std}(t_2) - R^c_{Std}(t_1)}{t_2 - t_1}(t_0 - t_1) \right] \right| \right\}$$

(b) Error associated with the concentration correction

The error is stated as the 3 s.d. of the concentration corrected standard R^c from the natural ratio of 137.88. This error is the same for all samples.

2.5. Conclusions

- Using platinum overplated filaments the $^{240}Pu/^{239}Pu$ atomic ratio can be measured by TIMS with a measurement error of 0.6% SdErr for sample loads of 20pg.
- The IsoProbe MC-ICPMS allows the determination of the $^{240}Pu/^{239}Pu$ down to 0.1pg and reproducibility ranges from 1.3% to 0.12% (2sd) for sample sizes between 0.1pg and 100pg.
- The measured $^{242}Pu/^{239}Pu$ needs a correction if the ratio was determined from the third measurement cycle.
- $^{238}U/^{235}U$ has been determined with errors of <0.2 % (2 s.d.) using Faraday collectors for both, mass 238 and mass 235 for concentrations between 15 and 40 ppb. Static Faraday/Daly measurement of the $^{238}U/^{235}U$ for concentrations between 5 and 15 ppb yields an error of <0.8 % (2sd).

CHAPTER 3

3. Application I: The record of uranium and plutonium isotopic ratios in weapons fallout

3.1. Introduction

After the big US tests in 1952 and 1954 the potential problem of contamination of the entire world population by radioactive fallout from nuclear tests was realised. The DASA (Defense Atomic Support Agency) concluded in 1955 that the largest uncertainty in the prediction of the distribution and concentration of world-wide fallout debris on the surface of the earth was the quantity of fission products in the stratospheric reservoir and the rate and mode of their transfer. For this reason in 1956 a research program to define and delineate the stratospheric reservoir of fission debris was initiated. This program became known as the High Altitude Sampling Program, or Project HASP. More than 20,000 airfilters were collected during the period between 1957-1983 and analysed for approximately 40 different radionuclides. All of the available data characterising each filter are included in the database "RANDAB" (EML, 1997). Some of these filters were not only analysed for plutonium concentration, but also for its isotopic composition, partly to gain knowledge about the nuclear tests by other countries. This knowledge was of high importance during the 1950s and 1960s, but the interest decreased in the 1970s when France and China were the only countries conducting atmospheric nuclear tests. This can explain why plutonium isotopic ratio data from these filters are rare for the 1970s.

Besides these filters some natural archives, like ice cores, corals or lake sediments can be used to study the chronology of the $^{240}Pu/^{239}Pu$ of weapons fallout. For the 1950s and 1960s a good chronology exists from Arctic and Antarctic ice cores (Koide *et al*, 1985). However, the more-commonly used technique of Thermal Ionisation Mass Spectrometry (TIMS) needs large sample sizes to investigate the $^{240}Pu/^{239}Pu$, which explains why data for natural archives are rare. For the interpretation of a time-resolved measurement of plutonium pollution (e.g. in sediment cores) a good knowledge of the chronology of the isotopic ratios in the weapons fallout is essential. The variation of the plutonium isotopic ratio with time depends on differences in weapon design and parameters of the tests. The goal of this Chapter is to compile existing data and to add new data to improve the chronology of $^{240}Pu/^{239}Pu$ in weapons fallout. For the following Chapters also the other Pu isotopic ratios and the $^{239,240}Pu/^{137}Cs$ are of interest. Therefore these ratios are also reviewed. In addition a

chronology of $^{238}U/^{235}U$ in grass is presented. Uranium isotope ratio data for atmospheric fallout from weapon testing have not been previously reported. This is presumably because it is easily masked by the presence of any natural uranium.

3.2. Transport of radionuclides from tests with stratospheric input to the UK

In areas without a local source of plutonium contamination, the main input of any plutonium is global fallout from nuclear tests. The term "global fallout" is used for material that was injected into the stratosphere and then distributed globally. Whether a test has stratospheric input or not is determined by the explosive yield, the height at which the detonation occurred and the meteorological conditions existing at the time of detonation. Figure 3.1 shows the height of the centre of the fireball *versus* explosive yield. It can be seen that the centre of the fireball penetrates the tropopause in Polar Regions for yields greater than 400kt and in equatorial regions for yields of 1-1.5 Mt.

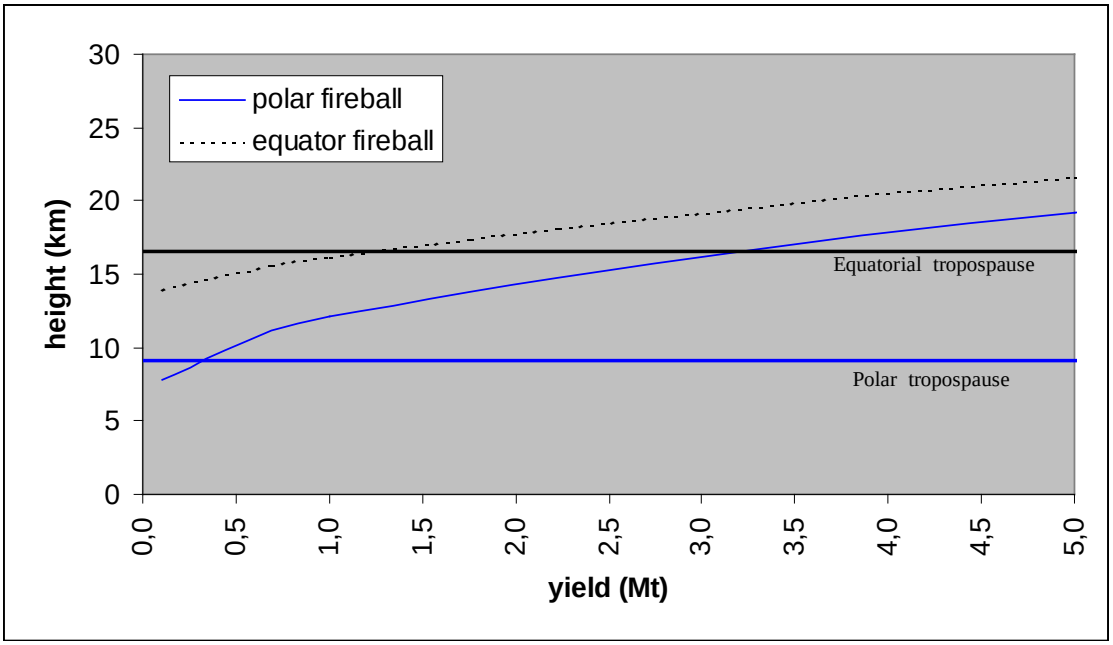

Figure 3.1 Height of the centre of the fireball *versus* explosive yield (from Bauer and Gilmore, 1975)

During any particular year 60-80% of the stratospheric mass is exchanged with the troposphere, which represents a residence time in the stratosphere of 15-18 month (Roedel, 1994). This residence time can be different if aerosols of interest are not distributed like the total mass of the stratosphere. For example, the plutonium of the SNAP-9A satellite,

introduced at the top of the stratosphere would have a longer residence time than would plutonium from weapons testing which was mainly introduced to the lower parts. Besides the location of injected particles, other physical properties such as density also influence the residence time. A time lag of one year between test and deposition was observed for ^{239,240}Pu in ice cores (Koide *et al*, 1979). The same time is observed by comparing the plutonium ratio data from the stratosphere with the ice cores. The mean residence time of plutonium in the troposphere is 71 days (Holloway and Hayes, 1982). Since the processes responsible for stratospheric-tropospheric exchange depend on the time of the year (details in Appendix A.7), the occurrence of stratospheric fallout products at the earth surface is seasonally modulated. The maximum stratospheric-tropospheric exchange occurs in spring (March-June). The amount of debris, which enters the troposphere during July-October, is insignificant (Roedel, 1994). The stratospheric-tropospheric transfer behaviour is illustrated by ^{137}Cs-data from Moosonee, Ontario, Canada (51° 16' N, 80° 30' W) in Figure 3.2. No tropospheric fallout was expected for this location and its latitude is similar to that of the UK. Therefore a similar behaviour to stratospheric fallout in Britain can be assumed. Large nuclear tests were conducted prior to 1958, 1958, 1961 and 1962 with the highest yield occuring in 1962. Apart from two small Chinese tests (yield<20kt), no tests were performed in 1963, 1964 and 1965. Therefore the fallout during these years originates mainly from the stratospheric reservoir. For this reason these years are chosen to demonstrate the seasonal modulation of stratospheric fallout using data from the EML “Surface Air Sampling” – database (EML, 2000). It can clearly be seen in Figure 3.2 that the greatest annual Cs-137 concentration at the earths surface occurs between March and June. This period is known as the "spring-peak".

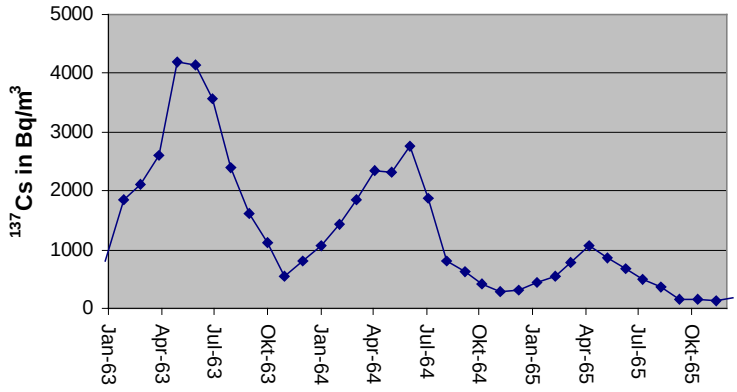

Figure 3.2 Cs-137 in surface air at Moosonee, Ontario, Canada in the years 1958-1966. Decay corrected to the time of sampling.

3.3. Transport of radionuclides from the Nevada test site to the UK

The ground-based small yield tests at the Nevada test site had no or little stratospheric input. At the time of the test the cloud rose to a certain height and then travelled eastwards with the prevailing westerly winds. During travel the cloud diffused laterally and vertically. Barriers of stable air prevented lateral diffusion south of 25-30°N, depending on the time of the year. The tropopause prevents vertical diffusion above 12km (Stewart *et al*, 1957, see also Appendix A.7). The cloud reached the UK for the first time about 5 days after the explosion and then every four to seven weeks as it circulated around the world. On its first circuit over the UK the cloud of the 1952 tests had not diffused to ground level and no increase of radionuclides in ground level air could be seen. However, the highest deposition occurred if rainfall intercepted the cloud on its first passage over the UK. The lateral diffusion was complete after one circuit (Stewart *et al*, 1957).

3.4. Existing Stratospheric and Ice core data

As described at the beginning of this Chapter, from 1957 to 1983 stratospheric measurements of radionuclides have been carried out by the U.S. Department of Energy Environmental Measurements Laboratory (EML). All plutonium ratios of interest (activity ratios $^{238}Pu/^{239,240}Pu$ and $^{241}Pu/^{239,240}Pu$, atom ratios $^{240}Pu/^{239}Pu$ and $^{242}Pu/^{239}Pu$) are extracted from their database "RANDAB" (EML, 1997). Reported ratios that were obviously incorrect, e.g. a $^{240}Pu/^{239}Pu$ of 100, were not taken into account. All other measurements of a particular year were averaged and the standard deviation was calculated. The standard deviations are plotted as error bars. (Figure 3.3a-3.3d) Besides these stratospheric measurements the ratios $^{238}Pu/^{239,240}Pu$, $^{241}Pu/^{239,240}Pu$ and $^{240}Pu/^{239}Pu$ have been investigated at the earth's surface using ice cores from Greenland and the Antarctic (Koide *et al*, 1981, Koide *et al*, 1985). Due to spiking with ^{242}Pu, no $^{242}Pu/^{239}Pu$ data have been published for these ice cores.

As discussed in Chapter 1 (Figure 1.1) nuclear testing in the 1950s was dominated by the US. Based on the ice cores the early 1950s fallout in the Antarctic had a $^{240}Pu/^{239}Pu$ greater than 0.3 and a $^{241}Pu/^{239,240}Pu$ of 25-30. The $^{241}Pu/^{239,240}Pu$ drops to about 10 in the late 1950s. The $^{240}Pu/^{239}Pu$ drops to 0.21-0.26 in the mid 1950s and to 0.16 in the late 1950s. The Arctic cores show the same trend, but the drop of the $^{240}Pu/^{239}Pu$ in the late 1950s is only to about 0.2. This might be due to the influence of the smaller but very close USSR tests. In the early

1960s the $^{240}Pu/^{239}Pu$ was between 0.17 and 0.19 and the $^{241}Pu/^{239,240}Pu$ around 10. No remarkable difference between northern and southern hemisphere exists and stratospheric ratios correspond well with the ice core data. In 1963 a maximum occurs in $^{240}Pu/^{239}Pu$, $^{241}Pu/^{239,240}Pu$ and $^{242}Pu/^{240}Pu$ in the Northern Stratosphere data and this maximum can also be seen in the $^{240}Pu/^{239}Pu$ in Arctic ice from 1964. In the Southern Hemisphere this maximum appears one year later. From 1965 to 1967 Northern and Southern Stratospheric ratios are similar. The $^{240}Pu/^{239}Pu$ is around 0.18, the $^{241}Pu/^{239,240}Pu$ around 12 and the $^{242}Pu/^{240}Pu$ around 0.004. In 1968 the three ratios show a significant drop in the Southern Stratosphere, but almost no change for the Northern Stratosphere. This can be explained by the French tests on Mururoa Island. The Chinese tests at Lop Nor hold the ratios almost constant in the north. No data are available between 1971 and 1974. The low ratios in 1975 can probably be attributed to the Chinese test in September 1974 (N.B. the last French atmospheric tests were in 1974). The Chinese atmospheric testing stopped in 1980.

The main feature of the $^{238}Pu/^{239,240}Pu$ is not produced by weapons testing, but by the burn-up of a ^{238}Pu powered satellite over the Indian Ocean in April 1964, the impact of which was three times greater in the Southern Stratosphere. The highest $^{238}Pu/^{239,240}Pu$ is observed in 1967 and 1968 for sampling heights between 12km and 20km. A longer stratospheric residence time of ^{238}Pu from the SNAP-9A burn-up in comparison to the weapon test $^{239,240}Pu$ was also observed in Antarctic ice cores (Koide *et.al*., 1979). This delay of the appearance of the SNAP-9A plutonium can be explained by the fact that the satellite burn-up occurred at 50 km, whereas the plutonium from the tests was introduced at the bottom of the stratosphere.

The $^{239,240}Pu/^{137}Cs$ in the Northern Hemisphere is about 0.01 for the period between 1961 and 1966 (Figure 3.5) and slightly higher from 1968 until 1983. These values agree well with ice core data (Koide *et al*, 1979). In addition ice cores data reveal that the ratio was between 0.01 and 0.02 from 1956 until 1962, but higher ratios of up to 0.05 were measured for the pre-1956 period (Koide *et al*, 1979). In the Southern Stratosphere the ratio changes more dramatically with values between 0.007 and 0.023.

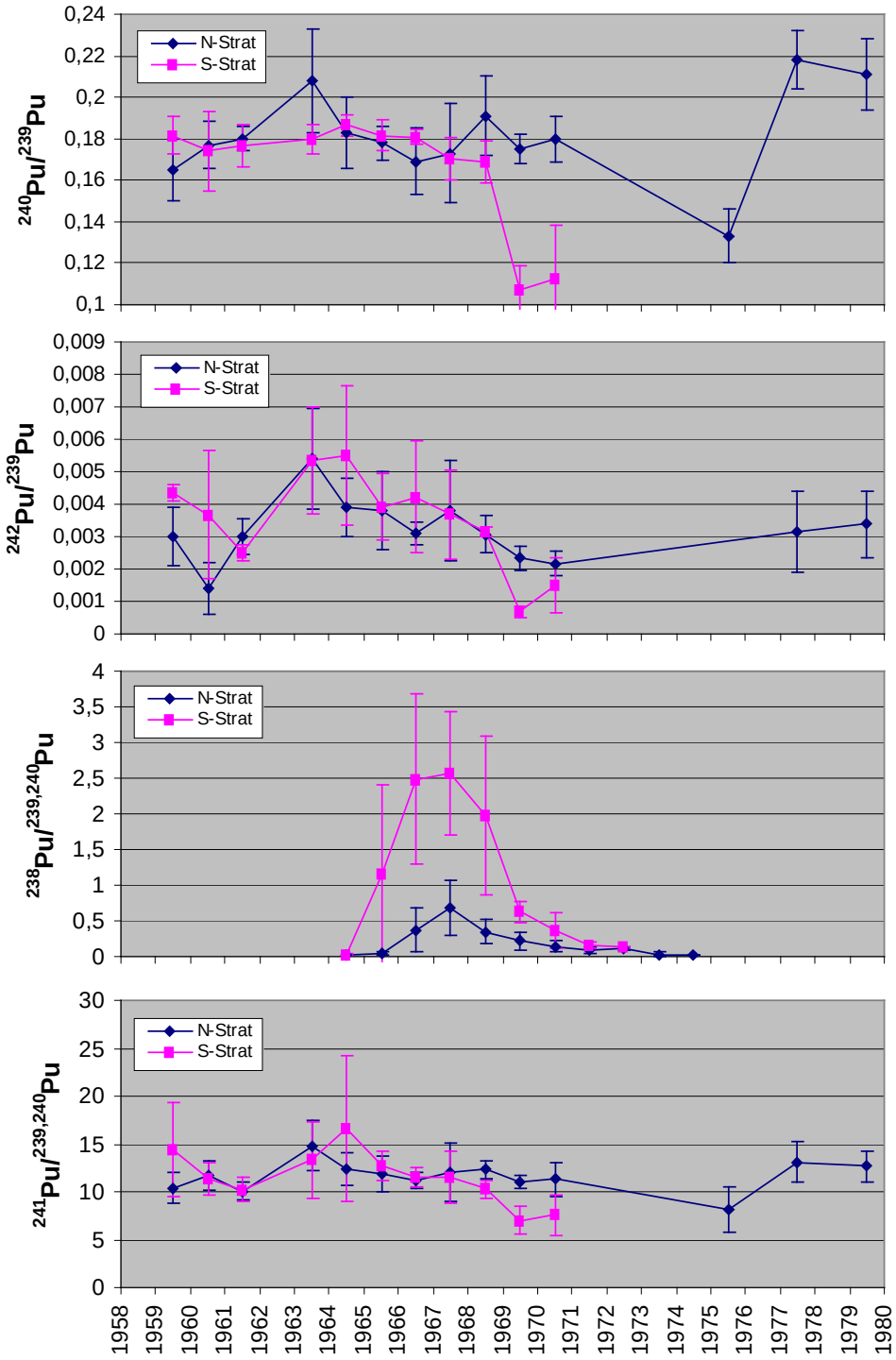

Figure 3.3 (a-d) Plutonium isotopic ratios in the stratosphere based on measurements by EML (1997). All measurements of a particular year are averaged and the standard deviations are shown as error bars. The blue line represents the Northern Stratosphere and the red line the Southern Stratosphere. Data are decay corrected to the time of sampling.

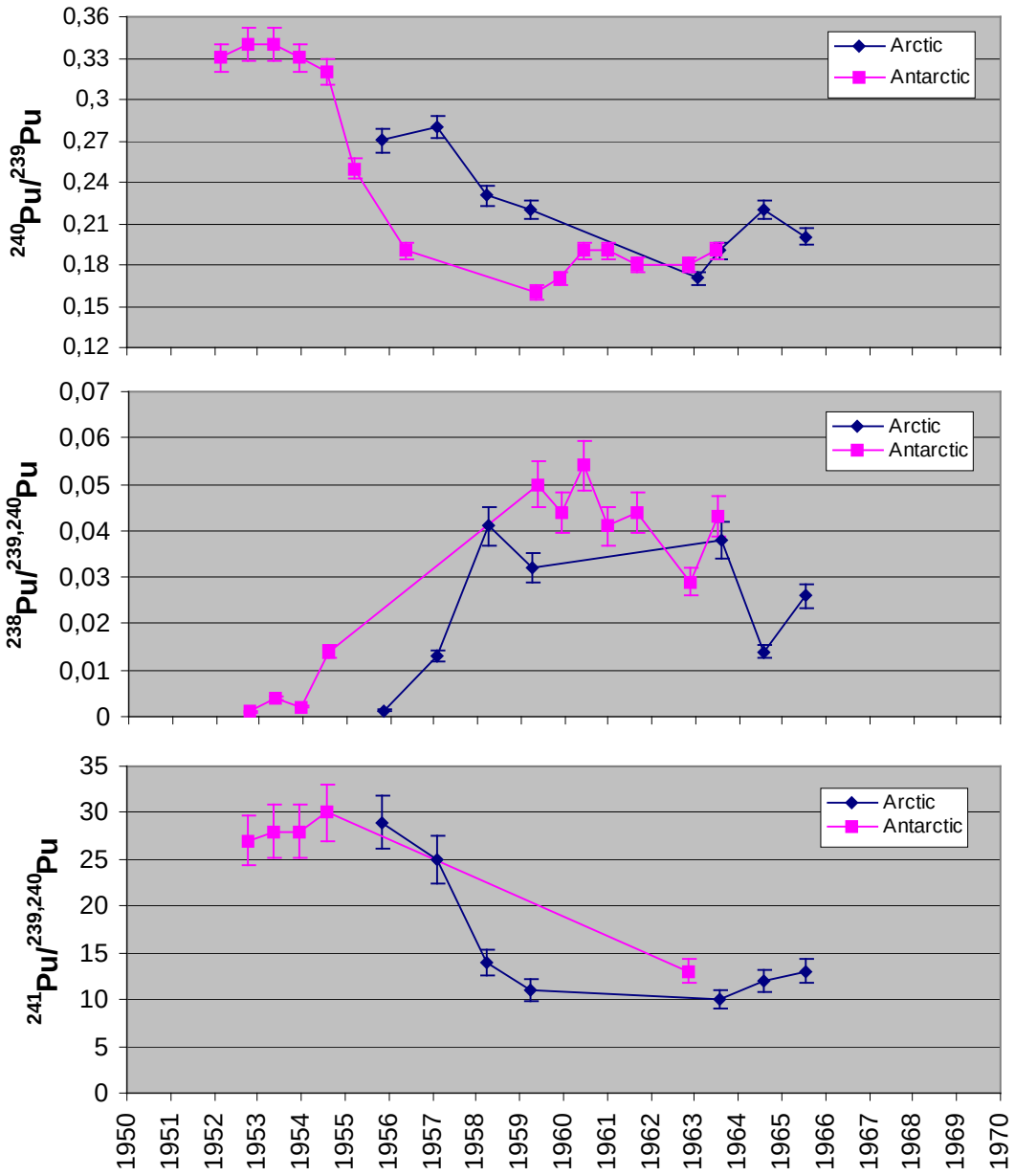

Figure 3.4 (a-c) Plutonium isotopic ratios in ice cores (Koide *et al*, 1981, 1985). The blue line shows data from South Dome, Greenland (63°31.6'N, 44°34.5'W) and the red line from J-9 Ross Ice Shelf, Antarctica (82°22'S, 168°40'W). Data are decay corrected to the time of deposition, based on a ^{210}Pb chronology.

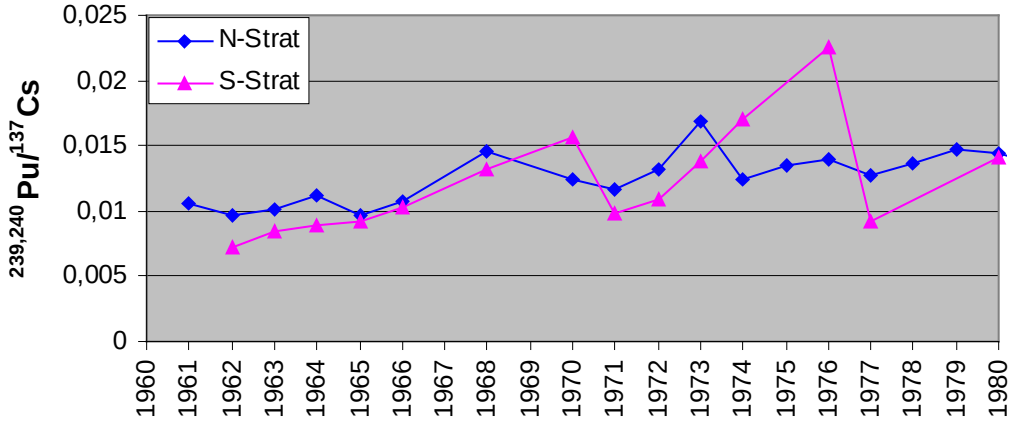

Figure 3.5 ^{239,240}**Pu/**^{137}**Cs activity ratio in the stratosphere**. Data are extracted from the database "RANDAB" (EML, 1997) and are decay corrected to the time of sampling, based on a ^{210}Pb chronology.

3.5. Grass samples from the IACR Rothamsted archive and an ice core from Dome du Gouter, Mont Blanc, French Alps

The IACR-Rothamsted (Harpenden, Hertfordshire) archive is a unique collection, with continuity from 1843 until now, of some 200,000 samples of crops and soils taken from agricultural field experiments. Permission was granted to take 50 grams of dried grass from the so-called Park Grass experiment to investigate the variation of ^{240}Pu/^{239}Pu as seen at ground level in the UK. The ice core from Dome du Gouter (4300m), Mont Blanc, French Alps was provided by the "Laboratoire de Glaciologie et Geophysique de l'Evironment" at the "Centre National de la Recherche Scientifique" (CNRS) in Grenoble. The core was collected in 1994 and has a length (depth) of 116 m. The core (core 2) has been studied previously by Vincent *et al* (1994) which included a model for the relation between snow/ice age and depth and ^{137}Cs variations with depth.

The grass and the ice core samples examined in this study represent two different locations within the latitude band of the Westerlies in the Northern Hemisphere (northern temperate latitudes). In the absence of local sources the measured variations in plutonium isotopic composition are expected to be representative for the northern temperate latitudes. The

measured concentrations will be influenced by differences in meteorological conditions and the $^{238}U/^{235}U$ by dilution with natural uranium. A manuscript about the record of uranium and plutonium isotopes obtained using the grass and ice data and its implications for nuclear fallout at northern temperate latitudes has been written (Appendix 10).

3.5.1 Deposition onto the grass and presentation of the data

The ability to take up material from rain or air depends on grass type, state of growing and meteorological conditions. For example Clark and Smith (1988) showed that the Cs area-concentration (deposition density) of Chernobyl ^{137}Cs by grass of wet deposited material varied more than a factor 2. Also the meteorological conditions between deposition and sampling might influence the concentration, e.g. strong wind or rain can blow or wash off deposited material. The aim is to present the data in a way that the number of dependent parameters is as small as possible. By comparison with deposition data from Milford Haven (AEA, 1957-1991) the following section shows why the presentation of concentrations (Bq/kg) in the Rothamsted grass is used instead of the commonly used deposition per unit area (Bq/m^2). An examination of Figure 3.6 (dry weight of the grass harvested per m^2), Figure 3.7 (^{137}Cs in Bq/kg) and Figure 3.8 (^{137}Cs Bq/harvested area) shows that the Milford Haven deposition data fit better to the Cs concentration in Figure 3.7 than to the Cs area-concentration in Figure 3.8. The better fit in Figure 3.7 is mainly due to the years 1957, 1959 and 1965. In 1957 and 1959 the area-concentration in the grass is too low and in 1965 too high compared with the Milford Haven data. Looking at the dry matter yield shows that 1957 and 1959 are years of low dry matter yield and 1965 the year of the highest yield (average yield ~0.13). Hence the deposition density and the harvest yield are positively correlated. Thus, in the years of higher dry matter yield the grass more effectively intercepts ^{137}Cs (and other) fallout before it can pass through the grass to the ground. From the comparison with the Milford Haven deposition data it looks like the presentation in Cs-concentrations (Bq/kg) is more independent of the state of growing and is therefore used.

Estimation of the interception factor for the grass

The yield data can be used to estimate the fraction of total yearly deposited activity that is taken up by the first cut of the Rothamsted grass.

The following definitions are used for the calculation:

C^g =concentration in the grass in Bq/kg

D^{tot}= total activity deposited per area in Bq/m^2

D^g= activity in grass per harvested area in Bq/m^2

f= interception factor = fraction of total yearly deposited activity found in the grass

Y= dry weight of harvested grass per area in kg/m^2

From the definitions above it follows that $D^g = f * D^{tot}$ and $C^g = \frac{f}{Y} * D^{tot}$. It is assumed that the Milford Haven data present the annual deposited activity D^{tot}. As shown in Figure 3.7 the concentration C^g agrees well with total deposited activity D^{tot}, if D^{tot} is divided by 4, hence $\frac{f}{Y} \approx \frac{1}{4}$. From the yield data follows 0.01<f<0.07, which means that between 1% and 7% of the annual deposited activity is found in the grass.

Loss of deposited activity from the grass with time

The measured amount of Chernobyl deposition found in the grass can be used to estimate how long the Cs is able to stay on the grass without being washed off. The Chernobyl plume reached the United Kingdom on 2 May 1986. At Chilton the maximum concentration in the air was detected on the afternoon of 2 May. The concentration declined by a factor 10 overnight and by a further factor of ten during the day of the 3 May (Fry *et al*, 1986). At Rothamsted 0.3 mm rain was detected on 2nd May, no rain on 3rd May and 0.2 mm on 4th May (IACR Rothamsted, pers. com.). County averages for predominantly dry areas (less than 1mm rainfall) during the passage of the plume show initial ^{137}Cs deposition densities on grass of about 20-30 Bq/m^2 during the 3-6 May 1986 (Clark and Smith, 1988, Fry *et al*, 1986). The ^{137}Cs deposition density of the Rothamsted grass on 12.June 1986 was 3.6 Bq/m^2, hence less than 20% of the initial deposited Cs is present in the grass after about 40 days.

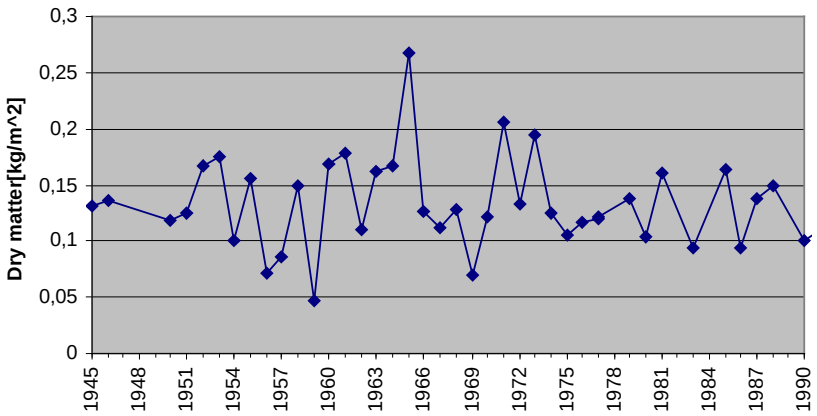

Figure 3.6 Dry matter yield of Rothamsted grass

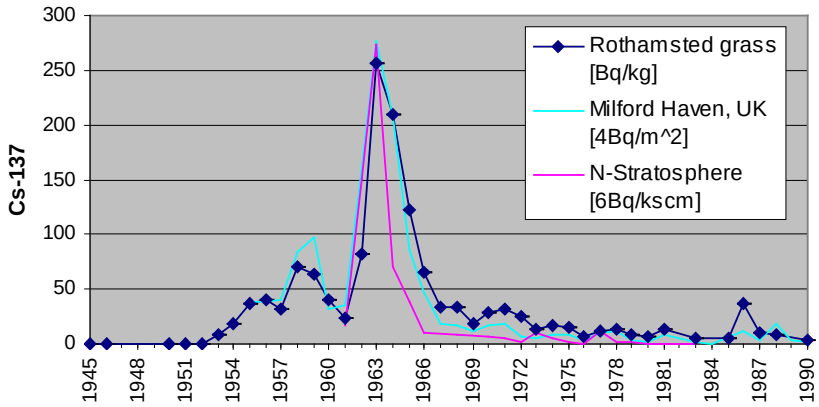

Figure 3.7 Cs-137 concentration in Bq/kg [dry grass]

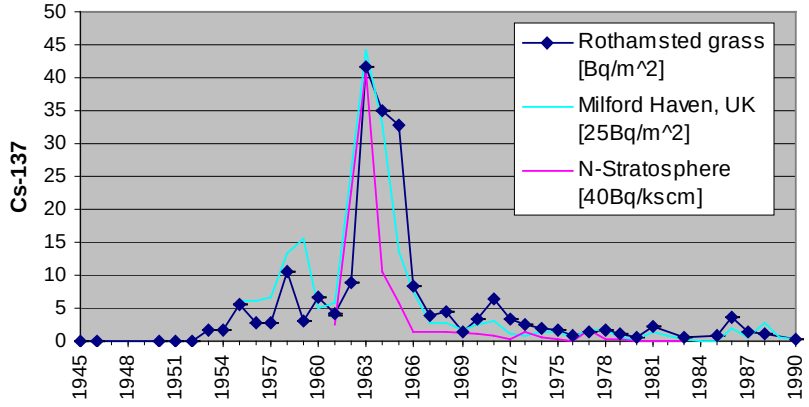

Figure 3.8 Cs-137 area-concentration (deposition density) [Cs activity / harvested area]

3.5.2 ^{137}Cs, plutonium (alpha), ^{240}Pu/^{239}Pu and ^{238}U/^{235}U in Rothamsted grass samples and the Mont Blanc ice core

The concentrations in the ice and the grass agree closely with records of device-testing (Lawson, 1998, Carter and Moghissi, 1977) and radiochemical monitoring of fallout (Koide *et al*, 1985, EML, 1997, AEA, 1957-1991) that took place at the time (Figure 3.9). The main stratospheric events that dominate the ratios during 1952-1962 are the U.S. and UK tests on Bikini, Eniwetok and Christmas Island in 1954, 1956 and 1958 and 1962 and Soviet tests in the Arctic in 1958, 1961 and 1962. In November 1958 the Partial Test Ban Treaty inhibited nuclear testing until the resumption of atmospheric testing first by the U.S.S.R. in September 1961 and then by the U.S. in April 1962. The U.S. and the U.S.S.R. finally ceased atmospheric testing in October 1962 and December 1962 following the ratification of the International Test Ban Treaty. Using a linear age-depth relation for the Mont Blanc ice core the ^{240}Pu/^{239}Pu profiles for the ice core and the Rothamsted grass are almost identical for the period 1955-1970. This good agreement indicates that the ^{240}Pu/^{239}Pu record is generally representative of northern temperate latitudes. This conclusion may not hold for areas influenced by relatively significant tropospheric fallout derived from a particular testing site. One of these is the Nevada Desert Test site NTS where eighty-four kiloton-range atmospheric nuclear tests were carried out between 1951-62 (Lawson, 1998, Carter and Moghissi, 1977) (Table 3.1). A 1953 air sampling study of NTS-derived radioactive fallout showed northeasterly dispersal of the test plume toward W. Europe (Eisenbud and Gesell, 1997). Hitherto the only record of this fallout in the UK was from measurements of beta/gamma activity in air carried out by UKAEA (Stewart *et al*, 1957). The 1952 Rothamsted grass (June-July harvest) shows a ^{240}Pu/^{239}Pu of 0.06. This grass was harvested before the first ever thermonuclear test at Eniwetok Atoll (10.4 Mt 'Mike' shot; 31 October 1952) which had a ^{240}Pu/^{239}Pu greater than 0.30, as inferred from ice cores (Koide *et al*, 1985). Similarly there were no USSR-tests in 1952 and therefore the 1952 Rothamsted ratio can only be due to fallout from one or more of the eight tests at the NTS between April-June 1952. The time-lag between a Nevada test and subsequent deposition in the UK could have been as short as 5 days if suitable weather conditions existed (Stewart *et al*, 1957). The 1952 second harvest (Sep-Nov) sample shows no measurable plutonium, which is consistent with the records of no summer testing at the NTS. It is notable that low ratios have been reported in North Atlantic, Gulf of Mexico and Mississippi Delta sediments (Buessler and Sholkovitz, 1987, Scott *et al.*, 1983, Noshkin and Gatrousis, 1974, Oktay *et al*, 2000)

and attributed to NTS testing but they did not have the good time control of the grass samples. Additional evidence for tropospheric fallout is also seen for later samples. For example, $^{240}Pu/^{239}Pu$ in the 1953 grass is 0.154 for the first cut and 0.135 for the second cut. Since fallout from the 1952 "Mike"-Shot had a $^{240}Pu/^{239}Pu$ greater than 0.30 the lower 1953 ratios must represent mixtures of tropospheric fallout and stratospheric fallout. There were no NTS tests carried out between the two 1953 grass harvests and any stratospheric fallout $^{240}Pu/^{239}Pu$ would have remained close to 0.30 so there must have been another tropospheric input. This could be from the first Soviet thermonuclear test (Kazakhstan site) that occurred in August 1953 (440kt) and this could have contributed low $^{240}Pu/^{239}Pu$ material to the second 1953 harvest.

Chinese and French atmospheric thermonuclear tests were carried out between 1964-1980 and 1966-1974 respectively (Lawson, 1998) and can also be related to the ratios seen in the grass. The small increase in the ratio during the late 1970s seen in N-stratosphere and Rothamsted data must be due to Chinese tests. There are no ice core $^{240}Pu/^{239}Pu$ data for this period although stratospheric aerosol measurements exist for 1975, 1977 and 1979. The Rothamsted isotope ratio data provide a useful alternative for this hiatus in the record.

Uranium isotope ratio data for atmospheric fallout from weapons testing have not been previously reported, perhaps because the small amounts of isotopically-altered uranium contamination are masked by the presence of natural uranium. The variation of the $^{238}U/^{235}U$ in the Rothamsted grass show three distinct negative inflections (enriched U ratio) at 1952, 1958 and 1963 and two small but significant positive inflections (depleted U ratio) at 1977/78 and 1983. The two negative inflections in the 1958 and 1963 grass data are also present in the ice record but no positive inflections are seen later in the ice core. The 1952 deviation in the Rothamsted grass, where Pu was also first detected, is likely to have been caused by tropospheric fallout from NTS. The 1953 deviation is likely to result from a mixture of tropospheric and stratospheric fallout, as also inferred from the Pu data, while the 1954 data can be attributed mostly to stratospheric fallout. The strongest deviations in $^{238}U/^{235}U$ in the grass record occur in 1958 and 1963 which coincide with the years of greatest atmospheric fallout from weapons testing by the U.S. and the U.S.S.R.. The measured ratios in both cases are about 0.55% lower than the natural ratio but the magnitude of the deviations for 1958 and 1963 are greater in the Mont Blanc ice. Enriched uranium isotopic ratios in the ice persist for the whole period of high yield atmospheric testing. It is likely that

the reason for the differences between ice and grass is a higher content of natural uranium in the grass compared with the ice. Enriched uranium was used as fissionable material in nuclear weapons. Enriched uranium and depleted uranium are both materials that could be used for the tamper in thermonuclear weapons. The excess ^{235}U found in fallout from nuclear testing could be unfissioned ^{235}U that was initially present in the weapon or origins from a nuclear reaction of some material present in the weapon, e.g $^{238}U(n,4n)^{235}U$. The possibility that the enrichment is due to alpha decay of ^{239}Pu can be excluded. Assuming a chemical recovery of 100%, the layers showing the strongest $^{238}U/^{235}U$ deviation contain about 1ng ^{238}U. From the measured plutonium concentrations it follows that the ^{235}U produced from the alpha decay of ^{239}Pu would lower the $^{238}U/^{235}U$ from 138.88 to 138.84 which is not sufficient to be detected. The depleted $^{238}U/\ ^{235}U$ in the grass in 1977, 1978 and 1983 is probably due to a local, but presently unidentified source, since no evidence of depleted ratios can be seen in the ice core. A possible though entirely speculative source for these very small perturbations could be from industrial uses of depleted uranium and/or the testing or fabrication of uranium-based weaponry (Barbante *et al*, 2001).

	Stratos-pheric input	Potential tropospheric input		Jun-Jul Rothamsted harvest			Sep-Nov Rothamsted harvest		
Year	Global fallout** $^{240}Pu/^{239}Pu$	Kazakhstan Tests USSR (yield)	Nevada Desert Tests USA (yield)	Date of harvest	$^{239,240}Pu$ Bq/kg	$^{240}Pu/^{239}Pu$	Date of harvest	$^{239,240}Pu$ Bq/kg	$^{240}Pu/^{239}Pu$
1945	-		16Jul (19kt)	n.r.+	-	-	n.r.+	-	-
1951	-	24Sep (38kt)	-	21 Jun	-	-	2 Oct	-	-
1952	-	-	1Apr-5Jun (104kt)	19 Jun	0.05	0.060	22 Sep	-	-
1953	0.33-0.34	12Aug-10Sep (440kt)	17Mar-4Jun (253kt)	21 Jul	0.04	0.154	19 Nov	0.08	0.135
1955	0.25-0.27	29Jul-5Aug (15kt)	18Feb-15May (163kt)	28 Jun	0.26	0.273	15 Sep	0.50	0.295
1957	0.19-0.22	8Mar-16Apr (1142kt) 22Aug-13Sep (526kt)	28May-7Oct (340kt)	18 Jun	0.19	0.165	24 Sep	0.44	0.113

* Only for the years where samples from both cuts were taken
** based on Arctic and Antarctic ice core measurements (Koide *et al*, 1985)
n.r. -· not recorded

Table 3.1 Nuclear test data and $^{240}Pu/^{239}Pu$ for Rothamsted grass samples (1945-1957)*

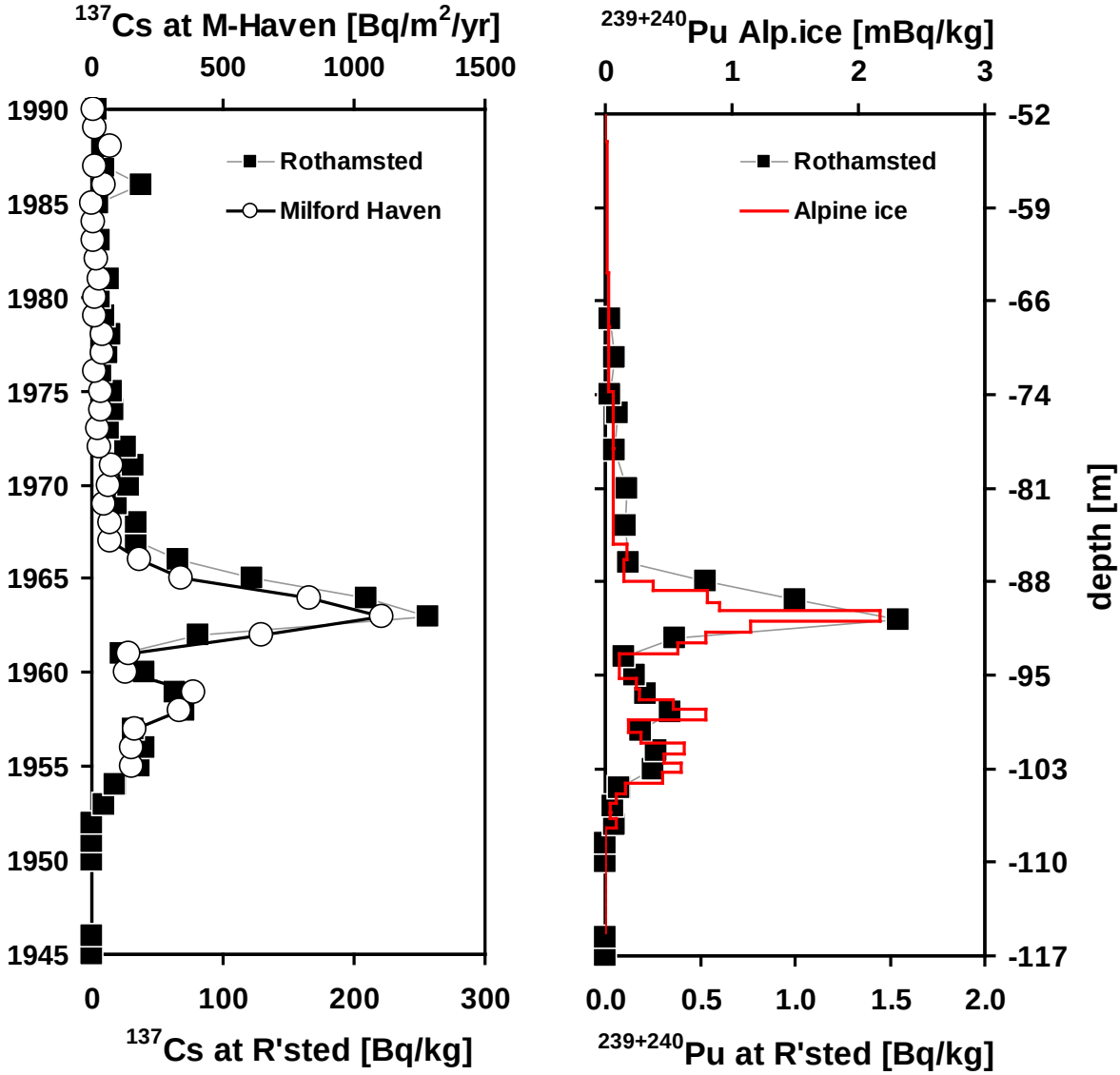

Figure 3.9 (a) ^{137}Cs concentration in the Rothamsted grass (Bq/kg) and deposition flux at Milford Haven (Bq/m^2/yr) from AEA monitoring from 1957-1991 (AEA, 1957-1991). (b) ^{239,240}Pu concentration in the Rothamsted grass and in Alpine ice.

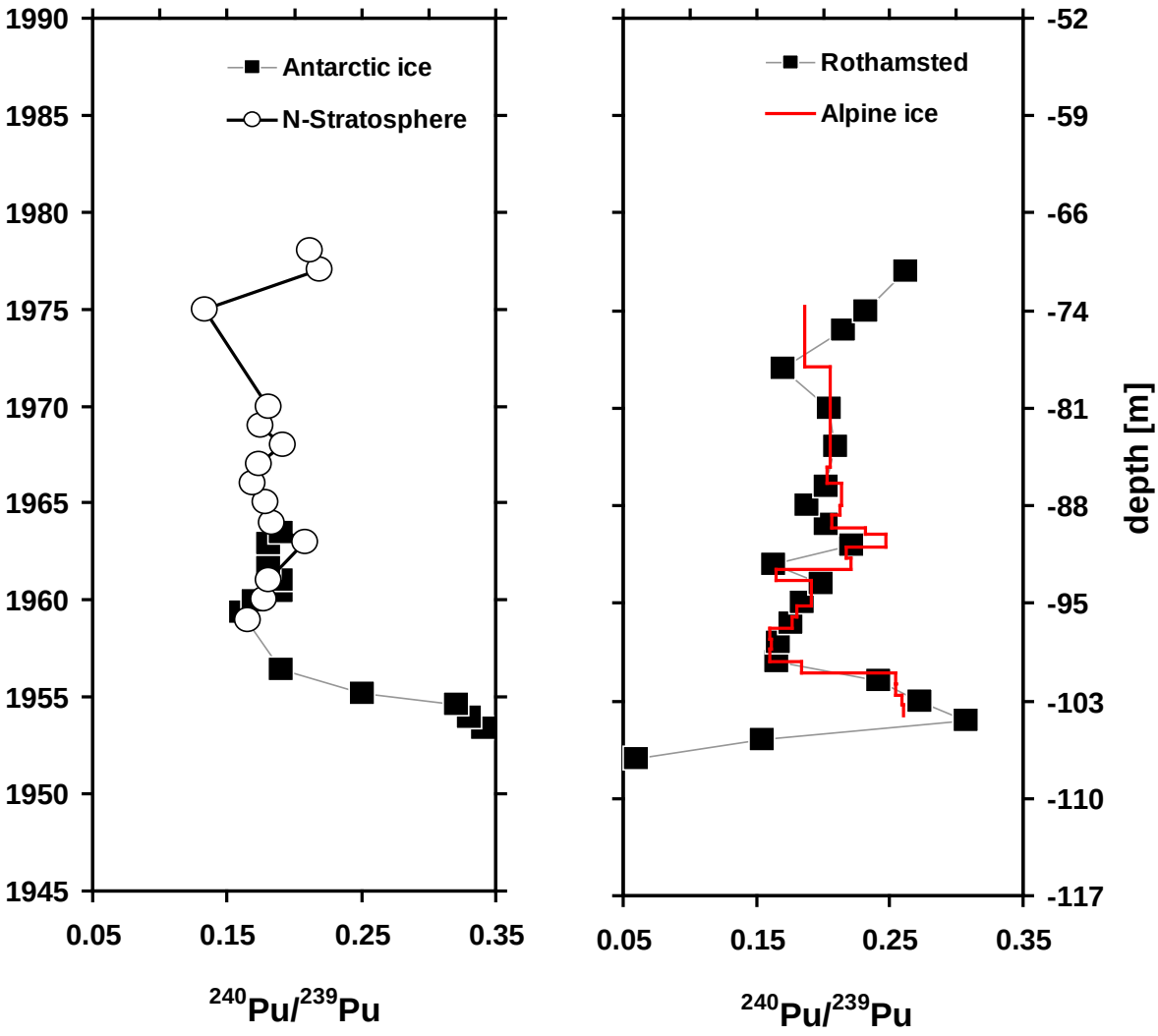

Figure 3.10 (a) $^{240}Pu/^{239}Pu$ atom ratio in an ice core from the J-9 Ross Ice Shelf, Antarctica (Koide *et al*, 1985) and in the northern Stratosphere (EML, 1997). (b) $^{240}Pu/^{239}Pu$ atom ratio in Rothamsted grass and Alpine ice.

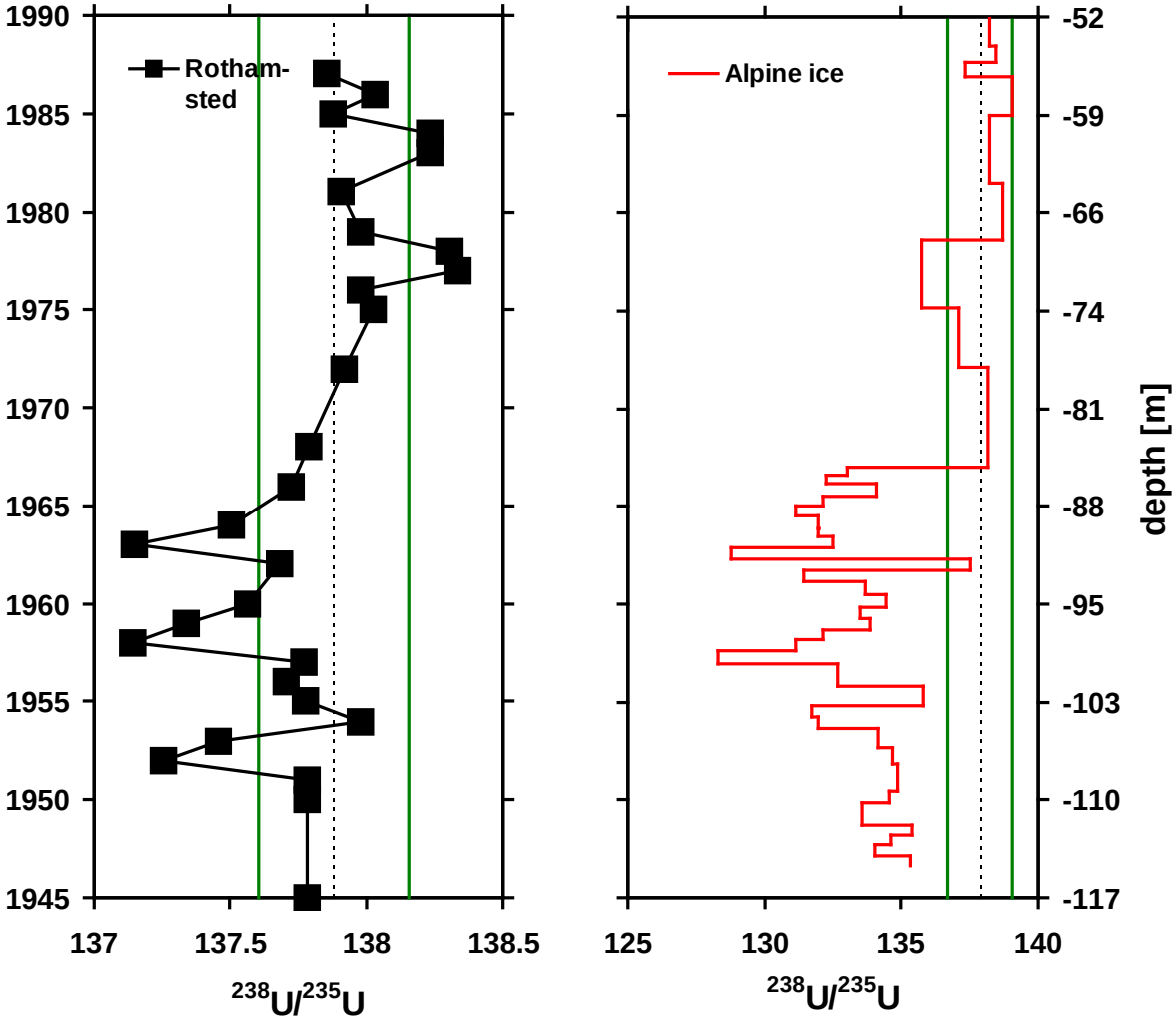

Figure 3.11 (a) $^{238}U/^{235}U$ in Rothamsted grass samples. The green lines represent the boundaries of the 3 s.d. analytical limit. (b) $^{238}U/^{235}U$ in Alpine ice from Dome du Gouter (4300m), Mont Blanc, France

3.6. Stratospheric air samples from Sweden

Three filters from stratospheric air sampling by the Swedish government (FDO Stockholm) were investigated. They were provided by officials at the Swedish Defense Agency. The exact sampling locations are unknown. The $^{240}Pu/^{239}Pu$ for the investigated filters are shown in the Table 3.1. The filter L212 has a $^{240}Pu/^{239}Pu$ of 0.10, which is significantly lower than the ratio measured in Arctic ice cores for this time. The filter was sampled during a Soviet testing period conducted between 10/10/1958 and 25/10/1958 in the Arctic (Carter and Moghissi, 1977). The ratio of 0.145 only 2.5 months later in sample L250 can be explained by mixing with other parts of the stratosphere. This suggests that the Soviet tests in October 1958 had an extremely low $^{240}Pu/^{239}Pu$. The filter L626 is in good agreement with ice- and US-stratospheric-data.

Sample	Sampling date	Sampling height	$^{240}Pu/^{239}Pu$	Expected 240Pu/239Pu Northern Stratosphere	Expected 240/239 ArcticIce core (Koide *et al*, 1985)
L212	17/10/1958	11.8 km	0.101	-	0.22
L250	01/01/1959	11.8 km	0.144	0.15-0.18	0.18
L626	18/09/1962	unknown	0.213	0.18-0.23	0.20

Table 3.2 $^{240}Pu/^{239}Pu$ results for stratospheric air filters from Sweden

3.7. Air filters from the PTB Braunschweig

The Physikalisch-Technische Bundesanstalt (PTB) is the German National Institute of Natural and Engineering Sciences. The PTB-Braunschweig has monitored radionuclides in ground-level air since 1963. Most of the older filters have been disposed of or have been used for destructive analysis. However, some filters from the 1970s still exist. As mentioned previously $^{240}Pu/^{239}Pu$ data from stratospheric air sampling exist for only a few years in the 1970s. Therefore the PTB filters are useful for verifying the $^{240}Pu/^{239}Pu$ for the years where measurements exist and for adding new data to some years where no measurements exist. Details about the filters and their $^{240}Pu/^{239}Pu$ are given in Table 3.3.

Year	Code	Sampling period	$^{240}Pu/^{239}Pu$	Relevant atmospheric tests
69				26Sep (China, 3000)
70				15May-6Aug (France, ~2500kt), 14Oct (China, 3000)
71				5Jun-22Sep (France, ~1500kt), 18Nov (China, 20)
72				1Jan (China, <20), 18Mar (China, 20-200)
73	PTB 73	May/Jun	0.165	26 Jun (China, 2000-3000)
74				16 Jun-15 Sep (France, ?), 17 June (China, 200-1000)
75	PTB 1	28 Apr – 2 Jun	0.156	21 Oct (China, low yield)
76	PTB 76	complete year	0,141	23 Jan (China, low yield), 26 Sep (China, 20-200kt), 17 Oct (China,?), 17 Nov (China, 4000kt)
77	PTB 4	14 Oct – 31 Oct	0.239	17 Sep (China, < 20 kT),
	PTB 5	31 Oct – 7 Dec	0.232	
78	PTB 78	May	0.226	24 Jan Cosmos 954 satellite burnup,
	PTB 7+8	Apr/Jun/ Jul/Aug	0.217	15 Mar (China, < 20 kT), 14 Dec (China, <20kt)
79	PTB 9+10	1Feb – 31 Aug	0.192	13 Sep 79 (China,?)
	PTB 11+12	15 Oct – 2 Jan 8 0	0.213	
80				16 Oct 80, (China, 200-1000kt)

Table 3.3 $^{240}Pu/^{239}Pu$ results for ground level air filters from Braunschweig (Germany)

To restate the main features of the profiles inferred from Stratospheric air sampling from 1963 until 1968 the $^{240}Pu/^{239}Pu$ lies between 0.17 and 0.19 for both the Southern and the Northern Stratosphere. In the Southern Stratosphere a drop occurs from 0.17 in 1968 to 0.11 in 1969 and 1970. In the Northern Stratosphere the $^{240}Pu/^{239}Pu$ ratios stay around 0.18 until 1970. In 1970 a gap in the stratospheric data occurred and the next measurements were in 1975 with a value of 0.133.

The measured PTB samples of filtered ground level air show the $^{240}Pu/^{239}Pu$ in 1973 to be 0.165. Assuming no local sources are present, the source of this ratio is stratospheric fallout. The lower value in comparison to the 1970 Northern Stratosphere measurement is either due to mixing with low ratio material from the Southern Stratosphere or, more likely, due to the input of the Chinese tests between 1970 and 1973. In 1975 the ground level air $^{240}Pu/^{239}Pu$ is 0.156 and 0.141 in 1976. This drop is in agreement with measurements in the Northern Stratosphere in 1975. In 1977 the $^{240}Pu/^{239}Pu$ in ground level air increases strongly to 0.23-0.24. This increase can also be seen in the stratosphere and can be attributed the Chinese testing in Oct/Nov1976. The measured $^{240}Pu/^{239}Pu$ in 1978 is only slightly lower than that in 1977, which can be explained by stratospheric mixing. In February-August 1979 the $^{240}Pu/^{239}Pu$ drops to 0.192 but increases again to 0.213 in Oct-Dec 1979. The drop could be explained by stratospheric mixing. However, the increase in the same year can only be explained by tropospheric fallout from the Chinese test in September 1979 or input from a local source.

3.8. Summary plot of data, suitable for a $^{240}Pu/^{239}Pu$ chronology

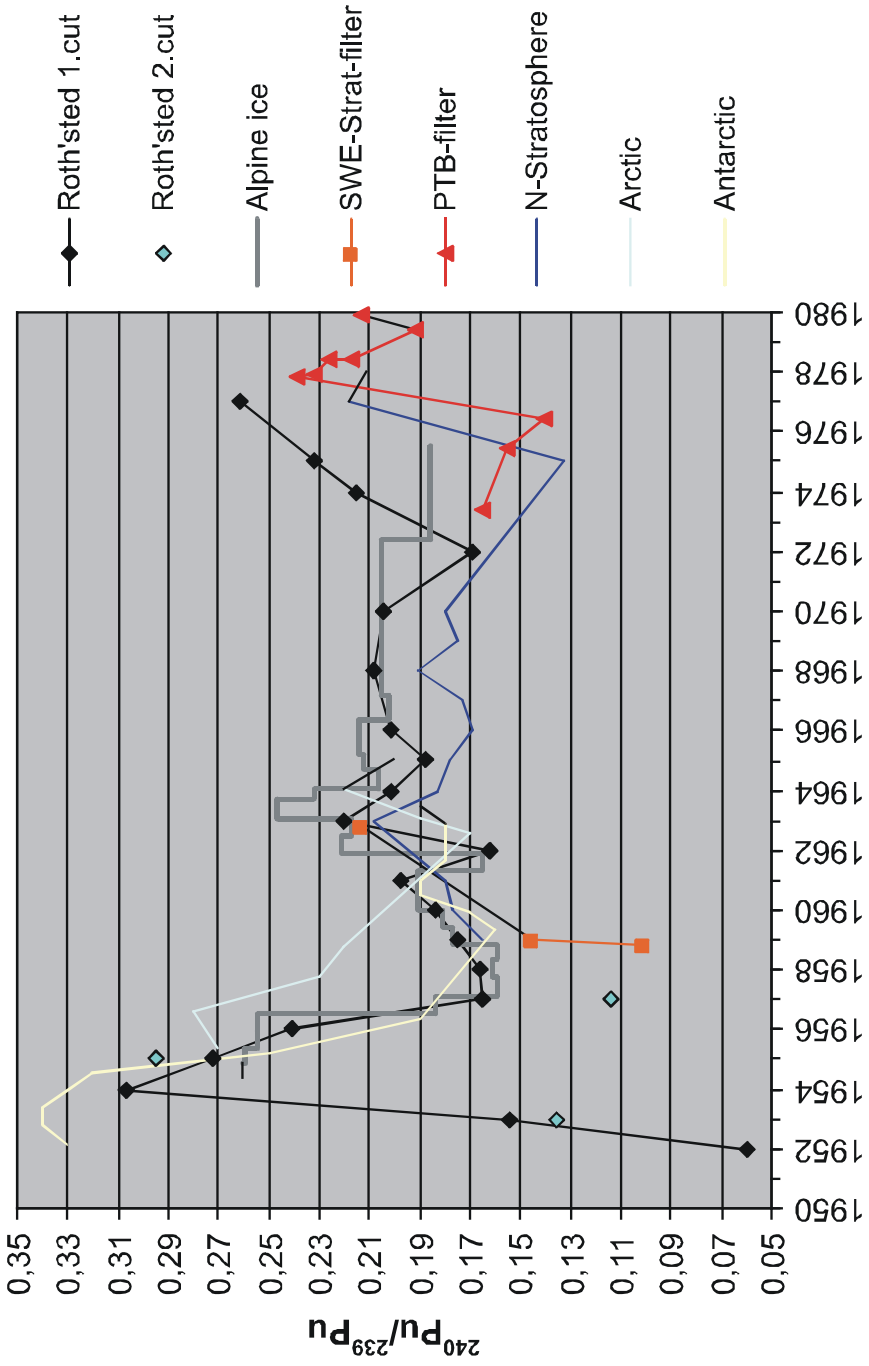

Figure 3.12 Summary plot of $^{240}Pu/^{239}Pu$ data. The plot shows a summary of all previously discussed data. The data for the Northern Stratosphere, the Arctic and the Antarctic are from EML, (1997) and Koide *et al*, (1985). The data for the Rothamsted grass, Alpine ice, Swedish Stratospheric filters and the PTB-filters was added during this research. Assuming a linear age-depth relation the data for the Alpine ice was fitted into the other data.

3.9. Conclusions

Previously existing data from stratospheric sampling (EML, 1997) and Polar ice cores (Koide *et al*, 1985) have been compiled. Using grass samples from the IACR-Rothamsted herbage archive in England, an ice core from the Mont Blanc glacier (French Alps) and ground-level air filters from Germany, for the first time a ground level record of $^{240}Pu/^{239}Pu$ for northern temperate latitudes is presented. One remarkable finding is that tropospheric fallout from the earliest US tests in the Nevada Desert is identified in the UK. For later years the data compare well with the incomplete chronological record obtained from the Stratosphere (EML, 1997) and Polar ice cores (Koide *et al*, 1985). In addition to the $^{240}Pu/^{239}Pu$ hitherto unseen fluctuations in the $^{238}U/^{235}U$ related to fallout from weapons testing are reported.

4. Application II A: Plutonium from the BNFL Sellafield site – results for a sediment core from the Wyre saltmarsh

4.1. Introduction

The Wyre saltmarsh is located on the estuary of the River Wyre, about ~68 km south of the BNFL Sellafield reprocessing plant (Figure 4.1). The core was studied previously and clearly shows a redox zonation as inferred from Mn and S profiles. (Thomson et al, 2002) Radionuclides in the core clearly reveal the discharges from BNFL Sellafield. However, none of the studied radionuclides (^{137}Cs and ^{241}Am) shows evidence of redox driven redistribution (Thomson et al, 2002). The reason for the lack of redistribution can be either that no post-depositional migration has occurred or that the processes of migration are too slow to be visible. In this Chapter plutonium and caesium data for the sediment core from the Wyre saltmarsh are presented. Based on these data a model was developed for the transport from the Sellafield plant to the sampling site. The model is then applied to reconstruct the ^{240}Pu/^{239}Pu in the Sellafield discharge. The existing record of the composition of the discharge from the Sellafield reprocessing plant does not differentiate between the isotopes ^{239}Pu and ^{240}Pu (Gray *et al*, 1995).

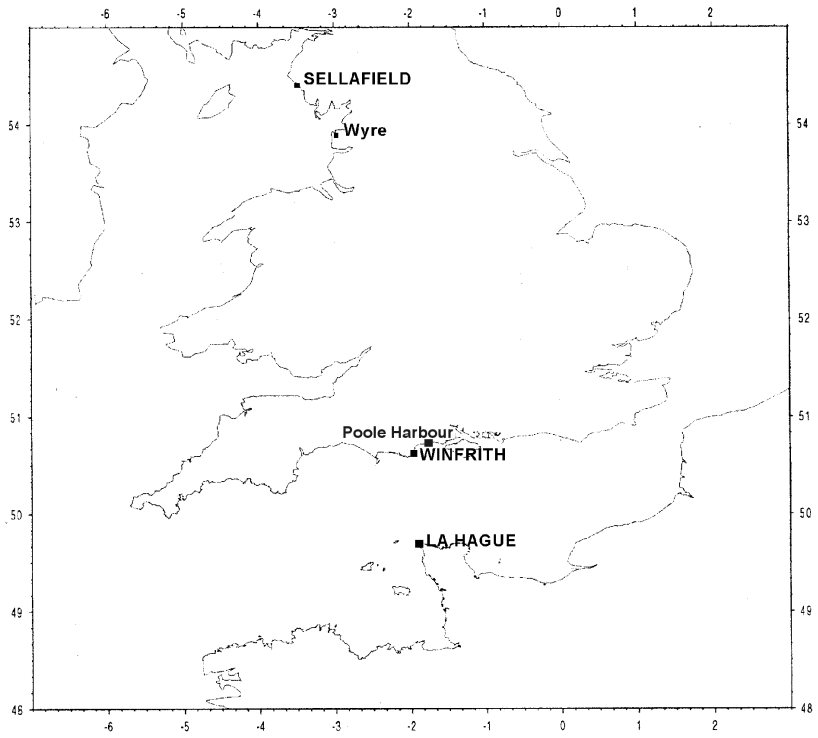

Figure 4.1 Location-map

4.2. Radionuclides in the Irish Sea and the transport to the sampling site

To understand radionuclide transport to the site of deposition it is important to know if the transport takes place mainly through solution or through particle adsorption. The consequences for the measurement of radionuclides in sediment cores for the two transport mechanisms, solution transport and particle transport, are investigated in a review paper by MacKenzie and Scott (1993). In **solution transport** the radionuclide is dissolved in the seawater. As the radionuclide is transported away from the discharge point its concentration decreases by continuous removal to sediments and by dilution with less contaminated seawater. Assuming both processes follow first order kinetics, the concentration decreases exponentially with distance from the source. Since the removal to the sediments depends on the K_d, the ratio of two radionuclides with different K_d values would also vary exponentially with distance from the source point. An accumulating, non-mixing sediment would exhibit radionuclide concentrations at different depths as a constant function of the annual discharge. In **particle transport** the radionuclide becomes attached to sediments at the discharge point and is then distributed by movement of the sediment. Assuming that that the sediment which is available for redistribution is subject to rapid, total vertical mixing, an accumulating, non-mixing sediment would exhibit time integrated radionuclide concentrations at different depths.

To quantify the tendency of a radionuclide to adsorb onto particles the distribution coefficient (K_d) is used. It describes the equilibrium distribution of species between the dissolved and particle-associated phases and is defined as:

$$K_d = \left(\frac{\text{Activity per unit mass of particulate}}{\text{Activity per unit mass of solution}} \right)$$

To apply the K_d - concept to systems in the environment one has to keep in mind that the K_ds depend on chemical and physical conditions of the radionuclide and the sampling location. The K_d of plutonium depends on the oxidation state. Pu can exist in the five oxidation states III, IV, V, VI and VII. Oxidation state VII is very rare in environmental systems. In the Irish Sea Pu (III & IV) have K_ds of 10^6, Pu (V & VI) K_ds of the order 10^4 and radiocaesium between 10^3 – 10^5 (Nelson and Lovett, 1978, MacKenzie *et al*. 1998). After the discharge about 10% of the plutonium and 90% of the radiocaesium remains in solution and is transported out of the Irish Sea via the North Channel (MacKenzie and Scott 1993). The

remaining 10% of the Cs, along with virtually all ^{241}Am and 90% of the Pu is incorporated in a deposit of fine sediment (the Sellafield mud patch) close to the discharge point (MacKenzie and Scott, 1993). The sediments close to the discharge point that are associated with the radionuclides show rapid mixing and a negligible accumulation rate (MacKenzie and Scott, 1993, MacKenzie *et al*. 1998). Within the last 20 years the surface concentration and inventories of plutonium and americium have been decreasing near the Cumbrian coast and are dispersed to more distant areas (Kershaw *et al*, 1999). In contrast to Am and Pu the incorporated caesium shows significant re-dissolution from the sediments (MacKenzie and Scott, 1993, MacKenzie *et al*. 1998). Particle transport is the most important transport mechanism for the dispersion of Cs, Pu and Am to intertidal and offshore sediments in the Irish Sea (MacKenzie and Scott 1993).

4.3. Plutonium and caesium concentrations in the core

The activity concentrations of ^{239,240}Pu, ^{238}Pu and ^{137}Cs in the Wyre core and the discharge from Sellafield are shown in Figure 4.2 (decay corrected to 1998). ^{137}Cs has been determined in the discharge since 1952 while plutonium isotopes ^{239,240}Pu and ^{238}Pu have been measured separately since 1978 with separate measurements of ^{241}Pu since 1972. However, separate estimates of ^{239,240}Pu, ^{238}Pu and ^{241}Pu exist for all years of operation. (Gray *et al*, 1995).

The patterns of the ^{239,240}Pu concentration observed in the core clearly reflect the pattern of the Sellafield discharge record. The two main maxima in the discharge record in 1973 and 1978 are also observed in the core at depths of 31 cm and 25 cm. The minima between those maxima can be seen at a single increment in the core compared to 4 years in the discharge. The small minima in the core at 47 cm and 39 cm could be attributed to the minima in 1964 and 1969 in the discharge record. The minimum in the core at 33 cm cannot be explained by the discharge record. The deviations from the exponential decrease in the core at 21 cm, 17 cm and 3cm are too small to be linked with certainty to the discharge record. However, it should be noted that those features could find attributions in the discharge for 1982, 1984 and 1993. Assuming that the sediment from the Sellafield mudpatch is the dominant source of radionuclides to the saltmarsh, it would be especially surprising to see such small discharge features in the core following periods of high activity discharge. The ^{238}Pu concentration in the core also closely reflects the discharge pattern. The maxima in the core at 29/31 cm and 25 cm can be seen in the discharge in 1973 and 1978/79.

The ^{137}Cs concentration in the core shows one maximum at a depth of 31 cm, which probably represents the years of high discharge between 1975 and 1977. Otherwise it looks as if the Cs concentration does not resolve as many features of the discharge record as the plutonium. The reason for this might be that the distinct features in the Cs discharge are too close in time to be resolved in the core. The second discharge maximum in 1977 appears just 2 years after the first one, whereas in the case of plutonium the time between the maxima is 5 years. The minima between those plutonium maxima is just seen as a single depth which shows that also the plutonium would not resolve two maxima that are adjacent by 2 years.

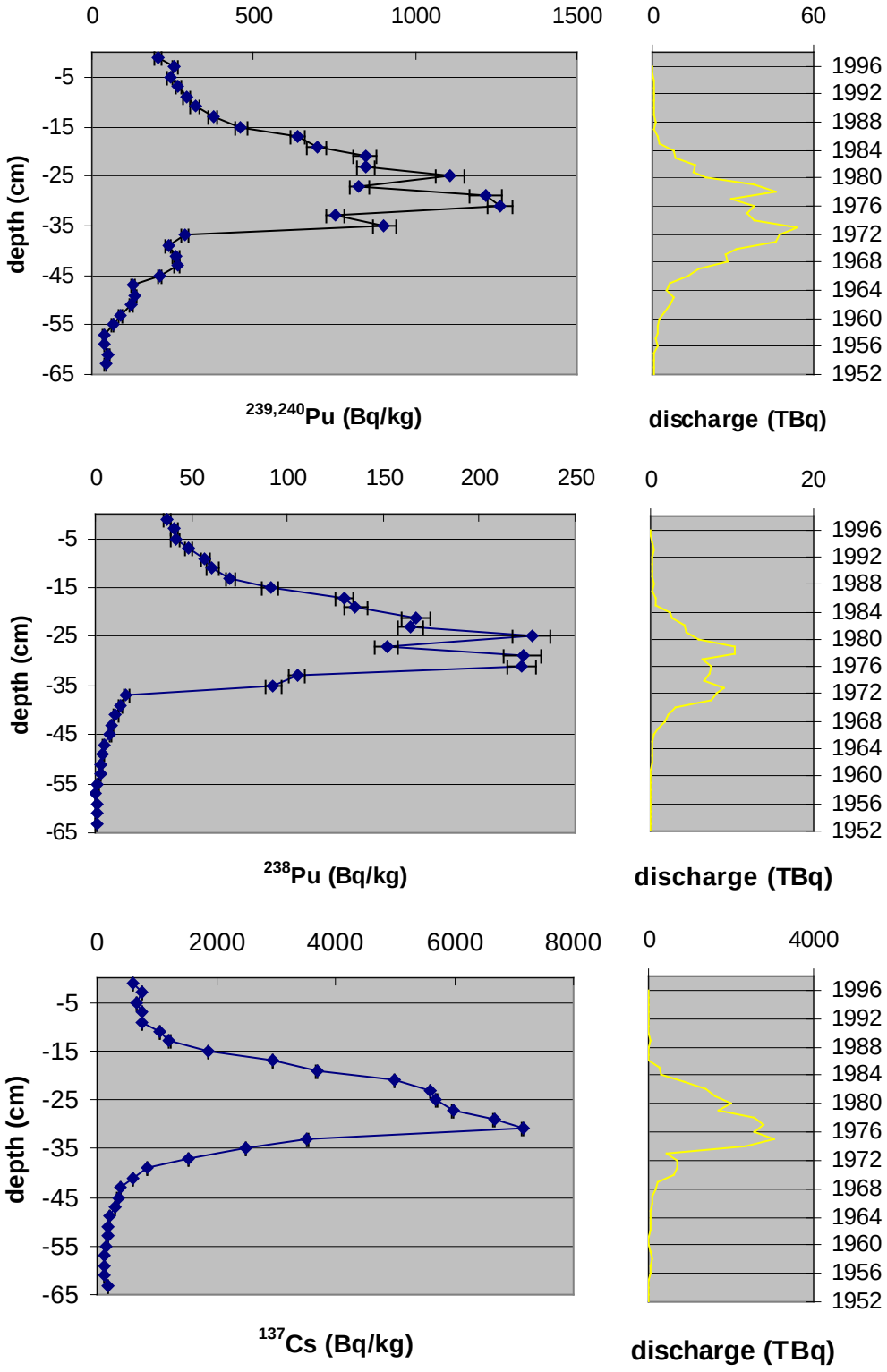

Figure 4.2 (a) ^{239,240}Pu (b) ^{238}Pu (c) ^{137}Cs in the Wyre core. The figures on the right hand column show Sellafield discharge. The data are decay corrected to 1998.

4.4. $^{238}Pu/^{239,240}Pu$ and $^{239,240}Pu/^{137}Cs$ activity ratios in the core

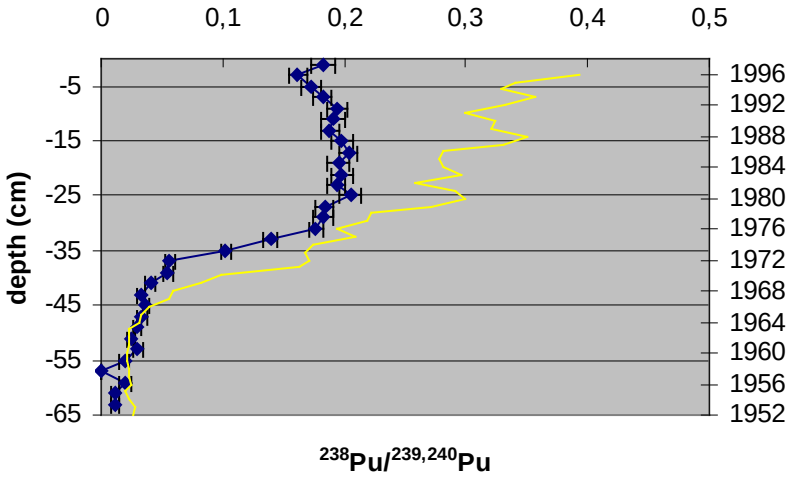

Figure 4.3 $^{238}Pu/^{239,240}Pu$ activity ratio in the Wyre core. The blue line shows the $^{238}Pu/^{239,240}Pu$ activity ratio in the core and is plotted against the depth of the core on the left vertical axis. The yellow line is the $^{238}Pu/^{239,240}Pu$ activity ratio in the discharge and is plotted against the right vertical axis. The data are decay corrected to 1998.

The **$^{238}Pu/^{239,240}Pu$** activity ratio in the core (Figure 4.3) increases slowly from 0.019 at 63 cm depth to 0.058 at 37 cm depth. This is the expected behaviour since the potential plutonium sources (weapons fallout and Sellafield discharge) have similar ratios at this time. The $^{238}Pu/^{239,240}Pu$ activity ratio in the Sellafield discharge is between 0.02 and 0.06 until 1968 and stays less than 0.1 until 1970. Until 1970 9% of the total ^{238}Pu and 26% of the total $^{239,240}Pu$ have been discharged (the stated totals are to 1998). From 37 cm the $^{238}Pu/^{239,240}Pu$ activity ratio increases strongly to 0.18 at 31 cm depth. The increase can also be seen in the Sellafield discharge, which has ratios between 0.166 and 0.226 for the period from 1971 until 1978. In this period Sellafield discharged 52% of its total ^{238}Pu and 48% of its total $^{239,240}Pu$. From 31 cm depth until the top of the core the ratio stays almost constant with values between 0.16 and 0.21. These ratios are significantly lower than the ratios in the discharge during that time. The $^{238}Pu/^{239,240}Pu$ activity ratio in the discharge is between 0.26 and 0.3 for the period from 1979 - 1986 and between 0.3 and 0.4 for the period from 1986 - 1998. In the former period 20% of its total ^{238}Pu and 12% of its total $^{239,240}Pu$ and in the latter period only 2% of its total ^{238}Pu and 1% of its total $^{239,240}Pu$ have been discharged. From the fact that the core does not reflect the ratios seen in the discharge from 1979 onwards it can

be concluded that the sediment has partly undergone mixing prior to deposition. At 3 cm depth the core exhibits clearly a small minimum, which cannot be attributed to the discharge.

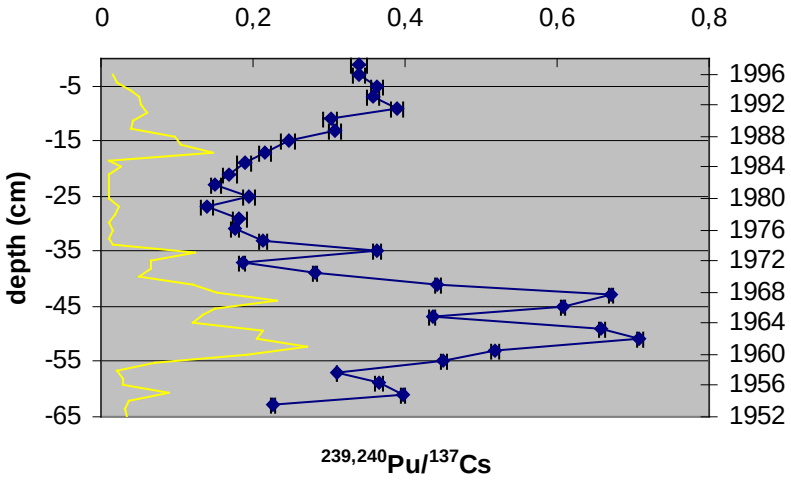

Figure 4.4 ^{239,240}Pu/^{137}Cs activity ratio in the Wyre core. The blue line shows the ^{239,240}Pu/^{137}Cs activity ratio in the core and is plotted against the depth of the core on the left vertical axis. The yellow line is the ^{239,240}Pu/^{137}Cs activity ratio in the discharge and is plotted against the right vertical axis. The data are decay corrected to 1998.

The **^{239,240}Pu/^{137}Cs** activity ratio in the discharge is significantly lower than the ratio in the core. However, the pattern of the discharge and the core match very well. The maxima in the discharge in 1955, 1961, 1967, 1973 and 1986 can be seen at depths of 61 cm, 51 cm, 43 cm, 35 cm and 9 cm. This suggests that the plutonium is transported more effectively to the sampling site than the caesium. The fact that the core reflects the pattern of the ^{239,240}Pu/^{137}Cs in the discharge very well, implies that the fractions of plutonium and caesium that are transported to the sampling site are constant with time. Previous studies suggest that about 10% of the caesium and 90% of the plutonium is incorporated into sediments and that those sediments are the main supply of radionuclides to saltmarsh sediments (MacKenzie and Scott 1993). This scenario would qualitatively explain the higher ratios in the core than in the discharge.

4.5. $^{240}Pu/^{239}Pu$ and $^{242}Pu/^{239}Pu$ atom ratios in the core

For the plutonium isotopes ^{242}Pu, ^{240}Pu and ^{239}Pu no separate discharge data exist. In Figures 4.5 and 4.6 the $^{240}Pu/\ ^{239}Pu$ and $^{242}Pu/\ ^{239}Pu$ atom ratios in the Wyre core are compared with published ratios for a core from Maryport harbour, about 40 km north of Sellafield (Kershaw *et al*, 1995). The $^{240}Pu/\ ^{239}Pu$ in the Wyre core and in the Maryport core are almost identical, if it is assumed that a depth of 235 cm in the Maryport core corresponds to a depth of 65 cm in the Wyre core and that the top of the Maryport core corresponds to 14 cm in the Wyre core. The $^{240}Pu/^{239}Pu$ in the core reflect the history of purposes of the Sellafield site. The continuous increase of the ratio until 21 cm results from an increase of burn up time of the fuel. In the early years of operation the principal purpose was to provide plutonium for the nuclear weapons program. Weapons grade plutonium ($^{240}Pu/^{239}Pu < 0.075$) is found for all depths below 45 cm. The continuous increase of the ratio has two reasons. In the earlier years it is due to the increasing proportion of fuel for civilian purposes. After the period of production of military plutonium the increase could be explained by developments in fuel rod and reactor design which allowed longer burn up times. The slight decrease of the ratio above 21 cm appears after the period of highest concentration in the core and corresponds to years later than 1980. The absolute values of the $^{240}Pu/^{239}Pu$ at the top of the core are slightly lower than the values of burned fuel from Magnox reactors which are 0.23. However, the $^{240}Pu/\ ^{239}Pu$ in burned fuel from other common reactor types is much higher than the ratios at the top of the core (Table 1.6 , Chapter 1). This discrepancy will be resolved by reconstructing the $^{240}Pu/\ ^{239}Pu$ in the discharge (4.9). The $^{242}Pu/\ ^{239}Pu$ in the Wyre core shows the same trend as the $^{242}Pu/\ ^{239}Pu$ in the Maryport core. However, the measured ratios in the Wyre core are significantly higher than in the Maryport core. This deviation might be due to the correction applied to the $^{242}Pu/\ ^{239}Pu$ measurement (see 2.4.3).

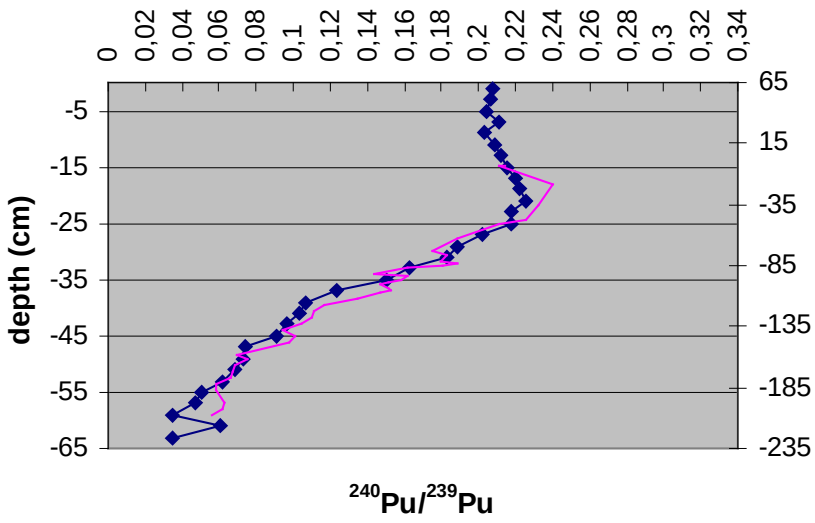

Figure 4.5 $^{240}Pu/^{239}Pu$ in the Wyre core. The blue line shows the $^{240}Pu/^{239}Pu$ atom ratio in the Wyre core and is plotted against the depth of the core on the left vertical axis. The red line is the $^{240}Pu/^{239}Pu$ atom ratio in the Maryport core (Kershaw *et al*, 1995)

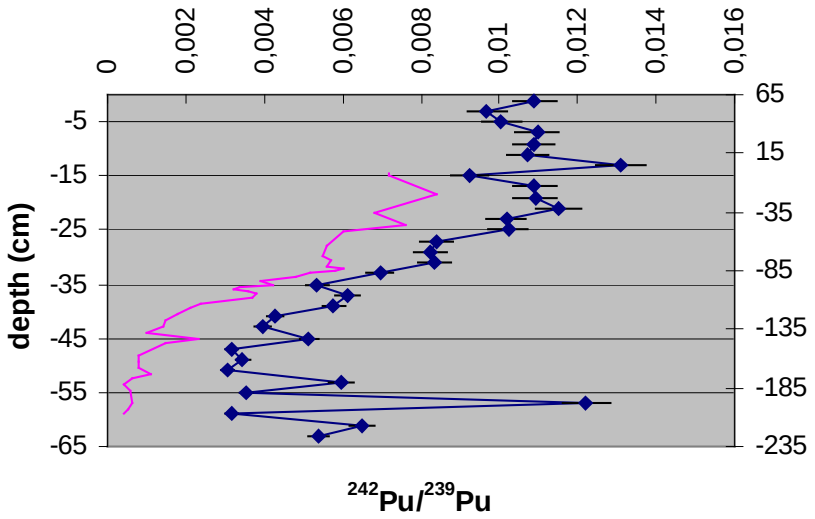

Figure 4.6 $^{242}Pu/^{239}Pu$ in the Wyre core. The blue line shows the $^{242}Pu/^{239}Pu$ atom ratio in the Wyre core and is plotted against the depth of the core on the left vertical axis. The red line is the $^{242}Pu/^{239}Pu$ atom ratio in the Maryport core (Kershaw *et al*, 1995)

4.6. A model for the dispersion of plutonium

In section 4.2 it has been discussed that radionuclides deposited in Cumbrian saltmarsh environments on the eastern coast of the Irish Sea undergo mixing with the previous year's material prior to deposition. This was also suggested for the Wyre core from the $^{238}Pu/^{239,240}Pu$ activity ratio in section 4.4. However, because distinct features of the Sellafield discharge can be seen in the Wyre core (4.3), even after years of high discharge it has been considered useful to model the transport of particle associated radionuclides (like plutonium).

The model is based on the following assumptions:

1. Following discharge the radionuclides are partly transported directly to the sampling site and partly become mixed in the mudpatch before being transported to the sampling site. The model also allows that the total discharge of the radionuclides become incorporated into the sediment before being transported to the sampling site.

2. The probability p that an activity unit (since all equations are linear with respect to A, instead of activity unit the number of particles can be used) leaves the sediment in a time interval Δt is proportional to Δt, hence
   $p(\text{leaves sediment in } \Delta t) = \xi \Delta t$.
   Therefore the probability that it stays in the sediment is
   $p(\text{stays in sediment in } \Delta t) = 1-\xi \Delta t$.
   The probability that the time $t=n\Delta t$ is survived in the sediment is
   $p(\text{stays in sediment in } t=n\Delta t) = (1-\xi \Delta t)^n = (1-\xi t/n)^n$
   For fixed t $\Delta t \rightarrow 0$ equals $n \rightarrow \infty$, hence
   $p(\text{stays in sediment in } t) = \lim_{n\rightarrow\infty} (1-\xi t/n)^n = e^{-\xi t}$
   ξ can be expressed by $\xi = \ln 2/R_{1/2}$ where $R_{1/2}$ is the half time of the discharged activity in the mudpatch.

The second assumption should be good as long as the sediment accumulation at the location where the mixing takes place can be neglected and rapid mixing takes place. This is a

common assumption that is supported by the study of offshore cores (MacKenzie *et al*, 1998).

Let $A_i^{discharge}$ be the discharged activity in a year i. Introducing a parameter w with $0 \leq w \leq 1$, the fraction of the discharged activity in a year i that enters the mudpatch and undergoes mixing can be described by

$w \times A_i^{discharge}$

and the fraction that is transported directly to the sampling site by

$(1-w) \times A_i^{discharge}$.

The concept of the model is illustrated in Figure 4.7.

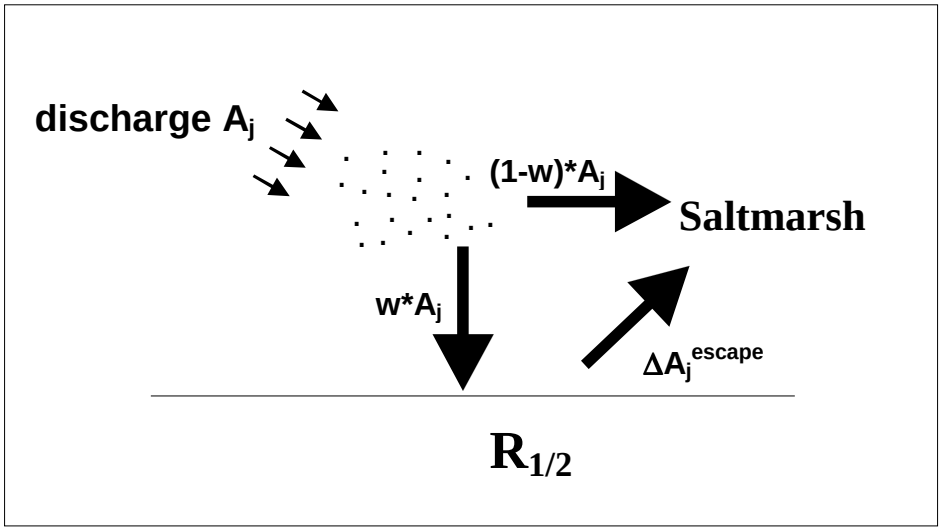

Figure 4.1 Schematic diagram of the model

For stable isotopes the activity in the mudpatch sediment at time t is given by

$$A^{sediment}(t) = \sum_{i=1952}^{t} wA_i^{discharge} e^{-\xi(t-i)}$$

However, in the more general case the decay of the isotopes has to be taken into account. If λ^{decay} is the decay constant of the isotope the activity in the sediment at time t is given by

$$A^{sediment}(t) = \sum_{i=1952}^{t} wA_i^{discharge} e^{-\xi(t-i)} e^{-\lambda^{decay}(t-i)}$$

The activity that left the sediment and is observed at time t is given by the decay corrected total activity that entered the sediment until time t minus the activity in the sediment at time t:

$$A^{escape}(t) = \sum_{i=1952}^{t} wA_i^{discharge} e^{-\lambda^{decay}(t-i)} - \sum_{i=1952}^{t} wA_i^{discharge} e^{-\xi(t-i)} e^{-\lambda^{decay}(t-i)}$$
$$= \sum_{i=1952}^{t} wA_i^{discharge} (1 - e^{-\xi(t-i)}) e^{-\lambda^{decay}(t-i)} \quad \textbf{(Equation 1)}$$

The activity that leaves the sediment and is observed in a time interval t_2-t_1 is given by

$$\Delta A_{t_2}^{\ escape} = A^{escape}(t_2) e^{\frac{1}{2}\lambda^{decay}(t_2 - t_1)} - A^{escape}(t_1) e^{-\frac{1}{2}\lambda^{decay}(t_2 - t_1)} \quad \textbf{(Equation 2)}$$

The correction of $e^{\frac{1}{2}\lambda^{decay}(t_2 - t_1)}$ is done to correct for decays within the year. In our case t_2 and t_1 are two adjacent years from 1952 until 1996. A scaling factor C (Equation 3) accounts for the fraction that reaches the sampling location. The total activity that arrives at the sampling location in a year j is

$$\Delta A_j^{arrive} = C\left(\Delta A_j^{escape} + (1-w)\Delta A_j^{discharge}\right) \quad \textbf{(Equation 3)}$$

(N.B. This is the main working equation used and incorporates Eqn 1&2)

The model allows for variations in the following parameters:

1. Half time in the mudpatch sediment $R_{1/2}$ (constant for all isotopes of an element)
2. Mixed fraction factor w (constant for all cores, constant for all isotopes of an element)
3. Sediment accumulation rate S of the core (constant for a particular core)
4. Scaling factor C (constant for a particular core, constant for all isotopes of an element)

4.7. Model response to the variation of the parameters

The initial settings for the model parameters were $R_{1/2} = 10^{-10}$, w=0, C=0, and S=1. In this way the modelled curves appear on the same plot window as the measured ones, if the measured and the modelled values are plotted *versus* time. The modelled concentrations appear as zero values and the modelled ratios show the ratios in the discharge. In the next step the scaling factor C is set that the maximum modelled concentrations match approximately the measured ones. After that the sediment accumulation rate is determined. Then $R_{1/2}$ and w are increased until a reasonable fit is observed. After each step C and S are adjusted. The determination of the sediment accumulation rate is straightforward. The scaling factor C only affects the concentration values as a multiplier. Both S and C can be determined with reasonable confidence and do not give any information about the transport mechanism. The important parameters for the transport are the residence half time $R_{1/2}$ in the sediment and the mixed fraction factor w. In Figures 4.8 and 4.9 it is demonstrated for the Wyre core how the modelled ^{238}Pu, ^{239,240}Pu and ^{238}Pu/^{239,240}Pu respond to a variation of $R_{1/2}$ and w.

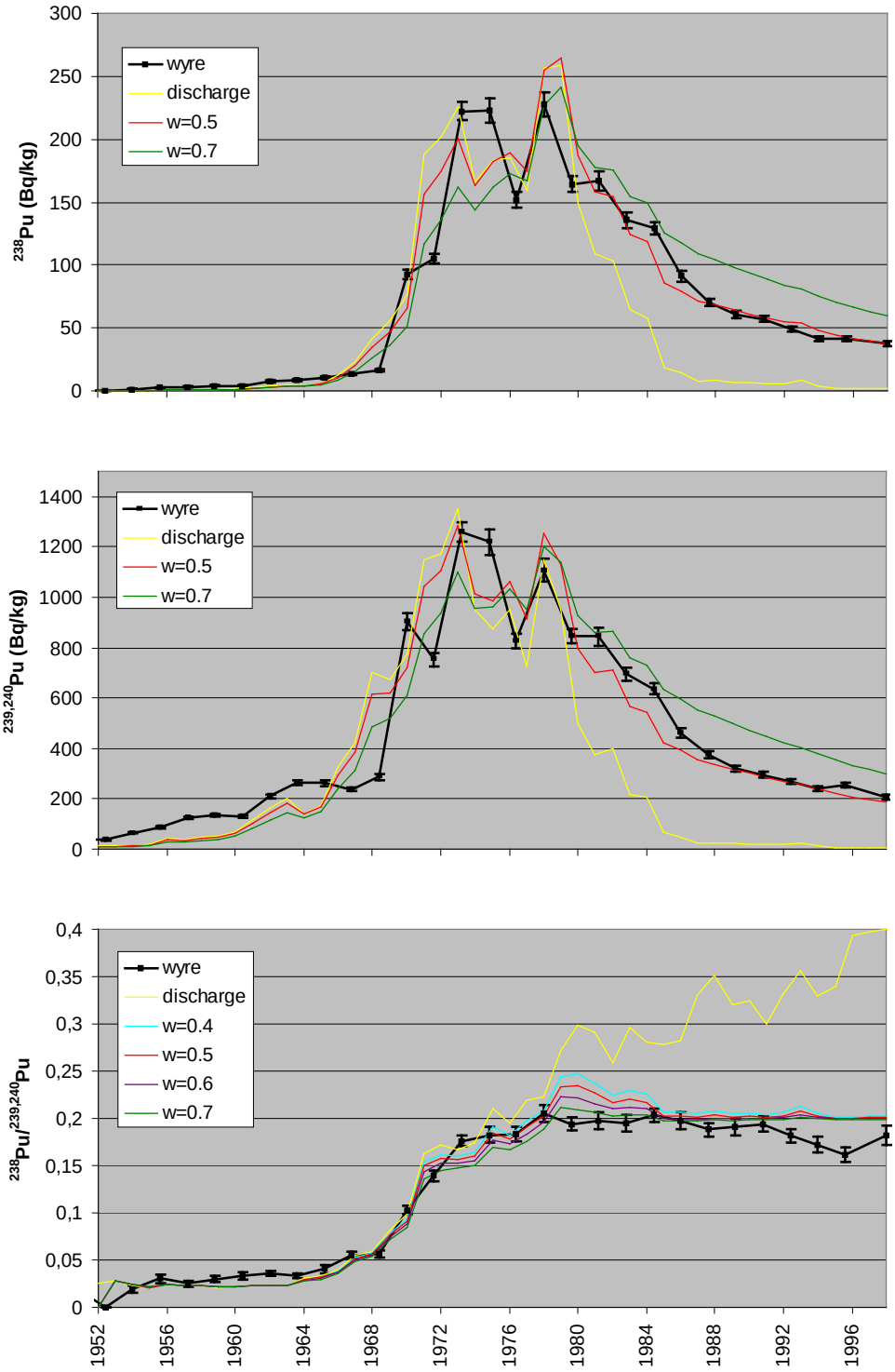

Figure 4.2 Modelled ^{238}Pu, ^{239,240}Pu and ^{238}Pu/^{239,240}Pu for different values of w. The residence half time $R_{1/2}$ is constant with a value of 12 years. The actual Wyre data is plotted with error bars. The data are decay corrected to 1998.

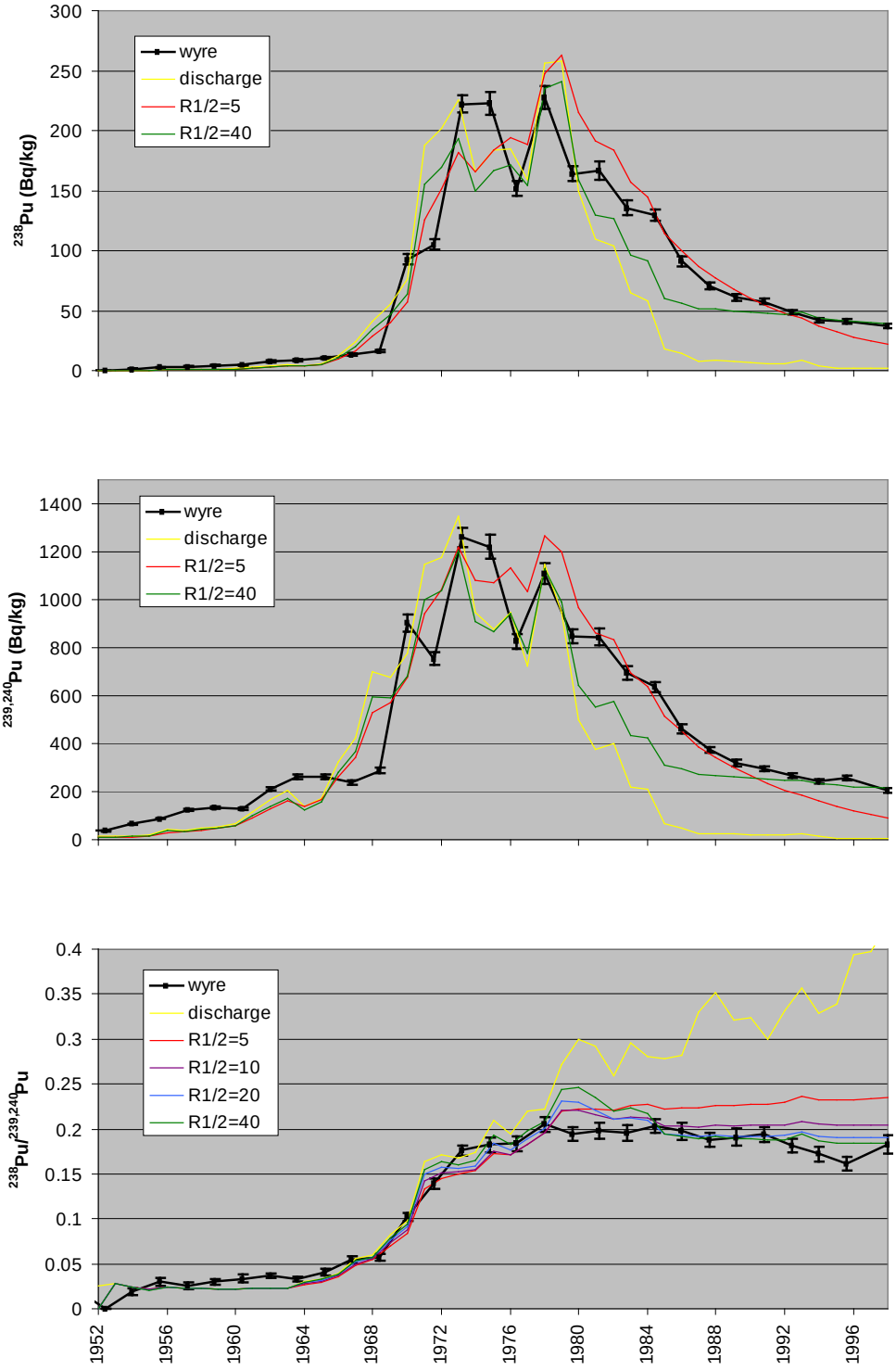

Figure 4.3 Modelled ^{238}Pu, ^{239,240}Pu and ^{238}Pu/^{239,240}Pu for different values of $R_{1/2}$. The parameter w is constant with a value of 0.6. The actual Wyre data is plotted with error bars. The data are decay corrected to 1998.

Using a parameters w between 0.4 – 0.7 the modelled curve approximates the measured one much better than the discharge (Figure 4.8). The residence half time of 12 years was found to be the best after the initial variation of the parameters. For w=0.4 the main deviations between the modelled $^{238}Pu/^{239,240}Pu$ and the measured one are in 1979-1984 and 1991-1996. The deviation 1991-1996 is almost the same for all w. With increasing w the deviation for the years 1979-1984 decreases and disappears for w=0.7. However, for w=0.7 the values for 1973-1977 are lower than the measured curve. Looking at the $^{239,240}Pu$ concentration it can be seen that the curve for w=0.5 is in fairly good agreement with the measured curve. If w becomes greater than 0.5 the approximation of the double peak in the measured curve gets worse. Besides that the tailing for the years after high discharge is not strong enough for w>0.5. It can be seen that the plutonium in the Wyre core can neither be described by direct transport of the discharge nor by integrated discharge alone.

The best approximation is obtained for $0.5<w<0.7$.

The response of the model to the residence half time $R_{1/2}$ in the sediment is not that sensitive (Figure 4.9). The parameter w is constant with a value of 0.6 in both figures. For $R_{1/2}$ =5 the modelled $^{238}Pu/^{239,240}Pu$ is too low for the years 1973-1974 and too high from 1979 until the top of the core. The curve $R_{1/2}$ =10 shows the same deviation as the $R_{1/2}$ =5 curve in 1973-1974 and in 1979, but for all other years the approximation increases significantly. For the later years the $R_{1/2}$ =10 curve shows only a deviation for the years 1991-1995. $R_{1/2}$ =20 improves slightly the approximation from the mid 1980s onwards. However, the approximation for 1979-1982 gets worse. $R_{1/2}$ =40 does not approximate the measured curve very well because of a strong deviation for 1979-1984. The $^{239,240}Pu$ concentration is less sensitive to the variation of $R_{1/2}$ and does not give a further restriction for $R_{1/2}$.

The best approximation is obtained for $10< t_{1/2}<20$.

4.8. Best fit parameters for the Wyre core

The parameters that appear to best fit are given in Table 4.1 and the corresponding curves in Figure 4.10.

w	S (cm/yr)	$R_{1/2}$ (yrs)	C
0.6	1.25	12	40

Table 4.1 Best fit parameters for the Wyre model

Prior the mid 1960s the modelled ^{239,240}Pu concentration and the weighted discharge are up to 50% lower than the measured concentration. From the mid 1960s the modelled ^{239,240}Pu concentration increases to a maximum in 1973, which can also be seen in the measured ^{239,240}Pu concentration. The measured maximum is broader and the maximal modelled values are 9% lower than the measured ones. The second maximum in 1978 has similar values in the model than in the core. After the second maximum both modelled and measured ^{239,240}Pu concentrations drop exponentially until 1996 with a slightly stronger tailing in the measured concentrations. The modelled ^{238}Pu concentration matches the measured one prior the first maximum in 1973. The maximum in 1973 is not very well approximated by the model. The measured maximum is broader and the modelled maximal ^{238}Pu concentration are 20% lower than the measured ones. The second maximum in 1978/79 is fairly well approximated but appears about one year later in the model. After this maximum both modelled and measured concentrations decrease with slightly greater tailing in the measured concentrations. Besides the deviations mentioned both, the measured ^{239,240}Pu concentration and the measured ^{238}Pu concentration deviate for individual years from the model. The ^{238}Pu/^{239,240}Pu isotopic ratio is well approximated by the model. Deviations occur in 1973/74, 1979-1981 and 1991-1996. In 1973/74 the modelled concentrations are about 10% lower than the measured ones and in 1979-1981 up to 10% higher. The 1991-1996 deviation is fairly large with the measured ratio being 20% lower. However, as discussed previously, the lower values in the core in 1991-1996 cannot be attributed to direct transport from Sellafield.

The good agreement between the modelled and measured ^{238}Pu/^{239,240}Pu isotopic ratio suggests that the deviations between the modelled concentrations and the measured ones result from differences in transport for individual years. The efficiency of the transport to the sampling site is determined by the parameter C, which is constant for all years. Since the transport is the same for ^{238}Pu and ^{239,240}Pu the ^{238}Pu/^{239,240}Pu is independent of differences in the yearly transport efficiency to the sampling site. The accumulation rate of 1.25 cm/year compares with 1.4 cm/year and 2 cm/year reported by Thomson *et al* (2002) inferred from ^{137}Cs and ^{210}Pb.

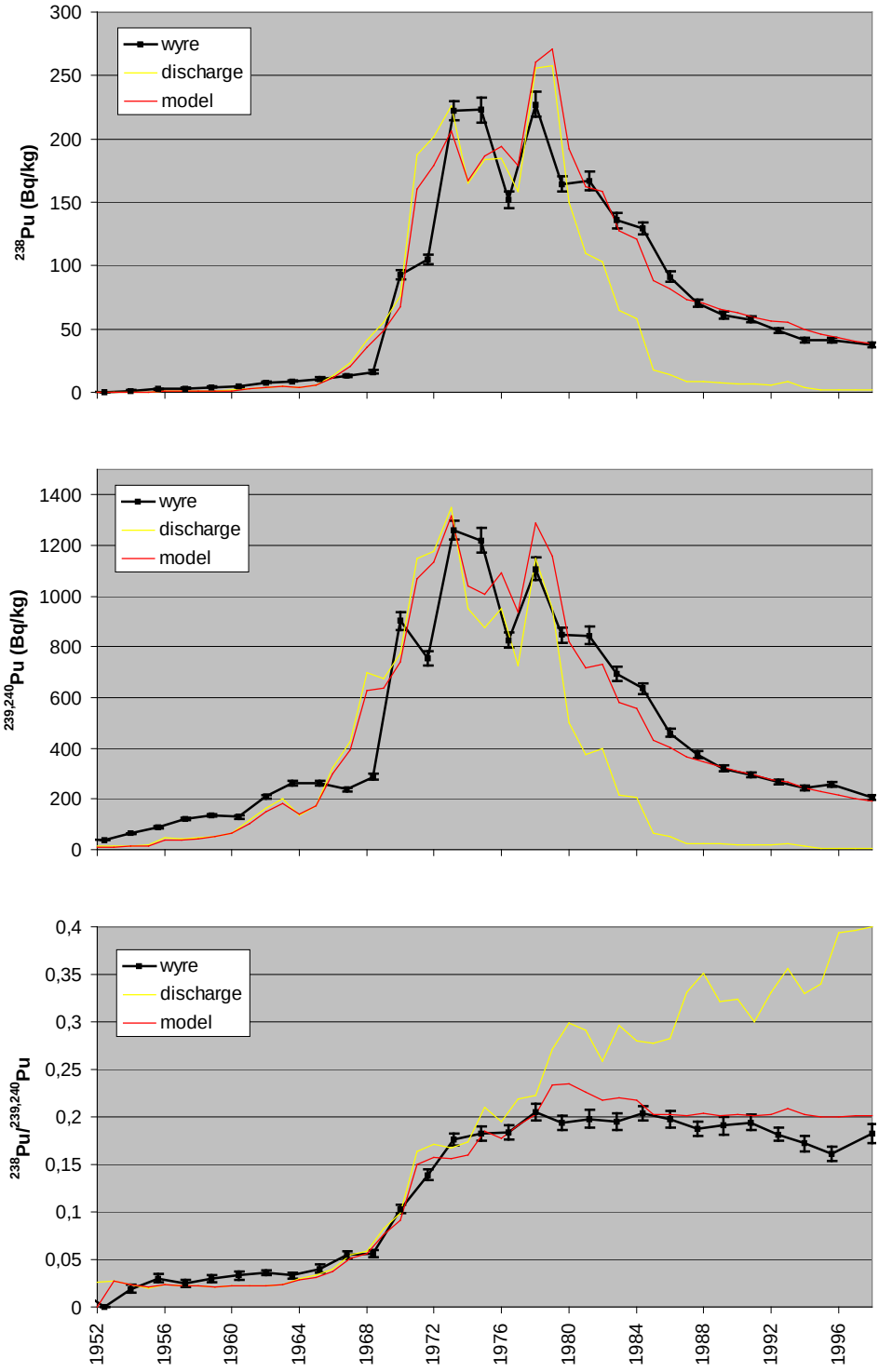

Figure 4.4 Measured curves and modelled curves for the best fit parameters The data are decay corrected to 1998.

4.9. Reconstruction of the $^{240}Pu/^{239}Pu$ atom ratio in the discharge

Using the same transport model described in section 4.6 (Equation 3, p.76) and by applying the best fit parameters already determined (Table 4.1) the $^{240}Pu/^{239}Pu$ atom ratio in the discharge is reconstructed using the measured $^{240}Pu/^{239}Pu$ ratio in the Wyre core. Since the $^{240}Pu+^{239}Pu$ activity concentration in the discharge is published, the discharged activity of one of the isotopes is fixed by a knowledge of the other. Starting in 1952 the discharged ^{240}Pu activity is determined in this way that the modelled $^{240}Pu/^{239}Pu$ ratio fits the measured ratio. This is done for each year until the top of the core. The fit can be done with reasonable confidence as long the discharged activity is fairly high, which is the case up until the early 1980s. With decreasing discharged activity in the mid 1980s the modelled curve gets less sensitive to the discharged ratio. For that reason the reconstructed $^{240}Pu/^{239}Pu$ in the discharge is only shown until 1984 (Figure 4.11) but by this time more than 98% of the total cumulative $^{239,240}Pu$ activity had been discharged.

It has been mentioned previously that the measured $^{240}Pu/^{239}Pu$ ratios at the top of the core are fairly low compared with burned reactor fuel. From Figure 4.11 it can be seen, that the $^{240}Pu/^{239}Pu$ in the reconstructed discharge is above 0.2 after 1974 and above 0.25 after 1979, whereas the maximum value in the core is 0.225. The core shows lower ratios in 1983/84 after the maximum in 1981/82. The reconstructed ratios in the discharge are even higher in 1983/84 than in 1981/82. The explanation is that the drop has its origin in plutonium discharges from the earlier years. The fact that a maximum occurs shows that direct transport plays a role for the plutonium. Assuming no direct transport and rapid mixing of the sediment the ratio could stay constant but could never go down without a drop in the discharged ratio below the measured ratio in the core.

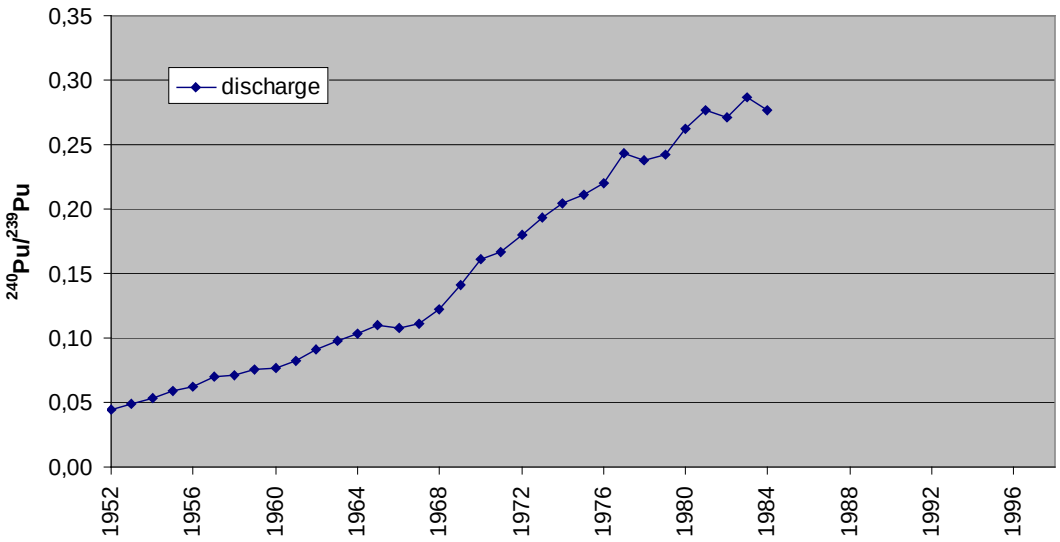

Figure 4.5 Reconstructed $^{240}Pu/^{239}Pu$ in the Sellafield discharge

4.10. Conclusions

The concentrations of ^{137}Cs, ^{238}Pu and $^{239,240}Pu$ in a sediment core from the Wyre saltmarsh, located approximately 68km south of the Sellafield reprocessing plant, reflect well the pattern of the discharge from BNFL Sellafield. The $^{238}Pu/^{239,240}Pu$ activity ratio suggests that the sediments transported to the sampling site have undergone mixing with sediment material of earlier years. The $^{239,240}Pu/^{137}Cs$ shows that a higher fraction of discharged plutonium is transported to the sampling site than caesium and that the relative fractions are constant with time. A model based on a constant mixing half-time of the discharge in a mixing reservoir is able to explain the ^{238}Pu and $^{239,240}Pu$ concentrations and the $^{238}Pu/^{239,240}Pu$ activity ratio observed in the core. Using the model the $^{240}Pu/^{239}Pu$ in the Sellafield discharge was reconstructed from the measured $^{240}Pu/^{239}Pu$ ratio in the core.

CHAPTER 5

5. Application II B: Plutonium in a sediment core from Poole Harbour

5.1. Introduction

Poole Harbour is located in Dorset in Southern England. Possible sources of anthropogenic radionuclides in this region are:

- Fallout from atmospheric nuclear weapons testing.
- Discharges from the Atomic Energy Establishment at Winfrith in Dorset (1970-1990; Appendix A.4).
- Discharges from the reprocessing plants Sellafield and La Hague (Appendices A.5 & A.6).
- Fallout from the Chernobyl accident in 1986.

The Atomic Energy Establishment at Winfrith in Dorset has undertaken reactor research and operated a prototype steam-generating heavy water reactor on site. The AEE discharged via a 2km long pipeline into the marine environment off the Dorset coast. Discharge records for the actinides are only reported as 'total alpha activity'. Since a variety of designs of research reactors were investigated it is difficult to predict the plutonium activity or the isotopic composition in the discharges. The reprocessing plants at Sellafield and La Hague are unlikely to have a significant impact in this area because there are no effective marine transport mechanisms (Bailly du Bois and Guegueniat, 1999). However, since they have discharged large quantities of radionuclides, a possible input should be considered. The plutonium isotopic composition of the discharges from both sites is well known (Figure 5.4). The Chernobyl incident (Figure 1.6) produced a small impact in this area and a ^{137}Cs-deposition of 25 Bq/m^2 is reported as the county average for Dorset (Clark and Smith, 1988). Actinides were primarily contained in the larger and heavier particulates and were therefore mostly deposited close to the accident site (NEA, 1995). The Chernobyl accident is unlikely, therefore to have transported significant quantities of plutonium to this area.

5.2. Core Geochemistry

A sediment core from a Wytch Farm mudflat, previously collected and studied by Cundy and Croudace (1996) was chosen for further investigation by this study. The geochemistry of the core has been reported by Cundy and Croudace, (1996). Little redox zonation can be identified from the profiles of Fe_2O_3, MnO and S (Figure 5.1). Al_2O_3, which is an indicator of clay mineral content, does not show any significant variations. Thus, preferential enrichment of radionuclides due to mineralogical variations or diagenetic processes are not expected over the length of the core.

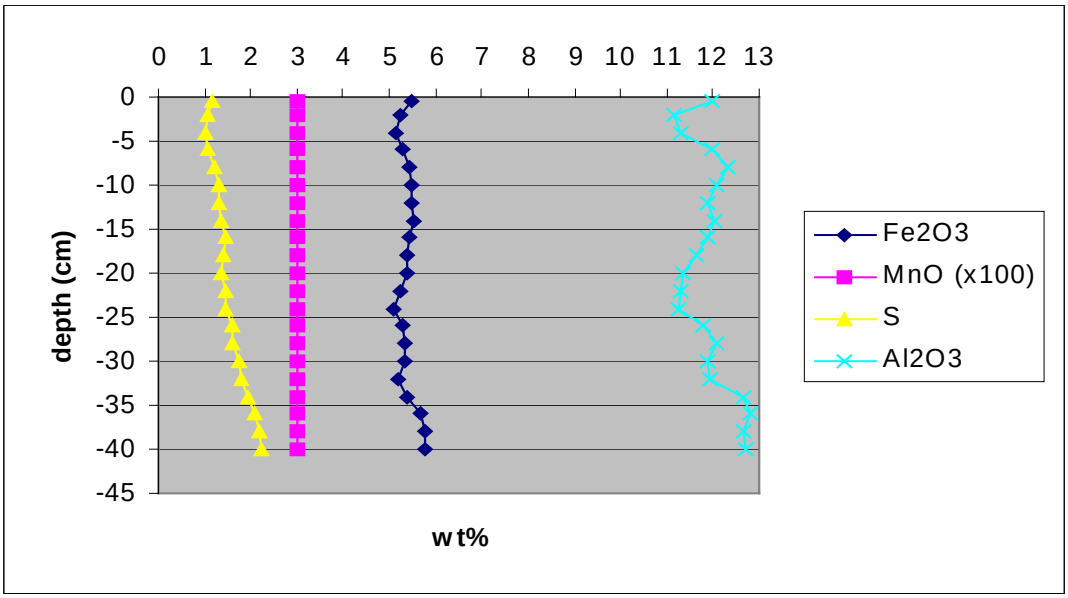

Figure 5.1: Profiles of Fe_2O_3, MnO, S and Al_2O_3 in the Poole Harbour core.

Sediment accumulation rates have been determined by several radiometric methods: These include ^{210}Pb dating and the application of ^{137}Cs, ^{241}Am, ^{239,240}Pu activity and ^{240}Pu/^{239}Pu isotopic ratio variations in atmospheric fallout deposition. Lead-210 dating gives a sediment accumulation rate of 8.4 mm/year (Cundy and Croudace, 1996). The variation in ^{137}Cs activity concentration (Figure 5.2) reveals a broad maximum and the sharp rise shows that mixing in the core is not significant. Since 1958 is known to be the first year of high ^{137}Cs fallout, the calculated accumulation rate is 10.3 – 10.9 mm/year. The ^{241}Am and ^{239,240}Pu profiles (Figures 5.3 and 5.8) show an increase between 30 and 34 cm, which should correspond to 1963. The resulting sedimentation accumulation rate is 10.7 – 12.1 mm/year. Fitting the ^{240}Pu/^{239}Pu chronology, established from Rothamsted grass (Chapter 3) to the ^{240}Pu/^{239}Pu ratio measured in the core yields a sedimentation accumulation rate of 10.5 – 10.9

mm/year (Figure 5.5). The sedimentation accumulation rates determined using different dating methods are compiled in Table 5.1. It can be seen that the rates determined from weapons' fallout products are significantly higher than that from ^{210}Pb dating and the model for the Winfrith discharges.

The determination of the accumulation rate from fallout spikes must make the assumption that variations in meteorological conditions (e.g. amount of rain) do not affect the appearance of the spike and that the observed radionuclides are geochemically not mobile. The first assumption is not needed if isotopic ratios are used, which makes the use of ratios superior to individual radionuclides. Plutonium isotopic ratios have distinct fallout features that can be used to establish the chronology of the core. Plutonium also fulfils the criterion of geochemical immobility. It is strongly sorbed on common minerals (e.g. clays with Fe-Mn oxyhydroxide grain coatings) and can remain fixed over a range of environmental eH-pH ranges (Allard *et al*, 1984) and is therefore likely to be a reliable recorder of the chronology in sediment cores (Oktay *et al*, 2000).

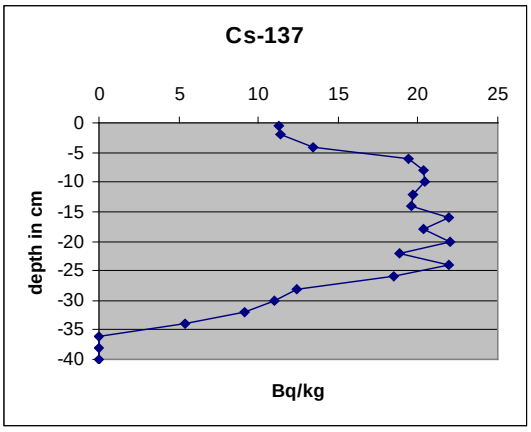

Figure 5.2: ^{137}Cs profile in the Poole Harbour core (decay corrected to 1991)

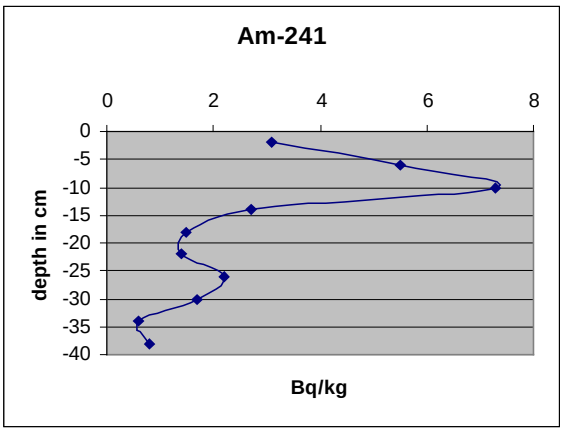

Figure 5.3: ^{241}Am profile in the Poole Harbour core (decay corrected to 1991)

Dating method	Sediment accumulation rate (mm/year)
^{210}Pb	8.4*
^{239,240}Pu from model for Winfrith discharges	8.4
^{137}Cs concentration (weapons fallout)	10.3 – 10.9
^{241}Am concentration (weapons fallout)	10.7 – 12.1
^{239,240}Pu concentration (weapons fallout)	10.7 – 12.1
^{240}Pu/^{239}Pu atomic ratio (weapons fallout)	10.5 – 10.9

*** from Cundy and Croudace (1996)**

Table 5.1 Sediment accumulation rates from different methods

5.3. Plutonium in the core

The concentration of ^{239}Pu and ^{240}Pu (Figure 5.8), the atom ratio $^{240}Pu/^{239}Pu$ (Figure 5.5) and the decay corrected activity ratios $^{238}Pu/^{239,240}Pu$ and $^{241}Pu/^{239,240}Pu$ (Figure 5.6 and Figure 5.7) have been determined for the core. Figure 5.5 –Figure 5.7 also contain Rothamsted grass-, stratospheric- and Arctic ice core data. One year is added to the stratospheric data to account for the lag time required for deposition. All data are decay corrected to 1991.

Between 40 and 34cm depth the plutonium concentration is below 0.3 Bq/kg. The $^{240}Pu/^{239}Pu$ shows qualitatively the same pattern as the ratios in the Rothamsted grass, but the magnitude of the variations are much smaller in the core. The reason might be mixing in the core or mixing prior to deposition. However, the increase from the bottom of the core to 38 cm depth is not expected from global fallout at this time and could be attributed to mixing with tropospheric fallout from the Nevada test site. The $^{241}Pu/^{239,240}Pu$ and the $^{238}Pu/^{239,240}Pu$ in this depth range are significantly higher than the corresponding ice core ratios. The reason for these high ratios is unclear.

From 34 to 26cm depth the plutonium concentration increases to 0.85 Bq/kg at 30 cm and over 1.1 Bq/kg at 26 cm. This increase can be attributed to the high yield USSR tests in 1961 and 1962. The $^{240}Pu/^{239}Pu$ in the core shows the same pattern than the $^{240}Pu/^{239}Pu$ in the grass, the most striking feature being the maximum at 30 cm depth that appears in the grass in 1963. The absolute values in the core are higher than in the grass which can be due to mixing with plutonium of the early US tests that was present in the water at that time. The $^{238}Pu/^{239,240}Pu$ drops to about 0.005, which is the expected value from weapons' fallout. The $^{241}Pu/^{239,240}Pu$ drops to a value of about 2 at 30 cm depth, which is in agreement with the values observed in the stratosphere and in the ice cores. However, this value is followed by an increase of the $^{241}Pu/^{239,240}Pu$ that cannot be seen in the other datasets.

Between 26 and 18 cm the concentration has values of 1.1 Bq/kg at 26 cm and 1.9 Bq/kg at 22 cm. The concentration in the core does not show a drop after the years of highest testing yields. The reason could be that most of the plutonium from the high yield tests is still in the water column and the concentration shows an integration of the plutonium from the high yield tests and plutonium that was introduced later. Another explanation could be that a local source contributes to the plutonium concentration. The plutonium isotopic ratios in this depth range do not clarify if a local source is present or not.

Above 18cm the concentration strongly increases and peaks at 10cm to over 5 Bq/kg. This clearly reveals the additional source. The start of the second source can also be seen by an increase of the $^{238}Pu/^{239,240}Pu$ to about 0.2. Between 18 cm and 12 cm the $^{240}Pu/^{239}Pu$ slowly increases from 0.17 to 0.185 and then strongly increases to values of 0.23 at 6 cm. The $^{241}Pu/^{239,240}Pu$ shows a steady increase that could also be attributed to a local source.

Comparing the concentration and the ratio data it becomes obvious that either one source of varying isotopic composition or more than one source of constant isotopic composition must be present. A varying isotopic composition can be seen in discharges from reprocessing plants, depending on the material being reprocessed. However, at the AEE Winfrith, research and development of different reactor types took place, which could also explain variations in isotopic composition. The two reprocessing plants that could have an impact are La Hague and Sellafield (Figure 5.4). A study of conservative radionuclides shows that the discharges from Sellafield are partly transported southwards along the east coast of Britain (Herrmann *et al*, 1995). A transport through the Channel to the South Coast of England is unlikely. However, an input from BNFL Sellafield will be considered for completeness. Discharges from COGEMA La Hague are mainly transported eastwards (of the more conservative radionuclides) in a near coastal plume and the observed westward transport is small (Herrmann *et al*, 1995). The plume reaches the waters at the South coast of England, but due to influx of Atlantic water it is questionable if the plume extents as far west as Poole Habour.

The start of the La Hague discharges corresponds well with the onset of a local source in the core. Also the peak in plutonium concentration covers about the same time period in the core as in the La Hague discharge. However, for the post 1980 period the $^{238}Pu/^{239,240}Pu$ and the $^{241}Pu/^{239,240}Pu$ are more than a factor 3 greater in the discharge than in the core. Therefore La Hague can be excluded as a major contributor.

Sellafield discharged plutonium since 1952. A major increase occurred in the second half of the 1960s and the discharges remained high throughout the 1970s and decreased in the 1980s. The time of high plutonium concentration in the core of about 15 years agrees well with the time period of high discharge from Sellafield. During the time of highest discharge from Sellafield the $^{238}Pu/^{239,240}Pu$ was between 0.2 and 0.25 that is in agreement with the values measured in the core. Due to measurements in cores close to Sellafield, also the $^{240}Pu/^{239}Pu$ in the core could be explained by the discharge. The isotopic ratio that excludes

Sellafield as the source for the high plutonium concentration in the core is the $^{241}Pu/^{239,240}Pu$. During the time of highest discharge the $^{241}Pu/^{239,240}Pu$ in the discharge was above 20, whereas the $^{241}Pu/^{239,240}Pu$ in the Poole Harbour core is well below 20 for the times of high plutonium concentrations (Figure 5.4 and 5.7).

The AEA Winfrith started discharging in 1964. The discharge records (Figure 5.8) contain only information about the total alpha activity and no information about the discharged plutonium and its isotopic composition exist. This makes the source attribution more difficult and only the plutonium concentration in the core could be useful assuming that the discharged plutonium activity is proportional to the reported total alpha activity. The core does not reflect details of the Winfrith discharge (Figure 5.8). In contrast to the four maxima seen in the discharge record, the core shows only one maximum. However, by using the model developed in Chapter 4, the plutonium concentration in the core can be linked to the alpha discharge from Winfrith (Figure 5.8). The model parameter are w=0.6, S=0.84 cm/year and a half life in the sediment of 12 years. The sedimentation rate agrees with ^{210}Pb dating of the core. It can be seen that the model results are in very good agreement with the measured concentration in the core from 1968 onwards. As described previously the higher concentrations in the core for the years prior to 1968 are due to fallout from weapons testing and are therefore not presented by the model. The model parameter w and the half life in the sediment are the same as for the transport from the Sellafield site (Chapter 4). These two parameters are the only ones that describe the transport from the site to the core. This suggests the plutonium from the AEA Winfrith behaves in a similar manner to that from Sellafield and a reservoir exist where the plutonium is mixed with previous years material.

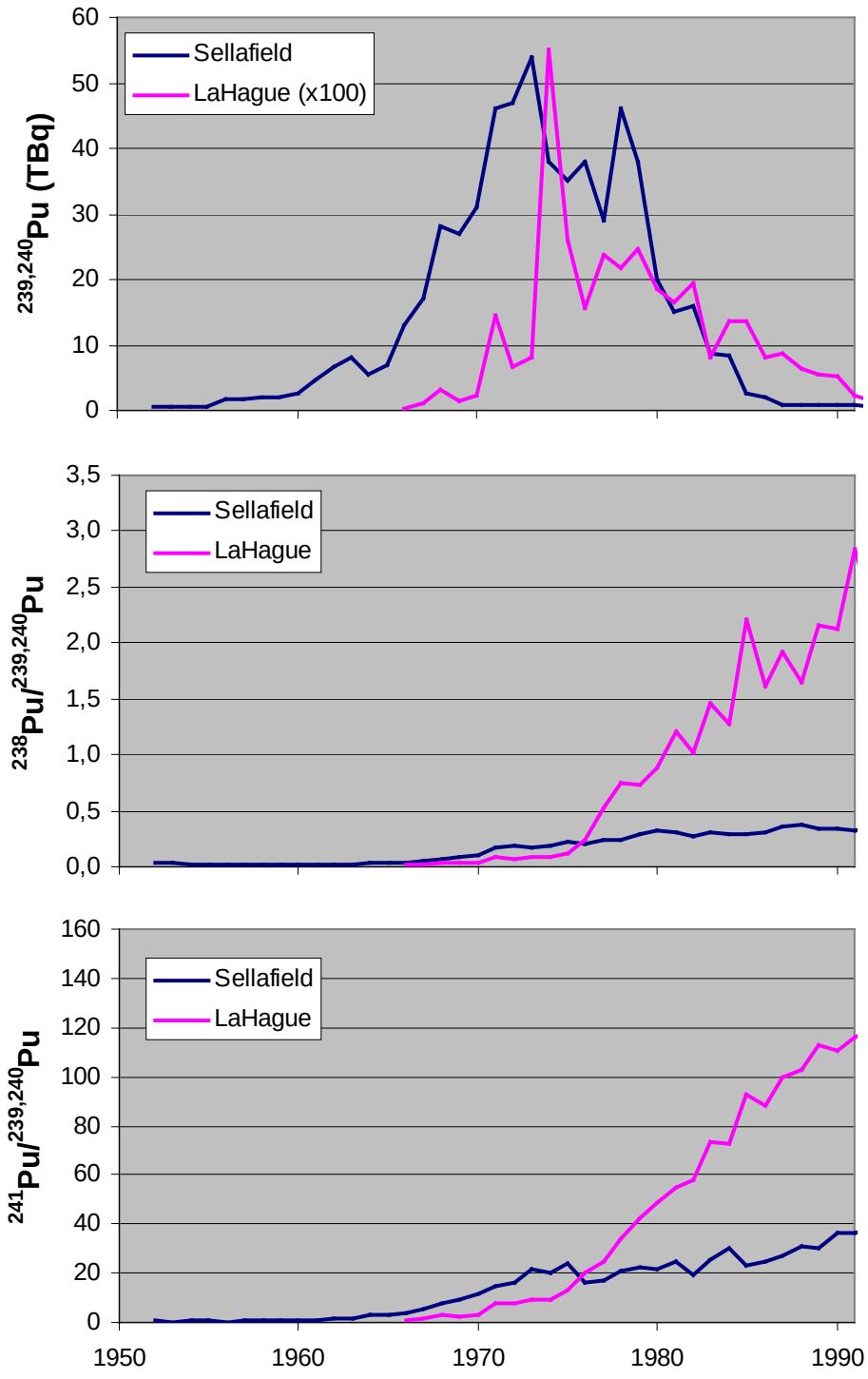

Figure 5.4 Plutonium in the discharge from COGEMA La Hague and BNFL Sellafield. (a) ^{239,240}Pu concentration (b) ^{238}Pu/^{239,240}Pu (c) ^{241}Pu/^{239,240}Pu (from Gray *et al*, 1995 and COGEMA La Hague, pers.com). All records are decay corrected to 1991.

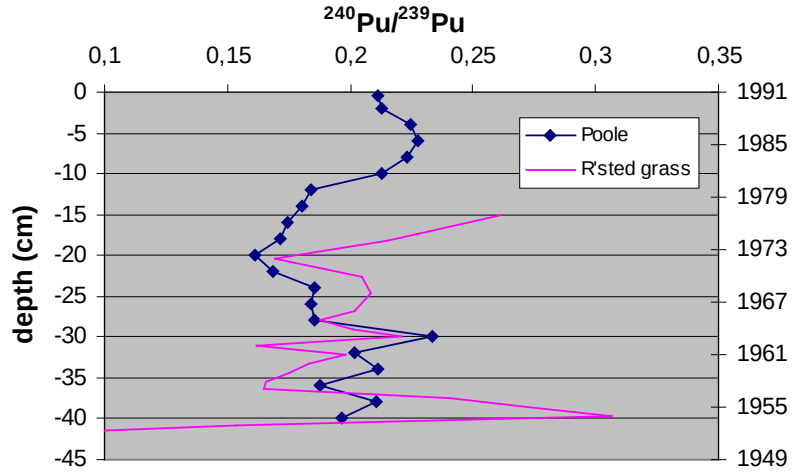

Figure 5.5 $^{240}Pu/^{239}Pu$ in the core from Poole Harbour

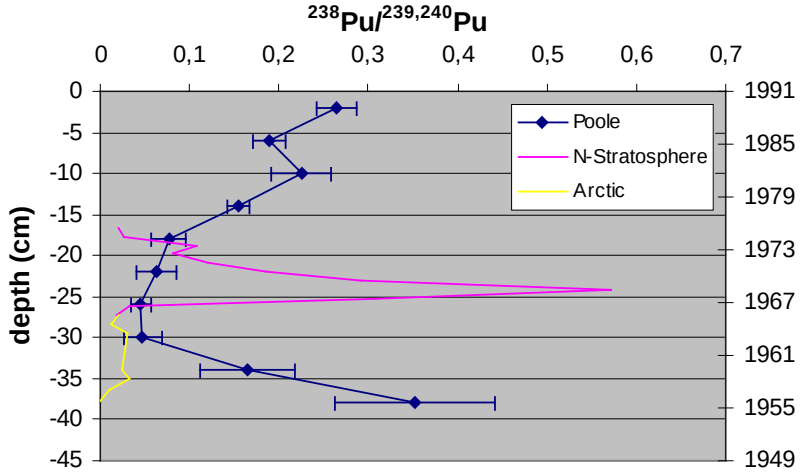

Figure 5.6 $^{238}Pu/^{239,240}Pu$ (decay corrected to 1991) in the core from Poole Harbour

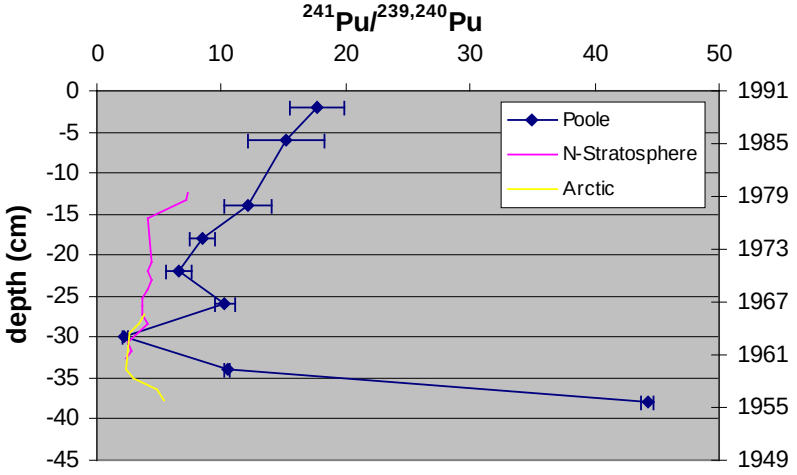

Figure 5.7 $^{241}Pu/^{239,240}Pu$ (decay corrected to 1991) in the core from Poole Harbour

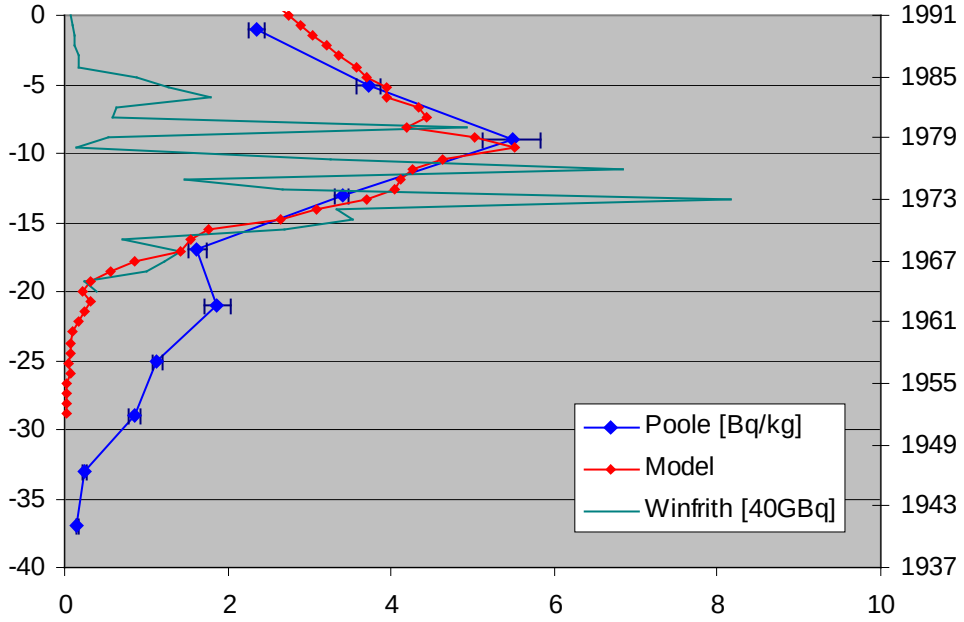

Figure 5.8 Measured ^{239,240}Pu concentration in the core (blue line), discharge of total alpha from AEE Winfrith (green line) and modelled concentration in the core (red line). The model parameters are w=0.6, S=0.84 cm/year, half life in the sediment:12 years

5.4. Conclusions

In the pre-1970 period the plutonium in a sediment core from Poole Harbour can be linked to atmospheric fallout via the ^{240}Pu/^{239}Pu. It should especially be noted that the ^{240}Pu/^{239}Pu in the core shows evidence of tropospheric fallout from the Nevada tests in the early 1950s. The ^{238}Pu/^{239,240}Pu and the ^{241}Pu/^{239,240}Pu in the pre-1970 period cannot always be attributed to the existing data of weapons fallout. Sediment accumulation rates inferred from radionuclides introduced by global weapons fallout (^{137}Cs, ^{241}Am, ^{239,240}Pu and ^{240}Pu/^{239}Pu) are similar. The sediment accumulation rate determined by ^{210}Pb is about 20% lower. In the post-1970 period the core reveals a local source of plutonium. The reprocessing plants Sellafield and La Hague can be excluded by the isotopic composition of the plutonium. Allowing mixing with previous years material, the plutonium in the core can be attributed to the Atomic Energy Establishment at Winfrith in Dorset, which is approximately 20 km west of Poole Harbour.

CHAPTER 6

6. Application III: Distribution of U and Pu from AWE Aldermaston and Burghfield

6.1. Introduction

This PhD project was funded as part of a 3-year research programme to examine the amount and distribution of U and Pu around the two UK weapons factories AWE Aldermaston and AWE Burghfield. The survey was recommended after small amounts of uranium and plutonium contamination around the two sites had been detected during a survey around the former USAF Greenham Common airbase and surrounding areas (Croudace *et al*. 2000). The results of the survey have been published in 3 reports (Croudace *et al*, 1999, 2000, 2001) on behalf of AWE.

- In the first part of this chapter an aerial dispersion model is presented and the predicted deposition pattern is discussed.
- The second part presents the results from the ground survey with the focus being on plutonium and uses selected results from the reports for the individual years. It also discusses the depth distribution of plutonium.
- In the last part of this chapter the observed contamination pattern is discussed.

6.2. The discharges from AWE Aldermaston

Figure 6.1 shows the annual discharge of plutonium and uranium from the AWE Aldermaston. The total discharge between 1952 and 1998 is 2131.2MBq for uranium and 86.9MBq for plutonium. Depending on the isotopic composition the total discharged mass of uranium is between 29kg-168kg and only 0.03g for plutonium. Approximately 80% of the total uranium and about 60% of the total plutonium were discharged prior 1970. Up to 1980 97% of the total uranium and about 93% of the total plutonium had been discharged. In the last 10 years (until 1998 where the first sampling took place) only 1.6% of the total plutonium and 0.07% of the total uranium had been discharged.

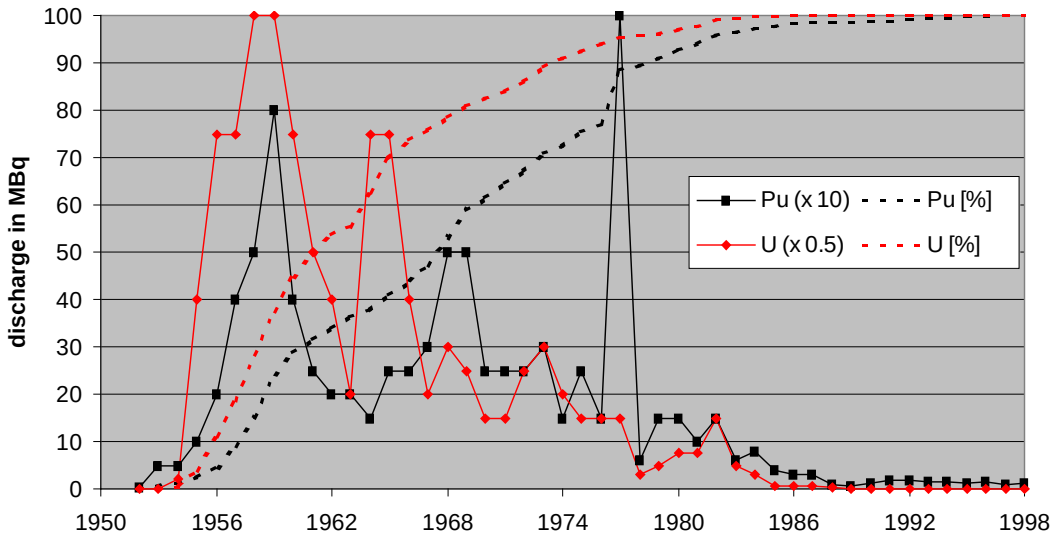

Figure 6.1 Aerial Discharge from AWE Aldermaston. The continuous black line shows the Pu discharge multiplied by 10 and the red line the uranium discharge divided by 2. The dotted lines show the cumulative percentage of the total discharge (from COMARE, 1989, AWE, 1990, 1992, 1995, 1998)

	Isotopic composition	Mass of 1MBq (g)
Uranium	Natural ($^{238}U/^{235}U$=137.88)	78
	Enriched ($^{238}U/^{235}U$=0.07)	14
	Depleted ($^{238}U/^{235}U$=250-500)	79-80
Plutonium	Fallout ($^{240}Pu/^{239}Pu$=0.18)	0.0003
	Weapons grade ($^{240}Pu/^{239}Pu$=0.05)	0.0004

Table 6.1 Mass equivalents of 1MBq for different isotopic compositions

6.3. Results from the dispersion model

The dispersion model is described in Appendix A.8 and the results are presented below. The figures show the deposition density from washout (WO) in Bq/m^2 and surface air concentration (SAC) in Bq/m^3. Both WO and SAC are the integrated values over the time period from 1952-1998. The integrated dry deposition density can be obtained by multiplying the SAC by 5.4m (see A.8). Discharge records are published on a yearly basis by AWE and in this study a continuous discharge is assumed for the calculation during each year. This is the most correct assumption that can be made using the available discharge

data, but even if the discharge is not continuous during the year, the calculated dispersion still represents a dispersion probability.

6.3.1 Modelled angular distribution of AWE discharge fallout

The angular distribution of the surface air concentration (SAC) and the washout ground concentration (WO) is studied on a circle at a distance of 1000m from the source. Because the Meteorological-Office data are given in steps of ten degrees similar steps are chosen for the calculations. Smaller steps could result in apparent fluctuations due to insufficient angular information from the Meteorological-Office data and larger steps would leave out information. Differences between the angular distribution of Pu and U could occur because of differences in the annual discharge, e.g. years of high U discharge do not necessarily correspond to high Pu discharge. However, the differences appear to be very small (Figure 6.2 and Figure 6.3). Both, SAC and WO, suggest a high deposition in a north-eastern direction. The general WO-maximum is not as broad as the SAC maximum and extends further north and the SAC maximum further east. If dry deposition is more important the expected deposition extends further east and if the washout is more important the expected deposition is shifted in a northerly direction.

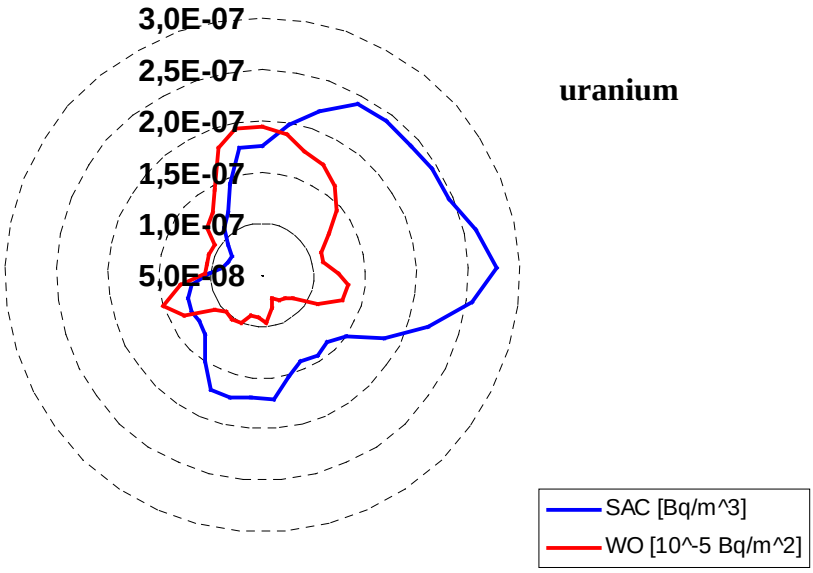

Figure 6.2 Angular distribution of uranium surface air concentration (SAC) and uranium wash-out (WO) at a distance of 1km

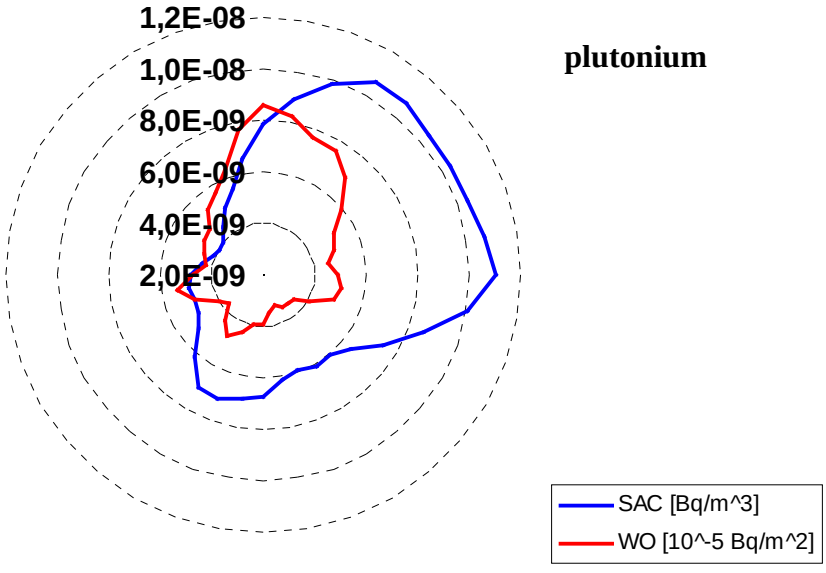

Figure 6.3 Angular distribution of plutonium surface air concentration (SAC) and plutonium wash-out (WO) at a distance of 1km

6.3.2 Modelled lateral distribution of AWE discharge fallout

As discussed above the model does not incorporate calm conditions. For this reason the calculated concentration close to the source is incorrect. However, it is interesting to discuss the variation of the concentration close to the source, because it gives an insight to the distribution if a wind is present. The SAC at the ground (Figure 6.4) shows a maximum at 200m and the Pu-washout has its highest value directly at the source. This behaviour can be explained by the development of the plume. The horizontal spreading of the plume leads to a decreasing concentration with distance. As the plume spreads vertically it gradually reaches the ground, which explains the low SAC close to the source. The washout only depends on the total amount of material in a particular vertical column of air and is independent of the vertical extent.

Soil sampling in the AWE survey was carried out using a radial grid with distances of 1,2,3,4 and 5km and therefore the modelled fallout in this range is particular interesting. The SAC of uranium drops by a factor 20 between 1000 and 5000m and the WO only by a factor 5 (Figure 6.6). For Pu the behaviour with distance is the same than in the case of U. This is not trivial, because the distance behaviour depends also on the wind velocities.

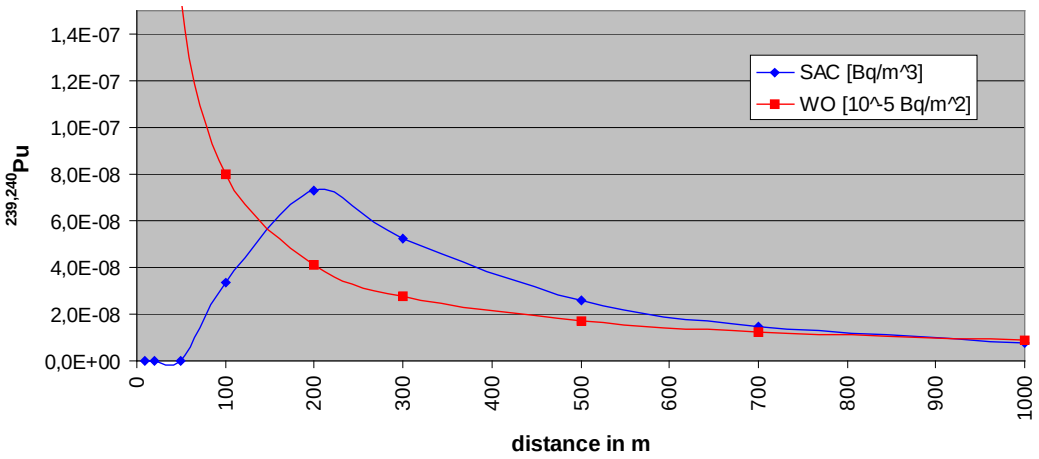

Figure 6.4 Lateral distribution of plutonium surface air concentration (SAC) and plutonium wash-out (WO) in northern direction for the first km

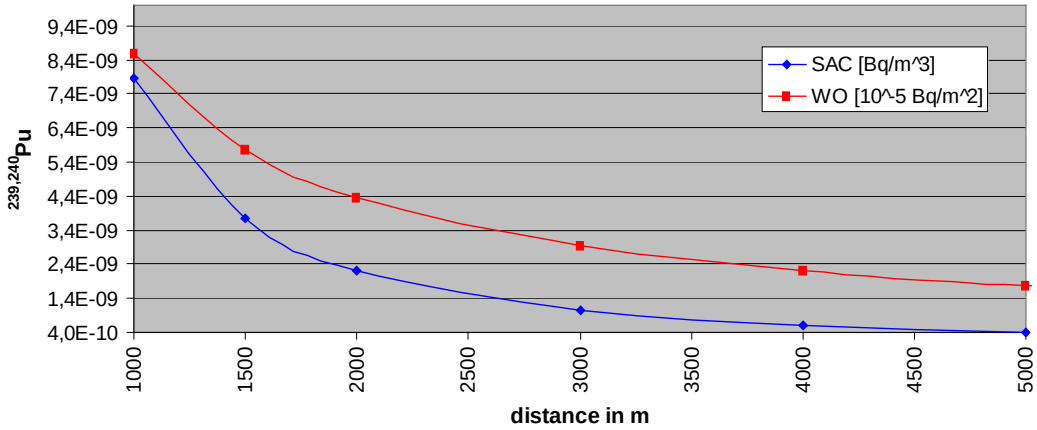

Figure 6.5 Lateral distribution of plutonium SAC and WO in northern direction for 1km – 5km

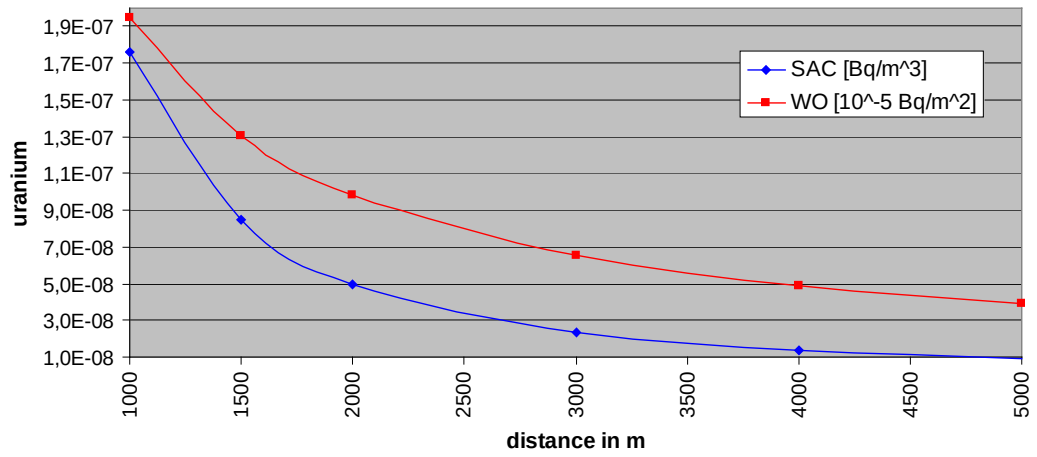

Figure 6.6 Lateral distribution of uranium SAC and WO in northern direction for 1–5km

6.3.3 Implications of the dispersion to the AWE survey results (Appendix A10)

For the survey it is important to see what the impact of the modelled SAC and WO would have on the uranium and plutonium in the soils.

Assumptions:

- A generalised natural uranium concentration of 1.6ppm is assumed. The natural $^{238}U/^{235}U$ ratio is 137.88. Since the discharged material is a mixture of enriched and depleted uranium of unknown composition, the extreme cases of only enriched discharge and only depleted discharge are investigated. A $^{238}U/^{235}U$ of 285 for depleted and a ratio of 0.07 for enriched uranium is assumed.
- A generalised plutonium concentration from weapons' fallout in the soils of 1Bq/kg is assumed. The assumed $^{240}Pu/^{239}Pu$ for weapon fallout is 0.18 and 0.075 for the discharged Pu.

Results:

For both uranium and plutonium the change in concentration and ratio in the soil is investigated for the highest values of dry deposition and washout at a distance of 1000m from the stack. The dry deposited uranium (enriched or depleted) increases the concentration in the soil sample by about 10^{-10}ppm and the ratio is affected only in the sixth decimal place. The effect of the washout deposition on concentration and ratio is even lower. Plutonium soil concentrations change by about 10^{-9} Bq/kg and the ratio is affected only in the 10^{th} decimal place. Such small would not be detectable. Therefore all the anomalies discovered in the soil are in clear contrast to the dispersion modelling using the discharge records.

6.4. The environmental monitoring survey around AWE Aldermaston and AWE Burghfield

The first sampling phase involved sample collection dominantly from woodland sites. Woodland was chosen as potentially the most sensitive environment where airborne particulates, derived from the AWE sites and elsewhere, might preferentially concentrate due to falling wind velocities. Subsequent sampling consisted of four radial networks centred at AWE(A), AWE(B), a control site (near Marlborough) and another at Hungerford. Soils were sub-sampled by collecting fractions normally at 5 cm depth intervals. The collected samples were investigated for plutonium concentration by alpha spectrometry and $^{238}U/^{235}U$ and $^{240}Pu/^{239}Pu$ by mass spectrometry.

6.4.1 Depth distribution of plutonium

The mobility of plutonium in soil depends on its chemical form. Different chemical forms in weapons fallout or chemical differences between weapons fallout and AWE derived plutonium might result in different downward-migration velocities.

Pu concentration

The percentage of ^{239,240}Pu in the first 3 soil layers (0-5 cm, 5-10 cm, 10-15cm) assuming that these 3 layers contain all the deposited plutonium is shown in Figure 6.7. The percentage of ^{239,240}Pu in the first 2 layers (0-5 cm, 5-10 cm) assuming that all the deposited plutonium is in these 2 layers is shown in Figure 6.8. The anomalous samples are characterised by a deviation of the ^{238}U/^{235}U from the natural value of 137.88. The reason for using this criterion is the limited number of samples investigated for ^{240}Pu/^{239}Pu. However, a deviation from the natural uranium ratio indicates AWE derived uranium contamination and therefore these samples are the most likely ones to have plutonium contamination. From the figures it can be seen that the standard deviations (error bars) of the percentages are great. The reason is probably that the downward migration depends on the soil type. Detailed information about the soil type was not recorded. However, a general trend can also be seen from the distributions over all samples. The percentage of plutonium is approximately evenly distributed over the three layers, with the third layer containing slightly less than the first ones. Within the errors no difference in downward migration between the natural and the anomalous samples can be seen.

For an initial assumption all plutonium is considered to be derived from weapons' fallout and deposited in 1963 and all of that plutonium resides in the investigated layers, the half-life in the top layer has been calculated for all samples where 3 layers have been investigated using

$$C_1 = C_0 \exp(-\lambda_1 t) \Leftrightarrow \lambda_1 = -\frac{1}{t}\ln\left(\frac{C_1}{C_0}\right)$$

where

C_1 = percentage of plutonium in layer 1

$\lambda_i = \ln 2/t_{1/2,i}$ where $t_{1/2,i}$ is the half-life in layer i

C_0=C(t=1963)=100

The percentage of samples *vs* half lives in the top layer is shown in Figure 6.9. The half life has been calculated for each sample individually and after that the percentages are determined. In this way differences in downward migration depending on soil type can be detected from the plot. Though the soil types were very variable almost 80% of the samples with a natural $^{238}U/^{235}U$ show half-lives between 10 and 30 years, with almost 50% of all samples having half-lives between 20 and 30 years. Less than 5% of all natural samples show half-lives of less than 10 years. These small half-lives could be attributed to a top layer that has a small capacity for plutonium. Also the majority of anomalous samples have half-lives between 10-30 years. The percentage with half-lives of less than 10 years is higher. This could be due to a plutonium component of a different chemical form, possibly AWE derived, or to a higher percentage of soils with a small capacity for plutonium in the top layer. Another difference is that half-lives above 60 years are dominated by anomalous samples. A higher half-life could be due to the following reasons or a combination of them:

- high capacity for plutonium of the top layer: most of the plutonium stays in this layer and has not reached the layers beneath
- very low capacity of layer 2 and layer3: the plutonium that has passed layer 1 drops through layer 2 and layer 3 and resides at greater depths.
- the plutonium was deposited after 1963: the calculation results in a apparently high half life

Therefore it is likely that the third point is the explanation for the observation that the half-lives above 60 years are dominated by anomalous samples.

$^{240}Pu/^{239}Pu$

As mentioned previously the number of samples investigated for the $^{240}Pu/^{239}Pu$ is much smaller than the number investigated for the plutonium concentration. Therefore a statistical treatment is less reliable. However, for the samples where no contamination is expected, it is interesting to look at the distribution of the $^{240}Pu/^{239}Pu$ for the different layers (Figure 6.10). The samples include control site samples and samples from the Burghfield area that show neither an anomalous plutonium concentration nor an anomalous $^{238}U/^{235}U$. The numbers of samples used in Figure 6.10 are: 18 for the first layer, 5 for the second and just two for the third layer. The error bars represent the standard deviation. The average $^{240}Pu/^{239}Pu$ is around 0.18 for all three layers. Therefore no differences in migration velocities due to chemical differences of weapons fallout could be detected.

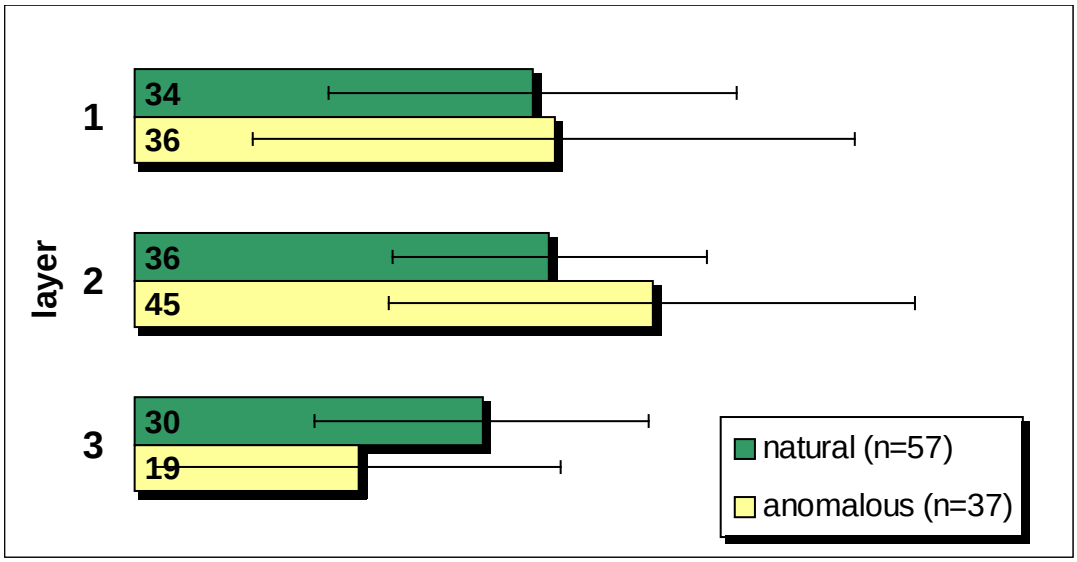

Figure 6.7 Percentage of ^{239,240}Pu in the first 3 layers (0-5 cm, 5-10 cm, 10-15cm) assuming that these 3 layers contain all the deposited plutonium. The anomalous samples are characterised by a deviation of the ^{238}U/^{235}U from the natural value of 137.88.

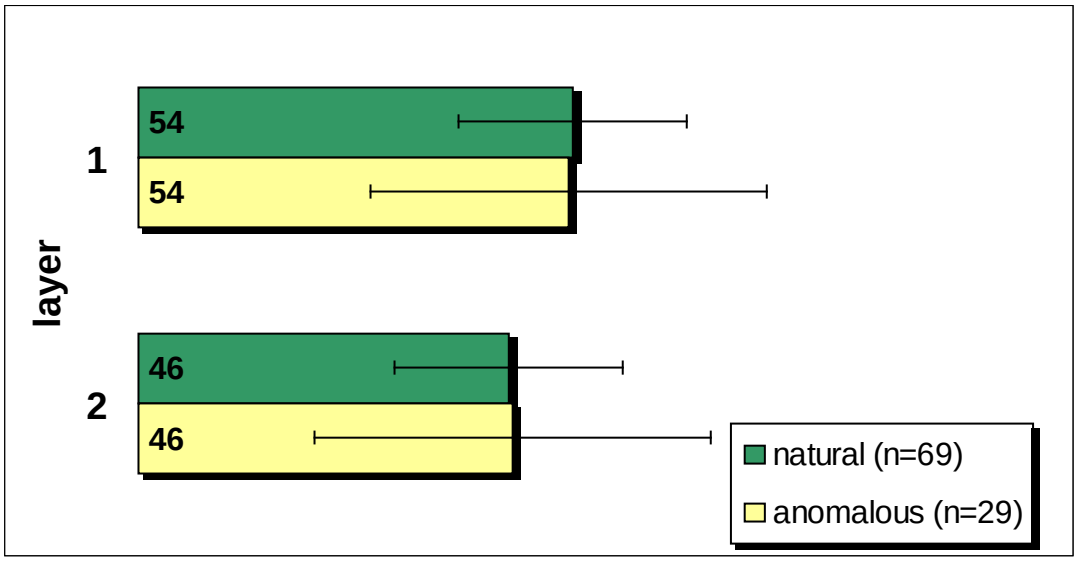

Figure 6.8 Percentage of ^{239,240}Pu in the first 2 layers (0-5 cm, 5-10 cm) assuming that these 2 layers contain all the deposited plutonium. The anomalous samples are characterised by a deviation of the ^{238}U/^{235}U from the natural value of 137.88.

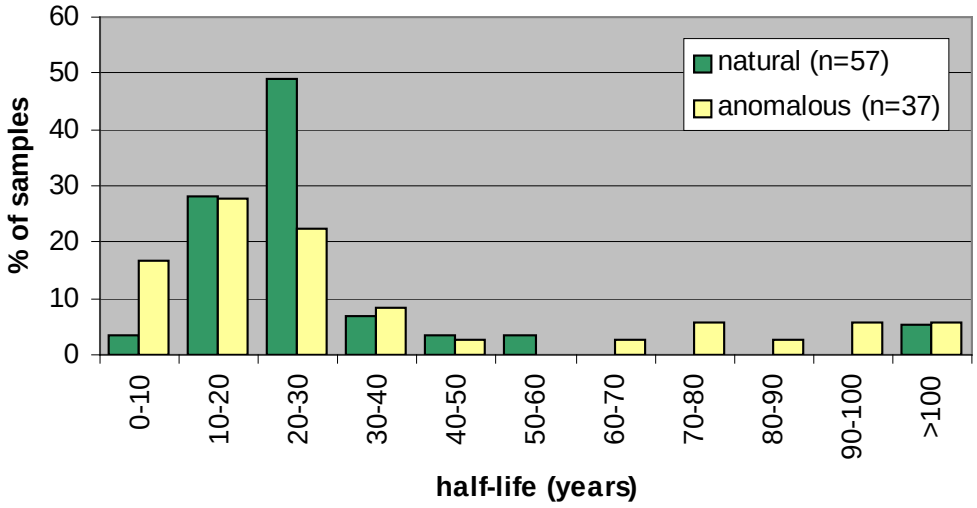

Figure 6.9 Half life of ^{239,240}Pu in the first layer (0-5 cm). The plot includes samples from all locations where 3 layers were sampled (same samples as in Figure 6.7). The anomalous samples are characterised by a deviation of the ^{238}U/^{235}U from the natural value of 137.88.

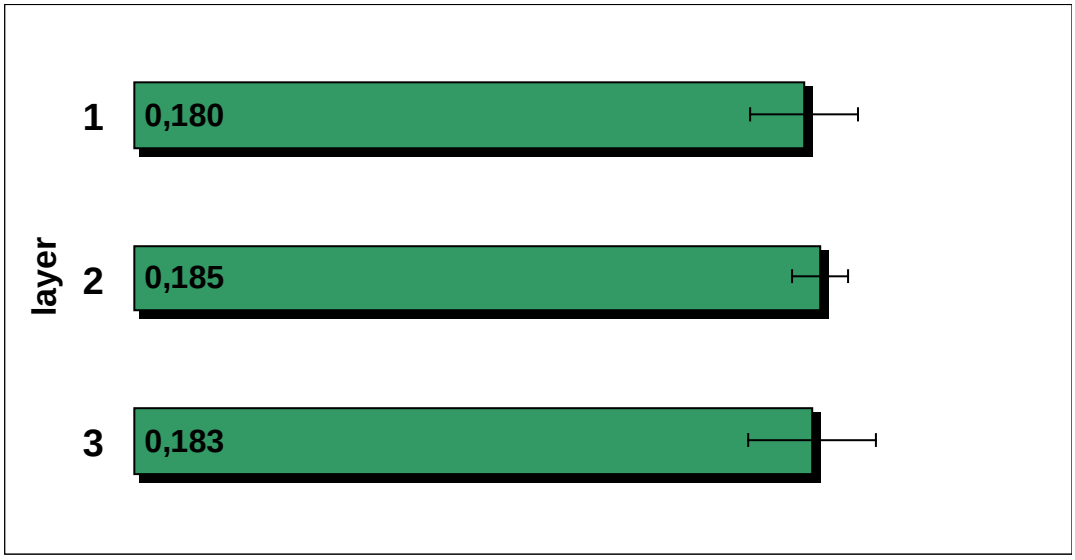

Figure 6.10 Depth distribution of the ^{240}Pu/^{239}Pu for non-contaminated sites. The numbers of samples used are: 18 for the first layer, 5 for the second and 2 for the third layer.

6.4.2 Contamination around the AWE sites

The main results from the survey are presented in the maps (Figure 6.11 – 6.13). For each location only the greatest $^{238}U/^{235}U$ deviation, the lowest $^{240}Pu/^{239}Pu$ and highest plutonium-concentration out of the investigated layers is shown. The selection of samples for $^{240}Pu/^{239}Pu$ analysis was based mainly on having an anomalous $^{238}U/^{235}U$ and an elevated plutonium concentration. After these criteria further samples were selected over the whole sampling area so that there was a good geographical coverage. All samples analysed for a particular isotope ratio or activity concentration are plotted on each map and only anomalous data are colour coded.

Control sites

The plutonium concentration in the control area soils varies between 0.1 Bq/kg and 2 Bq/kg. Exceptions are samples CG3/1 with 10.9 Bq/kg and IT1/2-2 with 4.5 Bq/kg. The sample CG3/1 was investigated for its $^{240}Pu/^{239}Pu$, showing a ratio typical for fallout from weapons testing. The high concentration could not be verified for a sample taken one year later at the same location. The sample IT1/2-2 has not been re-sampled. Contamination or error in sample handling cannot be excluded. However, it should be kept in mind that under special circumstances a plutonium concentration as high as 11Bq/kg could be possible in areas with no local source of contamination. The $^{240}Pu/^{239}Pu$ at the control sites varies between 0.16 and 0.20 (Figure 6.14). The only exception is the sample IG3 that shows a $^{240}Pu/^{239}Pu$ of 0.11 in the first layer. The reason for this small ratio remains unclear. The sample was reanalysed and gave the same result. No anomalous $^{238}U/^{235}U$ was detected. A correlation between plutonium concentration and $^{240}Pu/^{239}Pu$ cannot be seen.

Spatial pattern of contamination

AWE Aldermaston

West of AWE Aldermaston: The main contamination is confined to a small area close to the west boundary of the site. In this area the number of enriched uranium samples clearly dominates over the number of depleted uranium samples. Plutonium concentrations of up to 12 Bq/kg and $^{240}Pu/^{239}Pu$ as low as 0.07 are found in this area. Some of the samples with relatively high plutonium concentration and strong deviation from the $^{238}U/^{235}U$ show weapons fallout ratios (Figure 6.15).

North-west of AWE(A): No contamination has been found.

North of AWE(A): Some samples close to the boundary of the site show slightly depleted uranium and slightly low $^{240}Pu/^{239}Pu$.

North-east of AWE(A): Contamination has been found in two woodland sites, one about 0.5km away from the site and the other one about 1.5km away. The maximal spatial extent of contamination in this direction is about 2.5km, which includes depleted uranium and elevated plutonium concentrations. Though the plutonium concentrations are up to 11Bq/kg, no deviation from the fallout ratio could be detected.

East of AWE(A): Contamination is found in a woodland area adjacent to the eastern boundary of the AWE site. Contamination in this area consists of depleted uranium and high plutonium concentrations. As for the other contaminated areas, only some of the samples of high plutonium concentration show a deviation from the weapons fallout $^{240}Pu/^{239}Pu$.

South-east of AWE(A): Contamination is found in a woodland about 1km away from the AWE boundary, characterised by deviations from the $^{238}U/^{235}U$.

South and south-west of AWE(A): Small depletions in the $^{238}U/^{235}U$ are found within 1km distance from the site.

AWE Burghfield

Published discharge records for AWE Burghfield do not include any plutonium or uranium. However, **north and north-east** of the site only anomalous $^{238}U/^{235}U$ has been detected for some samples. The locations of these samples are up to 2km away from the boundary of the AWE Burghfield.

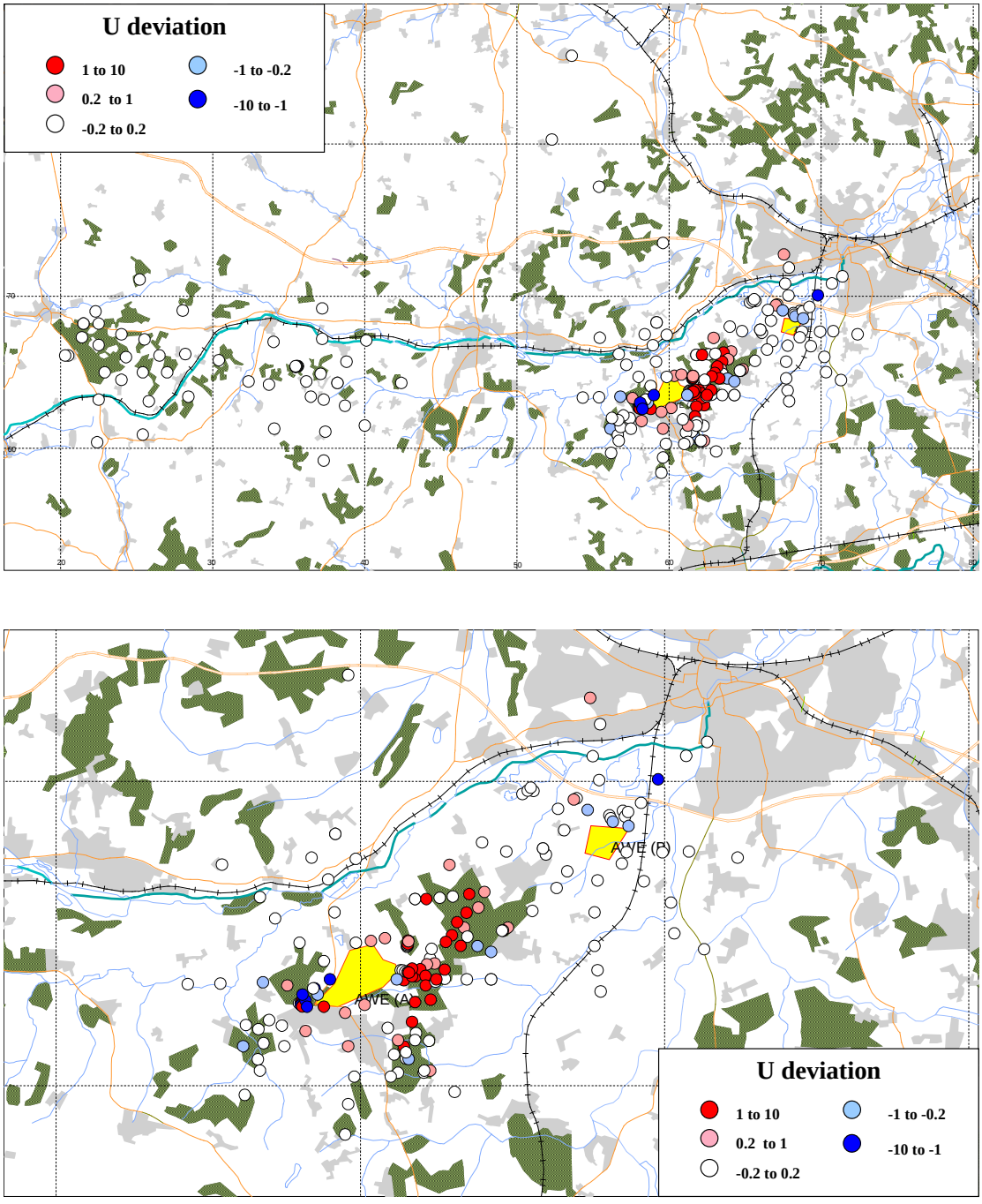

Figure 6.11 Deviation from the natural $^{238}U/^{235}U$ around the AWE sites. The deviation is defined as $[(^{238}U/^{235}U)_{measured} - 137.88]$

Negative values indicate contamination by enriched uranium; Positive values indicate contamination by depleted uranium.

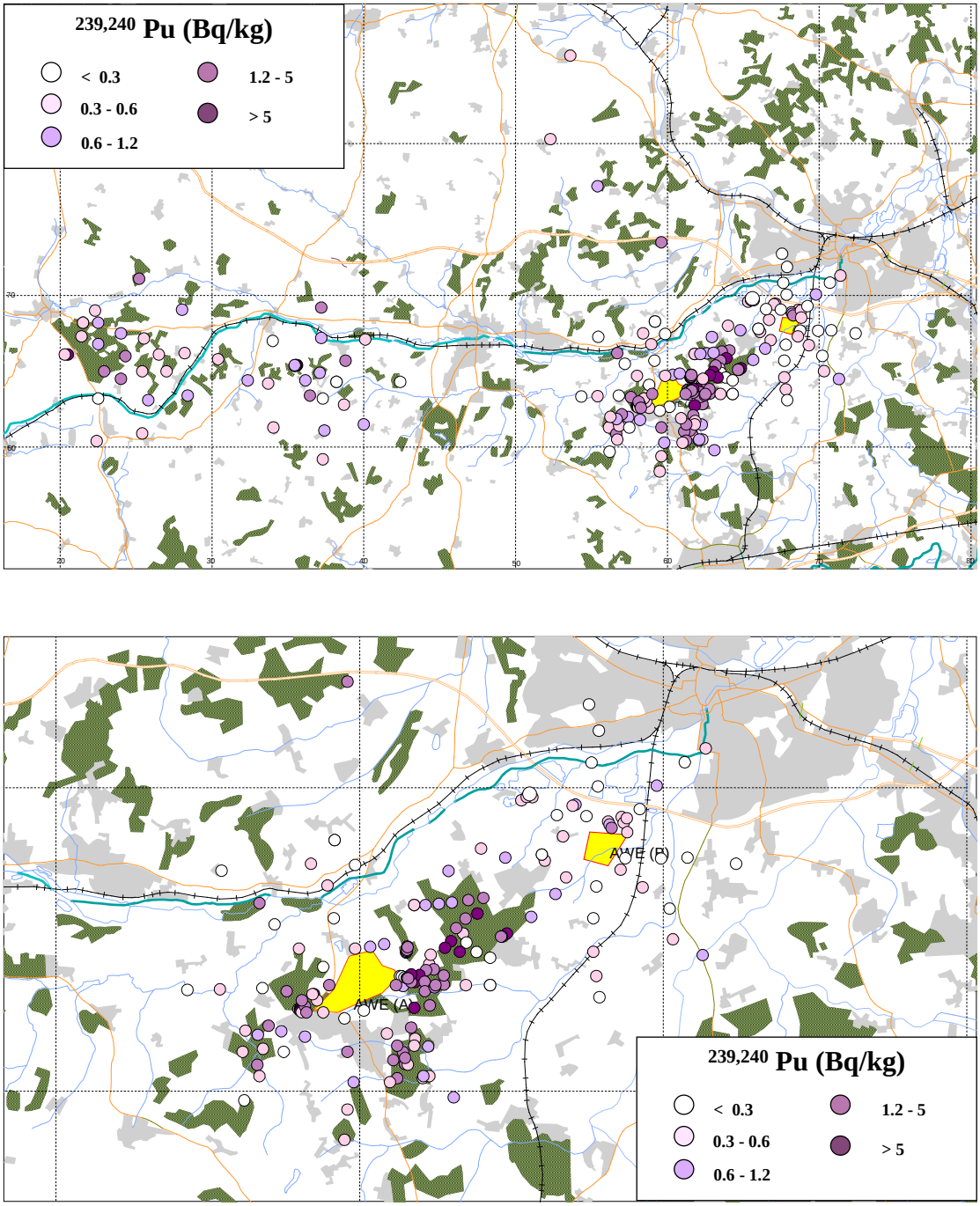

Figure 6.12 ^{239,240}Pu concentration around the AWE sites.

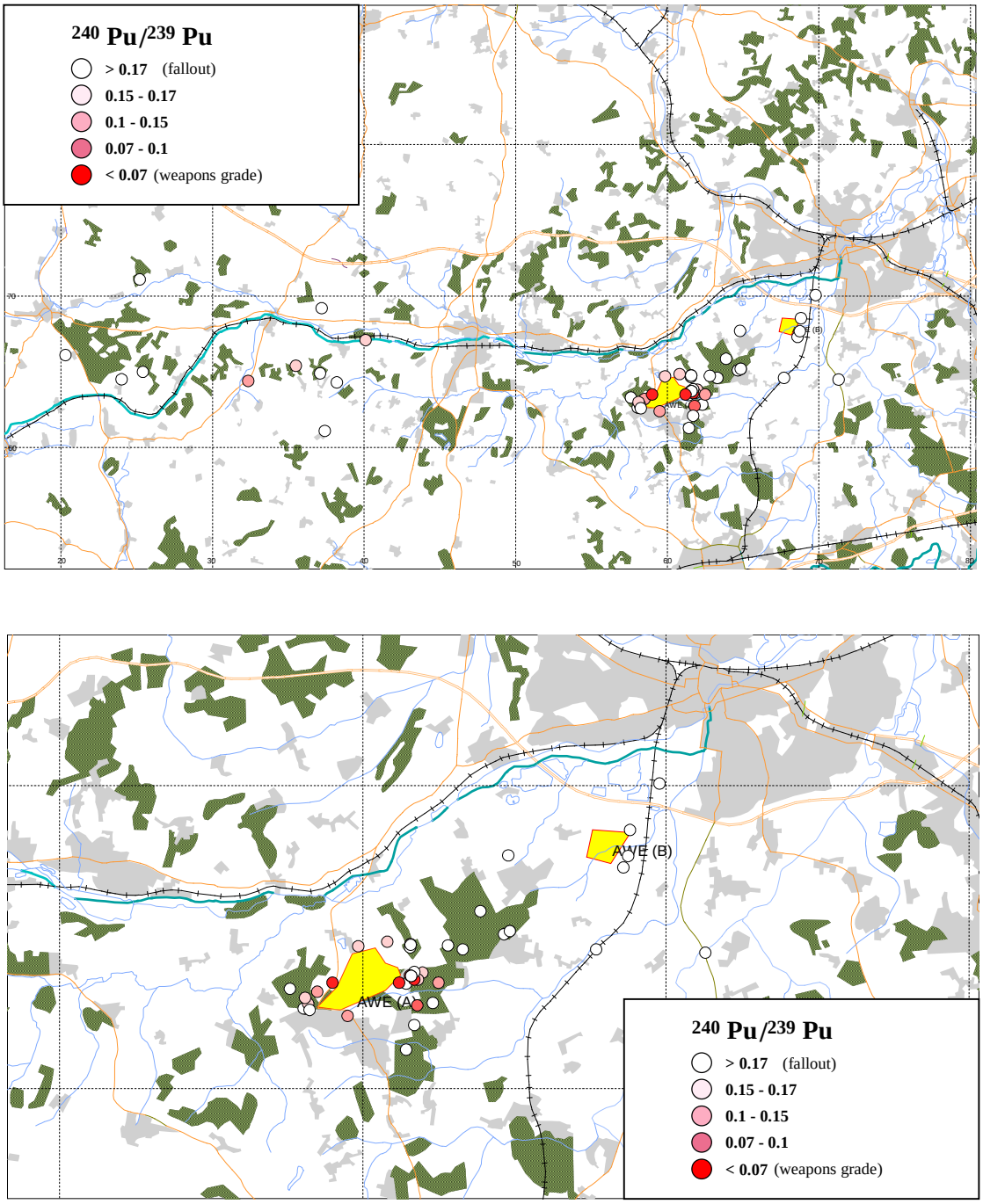

Figure 6.13 $^{240}Pu/^{239}Pu$ around the AWE sites from the AWE survey.

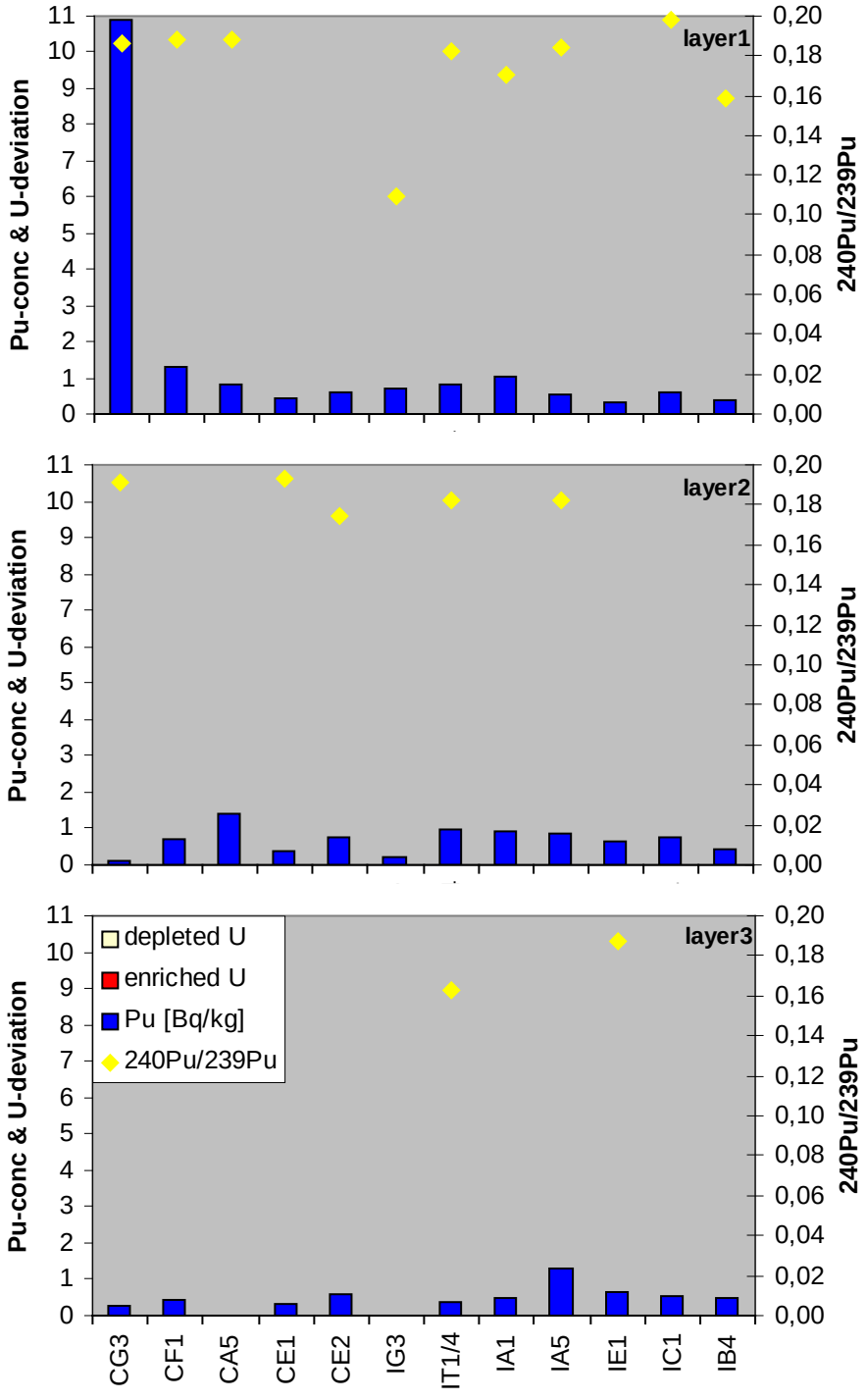

Figure 6.14 $^{240}Pu/^{239}Pu$, $^{239,240}Pu$ and deviation of the $^{238}U/^{235}U$ for Control site samples (all samples that have been investigated for $^{240}Pu/^{239}Pu$ for at least one layer) Any difference from the natural $^{238}U/^{235}U$ of 137.88 is shown as bars stacked on the plutonium bars.

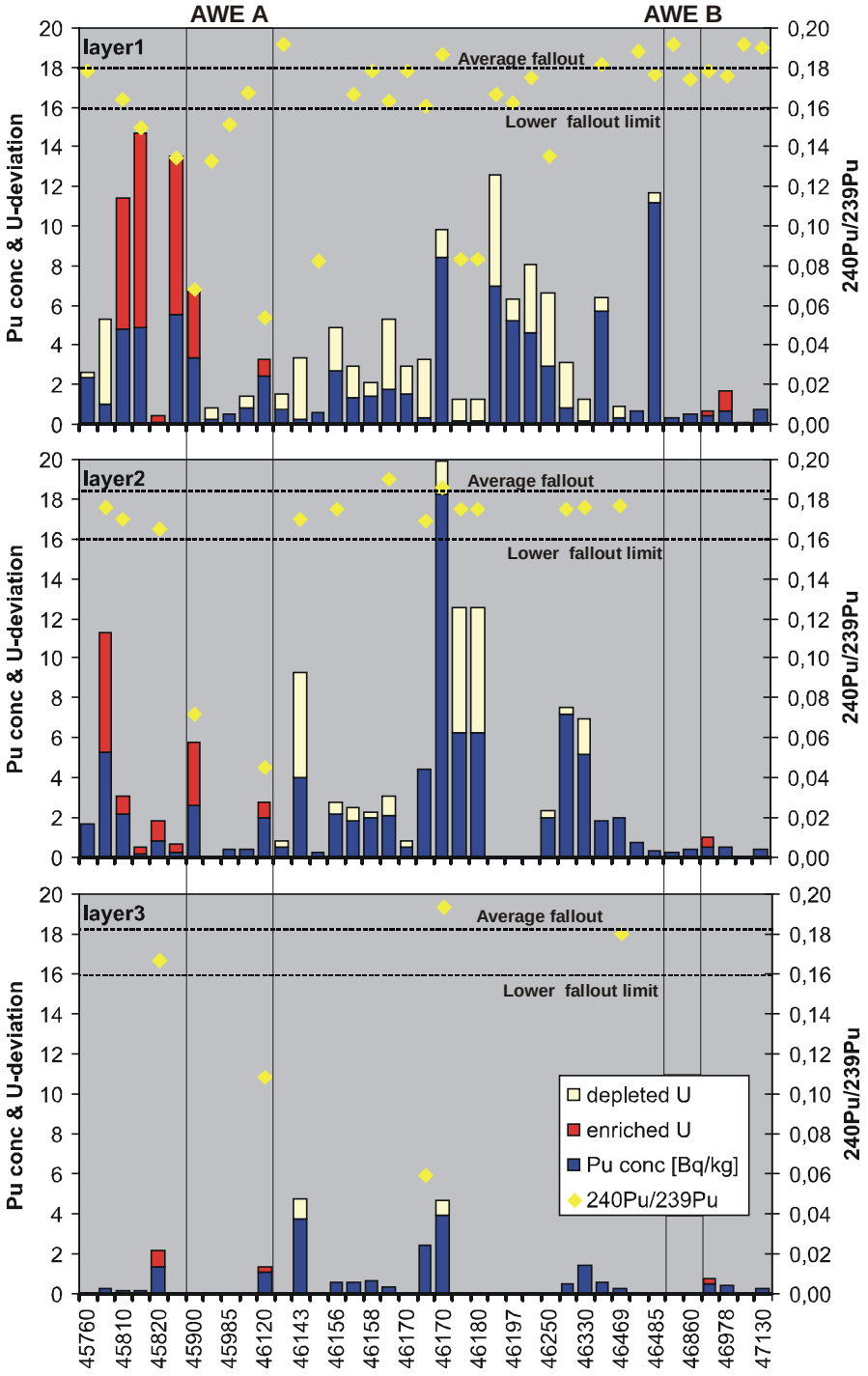

Figure 6.15 ^{240}Pu/^{239}Pu, ^{239,240}Pu and deviation of the ^{238}U/^{235}U for samples around the AWE sites. (all samples that have been investigated for ^{240}Pu/^{239}Pu for at least one layer) The samples are ordered by their eastings (west left and east right). The locations of the AWE sites is shown by two vertical lines for each sites. Samples to the left (right) of these lines are west (east) of the sites. Samples within the two lines are taken north or south of the sites. The lower limit for the ^{240}Pu/^{239}Pu in fallout from weapons testing is chosen to be 0.16. This represents the minimum found in control site samples (ignoring sample IG3). Any difference from the natural ^{238}U/^{235}U of 137.88 is shown as bars stacked on the plutonium bars.

6.5. Discussion of the observed contamination pattern

1. The highest spatial extent of the contamination is found to the eastern and north-eastern side of the site. Another 'hot-spot' of contamination is found at the west-boundary of the site.

The highest contamination towards the east and north-east can also be seen in the SAC of the model (Figure 6.2 and Figure 6.3). The lack of detected contamination between the north-west and north agrees well with the minimum in modelled SAC and WO in north-western direction. The 'hot-spot' at the western boundary of the site cannot be explained by the model. Besides that the contamination at the western boundary deviates from the contamination in other directions.(see 4.). This suggests that the contamination at the west-boundary is due to special circumstances, for example:

- the discharge of enriched uranium occurs close to the west-boundary and the one for depleted uranium at a greater distance from the west-boundary.
- the contamination is due to a single discharge event (possibly accidental or unintended) that occurred during an easterly wind
- the transport to this area is different from the other areas, e.g. by surface-water run-off or flooding

The fact that the measured contamination pattern agrees better with the modelled SAC than with the modelled WO suggest that dry deposition is more important. This is expected from the model, that predicts a 10^5-times higher dry deposition.

2. Contamination is only detected at distances of less than 2.5 km from the boundary of the site.

As discussed in 6.2.3 the modelled deposition does not result in measurable contamination. Ignoring the magnitude of contamination, the SAC is 4 times lower at 2.5km than at 1km and the WO drops by a factor 2 of over the same distance. The differences between 1km and 5km are a factor 20 for the SAC and a factor 5 for the washout. Therefore it is not surprising that the contamination is confined to a small area around the site.

3. Contamination around AWE Aldermaston is found in woodlands or at sites adjacent to woodlands.

Woodlands slow the air down and the wind starts effectively above the top of the trees. Besides that re-distribution of material deposited in woodlands is unlikely. These two reasons lead to an increased deposition in woodlands. It is remarkable that the contamination around AWE Aldermaston is found almost exclusively in woodlands. The pattern suggests that woodlands act like a filter for the contamination. This behaviour is best demonstrated in the direction of highest SAC: Towards the east and north-east a contamination of the same magnitude is expected from the SAC (Figure 6.2 and 6.3). In an easterly direction anomalies are found only in a woodland adjacent within 1 km of the boundary of the site and east of this woodland no further anomalies are detected. In a north-eastern direction the contamination is also mainly found in woodland sites. However, the woodlands in this wind-direction are further away from the site, which results in a greater spatial extent of the contamination of up to 2.5km away from the site boundary.

4. The majority of samples showing a deviation from the natural $^{238}U/^{235}U$ are depleted in ^{235}U. Sample sites where enriched and depleted U are found are rare. The only area around AWE Aldermaston showing predominantly enriched uranium is close to the western boundary of the site.

The dominance of depleted samples suggests that more ^{238}U (in comparison to natural uranium) is discharged than ^{235}U. The area at the west boundary, showing predominantly enriched uranium does not fit into the general pattern. Possible reasons are given in 1. The fact that some samples (exceptions) are enriched at the east boundary, an area characterised by depleted samples, could be explained by a small discharge of enriched uranium. A small discharge of enriched uranium could be masked by depleted uranium at most of the locations of favoured deposition. Special circumstances, e.g. meteorological conditions or plant growth might slightly change the locations of favoured deposition. If this change occurs between enriched or depleted discharge the enriched samples at the east boundary could be explained.

5. **Samples showing a deviation from the natural $^{238}U/^{235}U$ have often have a high plutonium concentration. However, the $^{240}Pu/^{239}Pu$ of those samples often show ratios typical of weapons fallout. Only a small number of samples show low ratios that are likely to be AWE-derived plutonium.**

It is likely that AWE derived uranium is found at the same locations as AWE-derived plutonium. The reason is that both radionuclides are transported via the air and areas of deposition are sinks for particles. Slight changes might occur due to different meteorological conditions between uranium and plutonium discharge, but the general contamination pattern should be the same. Samples having significant uranium anomalies often show a high concentration of plutonium. Only some of these samples show a $^{240}Pu/^{239}Pu$ attributed to AWE-derived contamination. This suggests that the AWE discharges not only consisted of weapons-grade plutonium but also of plutonium with a higher $^{240}Pu/^{239}Pu$.

6.6. Conclusions

Radioactive contamination as a result of operations at the Berkshire AWE sites at Aldermaston and Burghfield has been investigated by the Geosciences Advisory Unit at the Southampton Oceanography Centre over the period 1998-2001. The results are published in three reports (Croudace *et al*., 1999, Croudace *et al*., 2000, Croudace *et al*., 2001). Isotope ratio data show that contamination of the environment around the sites is patchy and mostly found in woodland sites. The contamination is too small to be a radiological hazard to the public. A dispersion model using the annual discharge records can explain the observed contamination qualitatively, but not quantitatively. Examination of the depth distribution shows that weapons fallout plutonium is evenly distributed over the investigated 3 layers (0-5cm, 5-10cm and 10-15cm). The average $^{240}Pu/^{239}Pu$ is 0.18 in all 3 layers.

CHAPTER 7

Overall conclusions and possible future work

Using the IsoProbe multi-collector ICPMS high precision $^{240}Pu/^{239}Pu$ and $^{238}U/^{235}U$ can be determined in environmental samples containing concentrations as low as 0.1pg of Pu. The reproducibility ranges between 1.3% and 0.12% (2sd) for sample sizes between 0.1pg and 100pg. This precision could not be achieved by thermal ionisation mass spectrometry (TIMS), which until recently has been more commonly used for $^{240}Pu/^{239}Pu$ determinations. Therefore the IsoProbe MC-ICPMS expands the range of environmental samples in which the $^{240}Pu/^{239}Pu$ can be determined. The accuracy of the measurement is limited by the need to subtract the background and this is affected mostly by possible organic and elemental components of the solutions. Hence a good chemical separation and effective oxidation of the analyte residue is required to keep matrix effects low.

A ground level record of $^{240}Pu/^{239}Pu$ and $^{238}U/^{235}U$ for northern temperate latitudes is presented (Chapter 3) which was obtained using grass samples from the IACR-Rothamsted herbage archive in England, an ice core from the Mont Blanc glacier, French Alps and ground-level air filters from Germany. This is the first time that a generalised annual fallout record for $^{238}U/^{235}U$ has been reported. No ^{233}U and ^{236}U could be detected in the samples. However, the aim of detecting ^{233}U and ^{236}U prohibited the measurement of the uranium concentration, which would have been useful for quantification of the fallout. $^{240}Pu/^{239}Pu$ data previously existed for Arctic and Antarctic ice cores and for individual flights in the stratosphere. However, none of the existing data was applicable to northern temperate latitudes. The agreement of the $^{240}Pu/^{239}Pu$ in the Mont Blanc ice core and the Rothamsted grass strongly suggest that the measured $^{240}Pu/^{239}Pu$ is representative for the northern temperate latitude band. Both records, the $^{240}Pu/^{239}Pu$ and the $^{238}U/^{235}U$, are of great importance for source characterisation in environmental studies. Besides that both ratios can be used as a post-1950 geochronometer. One remarkable finding was that uranium and plutonium from early, relatively small, nuclear tests at the Nevada test site were transported to the U.K..

Two studies on plutonium in marine sediment cores collected from southern England (Poole Harbour) and from north-western England (Wyre estuary) have been presented. The core from the Wyre saltmarsh, approximately 68km south of Sellafield, shows $^{239,240}Pu$ activity

concentrations up to 1300 Bq/kg. The pattern of ^{137}Cs-, ^{238}Pu- and ^{239,240}Pu concentrations and the ^{238}Pu / ^{239,240}Pu can clearly be linked to the discharge from BNFL Sellafield. A transport model based on a constant mixing half-life for discharged Pu radionuclides in a sediment reservoir (Sellafield mudpatch) is able to explain the ^{238}Pu and ^{239,240}Pu concentrations and the ^{238}Pu/^{239,240}Pu activity ratio observed in the core. Using the model the ^{240}Pu/^{239}Pu in the Sellafield discharge, not previously reported, has been reconstructed from the measured ratio in the core. The ^{240}Pu/^{239}Pu reveals the changing priorities of reprocessing at the Sellafield site. In the early years reprocessing was mainly applied to separating plutonium for military purposes (British nuclear weapon programme) while in later years the reprocessing of spent fuel from civil reactors became more important. The second sediment study was of a mudflat core collected from Poole Harbour, southern England. A comparison of the ^{240}Pu/^{239}Pu in the core with the ^{240}Pu/^{239}Pu Rothamsted-grass-record clearly shows that the source of plutonium until the mid-1960s was atmospheric fallout from nuclear weapons testing. From the mid-1960s until 1991 (collection time of the core) a local plutonium source was identified. The reprocessing plants at Sellafield and La Hague can be excluded by the isotopic composition of the plutonium. Applying the same transport model developed for plutonium transport in the Irish Sea, the plutonium in the Poole core can be linked to the Atomic Energy Establishment at Winfrith in Dorset, which is approximately 20 km west of Poole Harbour.

The last case study using the Isoprobe MC-ICPMS involved an investigation of the terrestrial environment around the two AWE sites at Aldermaston and Burghfield in Berkshire. The ^{240}Pu/^{239}Pu and ^{238}U/^{235}U records, already established in case study 1 (Ch 3), are useful for attributing the measured uranium and plutonium to the AWE sites or a weapon fallout source. Uranium and plutonium isotope ratios in soils reveal contamination that is clearly attributable to the AWE sites. The contamination is rather heterogeneous in nature and it is mostly found in woodland sites. The spatial extent of the detected contamination is confined to an area up to 2.5 km from the boundary of the site. From the existing data it can be concluded that the contamination is too small to be a hazard to the public. Modelling the dispersion using the AWE annual aerial discharge records can explain the observed contamination qualitatively, but not quantitatively. The modelling shows that dry deposition dominates over wet deposition.

CHAPTER 7

The origin of any plutonium and uranium contamination in the environment is of public interest. The studies already undertaken (e.g. alleged nuclear weapons incident at the former USAF Greenham Common) show what can be achieved using forensic geochemistry employing mass spectrometry. An essential requirement for any such study is a good knowledge of the isotopic composition of the sources (military and civil) and the background. Records of $^{240}Pu/^{239}Pu$ in the effluents of nuclear facilities are often not known or reported (e.g. BNFL Sellafield and COGEMA La Hague) but it is shown that it is possible to reconstruct these by measurements of the ratio in sediment cores (Ch 4). A potential future study would be to apply a similar reconstruction of historical $^{240}Pu/^{239}Pu$ in the COGEMA La Hague discharge. Additionally, it would be useful to complete the stratospheric $^{240}Pu/^{239}Pu$ record (Figure 3.3) and establish a stratospheric record of $^{238}U/^{235}U$ from stratospheric filters from collections such as those held by the Environmental Measurement Laboratory in New York.

The $^{240}Pu/^{239}Pu$ and $^{238}U/^{235}U$ ratios are also useful in studies of environmental transport mechanisms. One possible application is the $^{240}Pu/^{239}Pu$ and the $^{238}U/^{235}U$ measurement in Polar ice sheets where they could be used to determine the rate of snow accumulation over the last 50 years and as tracers in atmospheric transport and circulation studies. The process of deposition of radionuclides is for example not uniform over Antarctica and is not well understood (Pourchet *et al*, 1997) due to the limited number of studies and the limited data. Plutonium concentration and high-precision isotope ratio data are rare for Antarctica and could provide valuable data to improve our understanding of atmospheric transport mechanisms. The $^{240}Pu/^{239}Pu$ in the Southern Stratosphere shows a distinct minimum in the early 1970s (Figure 3.3a) due to French nuclear testing. It is likely that this minimum will be observed in Antarctic ice. Since the appearance of the minimum is about 7 years later than the well-known 1963 peaks in radionuclide concentration, it potentially sets a new reference level for the early 1970s.

The higher abundance of ^{235}U compared to natural uranium observed in northern temperate latitudes, for the period of high yield weapons testing (Chapter 3), deserves further investigation. The $^{238}U/^{235}U$ measured for different Antarctic locations could give an insight into the origin of the air masses, by quantifying the amount of natural and artificial uranium.

Finally, it would be interesting to search for plutonium derived from space, e.g. in Polar ice after removing the input from the Nuclear Age. The measurement of actinides in galactic cosmic rays is a current subject of reasearch by astrophysicists. One experiment to measure the abundances of actinides in galactic cosmic rays is the ECCO-project, deployed on the International Space Station (http://wwwmipd.gsfc.nasa.gov/ecco/ecco.htm).

8. References

AEA, 1957-1991, Annual Reports: Radioactivity in Air and Rainwater, United Kingdom Atomic Energy Authority, Harwell, Berkshire, UK.

Albarede F. (1995) Introduction to geochemical modelling, Cambridge University Press, Cambridge, ISBN: 0521454514.

Allard B. Olofsson U. and Torstenfelt B. (1984) Environmental actinide chemistry, *Inorganica Chim. Acta* 94, 205-221.

AMNA (1999) The Atomic Mirror Nuclear Atlas, Available from: *http://antenna.nl/nukeatlas*.

Arnold D., Kolb W. and Wershofen H. (1999) Die $^{(239+240)}$Pu Aktivitäetskonzentrationen in der bodennahen Luft Norddeutschlands von 1963 bis 1997, *Strahlenschutz Praxis* 2, 25-27.

AWE (1990) Report of AWE safety division: Radioactive and toxic waste disposals by AWE 1989, Ref: D/AWE/SFS/A23, AWE Aldermaston, Reading, Berkshire.

AWE (1992) Annual report: Discharges and environmental monitoring for 1991, AWE Aldermaston, Reading, Berkshire.

AWE (1995) Annual report: Discharges and environmental monitoring for 1994, AWE Aldermaston, Reading, Berkshire.

AWE (1998) Hunting-BRAE Annual report 1998, AWE Aldermaston, Reading, Berkshire.

Bailly du Bois P. and Guegueniat P. (1999) Quantitative assessment of dissolved radiotracers in the English Channel: Sources, average impact of La Hague reprocessing plant and conservative behaviour (1983, 1986, 1988, 1994). *Cont. Shelf Res.* 19, 1977-2002.

References

Barbante C., van de Velde K., Cozzi G., Capodaglio G., Cescon P., Planchon F., Hong S., Ferrari C. and Boutron C. (2001) Post-World war II uranium changes in dated Mont Blanc ice and snow, *Env, Sci Technol* 35, 4026-4030.

Bauer E. and Gilmore F.R. (1975) Effect of atmospheric nuclear explosions on total ozone, *Rev. Geophys.Space Phys.* 13, 451-458.

BMJ (Bundesminesterium der Justiz) (1994) Bekanntmachung einer Empfehlung der Strahlenschutzkommission, *Bundesanzeiger* 46, 222a. Available from: Bundesminesterium der Justiz, Berlin, Germany

Bondarenko G.N. and Sobotovich E.V. (1998) Report: Isotope fractionation of uranium in the process of leaching of nuclides of dispersed fuel of RBMK of the Chernobyl NPP, Available from: State Scientific Center of Environmental Radiogeochemistry NAS, Palladin av. 34, 252680 Kiev, Ukraine.

Boulyga S. F., Erdmann N., Funk H., Kievets M. K., Lomonosova E. M., Mansel A., Trautmann N, Yaroshevich O.I. and Zhuh I.V. (1997) Determination of isotopic composition of plutonium in hot particles of the Chernobyl area, *Rad. Meas.* 28, 349-352.

Buesseler K.O. (1986) Plutonium isotopes in the North Atlantic, PhD-thesis, Woods Hole Oceanographic Institution, Massachusetts Institute of Technology, WHOI-86-32, In SOC at N190/A/86-32.

Buesseler K.O. and Halverson J.E. (1987) The mass spectrometric determination of fallout ^{239}Pu and ^{240}Pu in marine samples, *J. Environ. Radioactivity* 5, No.6, 425-444.

Buesseler K.O. and Sholkovitz E.R. (1987) The geochemistry of fallout plutonium in the north atlantic: II. ^{240}Pu /^{239}Pu ratios and their significance, *Geochim. Cosmochim. Acta* 51, 2623-2637.

Buesseler K.O. (1997) The isotopic signature of fallout plutonium in the North Pacific, *J. Environ. Radioactivity* 36, 69-83.

References

Carlson J., Bardsley J., Bragin V. and Hill J. (1988) Plutonium Isotopics – Non proliferation and safeguards issues, Australian Safeguards Office, Canberra ACT, Australia, Report IAEA-SM-351/64.

Carter M.W. and Moghissi A.A. (1977) Three decades of nuclear testing, *Health Physics* 33, 55-71.

Chamberlain A.C. (1996) Emissions from Sellafield and activities in soil, *Sci. Total Environ.* 177, 259-280.

Chen J.H. and Wasserburg G.J. (1980) A search for isotopic anomalies in uranium, *Geophys. Res. Lett.* 7, 275-278.

Clark M.J. and Smith F.B. (1988) Wet and dry deposition of Chernobyl releases, *Nature* 332, 245-249.

COMARE (Committee on Medical Aspects of Radiation in the Environment) (1989) Third Report: Incidence of childhood cancer in the West Berkshire and North Hampshire area, in which are situated the AWE Aldermaston and the ROF Burghfield, HMSO Publications, London.

COMARE (Committee on Medical Aspects of Radiation in the Environment) (1996) Fourth Report: The incidence of cancer and leukaemia in young people in the vicinity of the Sellafield site, West Cumbria: Further studies and an update of the situation since the publication of the report of the Black Advisory Group in 1984, HMSO Publications, London.

Cooper L.W., Kelley J.M., Bond L.A., Orlandini K.A. and Grebmeier J.M. (2000) Sources of transuranic plutonium and neptunium in arctic marine sediments, *Mar. Chem.* 69, 253-276.

Cowan G.A. (1976) A natural fission reactor, *Scientific American* 235, 36.

References

Croudace I, Warwick P., Taylor R. and Dee S. (1997) An investigation of radioactive contamination at Greenham Common, Newbury District and surrounding areas Final Report, Geosciences Advisory Unit, University of Southampton, UK.

Croudace I, Warwick P., Taylor R., Bradshaw K. and Warneke T. (1999) An assessment of radioactive contamination in the environment as a result of operations at the AWE sites in Berkshire Report No.1, Geosciences Advisory Unit, University of Southampton, UK.

Croudace I, Warwick P., Cundy A., Warneke T., Oh J.S. and Taylor R.N. (2000) An assessment of radioactive contamination in the environment as a result of operations at the AWE sites in Berkshire Report No.2, Geosciences Advisory Unit, University of Southampton, UK.

Croudace I, Warwick P., Warneke T., Cundy A., Oh J.S. and Taylor R.N. (2001) An assessment of radioactive contamination in the environment as a result of operations at the AWE sites in Berkshire Report No.3, Geosciences Advisory Unit, University of Southampton, UK.

Croudace I, Warwick P., Taylor R. and Dee S. (1998) Rapid procedure for plutonium and uranium determination in soils using a borate fusion followed by ion-exchange and extraction chromatography, *Anal. Chim. Acta* 371, 217-225.

Croudace I.W., Warwick P.E., Taylor R.N. and Cundy A.B. (2000), Investigation of an alleged nuclear incident at Greenham Common airbase using TI-mass spectrometric measurements of uranium isotopes, *Env, Sci Technol.* 34, 4496-4503.

Cutter G.A., Bruland K.W. and Risebrough R.W. (1979) Deposition and accumulation of plutonium isotopes in Antarctica, *Nature* 279, 628-629.

Cundy A.B. and Croudace I.W. (1996) Sediment accretion and recent sea-level rise in the Solent, Southern England: Interferences from radiometric and geochemical studies, *Estuar. Coast. and Shelf Sci.* 43, 449-467.

References

Delmas R., and Pourchet M. (1977) Utilisation de filtres echangeurs d'ions pour l'etude de l'activite β globale d'un carottage glaciologique, International Association of Hydrological Sciences Publication 118 (Symposium at Grenoble 1975 – Isotopes and Impurities in Snow and Ice), 159-163.

Eisenbud M. and Gesell T. (1997) Environmental Radioactivity 4th edition, Academic Press, San Diego, ISBN: 0122351533.

EML (Department of Energy Environmental Measurements Laboratory) (1997) Stratospheric Radionuclide (RANDAB) and Trace Gas (TRACDAB) Databases Available from: CDIAC (Carbon Dioxide Information Analysis Center) *http://cdiac.esd.ornl.gov/by_new/bysubjec.html#atmospheric*.

EML (Department of Energy Environmental Measurements Laboratory) (2000) Surface Air Sampling Program, Available from: *http://www.eml.doe.gov/databases/sasp/*.

FAS (Federation of American Scientists) (2000) Available from: *http://www.fas.org/nuke/guide/uk/facility/index.html*.

Fry F.A., Clarke, R.H. and O'Riordan, M.C. (1986) Early estimates of UK radiation doses from the Chernobyl reactor, *Nature* 321, 193-195.

GEOMAR (1999) Online map creation, Available from: *http://www.aquarius.geomar.de/omc/make_map.html*.

Gordon R.L. (1983) Kinetics of the surface ionization of plutonium on carburized rhenium, *Int. J. Mass Spectrom. Ion Processes* 55, 31-46.

Gray J., Jones S. R. and Smith A. D. (1995) Discharges to the environment from the Sellafield Site, 1951-1992, *J. Radiol. Protect.* 15, 99-131.

Hardy E.P., Krey P.W. and Volchok, H.L. (1973) Global inventory and distribution of fallout plutonium, *Nature* 241, 444-445.

References

Harley J.H. (1980) Plutonium in the environment-a review, *J. Radiation Res.* 21, 83-104.

Herrmann J., Kershaw P. J., Bailly du Bois P. and Guegueniat P. (1995) The distribution of artificial radionuclides in the English Channel, southern North Sea, Skagerrak and Kattegat, 1990-1993, *J. Mar. Syst.* 6, 427-456.

Holloway R.W. and Hayes D.W. (1982) Mean residence time of plutonium in the tropophere, *Env, Sci Technol.* 16, 127-129.

Irlweck K. and Wicke J. (1998) Isotopic composition of plutonium immissions in Austria after the Chernobyl accident, *J. Radioanal. Nucl. Chem.* 227, 133-136

IUPAC (International Union of Pure and Applied Chemistry) (1991) *Pure and Applied Chemistry* 163, 991-1002.

Jackson D. I., Jackson A. A., Evans D., Wingfield R. T. R., Barnes R. P. and Arthur M. J. (1995) United Kingdom offshore regional report : The geology of the Irish Sea. HMSO for the British Geological Survey, London.

Junge C.E. (1963) Air chemistry and radioactivity, Academic Press, New York.

Kelley J.M. and Robertson D.M. (1985) Plutonium ion emission from carburized rhenium mass spectrometer filaments, *Anal. Chem.* 57, 124-130.

Kelley J.M., Bond L.A. and Beasley T.M. (1999) Global distribution of Pu isotopes and Np-237, *Sci. Total Environ.* 237/238, 483-500.

Kershaw P.J. (1986) Radiocarbon dating of Irish Sea sediments, *Estuar. Coast. and Shelf Sci.* 23, 295-303.

Kershaw P.J., Sampson K.E., McCarthy W. and Scott R.D. (1995) The measurement of the isotopic composition of plutonium in an Irish Sea sediment by mass spectrometry, *J. Radioanal. Nucl. Chem.* 198, 113-124.

References

Kershaw P.J., Denoon D.C. and Woodhead D.S. (1999) Observations on the redistribution of plutonium and americium in the Irish Sea sediments, 1978 to 1996: concentrations and inventories, *J. Environ. Radioactivity* 44, 191-221.

Koide M., Michel R., Goldberg E.D., Herron M.M. and Langway C.C. (1979) Depositional history of artificial radionuclides in the Ross Ice Shelf, Antarctica, *Earth Planet. Sci. Lett.* 44, 205-223.

Koide M., Michel R. and Goldberg E.D. (1981) $^{241}Pu/^{239,240}Pu$ ratios in polar glaciers, *Earth Planet. Sci. Lett.* 54, 239-247.

Koide M., Michel R., Goldberg E.D., Herron M.M. and Langway C.C. (1982) Characterization of radioactive fallout from pre- and post- moratorium tests to polar ice caps. *Nature* 296, 544-547.

Koide M. and Goldberg E.D. (1983) Uranium isotopes in the Greenland ice sheet, *Earth Planet. Sci. Lett.* 65, 245-248.

Koide M., Bertine K.K., Chow T.J. and Goldberg E.D. (1985) The $^{240}Pu/^{239}Pu$ ratio, a potential geochronometer, *Earth Planet. Sci. Lett.* 72, 1-8.

Krey P.W., Leifert R., Benson W.K., Dietz L.A., Hendrikson H.C. and Coluzza J.L. (1979) Atmospheric burnup of the Cosmos-954 reactor, *Science* 105, 583-585.

Lawson J.E. (1998) Nuclear Explosion Catalog, Oklahoma Geological Survey Observatory, Available from: *http://www.okgeosurvey1.gov/level2/nuke.cat.index.html*.

Leifert R., Russel Juzdan Z., Kelly W.R., Fassett J.D. and Eberhardt K.R. (1987) Detection of uranium from Cosmos-1402 in the stratosphere, *Science* 238, 512-514.

Leonard K.S., McCubbin D., Blowers P. and Taylor B.R. (1999) Dissolved plutonium and americium in surface waters of the Irish Sea, 1973-1996, *J. Environ. Radioactivity* 44, 129-158.

References

Lieser K.H. (1991) Einfuehrung in die Kernchemie, VCH Verlagsgesellschaft mbH, Weinheim, Germany.

MacKenzie A.B. and Scott R.D. (1993) Sellafield waste radionuclides in Irish Sea intertidal and salt marsh sediments, *Environ. Geochem. Health* 15, 173-184.

MacKenzie A. B., Cook G. T., McDonald P. and Jones S. R. (1998) The influence of mixing timescale and re-dissolution processes on the distribution of radionuclides in northeast Irish Sea sediments, *J. Environ. Radioactivity* 39, 35-53.

Muramatsu Y., Hamilton T., Uchida S., Tagami K., Yoshida S. and Robison W. (2001) Measurement of 240Pu/239Pu isotopic ratios in soils from the Marshall Islands using ICP-MS, *Sci. Total Environ.* 278, 151-159.

Matsunami T. and Mamuro T. (1968) Uranium in fallout particles, *Nature* 218, 555-556.

Makhijani A., Hu H. and Yih K. (1995) Nuclear Wastelands, The MIT Press, Cambridge, Massachusetts, USA.

McCarthy W. and Nicholls T.M. (1990) Mass-Spectrometric analysis of plutonium in soils near Sellafield, *J. Environ. Radioactivity* 12, 1-12.

MOD (2000) UK Ministry of Defence report: Plutonium and Aldermaston – an historical account. Available from: *http://146.80.12.194/policy/acsa/index.html.*

Momoshima N., Kakiuchi H., Maeda Y., Hirai E. and Ono T. (1997) Identification of the contamination source of plutonium in environmental samples with isotopic ratios determined by inductively coupled plasma mass spectrometry and alpha spectrometry, *J. Radioanal. Nucl. Chem.* 221, 213-217.

NEA (1995) Chernobyl Ten years on, Available from: *http://www.nea.fr/html/rp/reports/1995/chernobyl/allchernobyl.html#chap6.*

References

Nelson D.M. and Lovett M.B. (1978) Oxidation state of plutonium in the Irish Sea, *Nature* 276, 599-601.

Noshin V.E. and Gatrousis C. (1974) Fallout ^{240}Pu and ^{239}Pu in Atlantic marine samples, *Earth Planet. Sci. Lett.* 22, 111-117.

Oh J.S. (1999) The migration and accumulation of radionuclides in the Ravenglass saltmarsh, Cumbria, PhD-thesis, University of Southampton.

Oktay S.D., Santschi P.H., Moran J.E. and Sharma P. (2000) The ^{129}Iodine bomb pulse recorded in Mississippi River Delta sediments: Results from isotopes of I, Pu, Cs, Pb, and C, *Geochim. Cosmochim. Acta* 64, 989-996.

Pallmer P.G., Gordon R.L. and Dresser M.J. (1980) (a) The emissivity of carburized rhenium, *J. Appl. Phys.* 51, 1798-1801.

Pallmer P.G., Gordon R.L. and Dresser M.J. (1980) (b) The work function of carburized rhenium, *J. Appl. Phys.* 51, 3776-3779.

Pasquill F. and Smith F.B. (1983) Atmospheric Diffusion 3.Edition, Ellis Horwood Publishers, Chichester.

Perrin R.E., Knobeloch G.W., Armijo V.M. and Efurd D.W. (1985) Isotopic analysis of nanogram quantities of plutonium by using a SID ionisation source, *Int. J. Mass Spectrom. Ion Processes* 64, 17-24.

Pourchet M., Bartarya S.K., Maignan M., Jouzel J., Pinglot J.F., Aristarain A.J., Furdada G., Kotlyakov V.M., Mosley-Thompson E., Preiss N. and Young N.W. (1997) Distribution and fall-out of 137Cs and other radionuclides over Antarctica, *J. Glaciol.* 43, 435-445.

Reiter E.R. (1975) Stratospheric-Tropospheric Exchange Processes, *Rev. Geophys. Space Phys.* 13, 459.

Roedel W. (1994) Physik unserer Umwelt: Die Atmosphäre 2.Aufl., Spinger-Verlag Heidelberg, Germany.

Rokop D.J., Efurd D.W., Benjamin T.M., Cappis J.H., Chamberlin J.W., Poths H. and Roensch F.R. (1995) Isotopic signatures, an important tool in todays world, Los Alamos report LA-UR-95-3837.

Sakuragi Y, Meason J.L. and Kuroda P.K. (1983) Uranium and plutonium isotopes in the atmosphere, *J. Geophy. Res.* 88C, 3718-3724.

Salaymeh S. and Kuroda P.K. (1987) Variation of the isotopic composition of uranium in the atmosphere, *Radiochim. Acta* 41, 31-39.

Sampson K.E., Scott R.D., Baxter M.S. and Hutton R.C. (1991) The determination of $^{240}Pu/^{239}Pu$ atomic ratios and ^{237}Np concentrations within marine sediments, *Radionuclides in the study of marine processes* p. 177-186, ed. P.J. Kershaw and D.S. Woodhead.

Santschi P.H., Li Y.H., Bell J.J., Trier R.M. and Kawtaluk K. (1980) Pu in coastal marine environments, *Earth Planet. Sci. Lett.* 51, 248-265.

Scott M.R., Salter P.F. and Halverson J.E. (1983) Transport and deposition of plutonium in the ocean: evidence from Gulf of Mexico sediments, *Earth Planet. Sci. Lett.* 63, 202-222

Smith D.H., Christie W.H. and Eby R.E. (1980) The resin bead as a thermal ion source: A SIMS study, *Int. J. Mass Spectrom. Ion Processes* 36, 301-316.

Smith D.H. and Carter J.A. (1981) A simple method to enhance thermal emission of metal ions, *Int. J. Mass Spectrom. Ion Processes* 40, 211-215.

Steward N.G., Crooks R.N. and Fisher E.M.R. (1957) "The radiological dose to persons in the UK due to debris from nuclear test explosions prior to January 1956" AERE HP/R 2017, Harwell, Berkshire, UK.

References

Taylor R.N., Croudace I.W., Warwick P.E. and Dee S.J. (1998) Precise and rapid determination of $^{238}U/^{235}U$ and uranium concentration in soil samples using thermal ionisation mass spectrometry, *Chem. Geol.* 144, 73-80.

Taylor R.N., Warneke T., Milton J.A., Croudace I.W., Warwick P.E. and Nesbitt R.W. (2001) Plutonium isotope ratio analysis at femtogram to nanogram levels by multicollector ICP-MS, *J. Anal. At. Spectrom*. 16, 279-284.

Thirlwall M. (2001) Inappropriate tail corrections can cause large inaccuracy in isotope ratio analysis by MC-ICP-MS, *J. Anal. At. Spectrom.* 16, 1121-1125.

Thomson J., Dyer F.M. and Croudace I.W. (2002) Records of radionuclide deposition in two U.K. salt marshes with contrasting redox and accumulation conditions, *Geochim. Cosmochim. Acta* (in press).

UKAEA (1999) Report to the Local Liaison Committee on Radioactive Discharges & Environmental Monitoring, 1999, United Kingdom Atomic Energy Authority, Winfrith.

Vincent C., Vallon M., Pinglot J.F., Funk M. and Reynaud L. (1997) Snow accumulation and ice flow at Dome du Gouter (4300m), Mont Blanc, French Alps, *J. Glaciol.* 43, 513-521.

Appendix

M.1 Time independent mass fractionation laws in mass spectrometry

In the following the ratio $\frac{R}{r}$ of the measured ratio R and the true ratio r is expressed as a function of a second function, which is then approximated by the first term of a Taylor series. Any kind of functional relation could be assumed. The three most used ones, that have been shown suitable experimentally, are presented below. For most measurements the differences between the three laws are so small that they can be neglected within the errors of the measurement. The Isoprobe introduces an additional potential fractionation source by its collision cell and the best law has to be determined experimentally.

1. Linear law

The ratio $\frac{R}{r}$ is expressed as a function of the mass difference $\Delta m = m_2 - m_1$:

$$\frac{R}{r} = \alpha(\Delta m)$$

Expanding α to the first order yields $\alpha(\Delta m) \approx \alpha(0) + \xi\Delta m$. Since $\alpha(0) = 1$ one obtains:

$$R \approx r(1 + \xi\Delta m)$$

2. Power law

The ratio is expressed as $\frac{R}{r} = \exp[\beta(\Delta m)]$. First order approximation $\beta(\Delta m) \approx \beta(0) + \delta\Delta m$, where $\beta(0)$ equals 0 yields $R = r\exp[\delta\Delta m] = rg^{\Delta m}$ where g is the power law mass fractionation coefficient.

3. Exponential law

The ratio is expressed as $\frac{R}{r} = \exp[\beta(\Delta(\ln m))]$, where $\Delta(\ln m) = \ln m_2 - \ln m_1 = \ln\frac{m_2}{m_1}$.

First order approximation $\beta(\Delta(\ln m)) \approx \beta(0) + f\Delta(\ln m)$ with $\beta(0) = 0$ yields

$$R = r\exp[f\Delta(\ln m)] = r\left(\frac{m_2}{m_1}\right)^f = r\left(1 + \frac{\Delta m}{m_1}\right)^f$$

M.2 Derivation of an analytical formula for the sample ratio from a spike-sample mixture

In the case of the uranium measurements a ^{233}U-^{236}U-spike was added, that also introduces small quantities of the isotopes ^{234}U, ^{235}U and ^{238}U. Hence, the measured ratio has to be corrected for those contributions. In the following an analytical formula for this correction is derived:
The measured ratios $R_{i/j}^{m}$ are a superposition of the sample and the spike:

$$R_{i/j}^{m} = \frac{N_{sa}c_{sa}^{i} + N_{sp}c_{sp}^{i}}{N_{sa}c_{sa}^{j} + N_{sp}c_{sp}^{j}}$$

where N_{sa} and N_{sp} are the number of uranium atoms and c_{sa}^{i}, c_{sp}^{i} the abundances of the uranium isotope i in the sample and in the spike.
The calculation of the ratios for the sample is shown for the $^{238}U/^{235}U$ ratio as an example:
The ratio in the sample is given by

$$R_{8/5}^{sa} = \frac{N_{sa}c_{sa}^{238}}{N_{sa}c_{sa}^{235}}$$

Solving $R_{8/5}^{m}$ with respect to $N_{sa}c_{sa}^{238}$ the numerator can be replaced:

$$R_{8/5}^{sa} = \frac{R_{8/5}^{m}[N_{sa}c_{sa}^{235} + N_{sp}c_{sp}^{235}] - N_{sp}c_{sp}^{238}}{N_{sa}c_{sa}^{235}}$$

Since the sample does not contain ^{236}U uranium the measured $^{235}U/^{236}U$ ratio is

$$R_{5/6}^{m} = \frac{N_{sa}c_{sa}^{235} + N_{sp}c_{sp}^{235}}{N_{sp}c_{sp}^{236}}$$

Solving this with respect to $N_{sa}c_{sa}^{235}$ and plugging it into the equation for $R_{8/5}^{sa}$ one get

$$R_{8/5}^{sa} = \frac{R_{8/5}^{m}R_{5/6}^{m}c_{sp}^{236} - c_{sp}^{238}}{R_{5/6}^{m}c_{sp}^{236} - c_{sp}^{235}}$$

The $^{238}U/^{234}U$ ratio in the sample can be calculated in a similar manner.

A1. Atmospheric nuclear test data

Date	State	Location	Type	Yield (kt)	Name
03.10.52	GB	MBI	SHIP	<1000	
31.10.52	US	ENW	SURF	10400	MIKE
15.11.52	US	ENW	AIRD	500	KING
23.08.53	CP		ATMO		JOE 5-7
14.10.53	GB	EMU	TOWR	<1000	TOTEM
26.10.53	GB	EMU	TOWR	<1000	
28.02.54	US	BKN	SURF	15000	BRAVO
26.03.54	US	BKN	BARG	11000	ROMEO
25.04.54	US	BKN	BARG	6900	UNION
04.05.54	US	BKN	BARG	13500	YANKEE
13.05.54	US	ENW	BARG	1690	NECTAR
14.09.54	CP				
22.11.55	CP	KTS	AIRD	1600	
20.03.56	CP				
30.03.56	CP				
02.05.56	US	BKN	AIRD	3400	CHEROKEE
16.05.56	GB	MBI	TOWR	<1000	MOSAIC
27.05.56	US	BKN	SURF	3500	ZUNI
19.06.56	GB	MBI	TOWR	<1000	
25.06.56	US	BKN	BARG	1000	DAKOTA
08.07.56	US	ENW	BARG	1900	APACHE
10.07.56	US	BKN	BARG	4500	NAVAJO
20.07.56	US	BKN	BARG	5000	TEWA
24.08.56	CP		ATMO	<1000	
02.09.56	CP		ATMO		
10.09.56	CP		ATMO		
17.11.56	CP		ATMO		
19.01.57	CP		ATMO		
08.03.57	CP		ATMO		
03.04.57	CP		ATMO		
06.04.57	CP		ATMO		
10.04.57	CP		ATMO	200-1000	
12.04.57	CP		ATMO		
16.04.57	CP		ATMO	200-1000	
15.05.57	GB	CHR	AIRD	>1000	GRAPPLE
31.05.57	GB	CHR	AIRD	>1000	
19.06.57	GB	CHR	AIRD	>1000	
22.08.57	CP			HIGH	
24.09.57	CP	NZ		>1000	
06.10.57	CP	NZ	ATMO	HIGH	
08.11.57	GB	CHR	AIRD	1800	GRAPPLE
28.12.57	CP		ATMO		
23.02.58	CP	NZ	ATMO	>1000	
27.02.58	CP	NZ	ATMO	>1000	
27.02.58	CP	NZ	ATMO	HIGH	
14.03.58	CP	NZ	ATMO	<1000	
14.03.58	CP		ATMO	<1000	
15.03.58	CP		ATMO	<1000	
28.04.58	GB	CHR	AIRD	>1000	GRAPPLE
11.05.58	US	BKN	BARG	1300	FIR
12.05.58	US	ENW	SURF	1370	KOA
27.06.58	US	ENW	BARG	875	ELDER
28.06.58	US	ENW	BARG	8900	OAK
12.07.58	US	BKN	BARG	9300	POPLAR
26.07.58	US	ENW	BARG	2000	PINE
01.08.58	US	JON	ROCH	3800	TEAK
12.08.58	US	JON	ROCH	3800	ORANGE
02.09.58	GB	CHR	AIRD	>1000	
11.09.58	GB	CHR	AIRD	>1000	
20.09.58	CP	NZ	ATMO		

Date	State	Location	Type	Yield (kt)	Name
02.10.58	CP	NZ	ATMO		
05.10.58	CP	NZ	ATMO		
10.10.58	CP	NZ	ATMO	HIGH	
12.10.58	CP	NZ	ATMO	>1000	
15.10.58	CP	NZ	ATM0	>1000	
18.10.58	CP	NZ	ATMO	>1000	
20.10.58	CP	NZ	ATMO	>1000	
22.10.58	CP	NZ	ATMO	>1000	
24.10.58	CP	NZ	ATMO	HIGH	
25.10.58	CP	NZ	ATMO	HIGH	
10.09.61	CP	NZ	ATMO	>1000	
12.09.61	CP	NZ	ATMO	>1000	
14.09.61	CP	NZ	ATMO	>1000	
16.09.61	CP	NZ	ATMO	>1000	
18.09.61	CP	NZ	ATMO	>1000	
20.09.61	CP	NZ	ATMO	>1000	
22.09.61	CP	NZ	ATMO	>1000	
02.10.61	CP	NZ	ATMO	>1000	
04.10.61	CP	NZ	ATMO	>1000	
06.10.61	CP	NZ	ATMO	>1000	
20.10.61	CP	NZ	ATMO	>1000	
23.10.61	CP	NZ	ATMO	25000	
25.10.61	CP	NZ	ATMO	<1000	
30.10.61	CP	NZ	ATMO	58000	
31.10.61	CP	NZ	ATMO	<1000	
31.10.61	CP	NZ	ATMO	>1000	
04.11.61	CP	NZ	ATMO	>1000	
25.04.62	US	CHR	AIRD	20-1000	ADOBE
27.04.62	US	CHR	AIRD	20-1000	AZTEC
04.05.62	US	CHR	AIRD	20-1000	QUESTA
06.05.62	US	PAC	ROCH	600	FRIGATEB
08.05.62	US	CHR	AIRD	20-1000	YUKON
09.05.62	US	CHR	AIRD	20-1000	MESILLA
11.05.62	US	CHR	AIRD	20-1000	MUSKEGON
12.05.62	US	CHR	AIRD	20-1000	ENCINO
14.05.62	US	CHR	AIRD	20-1000	SWANEE
19.05.62	US	CHR	AIRD	20-1000	CHETCO
27.05.62	US	CHR	AIRD	20-1000	NAMBE
08.06.62	US	CHR	AIRD	20-1000	ALMA
09.06.62	US	CHR	AIRD	20-1000	TRUCKEE
10.06.62	US	CHR	AIRD	>1000	YESO
12.06.62	US	CHR	AIRD	20-1000	HARLEM
15.06.62	US	CHR	AIRD	20-1000	RINCONAD
17.06.62	US	CHR	AIRD	20-1000	DULCE
22.06.62	US	CHR	AIRD	20-1000	OTOWI
27.06.62	US	CHR	AIRD	>1000	BIGHORN
30.06.62	US	CHR	AIRD	>1000	BLUESTON
09.07.62	US	JON	ROCH	1400	STARFISH
10.07.62	US	CHR	AIRD	20-1000	SUNSET
11.07.62	US	CHR	AIRD	>1000	PAMLICO
05.08.62	CP	NZ	ATMO	30000	
10.08.62	CP	NZ	ATMO	<1000	
20.08.62	CP	NZ	ATMO	>1000	
22.08.62	CP	NZ	ATMO	>1000	
25.08.62	CP	NZ	ATMO	>1000	
27.08.62	CP	NZ	ATMO	1000+	
08.09.62	CP	NZ	ATMO	>1000	
15.09.62	CP	NZ	ATMO	>1000	
16.09.62	CP	NZ	ATMO	>1000	
18.09.62	CP	NZ	ATMO	>1000	
19.09.62	CP	NZ	ATMO	20000	
21.09.62	CP	NZ	ATMO	25000	
25.09.62	CP	NZ		25000	

Date	State	Location	Type	Yield (kt)	Name
27.09.62	CP	NZ	ATMO	>1000	
02.10.62	US	JON	AIRD	20-1000	ANDROSCO
18.10.62	US	JON	AIRD	>1000	CHAMA
22.10.62	CP	NZ	ATMO	>1000	
26.10.62	US	JON	ROCH	<1000	BLUEGIL
27.10.62	CP	NZ	ATMO	20-1000	
27.10.62	US	JON	AIRD	20-1000	CALAMITY
29.10.62	CP	NZ	ATMO	20-1000	
30.10.62	CP	NZ	ATMO	20-1000	
30.10.62	US	JON	AIRD	>1000	HOUSATON
01.11.62	CP	NZ	ATMO	20-1000	
01.11.62	CP	KTS	ATMO	20-1000	
01.11.62	US	JON	ROCH	<1000	KINGFISH
03.11.62	CP	NZ	ATMO	20-1000	
04.11.62	CP	KTS	ATMO	20-1000	
18.12.62	CP	NZ	ATMO	20-1000	
18.12.62	CP	NZ	ATMO	20-1000	
20.12.62	CP	NZ	ATMO	20-1000	
22.12.62	CP	NZ	ATMO	20-1000	
23.12.62	CP	NZ	ATMO	500-5000	
24.12.62	CP	NZ	ATMO	20000	
24.12.62	CP	NZ	ATMO		
25.12.62	CP	NZ	ATMO	500-5000	
17.06.67	PC	LNR	AIRD	3000	
03.08.68	FR	MUR	BALN	500	
24.08.68	FR	FAN	BALN	2600	CANOPUS
08.09.68	FR	MUR	BALN	1200	PROCYON
27.12.68	PC	LNR	AIRD	3000	
29.09.69	PC	LNR	AIRD	3000	
30.05.70	FR		BALN	>1000	DRAGON
03.07.70	FR		BALN	1000	LICORNE
14.10.70	PC	LNR	AIRD	3000	
14.08.71	FR		BALN	1000	RHEA
26.07.73	PC	LNR		2000-3000	
17.06.74	PC	LNR	ATMO	200-1000	
26.07.74	FR	MUR	AIRD		
29.07.74	FR	MUR	ATMO	HIGH	
15.08.74	FR	MUR	ATMO		
25.08.74	FR	MUR	ATMO		
15.09.74	FR	MUR	ATMO	1000	
17.11.76	PC	LNR	ATMO	4000	
16.10.80	PC	LNR	ATMO	200-1000	

Table A.1: Atmospheric nuclear tests with yields greater than 500Kt or expected high yield (from Lawson, 1998)

US=United States, GB=UK, CP=USSR, FR=France, PC=People's Republic of China

BKN Bikini, (11°N 165°E), (US atmospheric tests)
CHR Christmas Island, (2°N 157°W) (UK and US atmospheric tests)
ENW Enwetak, (11°N 162°E), (US atmospheric tests)
FAN Fangataufa Is., (21°S 137°W), (French atmospheric and underground tests)
JON Johnston Island, (17°N 169°E), (US atmospheric tests)
KTS Eastern Kazakh or Semipalitinsk test site (50°N 80°E), USSR (USSR atmospheric and underground tests)
LNR Lop Nor, PRC, (40°N 90°E), (PRC atmospheric and underground tests)
MBI Monte Bello Islands, Australia, (20°S 115°E), (UK atmospheric test)
MUR Muruora Is., (21°S 137°W), (French atmospheric and underground tests)
NTS Nevada Test Site, Nevada, USA, (31°N 116°W), (US atmospheric and underground and UK underground tests)
NZ Novaya Zemlya (75°N 55°E), USSR (USSR atmospheric and underground tests)
PAC Various Pacific Ocean sites

A.2 Discharge data for AWE Aldermaston

Year	Air discharges						Liquid discharge through pipe			Trade waste to sewer	
	Pu MBq	U MBq	Other α MBq	β MBq	^{3}Hd TBq	^{85}Kr TBq	α MBq	β MBq	^{3}H GBq	α MBq	β MBq
1952	0.025	0	0.03	0	0		60	100	0		
1953	0.5	0.15	0.1	0	0		1000	400	0		
1954	0.5	4	0.25	0	0		3000	1000	0		
1955	1	80	0.5	0	0		6000	1500	0		
1956	2	150	1.5	0	0		5000	1500	0		
1957	4	150	0.8	10	0		8000	2500	0		
1958	5	200	1	15	0		6000	400	0	30	80
1959	8	200	0.6	30	5		5000	500	0	200	300
1960	4	200	0.2	8	80		2500	400	0	200	800
1961	2.5	100	0.03	10	30		3000	300	0	300	600
1962	2	80	0.02	25	20		3000	500	0	250	300
1963	2	40	0.03	50	40		2000	1000	0	150	600
1964	1.5	150	0.1	15	25		2000	3000	0	150	500
1965	2.5	150	0.01	5	80		2000	5000	800	100	400
1966	2.5	80	0.06	20	60		2500	10000	400	100	400
1967	3	40	0.01	400	100		2000	5000	800	150	400
1968	5	60	0.02	25	150		4000	5000	500	200	300
1969	5	50	0.01	20	200		4000	4000	250	250	400
1970	2.5	30	0.01	20	250		3000	2500	150	250	400
1971	2.5	30	0.01	20	300		1000	2500	150	300	500
1972	2.5	50	0.01	20	500		1000	2500	150	200	500
1973	3	60	0.01	20	400		500	2500	200	100	500
1974	1.5	40	0.01	20	500		400	3000	150	150	600
1975	2.5	30	0.01	20	400		300	300	200	100	400
1976	1.5	30	0.01	20	400		800	1000	200	80	400
1977	10	30	0.02	20	400		600	1500	100	100	800
1978	0.6	6	0.03	20	400		150	300	80	100	500
1979	1.5	10	0.01	20	250		150	300	50	80	500
1980	1.5	15	0.01	20	200		200	500	80	80	400
1981	1	15	0.02	20	150	0.3	150	300	100	80	400
1982	1.5	30	0.01	20	200	0.3	200	300	800	80	400
1983	0.6	10	0.02	20	150	0.3	80	500	80	50	300
1984	0.8	6	0.01	20	150	0.3	100	300	100	50	300
1985	0.4	1.5	0.006	50	100	0.3	80	250	200	60	300
1986	0.3	1	0.004	30	80	0.3	150	250	100	80	500
1987	0.3	1	0.2								
1988	0.1	0.5	0								
1989	0.05	0.3	0								
1990	0.13	0.18	0								
1991	0.17	0.16	0								
1992	0.18	0.13									
1993	0.15	0.09									
1994	0.14	0.05									
1995	0.11	0.02									
1996	0.15	0.02									
1997	0.09	0.05									
1998	0.13	0									

Data from COMARE (1989) and AWE Reports for 1990, 1992, 1995, 1998)

A.3 Marine discharges from AEA Winfrith, Dorset (from UKAEA, 1999)

Year	1964	1965	1966	1967	1968	1969	1970	1971	1972	1973	1974	1975	1976	1977
GBq	16	10	40	49	57	29	108	142	134	326	107	59	274	130

Year	1978	1979	1980	1981	1982	1983	1984	1985	1986	1987	1988	1989	1990	1991
GBq	6	22	197	24	25	72	51	35	7	7	5	5	4	3

A.4 Marine discharges from COGEMA La Hague: (Units : TBq/yr)

Year	^{137}Cs	^{238}Pu	^{239,240}Pu	^{241}Pu	^{242}Pu	^{241}Am	^{238}Pu/^{239,240}Pu	^{241}Pu/^{239,240}Pu	^{242}Pu/^{239,240}Pu
1966	7	0.000	0.002	0.0		0.000	0.01	2.0	0.00E+00
1967	16	0.000	0.012	0.0		0.000	0.02	4.2	0.00E+00
1968	28	0.001	0.032	0.3		0.001	0.04	9.4	0.00E+00
1969	20	0.000	0.013	0.1		0.000	0.03	7.4	0.00E+00
1970	89	0.001	0.024	0.2		0.001	0.04	8.4	0.00E+00
1971	243	0.013	0.145	3.1		0.011	0.09	21.1	0.00E+00
1972	33	0.006	0.066	1.3		0.005	0.08	19.9	0.00E+00
1973	69	0.008	0.081	1.8		0.006	0.10	22.0	0.00E+00
1974	56	0.051	0.552	11.9		0.042	0.09	21.6	0.00E+00
1975	35	0.034	0.262	7.3		0.028	0.13	27.9	0.00E+00
1976	35	0.042	0.157	6.5	2.8E-05	0.023	0.27	41.5	1.75E-04
1977	51	0.140	0.239	11.6	9.6E-05	0.057	0.59	48.5	4.01E-04
1978	39	0.178	0.216	13.6	1.3E-04	0.064	0.82	63.0	6.02E-04
1979	23	0.199	0.245	18.5	1.8E-04	0.114	0.81	75.5	7.14E-04
1980	27	0.179	0.186	15.3	1.7E-04	0.111	0.96	82.3	8.87E-04
1981	39	0.213	0.164	14.5	1.7E-04	0.103	1.30	88.4	1.01E-03
1982	51	0.214	0.194	17.4	2.0E-04	0.139	1.10	89.7	1.02E-03
1983	23	0.126	0.081	8.7	1.1E-04	0.073	1.56	107.9	1.31E-03
1984	30	0.183	0.136	13.9	1.8E-04	0.118	1.35	102.2	1.33E-03
1985	29	0.315	0.136	16.9	2.7E-04	0.138	2.32	124.3	1.96E-03
1986	10	0.136	0.081	9.1	1.4E-04	0.439	1.67	112.1	1.66E-03
1987	8	0.170	0.086	10.4	1.6E-04	0.169	1.98	121.1	1.84E-03
1988	8	0.107	0.063	7.5	1.1E-04	0.147	1.69	118.6	1.78E-03
1989	13	0.123	0.056	6.9	1.2E-04	0.093	2.20	124.2	2.13E-03
1990	13	0.114	0.053	6.2	1.1E-04	0.120	2.14	116.3	2.03E-03
1991	6	0.066	0.023	2.7	5.2E-05	0.038	2.85	115.9	2.25E-03
1992	3	0.035	0.015	1.7	3.1E-05	0.018	2.28	113.8	2.03E-03
1993	4	0.023	0.012	1.3	2.3E-05	0.014	2.01	110.4	1.97E-03
1994	11	0.026	0.010	1.1	2.2E-05	0.010	2.67	112.2	2.28E-03
1995	5	0.016	0.006	0.6	1.3E-05	0.009	2.81	107.4	2.28E-03
1996	2	0.011	0.005	0.5	1.0E-05	0.005	2.47	106.1	2.21E-03

A.5 Selected radionuclides discharges to the Irish Sea from Sellafield (Units : TBq/yr)

Year	^{137}Cs	^{238}Pu	$^{239,240}Pu$	^{241}Pu	^{241}Am	$^{241}Pu/^{239,240}Pu$	$^{238}Pu/^{239,240}Pu$	$^{239,240}Pu/^{137}Cs$
1952	46	0.02	0.5	2	0.0	3.7	0.04	0.01
1953	46	0.02	0.5	1	0.0	2.0	0.04	0.01
1954	46	0.02	0.6	2	0.0	3.8	0.03	0.01
1955	21	0.02	0.7	2	0.0	2.7	0.03	0.03
1956	160	0.06	1.8	4	0.0	2.1	0.03	0.01
1957	140	0.05	1.6	3	0.0	2.1	0.03	0.01
1958	230	0.06	1.9	4	0.0	2.1	0.03	0.01
1959	73	0.06	2.1	4	0.0	2.1	0.03	0.03
1960	34	0.08	2.7	6	0.0	2.3	0.03	0.08
1961	40	0.14	4.6	18	0.0	3.9	0.03	0.12
1962	74	0.20	6.6	37	0.0	5.6	0.03	0.09
1963	85	0.25	8.1	55	0.0	6.8	0.03	0.10
1964	100	0.22	5.5	62	4.5	11.3	0.04	0.06
1965	110	0.30	6.9	81	8.1	11.7	0.04	0.06
1966	180	0.66	13.0	170	7.5	13.1	0.05	0.07
1967	150	1.20	17.0	290	17.0	17.1	0.07	0.11
1968	370	2.10	28.0	630	21.0	22.5	0.08	0.08
1969	440	2.80	27.0	730	14.0	27.0	0.10	0.06
1970	1200	3.80	31.0	1000	19.0	32.3	0.12	0.03
1971	1300	9.30	46.0	1800	38.0	39.1	0.20	0.04
1972	1300	9.90	47.0	1900	80.0	40.4	0.21	0.04
1973	770	11.00	54.0	2800	110.0	51.9	0.20	0.07
1974	4100	8.00	38.0	1700	120.0	44.7	0.21	0.01
1975	5200	8.80	35.0	1800	36.0	51.4	0.25	0.01
1976	4300	8.80	38.0	1300	12.0	34.2	0.23	0.01
1977	4500	7.50	29.0	980	3.7	33.8	0.26	0.01
1978	4100	12.00	46.0	1800	7.9	39.1	0.26	0.01
1979	2600	12.00	38.0	1500	7.8	39.5	0.32	0.01
1980	3000	6.90	20.0	730	8.2	36.5	0.35	0.01
1981	2400	5.00	15.0	600	8.8	40.0	0.33	0.01
1982	2000	4.70	16.0	480	6.4	30.0	0.29	0.01
1983	1200	2.90	8.7	330	2.2	37.9	0.33	0.01
1984	430	2.60	8.3	350	2.3	42.2	0.31	0.02
1985	330	0.80	2.6	81	1.6	31.2	0.31	0.01
1986	18	0.62	2.0	63	1.3	31.5	0.31	0.11
1987	12	0.35	1.0	32	0.7	33.0	0.36	0.08
1988	13	0.38	1.0	36	0.8	36.0	0.38	0.08
1989	29	0.31	0.9	30	1.1	33.3	0.34	0.03
1990	24	0.29	0.8	32	0.8	38.1	0.35	0.04
1991	16	0.26	0.8	30	0.7	36.6	0.32	0.05
1992	15	0.24	0.7	25	0.5	36.2	0.35	0.05
1993	22	0.36	1.0	38	0.9	39.2	0.37	0.04
1994	14	0.17	0.5	14	0.4	28.0	0.34	0.04
1995	12	0.08	0.2	8	0.1	33.5	0.35	0.02
1996	10	0.06	0.2	4	0.1	29.3	0.40	0.02

A.6 Atmospheric circulation (due to Roedel, 1994)

Tropospheric circulation

The idealised tropospheric circulation can be described by three cells. The lattitude range of these cells is approximately 0 – 30°/35°, 30°/35°-60°/70°, 60°/70°-poles.

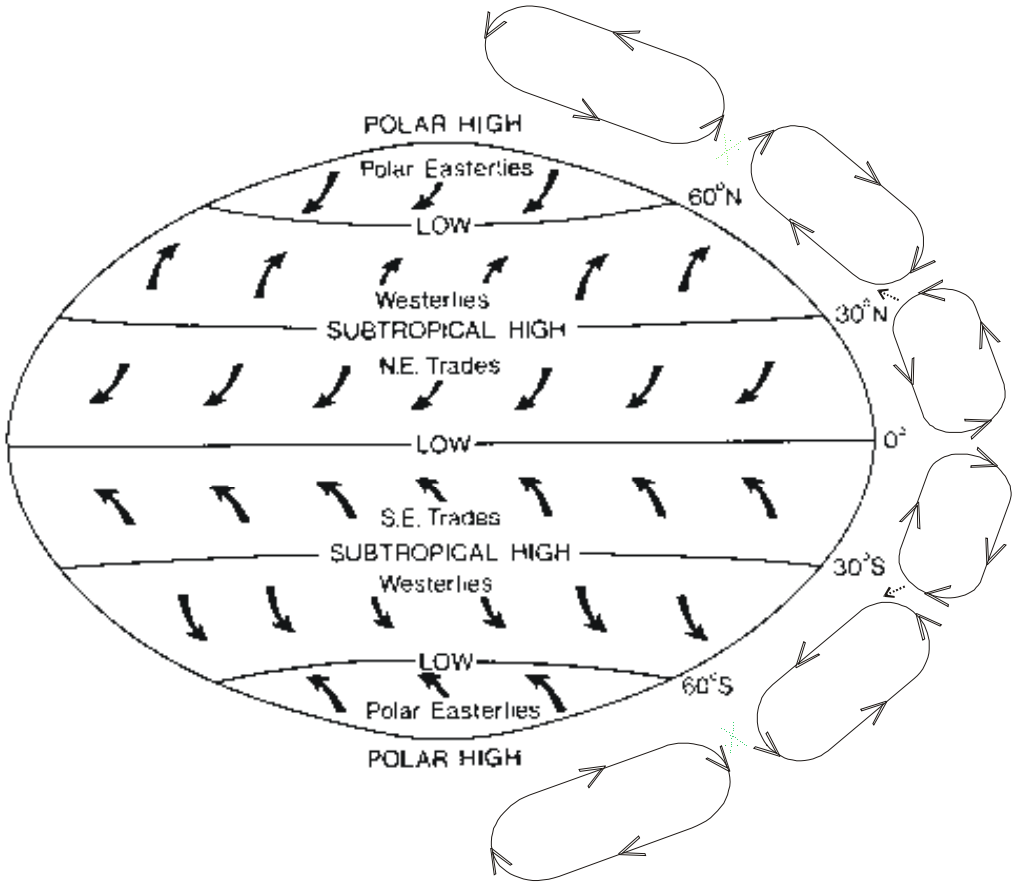

Figure A.1 Global circulation pattern in the troposphere

0 – 30°/35° (Hadley circulation)

The air rises in the zone of highest solar irradiation. The upper level air moves poleward, cools and descends near 30° and surface air returns to equator. The Coriolis force turns the surface winds to the right (left) in the Northern (Southern) Hemisphere (Trade winds). The line where winds from each hemisphere meet is called the Intertropical Convergence Zone (ITC).

30°/35° - 60°/70° (Ferrel Circulation)

The decending air at 30°/35° creates high surface pressure which causes surface air to move poleward. The polarward-moving air is deflected by the Coriolis force to the right (left) in the Northern (Southern) Hemisphere (Westerlies). This air meets equatorward moving polar air between 40°-70°. The boundary between poleward-moving air and polar air is called the polar front. The air ascends at the polar front and creates low pressure at the surface. The upperlevel flow is equatorwards. In contrast to the 0-30° zone the 35°-60° zone is subject to disturbances and wave action. Therefore the discribed circulation is only a rough approximation. For example, the polar front is not confined to a small lattitude band, but can move between 40° and 70°.

60°/70° - pole

The cooling of the air at the poles causes a high pressure and the air moves equatorwards until it meets the polewards moving air at the polar front.The equatorward-moving polar air is deflected by the Coriolis and becomes easterly in each hemisphere (Polar Easterlies). The convergence at the Polar front causes the air to move upward and return to the pole.

Tropopause

The border between the troposphere and stratosphere (the tropopause) is characterised by a minimum in temperature. In the troposphere a relative high temperature is maintained by back-scattering of thermal radiation (originating at the earth surface) mainly by water vapour. For that reason the tropopause coincides with the edge of the water-vapour-sphere around the earth. Therefore is the tropopause higher (and cooler) the greater the layer of water vapour. The height of the tropopause is 9-13km at temperate and high latitudes and reaches 17-18km in the tropics. The summer tropopause of the temperate and high latitudes is approximately 2km higher than the winter tropopause. Within the stratosphere the temperature rises, due to absorption of solar radiation. No exchange occurs if warmer air is above cooler air (Inversion). Therefore the stratosphere and the troposphere can be regarded as two different reservoirs and the convection and exchange in the stratosphere is small.

Stratospheric circulation

The tropopause and lower stratosphere is higher in the tropics and therefore fairly cool. The polar stratosphere is warmer (cooler) in the summer (winter) than the tropical stratosphere. Due to the pressure gradient the air would move polewards in the summer hemisphere and equatorwards in the winter hemisphere. From the equilibrium of Coriolis force and pressure gradient one get eastwinds in the summer stratosphere and westwinds in the winter-stratosphere. The eastwinds in the summer are more stable than the westwind in the winter. Single events like sudden warmings play a significant role in meridional exchange. In average the meridional exchange is small in summer and higher in winter. Besides that southern circulation is more stable which results in less exchange.

Troposphere/Stratosphere exchange

Due to the temperature inversion the troposphere and stratosphere can be regarded as two different reservoirs. Exchange between them occurs mainly by the following three processes:

1. As described above, the tropopause of the temperate and high latitudes is higher in the summer and lower in the winter. This seasonal rising and falling of the tropopause causes an exchange of stratospheric mass at temperate to high latitudes.
2. The hot air at the ITC can rise through the tropopause, which results in the Hadley-circulation going partially through the stratosphere. The main input of stratospheric air into the troposphere is around 30°.
3. At the two boundaries between the three tropospheric circulation cells high windspeeds occur in the region of the tropopause (Jetstreams). These Jetstreams have been shown to be very effective in stratospheric-tropospheric exchange. The subtropical jet at the boundary between the Hadley and Ferrel cell is much stronger than the sub-Polar-jet at the polarfront. Therefore more exchange occurs in the region of around 30° than around 60°. The jets are stronger (more exchange) in winter.

The first process is responsible for the exchange of about 10% of the total stratospheric mass per year and the latter two processes for about 50-60%. Various smaller processes contribute an additional 5% which adds to a yearly exchange of 60-75% of the total stratospheric mass.

A.7 A simple dispersion model for the AWE airborne discharge

A.8.1 General theory of the dispersion of airborne discharges (Gaussian plume equation)

The dispersion of material released into the atmosphere depends on atmospheric dynamics. Regarding dynamics the atmosphere can be divided into 4 layers. The first two layers above the earth's surface are dominated by the friction with the earth surface. The first layer is called the **molecular viscose layer**. Its thickness is of the order of mm and molecular diffusion is the most important transport mechanism. In the second layer, called **Prandl layer**, turbulent diffusion dominates over molecular diffusion. Its thickness is about 100m. Above these two layers the wind turns gradually and reaches the direction of the geostrophic wind of the free atmosphere (only pressure-gradient and Coriolis force is present, in equilibrium the wind is parallel to the isobars) at about 1000m. This layer of turning wind is called the **Ekman layer**.

Discharged material from stacks is usually released in the bottom 100m of the atmosphere. For this reason the Prandl layer is the one where the modelling should take place and turbulent diffusion must be assumed.

The Gaussian plume equation:

Conservation of mass yields the continuity equation:

$$\frac{\partial c}{\partial t} = -div\vec{j}$$

The flux j consists of a uniform flux in the wind-direction and the turbulent diffusion flux:

$$\vec{j} = \vec{j}_{turb} + \vec{j}_{unif}$$

The uniform flux in winddirection is given by

$$\vec{j}_{unif} = c\vec{v}$$

For the turbulent flux a gradient-ansatz is done similar to molecular diffusion:

$$j_x = -K_x \frac{\partial c}{\partial x}$$

$$j_y = -K_y \frac{\partial c}{\partial y}$$

$$j_z = -K_z \frac{\partial c}{\partial z}$$

where j_i is the flux, K_i (i=x,y,z) the turbulent diffusion coefficients and c the concentration,

hence

$$\frac{\partial c}{\partial t} = \sum_{i=x,y,z} \frac{\partial}{\partial i}\left(K_i \frac{\partial c}{\partial i}\right) - \frac{\partial}{\partial i}\left(c v_i\right)$$

In our case a continuous Emission from a stack is assumed. Taking x as the wind direction and neglecting diffusion in this direction the solution of the differential equation is

$$c(y,z,t) = \frac{const}{2\pi\sqrt{4K_yK_zt^2}} \exp\left[-\left(\frac{y^2}{4K_yt} + \frac{z^2}{4K_zt}\right)\right]$$

if we assume that K_i (i=y,z) is independent of t. Since we neglected diffusion in the x direction this solution equals a growing disk with the thickness of a unit-length in x direction. The disk is transported in the x direction with the velocity v_x. The integration constant can be obtained from

$$E = \int_{-\infty}^{\infty}\int_{-\infty}^{\infty} v_x c(x,y,z)dydz$$

where E is the emission rate (amount material/time). Integration yields const=E/v_x. Hence

$$c(y,z,t) = \frac{E}{2\pi v_x\sqrt{4K_yK_zt^2}} \exp\left[-\left(\frac{y^2}{4K_yt} + \frac{z^2}{4K_zt}\right)\right]$$

c(x,y,z) can be obtained using t=x/v_x

The diffusion coefficients K_i (i=x,y,z) can be obtained from sophisticated meteorological data (see Roedel,1994 for details). Since these data are usually not available the following common approach is used:

Instead of calculating c(x,y,z) via the diffusion constants one can express the diffusion constants by standard deviations (quadratic mean distance from origin) (Roedel, 1994, p.267). The relation between the standard deviations and the diffusion coefficients is given by

$$\frac{d\sigma^2}{dt} = 2K$$

hence the solution can be rewritten as:

$$c(x,y,z) = \frac{E}{2\pi v_x\sigma_y\sigma_z} \exp\left[-\left(\frac{y^2}{2\sigma_y^2} + \frac{z^2}{2\sigma_z^2}\right)\right]$$

In the above solution the stack height equals z=0. The concentration at the ground is:

$$c(x,y,-h) = \frac{E}{2\pi v_x\sigma_y\sigma_z} \exp\left[-\left(\frac{y^2}{2\sigma_y^2} + \frac{h^2}{2\sigma_z^2}\right)\right]$$

This is the correct solution, if the particles are completely absorbed by the ground.

The case of no absorption at the ground yields the boundary condition $\partial c/\partial z(-h)=0$, where h is the stack height. This condition can be satisfied by placing an image source at stack height below the ground. This yields the solution

$$c_{reflect}(x,y,z) = \frac{E}{2\pi v_x\sigma_y\sigma_z}\left\{\exp\left[-\left(\frac{y^2}{2\sigma_y^2} + \frac{z^2}{2\sigma_z^2}\right)\right] + \exp\left[-\left(\frac{y^2}{2\sigma_y^2} + \frac{(z+2h)^2}{2\sigma_z^2}\right)\right]\right\}$$

For the concentration at the ground follows

$$c_{reflect}(x,y,-h) = \frac{E}{\pi v_x\sigma_y\sigma_z} \exp\left[-\left(\frac{y^2}{2\sigma_y^2} + \frac{h^2}{2\sigma_z^2}\right)\right]$$

As one can see in the case of no absorption, the concentration at ground level is twice as high as in the case of complete absorption.

A.7.2 Calculations and assumptions for the dispersion from AWE Aldermaston

In A.8.1 solutions of the Gaussian plume equation have been derived for airborne discharge from a stack.

For a stack of height h the concentration at the ground is

$c(x,y,-h) = \frac{E}{2\pi v_x \sigma_y \sigma_z} \exp\left[-\left(\frac{y^2}{2\sigma_y^2} + \frac{h^2}{2\sigma_z^2}\right)\right]$ if the particles are completely absorbed by the ground and $c_{reflect}(x,y,-h) = \frac{E}{\pi v_x \sigma_y \sigma_z} \exp\left[-\left(\frac{y^2}{2\sigma_y^2} + \frac{h^2}{2\sigma_z^2}\right)\right]$

in the case of no absorption. The σ^2 are the mean quadratic replacements, e.g. $\sigma_y^2 = \left\langle (y - y_0)^2 \right\rangle$.

The stacks at AWE Aldermaston have a height of 30m. The standard deviations in the plume equation in dependent on the meteorological conditions and are taken from the German emergency guidelines for a reactor incident (BMJ, 1994). In these guidelines the standard deviations are parameterised by

$\sigma_y = \sigma_{0y} x^{s_y}$ and $\sigma_z = \sigma_{0z} x^{s_z}$

The values for σ_0 and s are listed in tables depending of the atmospheric stability class and stack height (BMJ, 1994). The stability class depends on the horizontal wind velocity and temperature gradient, which is correlated with solar irradiation. From wind and solar irradiation data, the mean stability class D is chosen for Aldermaston. The parameters for this stability class and a stack height of 50m are σ_{0y}=0.64, σ_{0z}=0.215, s_y=0.784 and s_z=0.885.

Dry deposition

The calculation of the deposited material per m^2 and time can be carried out by multiplying the surface air concentration by a deposition velocity v_g. The deposition velocity depends on the process of the deposition, which depends on particle size. For particles of a diameter smaller than 0.1 µm diffusion is most important, for particles between tens of a µm to about 10 µm inertial deposition is the most dominant process and for diameters greater than 10 µm gravitational deposition dominates. A recommended deposition velocity for aerosols from nuclear accidents is $v_g = 1.5\times10^{-3}$ m/s (BMJ, 1994). In the calculations for Aldermaston, the air concentrations are always calculated for periods of one hour. To get the ground concentration that arises from the deposition per hour, the air concentrations have to be multiplied by the distance that reaches the ground in one hour, hence 1.5×10^{-3} m/s × 60×60 s = 5.4m.

Wash out

For the deposition at distances close to the source the particles are not high enough to be involved in the droplet formation, hence the capture of particles by the falling drops is the only contribution to the concentration in the rain-water. Large particles can be captured directly by the drop. As the particles become smaller they follow the streamlines around the drop and the probability for direct capture decreases. The mechanism that incorporates smaller particles is diffusion, mostly thermal diffusion. The washout efficiency epsilon is defined by

$$\varepsilon = \frac{c_{RW}}{c_A V_A} = \frac{c_{RW}}{N_A}$$

where c_{RW} is the concentration in the rain water, c_A the average concentration in the air, V_A the volume of the air beneath the cloud and N_A the number of particles in the air beneath the cloud. Epsilon is given in Roedel (1994, p.201) (assumed epsilon=10^{-3})

Hence the number of deposited particles N_D is given by

$$N_D = N_A V_{RW} \varepsilon$$

Where V_{RW} is the total volume of rain.

If all is taken per m^2 then:

$$c'_{Deposited,Wash-out}(x,y) = c'(x,y) V'_{RW} \varepsilon$$

where V'_{RW} is the volume of rain per m^2 and c' an area concentration.

To get the concentration of c'(x,y), it is necessary to integrate:

$$c'(x,y) = \int_{-h}^{\infty} c_{reflect}(x,y,z)dz$$

From the symmetry of the image source it is obvious that

$$c'(x,y) = \int_{-h}^{\infty} c_{reflect}(x,y,z)dz = \int_{-\infty}^{\infty} c(x,y,z)dz$$

The integral yields

$$c'(x,y) = \frac{E}{\sqrt{2\pi} v_x \sigma_y} \exp\left[-\frac{y^2}{2\sigma_y^2}\right]$$

hence

$$c'_{Deposited,Wash-out}(x,y) = \frac{E}{\sqrt{2\pi}v_x\sigma_y}\exp\left[-\frac{y^2}{2\sigma_y^2}\right]V'_{RW}\varepsilon$$

We now have the number of deposited aerosol particles per m^2. For the deposited activity we need the activity per particle A_p. The total deposited activity is then $A_p*(c_{deposited,dry} + c_{deposited\ washout})$.

Transformation on a fixed coordinate system

The calculations presented above are designed for an accidental release with a single wind-direction. The wind-direction is taken as the x-coordinate. In our case it is desired to have the depositions in the same coordinate system to obtain the contribution at a specific point from different wind-directions. The reference-coordinate-system (RCS) is marked with *. The transformation onto this system is done by a rotation in the xy-plane. If φ is the angle between the coordinate axes one gets

$$\begin{pmatrix} x^* \\ y^* \end{pmatrix} = A\begin{pmatrix} x \\ y \end{pmatrix}$$

with

$$A = \begin{pmatrix} \cos\varphi & -\sin\varphi \\ \sin\varphi & \cos\varphi \end{pmatrix}$$

Taking the inverse matrix

$$A^{-1} = \begin{pmatrix} \cos\varphi & \sin\varphi \\ -\sin\varphi & \cos\varphi \end{pmatrix}$$

and the parameterisations of the standard deviations from BMJ (1994) one gets

$$c'_{Deposited,Wash-out}(x^*,y^*) =$$

$$\frac{E}{\sqrt{2\pi}v_x\sigma_{0y}(x^*\cos\varphi + y^*\sin\varphi)^{s_y}}\exp\left[-\frac{(-x^*\sin\varphi + y^*\cos\varphi)^2}{2\sigma_{0y}^2(x^*\cos\varphi + y^*\sin\varphi)^{2s_y}}\right]V'_{RW}\varepsilon$$

and

$$c_{reflect}(x^*,y^*,-30) =$$

$$\frac{E}{\pi v_x\sigma_{0y}\sigma_{0z}(x^*\cos\varphi + y^*\sin\varphi)^{s_y+s_z}}\exp\left[-\left(\frac{(-x^*\sin\varphi + y^*\cos\varphi)^2}{2\sigma_{0y}^2(x^*\cos\varphi + y^*\sin\varphi)^{2s_y}} + \frac{30^2}{2\sigma_{0z}^2(x^*\cos\varphi + y^*\sin\varphi)^{2s_z}}\right)\right]$$

For the calculation is convenient to introduce polar coordinates and plug them into the equations.

$$x^* = r\cos\xi$$

$$y^* = r\sin\xi$$

Meteorological Office data are used for the calculations. The data contain mean hourly wind speed, mean hourly wind direction and hourly rain volume. The wind direction is given in spacings of 10

degrees and the wind speed is measured at a height of 10m. The wind speed at stack height of 30m is calculated via (BMJ, 1994) $v = v_1\left(\frac{H}{z_1}\right)^m$

where v and v_1 are the wind speeds at the stack height H and the reference height z_1.
m is a parameter that depends on the atmospheric stability. For stability class D the value is 0.28.
The concentrations $c_{reflect}$ and the wash-out $c_{Deposited\ Wash\text{-}out}$ are calculated via the equations above for each hour and then summed for the whole year. To do this is has to be kept in mind that the original formula was derived for x>0. The parameterisation of the standard deviations, however, introduced a x dependence, which results in non-zero values for x<0. For this reason only sections of 90 degrees in the reference coordinate system can be processed at a time.

To get the correct results at the boundaries of each section, the data is processed for 8 sections Ω_k of approximately 90 degrees each (0-90, 40-140, 90-180, 140-220, 180-270, 230-330, 270-360, 310-50). The results are then taken for 40 or 50 degrees out of the middle of each section. The final equations for each section are

$$c_{reflect,\Omega}(r,\xi,-30) =$$
$$\sum_{i=1952}^{1998}\sum_{\varphi\in\Omega_k}\sum_{j}\frac{E_i/8760}{\pi v_j \sigma_{0y}\sigma_{0z}(r\cos\xi\cos\varphi+r\sin\xi\sin\varphi)^{s_y+s_z}}\exp\left[-\left(\frac{(-r\cos\xi\sin\varphi+r\sin\xi\cos\varphi)^2}{2\sigma_{0y}^2(r\cos\xi\cos\varphi+r\sin\xi\sin\varphi)^{2s_y}}+\frac{30^2}{2\sigma_{0z}^2(r\cos\xi\cos\varphi+r\sin\xi\sin\varphi)^{2s_z}}\right)\right]$$

$$c'_{Deposited,Wash-out,\Omega}(r,\xi) =$$
$$\sum_{i=1952}^{1998}\sum_{\varphi\in\Omega_k}\sum_{j}\frac{E_i/8760}{\sqrt{2\pi}v_j\sigma_{0y}(r\cos\xi\cos\varphi+r\sin\xi\sin\varphi)^{s_y}}\exp\left[-\left(\frac{(-r\cos\xi\sin\varphi+r\sin\xi\cos\varphi)^2}{2\sigma_{0y}^2(r\cos\xi\cos\varphi+r\sin\xi\sin\varphi)^{2s_y}}\right)\right]V'_j\varepsilon$$

$$c'_{Deposited,Dry,\Omega}(r,\xi,-30) = c_{reflect,\Omega}(r,\xi,-30)\times 1.5\times 10^3\,\tfrac{m}{s}\times 3600s = c_{reflect,\Omega}(r,\xi,-30)\times 5.4m$$

where j are the hours with wind-direction phi. $E_i/8760$ is the mean discharge per hour.
The Meteorological Office data report '***' for value not available, 'trace' for small amounts of precipitation and '999' for variable wind direction.

Steps used in Microsoft Excel to process the Meterological Office data

1. Sort data by rain-amount-column and set trace=***=0.

2. Sort data by windspeed and delete all rows with windspeed 0. This assumes that at zero windspeed all discharge is deposited on the site.

3. The file after step 1 and 2 is called "*Hsoco.xls*"

4. Copy 8 sections of 90 degree each out of "*Hsoco.xls*" and save them in "*x-y.a-b.xls*", where x is the starting year, y the ending year and a and b the angles of the octant.

5. A spreadsheet called "*Muster.xls*" was created that contains all the calculations described in the text

6. Each "*x-y.a-b.xls*" is copied into "*Muster.xls*" at a time and called "*mx-y.a-b.xls*".

7. For each year the discharge values from the discharge records are filled in the calculations and concentration and wash out are calculated for each hour and the summed over all the hours for each year. Then the values are calculated on circles with distance (in meter) 10, 20, 30, 50, 100, 200, 400, 600, 800, 1000, 1500, 2000, 3000, 4000, 5000, 8000, 10000 are calculated in spacings of 10 degrees.

A.7.3 Main assumptions and approximations used for the model

- The Gaussian plume equation approximates the dispersion well. The equation was derived for a uniform wind in one direction. It is obvious, that when the wind direction changes too frequently the plume cannot evolve completely.
- The atmosphere has neutral stability. This is the prominent stability due to Pasquill's criteria (Pasquill, 1983). However, the effect of this assumption is small.
- The materials are discharged continuously. However, even if this is not the case the calculated values give the probability of the dispersion.
- A single point source is assumed.
- At zero windspeed all material is deposited on site.
- Heathrow meteorological data are a reasonable approximation for the Aldermaston area.

A.7.4 Effects of the modelled deposition for the measurements

In the following it is shown how the calculated SAC and WO concentrations will affect the measured values (concentrations and isotopic ratios) in the soils. Both the SAC and the WO are stated in units of meters. The sampling area was 18cmx18cm, which equals 0.0324 m^2. For that reason the calculated SAC and WO are multiplied by 0.0324. In addition, the surface air concentration is multiplied by $1.5x10^{-3}$x60x60m to get the ground concentration for the dry deposition.

Uranium:

The average concentration of uranium in soils in the Aldermaston area is 1.6ppm. (average in UK is 2-3ppm). The natural $^{238}U/^{235}U$ ratio is 137.88. The concentration of the individual isotopes can be calculated from the ratio:

$$R_{8/5} = \frac{N_8}{N_5} = \frac{m_8}{m_5}\frac{M_5}{M_8} = \frac{T - m_5}{m_5}\frac{M_5}{M_8}$$

where N are the number of particles, m are the masses, M the molar masses and T the total mass of ^{235}U and ^{238}U. In the case of natural uranium it is a good assumption that T equals the total mass of uranium, since the abundance of ^{234}U uranium is low. For the mass of ^{235}U and ^{238}U follows:

$$m_8 = m_5 R \frac{M_8}{M_5}$$

and

$$m_5 = \frac{T\frac{M_5}{M_8}}{R + \frac{M_5}{M_8}}$$

Increase of U concentration in soils:

For the calculation of the masses from the activities, the ratio of the discharged uranium is needed. Since the discharged material is a mixture of enriched and depleted uranium of unknown composition, the extreme cases of only enriched discharge and only depleted discharge are investigated. A $^{238}U/^{235}U$ of 285 for depleted and a ratio of 0.07 for enriched uranium is assumed.

The discharge records are given in activities. The masses are calculated from the activities as follows:

$$A = A_{238} + A_{235} = \lambda_{238}N_{238} + \lambda_{235}N_{235}$$

Using $R_{8/5} = \frac{N_8}{N_5}$, $m = \frac{NM}{N_{Av}}$ and $\lambda = \frac{\ln 2}{t_{1/2}}$ one get

$$m_{238} = \frac{A}{\left(\frac{\ln 2}{t_{1/2}^{235}}\frac{1}{R_{8/5}} + \frac{\ln 2}{t_{1/2}^{238}}\right)}\frac{M_{238}}{N_{Av}} \text{ and } m_{235} = m_{238}\frac{M_{235}}{M_{238}}\frac{1}{R_{8/5}}$$

The total mass U is given by $m_U=m_{238}+m_{235}$. Assuming all deposited uranium stays in the top 5cm (thickness of sampling layer) the concentration is obtained by dividing m_U by the weight of the 5cm-layer.

Change of R8/5 ratio in soils:

Using $m = \frac{NM}{N_{Av}}$ one get

$$R_{8/5}^{mix} = \frac{N_{238}^{nat} + N_{238}^{AWE}}{N_{235}^{nat} + N_{235}^{AWE}} = \frac{M_{235}}{M_{238}}\frac{m_{238}^{nat} + m_{238}^{AWE}}{m_{235}^{nat} + m_{235}^{AWE}}$$

Plutonium:

The concentration in the soils from fallout is about 1Bq/kg. Weapon fallout Pu consists of 84.5% ^{239}Pu and 15.5% ^{240}Pu (^{240}Pu/^{239}Pu=0.18). For the discharged Pu weapon grade Pu with an isotopic composition of 93% ^{239}Pu and 7% ^{240}Pu ($R_{4/9}$=0.075) is assumed.

Change in concentration:

Since both the concentration in the soils and the discharge records are measured in activities, the added concentration is obtained by dividing the calculated SAC and WO by the weight of the soil.

Change in ratio:

Similar to the case of uranium, the numbers of particles N_{239}^{FO}, N_{239}^{WG}, N_{240}^{FO} and N_{240}^{WG} are calculated via:

$$N_{240} = \frac{A}{\left(\frac{\ln 2}{t_{1/2}^{239}}\frac{1}{R_{4/9}} + \frac{\ln 2}{t_{1/2}^{240}}\right)} \text{ and } N_{239} = \frac{N_{240}}{R_{4/9}}.$$

This assumes that the discharged plutonium consists only of ^{239}Pu and ^{240}Pu.

The ratio of the mixture is then obtained from

$$R_{4/9} = \frac{N_4^{FO} + N_4^{WG}}{N_9^{FO} + N_9^{WG}}$$

Results:

For both uranium and plutonium the change of concentration and ratio in the soil is investigated for the highest values of dry deposition and washout at a distance of 1000m. The dry deposited uranium (enriched or depleted) increases the concentration in the soil sample by about 10^{-10}ppm and the ratio is affected in the sixth decimal place. Plutonium soil concentrations change by about 10^{-9} Bq/kg and the ratio is affected in the 10^{th} decimal place. These small changes are not detectable. Therefore all anomalies that will be found are in contrast to the calculated values from the discharge records.

A.7.5 Calculation of the critical ratios and concentrations

It is interesting to see how the soil concentrations and ratio would change if the surface air concentration is that high that the intake by inhalation continuously succeed the recommended value of 1mSv. To do this the critical air concentration is defined as the concentration that gives an adult 1mSv each year. It can be calculated from

$$c_{crit} \times breathing\ \ rate \times CEDE = 1mSv\ /\text{year}$$

The breathing rate of an adult is 0.00023m^3/s which is 7253.28 m^3/year (BMJ, 1994). The CEDE values for the isotopes of interest are listed in the Table A.2.

For uranium the value 0.000033 is taken for enriched uranium and 0.000031 for depleted uranium.

	^{240}Pu	^{239}Pu	^{238}U	^{235}U	^{234}U
adult	0.00008	0.00008	0.000031	0.000033	0.000035
child	0.00011	0.00011	0.00005	0.000052	0.000056

Table A.2 CEDE values inSv/Bq(NRPB-GS7, 1987)

The critical concentrations are 0.001723 Bq/m^3 for Pu, 0.004447 Bq/m^3 for depleted U and 0.004178 Bq/m^3 for enriched uranium.

The critical ground concentration activities per m^2 are calculated via

$$c_{crit}^{ground} = c_{crit}^{air} v_d t$$

where v_d=1.5×10^{-3} m/s is the deposition velocity and t=46*365*24*60*60s the time of the 46 years between 1952 and 1988. The results are presented in Table A.7. The first column indicates the discharged material and the second column gives the critical air concentration. The third and fourth column give the concentration and isotopic ratio that we would measure if all the deposited material

stays in the top 5cm. As well the concentration as the ratios differ significantly from the background values and are detectable without a problem.

Discharged material	Crit. air conc. in Bq/m^3	Soil conc of top layer	Isotopic ratio
Pu	0.002	121 Bq/kg	0.076
U depl.	0.004	25 ppm	268
U enr.	0.004	4 ppm	0.50

Table A.3 Expected results from continuous air concentration above the limit

A8 Data

Abbreviations:

b.d. below detection limit (see detection limits)
n.r. not recorded
n.a. not analysed (either due to selection or due to analytical problems)

Detection limits:

The detection limit is defined here as the minimal concentration to get a quantitavely reliable result.
On the Isoprobe 60fg ^{239}Pu are needed for a reliable determination of the ^{239,240}Pu concentration.
Assuming ^{240}Pu/^{239}Pu=0.2 this equals 0.25mBq.
Depending on the sample size the detection limits in the units of the tables are:
Rothamsted grass: 5mBq^{239,240}Pu /kg
Alpine ice: 0.003mBq^{239,240}Pu /kg – 0.2mBq^{239,240}Pu /kg
The detection limit for the ^{240}Pu/^{239}Pu is about a factor 4 higher.
Detection limit ^{137}Cs: 50 mBq

Errors if not otherwise stated:

Error ^{239,240}Pu activity: <1%
Error ^{240}Pu/^{239}Pu: <1%
Error ^{137}Cs: 5% - 20%

Method blanks for low concentration measurements:

Air filters and Rothamsted grass
Pu method blank: (Method Blank voltage on 239)/(Sample voltage on 239) < 1/1000 (not subtracted)
U method blank: (Method Blank voltage on 238)/(Sample voltage on 238) < 1/40 (not subtracted)

Alpine ice
Pu method blank: (Method Blank voltage on 239)/(Sample voltage on 239) < 1/1000 (not subtracted)
U method blank: (Method Blank voltage on 238)/(Sample voltage on 238) < 1/5 (subtracted)

Data tables

Table A4 $^{240}Pu/^{239}Pu$ for air filters from the PTB Braunschweig (Chapter3)

Code	Year	Beginning of sampling	End of sampling	$^{240}Pu/^{239}Pu$
PTB73	1973	unknown	unknown	0.165
PTB 1	1975	28Apr	2Jun	0.156
PTB76	1976	complete year		0.141
PTB 4	1977	14Oct	31Oct	0.239
PTB 5	1977	31Oct	7Dec	0.232
PTB78	1978	May	May	0.226
PTB 7+8	1978	31Mar	1Sep	0.217
PTB 9+10	1979	1Feb	31Aug	0.192
PTB 11+12	1979	15Oct	2 Jan 1980	0.213

Table A5 $^{240}Pu/^{239}Pu$ for stratospheric filters from Sweden (Chapter 3)

Sample	Sampling date	Sampling height	$^{240}Pu/^{239}Pu$
L212	17.10.58	11.8 km	0.101
L250	01.01.59	11.8 km	0.144
L626	18.09.62	unknown	0.213

Table A.6 Radionuclide data for grass samples from the Rothamsted archive (Chapter 3)

Year	Begin of sampling	End of sampling	^{137}Cs Bq/kg	^{239,240}Pu Bq/kg	^{240}Pu/^{239}Pu	^{238}U/^{235}U
1945	n.r.	n.r.	b.d.	b.d.	b.d.	137.78
1946	n.r.	n.r.	b.d.	b.d.	b.d.	n.a.
1950	13-Jun	15-Jun	b.d.	b.d.	b.d.	137.78
1951	21-Jun	23-Jun	b.d.	b.d.	b.d.	137.78
1952	19-Jun	23-Jun	b.d.	0.05	0.060	137.26
1953	21-Jul	23-Jul	9.2	0.04	0.154	137.46
1954	24-Jun	26-Jun	17.7	0.07	0.306	137.98
1955	28-Jun	30-Jun	36.3	0.26	0.273	137.78
1956	11-Jul	12-Jul	40.2	0.27	0.241	137.70
1957	18-Jun	19-Jun	32.1	0.19	0.165	137.77
1958	7-Jul	8-Jul	70.7	0.34	0.166	137.14
1959	15-Jun	16-Jun	63.3	0.21	0.175	137.34
1960	16-Jun	16-Jun	39.6	0.16	0.183	137.56
1961	20-Jun	20-Jun	22.7	0.10	0.198	137.68
1962	13-Jun	13-Jun	81.5	0.36	0.162	137.15
1963	27-Jun	27-Jun	257.0	1.55	0.221	137.50
1964	26-Jun	30-Jun	209.0	1.00	0.201	n.a.
1965	28-Jun	29-Jun	122.6	0.53	0.188	n.a.
1966	7-Jun	7-Jun	66.1	0.12	0.202	137.72
1967	12-Jun	12-Jun	33.6	n.a.	n.a.	n.a.
1968	11-Jun	11-Jun	34.2	0.10	0.208	137.79
1969	9-Jun	10-Jun	18.6	n.a.	n.a.	n.a.
1970	15-Jun	15-Jun	28.3	0.11	0.205	n.a.
1971	24-Jun	24-Jun	31.2	n.a.	n.a.	n.a.
1972	15-Jun	16-Jun	25.5	0.05	0.169	137.92
1973	13-Jun	13-Jun	12.9	b.d.	b.d.	n.a.
1974	20-Jun	21-Jun	16.0	0.06	0.215	n.a.
1975	9-Jun	10-Jun	15.7	0.03	0.232	138.03
1976	9-Jun	9-Jun	7.4	b.d.	b.d.	137.98
1977	21-Jun	21-Jun	11.4	0.05	0.262	138.34
1978	19-Jun	20-Jun	14.1	n.a.	n.a.	138.30
1979	19-Jun	20-Jun	9.0	0.02	b.d.	137.98
1980	4-Jun	4-Jun	6.1	b.d.	b.d.	n.a.
1981	9-Jun	10-Jun	13.3	b.d.	b.d.	137.91
1983	15-Jun	15-Jun	5.7	b.d.	b.d.	138.23
1985	1-Jul	1-Jul	4.8	b.d.	b.d.	137.88
1986	12-Jun	12-Jun	37.6	b.d.	b.d.	138.03
1987	29-Jun	29-Jun	9.6	b.d.	b.d.	137.85
1988	14-Jun	15-Jun	7.9	b.d.	b.d.	n.a.
1990	2-Jul	2-Jul	3.4	b.d.	b.d.	n.a.
1945-2	n.r.	n.r.	12.9	b.d.	b.d.	n.a.
1951-2	2-Okt	5-Okt	b.d.	b.d.	b.d.	n.a.
1952-2	22-Sep	23-Sep	b.d.	b.d.	b.d.	n.a.
1953-2	19-Nov	23-Nov	24.3	0.08	0.135	n.a.
1955-2	15-Sep	20-Sep	48.4	0.05	0.295	n.a.
1957-2	24-Sep	26-Sep	55.6	0.44	0.113	n.a.

Table A.7 U and Pu data for the Mont Blanc Alpine ice core (Chapter 3)

Plutonium				Uranium	
Depth (cm)	^{239,240}Pu mBq/kg	^{240}Pu/^{239}Pu	Ice weight (kg)	Depth (cm)	^{238}U/^{235}U
-35.38	0.007	b.d.	82.42	-4.4	135.29
-36.4	0.058	b.d.	2.90	-9.29	136.18
-37.51	0.083	b.d.	2.00	-10.19	138.39
-38.61	0.058	b.d.	2.75	-14.68	136.80
-39.6	0.059	b.d.	3.02	-21.04	137.32
-40.65	0.069	b.d.	2.65	-24.75	137.59
-41.7	0.033	b.d.	2.41	-26.84	137.22
-42.65	0.135	b.d.	1.58	-31.24	136.81
-54.14	0.004	b.d.	38.25	-35.38	137.55
-64.21	0.018	b.d.	46.51	-37.51	135.82
-68.42	0.019	b.d.	22.70	-38.61	136.28
-73.37	0.019	b.d.	19.41	-39.6	134.74
-77.82	0.060	0.186	22.17	-40.65	136.12
-85.22	0.061	0.205	24.90	-41.7	135.51
-86.43	0.166	0.202	4.66	-42.65	135.20
-88.12	0.140	0.214	4.62	-45.135	137.53
-88.81	0.383	0.213	1.72	-47.62	137.43
-89.7	0.802	0.206	2.20	-51.532	137.61
-90.28	0.907	0.232	1.92	-54.14	138.22
-91.16	2.165	0.247	2.05	-55.2756	138.49
-92.02	1.141	0.217	2.53	-56.4111	137.36
-92.8	0.794	0.221	2.65	-59.25	139.03
-93.66	0.578	0.165	2.64	-64.21	138.20
-95.55	0.108	0.191	5.16	-68.42	138.70
-96.36	0.240	0.181	2.78	-73.37	135.74
-97.19	0.271	0.177	2.82	-77.82	137.11
-97.96	0.540	0.159	2.11	-85.22	138.17
-98.77	0.797	0.161	2.54	-85.82	133.05
-99.69	0.183	0.160	2.17	-86.43	132.26
-100.52	0.275	0.184	2.41	-87.32	134.08
-101.36	0.627	0.255	2.35	-88.12	132.17
-102.14	0.460	0.255	6.01	-88.81	131.14
-103.63	0.453	0.261	2.42	-90.28	131.95
-104.51	0.159	b.d.	2.25	-91.16	132.49
-105.19	0.080	b.d.	2.55	-92.02	128.77
-105.94	0.042	b.d.	3.06	-92.8	137.53
-106.4	0.038	b.d.	2.72	-93.66	131.45
-107.06	0.089	b.d.	2.49	-94.6	133.68
-107.61	b.d.	b.d.	2.68	-95.55	134.43
-108.46	b.d.	b.d.	1.67	-96.36	133.51
-109.14	b.d.	b.d.	1.35	-97.19	133.83
-109.96	b.d.	b.d.	1.76	-97.96	132.14
-110.83	b.d.	b.d.	1.33	-98.77	131.13
-111.66	b.d.	b.d.	1.86	-99.69	128.29
-112.35	b.d.	b.d.	1.47	-101.36	132.67
-113.05	b.d.	b.d.	1.28	-102.89	135.83
-113.85	b.d.	b.d.	1.48	-103.63	131.72
-114.65	b.d.	b.d.	1.42	-104.51	131.99
-115.16	b.d.	b.d.	1.88	-105.94	134.13
				-107.06	134.70
				-109.14	134.84
				-109.96	134.58
				-111.66	133.58
				-112.35	135.42
				-113.05	134.61
				-113.85	134.05
				-114.65	135.33

Sample	Depth (cm)	^{241}Pu (Bq/kg)	Error %	^{238}Pu (Bq/kg)	Error %	^{239,240}Pu (Bq/kg)	Error %	^{240}Pu/ ^{239}Pu	^{60}Co (Bq/kg)	^{137}Cs (Bq/kg)	S (wt %)	MnO (wt %)	Fe_2O_3 (wt %)	Al_2O_3 (wt %)
PH7/1	-0,5							0.212	37.3	11.3	1.185	0.03	5.5	11.99
PH7/2	-2	41.8	5.2	0.6	7.6	2.4	3.9	0.213	36.9	11.4	1.091	0.03	5.22	11.17
PH7/3	-4							0.225	50.1	13.4	1.002	0.03	5.13	11.3
PH7/4	-6	56.9	5.4	0.7	9.0	3.7	3.9	0.228	54.5	19.4	1.078	0.03	5.29	11.98
PH7/5	-8							0.223	48.7	20.3	1.202	0.03	5.45	12.32
PH7/6	-10	n.a.	n.a.	1.2	13.3	5.5	6.3	0.213	31.3	20.5	1.29	0.03	5.49	12.1
PH7/7	-12							0.184	21.5	19.7	1.306	0.03	5.46	11.9
PH7/8	-14	41.2	4.7	0.5	7.0	3.4	2.8	0.180	10.0	19.6	1.363	0.03	5.55	12.04
PH7/9	-16							0.175	7.7	21.9	1.431	0.03	5.44	11.87
PH7/10	-18	13.8	7.6	0.1	23.7	1.6	6.6	0.171	3.7	20.3	1.407	0.03	5.37	11.65
PH7/11	-20							0.161	0.0	22.0	1.364	0.03	5.37	11.36
PH7/12	-22	12.3	8.3	0.1	34.3	1.9	8.6	0.169	0.0	18.9	1.478	0.03	5.26	11.31
PH7/13	-24							0.185	0.4	21.9	1.461	0.03	5.11	11.27
PH7/14	-26	11.6	6.9	0.1	23.7	1.1	5.1	0.184	1.2	18.4	1.588	0.03	5.31	11.78
PH7/15	-28							0.186	0.0	12.4	1.599	0.03	5.34	12.1
PH7/16	-30	1.9	8.8	0.0	41.7	0.9	9.1	0.233	1.4	11.0	1.758	0.03	5.33	11.89
PH7/17	-32							0.202	0.0	9.1	1.807	0.03	5.2	11.93
PH7/18	-34	2.6	8.7	0.0	30.2	0.3	12.2	0.212	0.0	5.4	1.95	0.03	5.4	12.65
PH7/19	-36							0.188	0.0	b.d.	2.085	0.03	5.69	12.81
PH7/20	-38	6.9	7.4	0.1	22.1	0.2	13.1	0.211	0.0	b.d.	2.191	0.03	5.75	12.65
PH7/21	-40							0.196	0.0	b.d.	2.253	0.03	5.75	12.69

Table A.8 Radionuclide and geochemical data for Poole sediment core (Chapter 5)

Table A.9 U and Pu data for the AWE survey (West Berkshire) * (Chapter 6)

Sample code	Eastings	Northings	^{239,240}Pu Bq/kg dry	^{240}Pu/^{239}Pu	^{238}U/^{235}U	3 s.e.	Deviation from natural
001	457980	162710	2.17	n.a.	138.01	0.47	
002	458040	162720	12.39	n.a.	135.43	0.32	-2.45
003	458080	162730	4.32	n.a.	135.80	0.26	-2.08
004	458120	162740	2.23	n.a.	137.39	0.27	-0.49
005	458160	162750	4.09	n.a.	136.48	0.33	-1.4
006	458060	162770	1.02	n.a.	138.24	0.24	
007	458070	162750	5.00	n.a.	139.22	0.27	1.34
008	458090	162710	1.77	n.a.	136.84	0.28	-1.04
009	458050	162650	5.29	0.176	131.91	0.35	-5.97
010	458110	162640	4.86	0.149	128.02	0.34	-9.86
011	458090	162610	0.36	n.a.	140.23	0.42	2.35
012	468630	169040	0.43	n.a.	137.63	0.29	
014	468700	168850	0.57	n.a.	137.60	0.29	
017	468190	168890	0.48	n.a.	137.66	0.22	
018	468230	168790	0.64	n.a.	137.54	0.36	
019	468300	168680	1.48	n.a.	137.46	0.31	-0.42
022	467110	169450	0.88	n.a.	138.00	0.78	
023	467020	169410	0.50	n.a.	138.30	0.70	0.42
025	465690	169690	0.46	n.a.	137.80	0.20	
026	465330	169590	0.41	n.a.	137.61	0.28	
028	464080	166370	1.98	n.a.	138.49	0.33	0.61
029	463580	166300	1.27	n.a.	139.63	0.31	1.75
030	463880	165860	5.74	0.181	138.49	0.28	0.61
031	462610	166180	0.75	n.a.	137.90	0.27	
032	463040	166220	1.15	n.a.	138.04	0.31	
033	463490	165690	2.15	n.a.	139.13	0.25	1.25
034	463180	165380	2.46	n.a.	140.30	0.66	2.42
035	463410	165200	0.34	n.a.	138.36	1.21	0.48
036	463520	164900	0.10	n.a.	137.96	0.32	
037	463850	164590	0.14	n.a.	137.46	0.78	-0.42
038	463010	164950	5.04	n.a.	139.44	0.26	1.56
041	463300	164600	5.17	0.176	139.67	0.72	1.79
042	462810	164730	7.17	0.175	140.22	0.39	2.34
044	462340	164500	0.34	n.a.	137.77	0.23	
045	462290	164190	0.44	n.a.	138.03	0.27	
046	462440	164020	2.14	n.a.	138.74	0.38	0.86
047	462190	163990	4.10	n.a.	138.76	0.24	0.88
048	461970	163830	5.21	0.162	138.96	0.42	1.08
049	461820	163600	6.96	0.167	143.49	0.35	5.61
050	462140	163610	1.45	n.a.	141.05	0.34	3.17
051	462780	163520	1.53	n.a.	138.22	0.24	
052	462770	163820	3.78	n.a.	139.95	0.56	2.07
053	462310	162830	4.64	0.175	141.27	0.83	3.39
054	462150	163300	2.42	n.a.	139.79	0.30	1.91
055	462470	163420	3.29	n.a.	138.24	0.30	
056	461110	161030	2.58	n.a.	138.02	0.29	
057	461430	161290	4.02	0.170	143.12	0.46	5.24
058	461830	161730	0.54	n.a.	137.85	0.24	
059	461590	160880	0.45	n.a.	137.03	0.33	-0.85
060	461240	160430	1.51	n.a.	138.17	0.24	
061	462080	160430	0.58	n.a.	138.05	0.34	
062	462260	161480	0.91	n.a.	138.27	0.29	
063	461240	161500	1.33	n.a.	138.51	0.41	0.63
064	456150	161300	0.43	n.a.	137.38	0.47	-0.5
065	456630	160870	1.94	n.a.	137.93	0.25	
066	456820	161400	0.55	n.a.	137.74	0.30	
067	457420	161980	0.64	n.a.	137.93	0.25	
068	457000	162160	1.89	n.a.	137.95	0.33	
070	456650	161860	0.66	n.a.	137.61	0.30	
071	456240	162000	0.39	n.a.	137.97	0.44	
074	425450	117350	2.39	n.a.	138.09	0.32	
076	420500	128400	1.24	n.a.	138.10	0.20	
079	422400	160400	0.41	n.a.	137.77	0.22	
082	421500	168200	0.66	n.a.	138.02	0.23	
082	421500	168200	0.54	n.a.	137.89	0.32	

AWE Data (West Berkshire)cont.

Sample code	Eastings	Northings	^{239,240}Pu Bq/kg dry	^{240}Pu/^{239}Pu	^{238}U/^{235}U	3 s.e.	Deviation from natural
085	421400	167300	0.59	n.a.	138.01	0.28	
087	458400	167500	0.40	n.a.	137.83	0.28	
088	452300	180300	0.34	n.a.	137.98	0.36	
090	455400	177200	0.90	n.a.	138.05	0.23	
093	459600	173500	1.72	n.a.	138.16	0.31	
097	465500	169700	0.46	n.a.	137.97	0.25	
104	468800	169000	0.45	n.a.	138.03	0.32	
107	453600	185800	0.39	n.a.	137.71	0.18	
A1	459850	164700	0.52	0.151	138.04	0.21	
A2	459150	165700	0.12	n.a.	137.91	0.21	
A3	458940	166780	0.33	n.a.	138.00	0.21	
A4	459850	167460	0.10	n.a.	137.98	0.21	
A5	459180	168280	0.80	n.a.	137.81	0.21	
A5	459180	168280	0.27	n.a.	137.97	0.21	
B1	460350	164760	0.82	n.a.	138.84	0.21	0.96
B2	460810	164850	0.87	0.167	138.42	0.21	0.54
B3	461800	166140	0.32	n.a.	137.96	0.21	
B3	461800	166140	0.27	n.a.	138.00	0.21	
B4	462170	166140	0.66	n.a.	139.73	0.21	1.85
B5	462930	167260	0.65	n.a.	138.22	0.21	0.34
C2	461430	163470	0.78	0.191	139.01	0.21	1.13
C3	462500	163500	2.97	0.135	141.52	0.21	3.64
C4	463500	163500	0.34	n.a.	138.08	0.21	
C5	464300	163500	0.52	n.a.	137.90	0.21	
C5	464300	163500	0.28	n.a.	137.98	0.21	
D1	460140	162660	0.11	n.a.	138.74	0.21	0.86
D2	460900	161900	0.31	n.a.	137.90	0.21	
D3	461500	161100	1.49	n.a.	138.00	0.21	
D4	462300	160500	0.59	n.a.	138.16	0.21	0.28
D5	463100	159800	0.81	n.a.	137.96	0.21	
E1	459500	162400	0.23	0.133	138.47	0.21	0.59
E2	459600	161300	2.00	n.a.	138.10	0.21	0.22
E3	459800	160300	0.65	n.a.	137.96	0.21	
E4	459600	159400	0.55	n.a.	137.94	0.21	
E5	459500	158400	0.35	n.a.	138.07	0.21	
F1	458800	162600	0.44	n.a.	144.44	0.21	6.56
F2	458200	161800	0.85	n.a.	138.13	0.21	0.25
F3	457500	161300	0.28	n.a.	138.06	0.21	
F4	456700	160500	0.42	n.a.	137.86	0.21	
F5	456200	159700	0.17	n.a.	137.89	0.21	
G1	458500	163200	5.57	0.134	129.90	0.21	-7.98
G2	457600	163300	2.35	0.178	138.13	0.21	0.25
G3	456800	163400	0.19	n.a.	137.39	0.21	-0.49
G4	455400	163360	0.31	n.a.	137.98	0.21	
G5	454330	163340	0.15	n.a.	137.97	0.21	
H1	458800	164100	0.19	n.a.	137.94	0.21	
H2	458000	164700	0.41	n.a.	138.03	0.21	
H3	457200	165500	0.13	n.a.	138.00	0.21	
H4	456700	166200	1.36	n.a.	137.91	0.21	
H5	455450	167270	0.15	n.a.	137.73	0.21	
BA1	467472	169065	0.22	n.a.	137.50	0.21	-0.38
BA2	467850	170048	0.25	n.a.	137.93	0.21	
BA3	467640	170832	0.21	n.a.	138.02	0.21	
BA4	467882	171882	0.16	n.a.	137.91	0.21	
BA5	467554	172744	0.11	n.a.	138.09	0.21	0.21
BB1	468815	168537	0.53	n.a.	137.44	0.21	-0.44
BB2	469227	169298	0.09	n.a.	137.97	0.21	
BB3	469789	170070	0.64	n.a.	136.84	0.21	-1.04
BB4	470710	170841	0.04	n.a.	137.92	0.21	
BB5	471400	171300	0.41	0.176	137.86	0.21	
BC1	468750	167680	0.29	n.a.	137.86	0.21	
BC2	469930	167670	0.27	n.a.	137.81	0.21	
BC3	470800	167700	0.09	n.a.	137.97	0.21	
BC4	472400	167500	0.10	n.a.	137.90	0.21	
BD1	468600	167300	0.54	n.a.	137.88	0.21	
BD2	469320	166720	0.53	n.a.	137.93	0.21	

AWE Data (West Berkshire)cont.

Sample code	Eastings	Northings	^{239,240}Pu Bq/kg dry	^{240}Pu/^{239}Pu	^{238}U/^{235}U	3 s.e.	Deviation from natural
BD3	470210	166020	0.16	n.a.	137.76	0.21	
BD4	470320	165010	0.40	n.a.	137.89	0.21	
BD5	471300	164490	0.79	n.a.	137.84	0.21	
BE1	467800	166750	0.17	n.a.	137.90	0.21	
BE2	467700	165700	0.13	n.a.	137.93	0.21	
BE3	467700	164600	0.31	0.188	138.03	0.21	
BE4	467800	163800	0.49	0.187	137.98	0.21	
BE5	467900	163100	0.17	0.192	137.93	0.21	
BF1	466800	167050	0.35	0.174	137.96	0.21	
BF2	466450	166500	0.68	0.192	137.91	0.21	
BF3	465650	165750	0.64	0.178	137.97	0.21	
BF4	464850	165200	11.21	0.176	138.31	0.21	0.43
BF5	464300	164400	0.28	0.190	137.64	0.21	-0.24
BG1	466100	167600	0.54	n.a.	138.05	0.21	
BG2	466000	167800	0.22	n.a.	137.89	0.21	
BG2	466000	167800	0.28	n.a.	137.94	0.21	
BG3	464800	167700	0.76	n.a.	137.93	0.21	
BG4	464000	168000	0.30	n.a.	137.82	0.21	
BH1	466700	168400	0.31	n.a.	137.89	0.21	
BH2	466500	169100	0.22	n.a.	137.80	0.21	
BH3	465600	169800	0.00	n.a.	137.87	0.21	
CA1	425510	167160	0.47	n.a.	137.96	0.21	
CA5	425200	171100	1.39	0.188	137.89	0.21	
CB4	428029	169055	0.76	n.a.	137.91	0.21	
CC1	426500	166100	0.39	n.a.	137.91	0.21	
CC3	428200	166200	0.32	n.a.	137.98	0.21	
CC5	430400	165800	0.56	n.a.	137.88	0.21	
CD2	427000	165000	0.40	n.a.	137.70	0.21	
CD4	428400	163400	0.80	n.a.	137.99	0.21	
CE1	425400	165000	0.44	0.193	137.88	0.21	
CE2	425800	163100	0.76	n.a.	137.85	0.21	
CE3	425400	160900	0.50	n.a.	137.87	0.21	
CF1	424000	164500	1.29	0.188	137.99	0.21	
CF2	422500	163200	0.22	n.a.	137.87	0.21	
CG1	424300	166000	1.20	n.a.	137.95	0.21	
CG3	420500	166100	10.87	0.186	137.93	0.21	
CH1	424000	167500	0.72	n.a.	137.98	0.21	
CH2	422300	169000	0.54	n.a.	137.97	0.21	
AS1	461700	163600	4.45	0.059	140.80	0.21	2.92
AS2	461700	163850	18.23	0.186	139.53	0.21	1.65
AS3	461800	162750	6.29	0.083	144.18	0.21	6.3
AS4	461200	163500	2.46	0.045	137.08	0.21	-0.8
AT1/1	461327	163795	0.30	n.a.	137.96	0.21	
AT1/2	461393	163790	0.10	n.a.	137.89	0.21	
AT1/3	461479	163756	0.08	n.a.	137.83	0.21	
AT1/4	461553	163737	0.60	0.082	137.88	0.21	
AT1/5	461567	163730	1.28	n.a.	138.34	0.21	0.46
AT1/6	461597	163720	2.13	0.163	141.46	0.21	3.58
AT2/1	461533	164571	0.36	n.a.	137.94	0.21	
AT2/2	461540	164600	0.39	n.a.	137.94	0.21	
AT2/3	461550	164630	3.43	n.a.	137.89	0.21	
AT2/4	461560	164660	2.68	0.175	140.05	0.21	2.17
AT2/5	461570	164770	1.38	0.167	139.44	0.21	1.56
AT2/6	461580	164750	2.05	0.179	138.54	0.21	0.66
M1	464700	165100	0.31	n.a.	138.29	0.21	0.41
M2	464690	165110	1.99	0.176	138.44	0.21	0.56
M3	464660	165100	2.67	0.180	137.85	0.21	
PF1	461700	162100	1.51	0.178	139.35	0.21	1.47
PF2	461800	161500	0.50	n.a.	137.90	0.21	
PF3	461500	160900	1.62	n.a.	138.00	0.21	
PF4	462100	160500	0.74	n.a.	137.98	0.21	
PF5	461000	160300	0.35	n.a.	137.93	0.21	
WC1	458200	162800	1.34	0.165	136.84	0.21	-1.04
WC2	458600	163000	0.39	n.a.	137.55	0.21	-0.33
WC3	458450	163200	0.41	n.a.	137.96	0.21	
WC4	458100	163000	4.80	0.164	131.28	0.21	-6.6

AWE Data (West Berkshire)cont.

Sample code	Eastings	Northings	^{239,240}Pu Bq/kg dry	^{240}Pu/^{239}Pu	^{238}U/^{235}U	3 s.e.	Deviation from natural
WC5	458250	162600	3.93	0.170	136.33	0.21	-1.55
WC6	459000	163500	3.35	0.068	134.44	0.21	-3.44
516	422500	168200	0.89	n.a.	137.89	0.21	
518	422900	165000	2.04	n.a.	138.00	0.21	
520	422500	166800	0.63	n.a.	137.89	0.21	
CG3	420300	166100	0.36	n.a.	137.89	0.21	
IA1	437100	164900	1.02	0.171	137.95	0.21	
IA3	437200	167200	0.75	n.a.	137.87	0.21	
IA5	437200	169200	1.27	0.184	137.92	0.21	
IB2	438800	165700	1.67	n.a.	137.80	0.21	
IB4	440100	167100	0.47	0.159	137.84	0.21	
IC1	438200	164300	0.73	0.198	137.92	0.21	
IC3	438200	164300	0.22	n.a.	137.94	0.21	
IC5	442400	164300	0.27	n.a.	137.92	0.21	
ID2	438700	162800	0.58	n.a.	137.92	0.21	
ID4	440000	161500	0.74	n.a.	137.82	0.21	
IE1	437400	161100	0.64	0.187	137.89	0.21	
IE3	437300	163200	0.28	n.a.	137.92	0.21	
IE5	437300	159200	0.55	n.a.	137.85	0.21	
IF1	436450	163400	1.44	n.a.	137.88	0.21	
IF2	434050	161300	0.46	n.a.	137.88	0.21	
IG1	436150	164400	0.76	n.a.	137.89	0.21	
IG2	433700	164200	0.45	n.a.	137.94	0.21	
IG3	432350	164400	0.70	0.110	137.93	0.21	
IH1	435450	165350	0.43	n.a.	137.89	0.21	
IH2	434000	167000	0.13	n.a.	137.88	0.21	
IT1/1	435600	165400	0.30	n.a.	137.88	0.21	
IT1/2	435570	165400	4.48	n.a.	137.85	0.21	
IT1/3	435540	165400	0.32	n.a.	137.90	0.21	
IT1/4	435500	165400	0.96	0.163	137.84	0.21	
IT1/5	435450	165400	0.76	n.a.	137.90	0.21	

*for each sample location only the highest Pu-concentration and strongest deviation from the natural ^{238}U/^{235}U out of the investigated layers is shown. More details about can be found in Croudace *et al.* (1999, 2000, 2001)

Table A.10 Radionuclide and geochemical data for Wyre sediment core (Chapter 4)

depth (cm)	^{238}Pu (Bq/kg)	error (%)	^{239,249}Pu (Bq/kg)	error (%)	^{240}Pu/ ^{239}Pu	^{242}Pu/ ^{239}Pu	^{137}Cs (Bq/kg)	S (wt %)	MnO (ppm)
-1	37.4	5.4	205.2	4.3	0.208	0.0090	605	0.29	1881.2
-2	n.a.	n.a.	n.a.	n.a.	n.a.	n.a.	n.a.	0.26	1573.7
-3	41.4	4.6	256.3	3.7	0.207	0.0078	753	0.21	3030.8
-4	n.a.	n.a.	n.a.	n.a.	n.a.	n.a.	n.a.	0.19	2961.5
-5	41.6	4.8	241.6	3.9	0.204	0.0081	666	0.19	2669.8
-6	n.a.	n.a.	n.a.	n.a.	n.a.	n.a.	n.a.	0.19	2098.3
-7	48.8	3.9	268.1	3.3	0.211	0.0090	750	0.18	2637.2
-8	n.a.	n.a.	n.a.	n.a.	n.a.	n.a.	n.a.	0.18	2387
-9	57.3	4.2	295.0	3.5	0.203	0.0089	757	0.18	2674.5
-10	n.a.	n.a.	n.a.	n.a.	n.a.	n.a.	n.a.	0.21	2120.6
-11	61.0	4.8	319.8	4.0	0.209	0.0088	1058	0.20	2902.7
-12	n.a.	n.a.	n.a.	n.a.	n.a.	n.a.	n.a.	0.20	2346.7
-13	70.4	3.9	374.6	3.3	0.212	0.0111	1217	0.23	2782.3
-14	n.a.	n.a.	n.a.	n.a.	n.a.	n.a.	n.a.	0.28	2638.4
-15	91.2	4.5	461.7	3.8	0.215	0.0074	1870	0.21	1917.9
-16	n.a.	n.a.	n.a.	n.a.	n.a.	n.a.	n.a.	0.22	1679.4
-17	129.3	3.6	636.1	3.2	0.220	0.0090	2940	0.21	1468.5
-18	n.a.	n.a.	n.a.	n.a.	n.a.	n.a.	n.a.	0.17	1278.2
-19	135.6	4.4	694.8	4.0	0.222	0.0090	3690	0.25	1178.5
-20	n.a.	n.a.	n.a.	n.a.	n.a.	n.a.	n.a.	0.28	996.8
-21	167.0	4.6	844.2	4.2	0.225	0.0096	4990	0.28	919.1
-22	n.a.	n.a.	n.a.	n.a.	n.a.	n.a.	n.a.	0.34	896.9
-23	164.3	3.8	846.6	3.4	0.217	0.0083	5600	0.31	810.8
-24	n.a.	n.a.	n.a.	n.a.	n.a.	n.a.	n.a.	0.28	950.5
-25	227.3	4.2	1108.1	3.9	0.218	0.0083	5690	0.33	841.9
-26	n.a.	n.a.	n.a.	n.a.	n.a.	n.a.	n.a.	0.50	892
-27	151.8	4.2	826.5	3.7	0.202	0.0066	5970	0.66	963.2
-28	n.a.	n.a.	n.a.	n.a.	n.a.	n.a.	n.a.	0.86	934.5
-29	222.7	4.3	1219.9	4.0	0.189	0.0064	6670	0.67	871.8
-30	n.a.	n.a.	n.a.	n.a.	n.a.	n.a.	n.a.	0.50	898.4
-31	222.0	3.2	1259.9	3.1	0.183	0.0065	7150	0.54	860.9
-32	n.a.	n.a.	n.a.	n.a.	n.a.	n.a.	n.a.	0.68	869.8
-33	105.0	3.9	754.1	3.6	0.163	0.0053	3530	0.68	883.5
-34	n.a.	n.a.	n.a.	n.a.	n.a.	n.a.	n.a.	0.73	832.5
-35	92.8	4.4	903.5	3.9	0.151	0.0038	2490	0.80	785.3
-36	n.a.	n.a.	n.a.	n.a.	n.a.	n.a.	n.a.	0.80	835.2
-37	16.3	6.7	286.9	3.9	0.123	0.0045	1540	0.76	914.1
-38	n.a.	n.a.	n.a.	n.a.	n.a.	n.a.	n.a.	0.86	907.9
-39	13.1	6.6	237.2	3.7	0.107	0.0042	843	0.74	981.9
-41	10.6	10.3	262.4	4.3	0.103	0.0029	592	0.86	998.6
-43	8.8	8.8	263.7	3.5	0.097	0.0027	393	0.88	1133.2
-44	n.a.	n.a.	n.a.	n.a.	n.a.	n.a.	n.a.	0.83	1150.9
-45	7.7	7.1	210.7	3.2	0.091	0.0036	346	1.12	1344.3
-46	n.a.	n.a.	n.a.	n.a.	n.a.	n.a.	n.a.	1.23	1511.9
-47	4.3	13.2	129.0	4.4	0.074	0.0020	296	1.20	1575
-48	n.a.	n.a.	n.a.	n.a.	n.a.	n.a.	n.a.	1.00	1706.8
-49	4.0	11.4	135.0	3.6	0.073	0.0022	205	1.03	1802.4
-50	n.a.	n.a.	n.a.	n.a.	n.a.	n.a.	n.a.	1.11	1680.1
-51	3.1	14.0	123.3	4.0	0.068	0.0019	174	1.28	1877.3
-52	n.a.	n.a.	n.a.	n.a.	n.a.	n.a.	n.a.	1.11	1817.9
-53	2.7	14.6	87.9	4.3	0.061	0.0044	169.5	1.26	1808.4
-54	n.a.	n.a.	n.a.	n.a.	n.a.	n.a.	n.a.	1.32	1809.7
-55	1.2	22.2	64.4	4.5	0.051	0.0023	143	1.35	1795.4
-56	n.a.	n.a.	n.a.	n.a.	n.a.	n.a.	n.a.	1.17	1756.7
-57	0.0	n.a.	37.1	4.3	0.048	0.0102	119.7	1.21	1909
-58	n.a.	n.a.	n.a.	n.a.	n.a.	n.a.	n.a.	1.35	2205.8
-59	0.8	25.5	40.1	4.8	0.034	0.0020	109.7	1.26	1928.8
-60	n.a.	n.a.	n.a.	n.a.	n.a.	n.a.	n.a.	1.33	1827.5
-61	0.6	31.2	52.0	4.7	0.060	0.0048	130.7	1.16	1541.8
-62	n.a.	n.a.	n.a.	n.a.	n.a.	n.a.	n.a.	1.39	1732.2
-63	0.5	24.7	42.6	4.0	0.035	0.0038	189	1.25	1806.1

Appendix 9

Paper:

Plutonium isotope ratio analysis at femtogram to nanogram levels by multicollector ICP-MS

Taylor R.N., Warneke T., Milton J.A., Croudace I.W., Warwick P.E. and Nesbitt R.W.

J. Anal. At. Spectrom. 16, 279-284 (2001)

JAAS FULL PAPER
www.rsc.org/jaas

Plutonium isotope ratio analysis at femtogram to nanogram levels by multicollector ICP-MS

Rex N. Taylor,* Thorsten Warneke, J. Andrew Milton, Ian W. Croudace, Phillip E. Warwick and Robert W. Nesbitt

School of Ocean and Earth Science, Southampton Oceanography Centre, Empress Dock, Southampton, UK SO14 3ZH. E-mail: rex@soc.soton.ac.uk

Received 13th November 2000, Accepted 25th January 2001
First published as an Advance Article on the web 23rd February 2001

Plutonium isotope ratios have been determined on solutions with concentrations covering four orders of magnitude, 100 fg ml^{-1} to 600 pg ml^{-1}, using multicollector ICP-MS (Micromass IsoProbe). Discrimination between different sources of anthropogenic plutonium requires both precise and accurate isotope ratio determination at environmental concentration levels. To achieve a precision of better than 1% at these concentrations, we have developed an analytical procedure in which an equal atom ^{236}U–^{233}U double spike was added to solutions to correct for drift in signal intensity between peak jump sequences. This double spike is also used to correct for instrument mass bias during each ratio determination. Analyses were made on about 1 ml of solution which, in the case of a 100 fg ml^{-1} sample with a fallout ^{240}Pu/^{239}Pu of about 0.18, means a ^{239}Pu content of about 80 fg in the analyte. ^{240}Pu/^{239}Pu can be reproducibly measured to within 1.4% (2*s*) at 100 fg ml^{-1} and better than 0.3% at >3 pg ml^{-1}. Using this same technique we have also successfully measured ^{242}Pu/^{239}Pu with a precision of better than 2% on solutions containing 30 fg of ^{242}Pu and better than 10% with 5 fg of ^{242}Pu.

Introduction

Plutonium is present in the environment as a consequence of the detonation of nuclear weapons and of authorised discharges from nuclear installations during the second half of the twentieth century. An additional contribution to the global plutonium budget has come from the SNAP-9a satellite, which has introduced ^{238}Pu during atmospheric burn up. Plutonium is present in varying concentrations in soils and surface sediments as well as biota. Measurement of the more abundant plutonium isotopes (^{239}Pu and ^{240}Pu) can provide information on the source of contamination, be it nuclear weapons production, weapon detonation, or reactor discharge.

Fissile ^{239}Pu is present in weapons-grade plutonium at high abundance (^{240}Pu/^{239}Pu typically 0.05) and at much lower abundances in mixed oxide fuels (^{240}Pu/^{239}Pu approximately 0.4; Fig. 1). The isotope is also produced during detonation of weapons and in nuclear reactors from ^{238}U *via* neutron capture and subsequent beta decay of the resulting ^{239}U ($t_{½}=23.47$ min) to ^{239}Pu. As well as being fissile, ^{239}Pu undergoes neutron capture, either briefly during weapons' detonation or for prolonged periods within a nuclear reactor, to produce ^{240}Pu and, through successive neutron capture, to generate the heavier isotopes of Pu. The ratio of ^{240}Pu/^{239}Pu will therefore depend on the composition of the source material and the subsequent irradiation history of the material. Nuclear weapon construction requires a low ^{240}Pu/^{239}Pu (<0.07). After detonation this ratio increases due to neutron capture, the exact value depending on the test parameters. For this reason the ^{240}Pu/^{239}Pu in weapon test fallout varies between 0.10 and 0.35, the integrated test ratio being about 0.18.[1] Weapons grade Pu, weapons fallout Pu and Pu produced in the nuclear fuel cycle, therefore, have ^{240}Pu/^{239}Pu ratios that are sufficiently different to permit discrimination of the various sources.

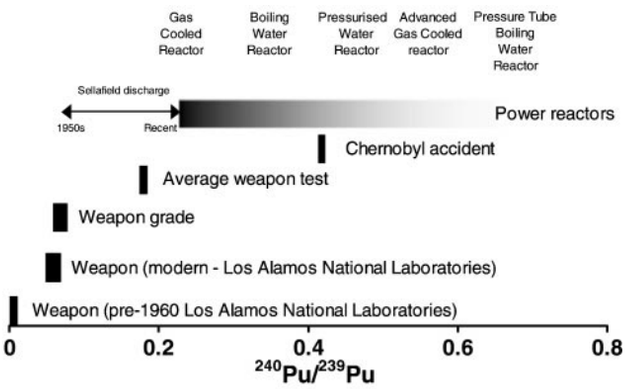

Fig. 1 ^{240}Pu/^{239}Pu in potential nuclear contamination sources.

Measurement of plutonium activity is routinely undertaken using a number of techniques such as alpha spectrometry and liquid scintillation counting.[2,3] However, it is difficult to distinguish ^{240}Pu and ^{239}Pu by these techniques due to the similarity of their alpha energies. Measurements of plutonium isotope ratios can be made by accelerator mass spectrometry on samples containing <50 fg Pu.[4] However, the precision of the ratios is around $\pm 18\%$ and the technique is expensive and not readily accessible.

Until recently thermal ionisation mass spectrometry (TIMS) has been the primary method for the determination of plutonium isotope ratios. TIMS analysis of Pu has been achieved by ionisation from carburised filaments,[5,6] platinum over-plating[7] or by loading on ion-exchange beads.[8,9] With relatively large sample loads (>1 ng Pu), TIMS is capable of a reproducibility of better than 0.1% (2*s*)[7,10] At 200–500 fg the reproducibility is about 1.5% (2*s*),[5,11] and about 10% at <50 fg.[6]

Plasma-source mass spectrometers (ICP-MS) with single ion-counting detectors have been used to measure plutonium isotope ratios in environmental materials.[12,13] However, quadrupole-based instruments do not produce sufficiently flat-topped peaks to enable precise ratio measurement, with precision around 5% on solutions of about 3 pg ml^{-1}. The recent addition of a sector field mass analyser to single detector

plasma instruments has generated more suitable peak shapes[14,15] and resulted in more reliable ratio determinations. A problem with plasma ionisation is the instability in signal intensity caused either by plasma "flicker" or by changes in the supply rate of analyte from the nebuliser to the ion source. Single detector instruments require that the ion beam at each mass be sequentially jumped into the detector. Thus, peak jumping is a limiting error on the precision of isotope ratio measurements.

Multicollector instruments circumvent the problem of ion beam instability by acquiring data from all required isotopes simultaneously. Thermal ionisation mass spectrometers have used multiple Faraday collector arrays for over 20 years, and have been the mainstay of high-precision isotope ratio analysis. In the mid-1990s multicollector, plasma source, sector field instruments (MC-ICP-MS) were developed.[16] These spectrometers combine the advantages of multiple collectors with flat-topped peaks, sample introduction by solution and high ionisation efficiency.

In the case of plutonium isotope measurement the amount of the element that is available and safe for analysis is usually quite low. Consequently, signal levels of ^{240}Pu and ^{242}Pu are generally too small to be reliably measured on Faraday collectors. Unless multiple ion-counting detectors are available, it is necessary to revert to the determination of Pu isotope ratios by peak jumping each mass into a single ion counting detector, which negates the advantages of multicollection.

In this paper we present a method for plutonium isotope ratio measurement by MC-ICP-MS involving a combination of Faraday and ion-counting detectors to eliminate imprecision caused by ion beam fluctuations. This method utilises a larger reference ion beam, suitable for Faraday collector acquisition, which is measured at the same time as each of the smaller objective ion beams. The measurement effectively becomes equivalent to a static multicollector analysis in which each isotope is counted simultaneously. TIMS multicollector analyses are generally limited to a reference isotope of the same element as the object isotope because of the significant influence of inter-element fractionation in the thermal source. To measure Pu by TIMS using a reference isotope would require spiking with a particular isotope such as ^{242}Pu. This would effectively rule out accurate determination of ^{242}Pu/^{239}Pu and would require that other ratios such as ^{240}Pu/^{239}Pu are corrected for impurities in the spike.

Multicollector ICP-MS is not restricted to corrections using the same element for two reasons. Firstly, elements of similar mass and ionisation efficiency respond to ion beam fluctuations in the same fashion in a plasma source, and secondly, elements with these similar characteristics exhibit comparable levels of mass bias during a run due to the constant sample flux. For example, it is possible to measure the mass bias between lead isotopes using ^{203}Tl–^{205}Tl of known isotope ratio.[17] In this study we present a method using multicollector detection of uranium and plutonium isotopes. We use uranium as both a reference signal and as an in-run measure of mass bias.

Experimental

Instrumentation and reagents

Data were acquired using an IsoProbe ICP mass spectrometer (Micromass Ltd., Withenshaw, UK) at the Southampton Oceanography Centre, UK. The instrument comprises an argon plasma torch ion source, a hexapole collision gas cell, a sector magnetic field and a multicollector array of nine Faraday detectors and an ion-counting Daly detector. The Daly detector is positioned after a retarding potential filter (WARP), which reduces the tail from large ion beams to <50 ppb at 1 u on the low mass side. Sample introduction to the argon plasma was *via* a desolvating nebuliser (MCN 6000, CETAC, Omaha, NE, USA). All samples were run using argon as collision gas (99.9999% purity; Air Products plc, Crewe, Cheshire, UK) admitted into the hexapole at a rate of about 1.2 ml min^{-1}.

For comparison, Pu isotope measurements were also made using a Sector 54 (Micromass Ltd.) TIMS at the Southampton Oceanography Centre, UK. This instrument has seven Faraday detectors and an axial ion-counting Daly detector. Pu solutions were loaded onto single de-gassed Re filaments either directly with a colloidal graphite suspension, or using anion resin beads.[5,6] Reagents used in all experiments were sub-boiled (in Teflon) nitric acid (distilled from Aristar grade HNO_3, Merck Ltd., Poole, UK) and high purity deionised water (resistivity higher than 18.2 MΩ cm) produced from a USF Elga Maxima system (USF Elga Ltd., High Wycombe, UK). All chemical work was undertaken in a Class 100 environment.

Sensitivity, background levels and interferences

On each measurement day the instrument was tuned for optimum sensitivity using a 100 ppt natural uranium solution. Typical analytical conditions are given in Table 1. Sensitivity for ^{238}U is typically in the range 0.3–0.4 V ng^{-1} ml [3–4×10^{-9} A μg^{-1} ml].

Minor background signals were found at all masses from *m*/*z* 239 to 242 (Table 2). After cleaning of the nebuliser, torch and cone assembly, the signal was optimised and, with an extract potential setting of 40%, the count rates were <50 cps for all Pu isotopes measured [Table 2 and Fig. 2(a)].

Interferences from ^{207}PbOO$^+$, ^{208}PbOO$^+$ and PbCl$^+$ were examined by admitting a 20 ppb solution of NIST SRM 981 Pb isotope standard, but no increase in signal was observed in the plutonium mass range. A potential matrix interference on ^{239}Pu is uranium hydride (^{238}UH$^+$). This was investigated using Pu-free natural uranium solutions and monitoring ^{238}U in a Faraday collector and *m*/*z* 239 simultaneously in the Daly. Two mass scans from 238.5 to 244.5 using the Daly collector are shown in Fig. 2. The upper trace (a) is a blank solution (0.3 M HNO_3), and the lower trace (b) a solution with 2 ng ml^{-1} uranium and a 7.2×10^{-12} A ^{238}U signal. In this case the background-subtracted signal at *m*/*z* 239 is 4.2×10^{-17} A (about 262 cps), which results in a UH$^+$/U$^+$ ratio of $5.8\times10^{-6}\pm3\%$ [2 standard error (SE)]. The average UH$^+$/U$^+$ ratio is $5.5\times10^{-6}\pm30\%$, which is a factor of two or more lower than results reported using similar nebulisation (MCN 6000) without a collision cell.[15,18,19] The results of two

Table 1 Operating conditions used on the IsoProbe MC-ICP-MS

Solution uptake rate	68 μl min^{-1}
Argon flow rates	
Cool gas	14.0 l min^{-1}
Auxiliary gas	1.0 l min^{-1}
Nebuliser gas	1.03 l min^{-1}
Collision gas flow rate (Ar)	1.2 ml min^{-1}
MCN6000 sweep gas flow	2.15 l min^{-1}
MCN6000 N_2 gas flow	0.10 l min^{-1}
Forward power	1350 W
Reflected power	<10 W

Table 2 Background signal at plutonium masses. Measurements taken a clean instrument and aspirating 2% (0.3 M) HNO_3. Equivalent concentration assumes a signal of 300 V (3×10^{-13} A) μg^{-1} ml

	Signal/μV	Signal/counts s^{-1}	Equivalent concentration/fg ml^{-1}
^{239}Pu	0.75	46	2.5
^{240}Pu	0.33	21	1.1
^{241}Pu	0.30	19	1.0
^{242}Pu	0.08	5	0.3

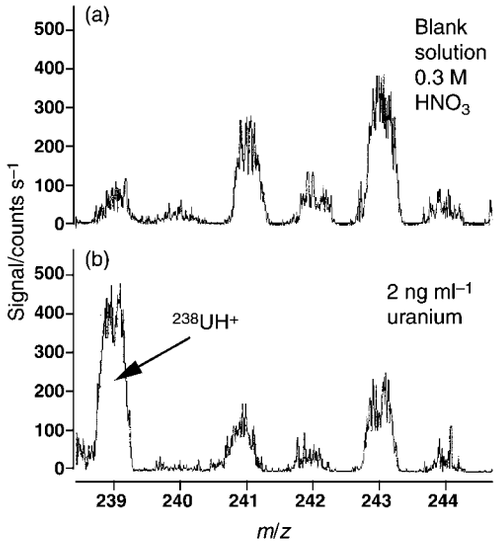

Fig. 2 Background mass scans *m/z* 238.5–244.5 admitting (a) a blank solution (0.3 M HNO_3) and (b) a solution with 2 ng ml^{-1} uranium producing a ^{238}U signal of 7.2×10^{-12} A (4.8×10^{8} counts s^{-1}). The resultant measured UH^+/U^+ ratio in this instance is $5.8\times10^{-6}+/-3\%$ (2 SE).

determinations of UH^+/U^+ using differing U concentrations are given in Table 3.

To achieve unbiased plutonium isotope ratios at ultra-trace Pu concentrations, it is essential to correct for the uranium interference at *m/z* 239. If UH^+ is not corrected for, it results in low $^{240}Pu/^{239}Pu$ and $^{242}Pu/^{239}Pu$ ratios in samples with $^{238}U/^{239}Pu > 1000$. For example, a sample with approximately 78 fg ml^{-1} ^{239}Pu and approximately 200 pg ml^{-1} U will have too low a $^{240}Pu/^{239}Pu$ ratio by about 1.5%. An additional interference at *m/z* 239 is tailing from ^{238}U. Abundance sensitivity behind the WARP filter is about 50 ppb at 1 u on the low mass side of a peak, but is about 200 ppb at 1 u on the high mass side. The low mass tail is reduced because the WARP filter eliminates lower energy ions caused by collisions, which would normally appear on the low mass side of the peak. Thus, the combined UH^+ and ^{238}U tail produces a signal at *m/z* 239 equivalent to about 5.7 ppm of the ^{238}U ion beam for an average level of hydride formation. In this study the magnitude of the correction was determined three times during an analysis period (every 2 h) by measuring a 1×10^{-11} A ^{238}U beam. During each analysis, ^{238}U was monitored by a Faraday collector and a UH^+/U and ^{238}U tail correction was applied to ^{239}Pu using the previously determined UH^+/U and tail determination. To minimise the correction and hence the propagated error, the ^{238}U concentration in the measurement solution is required to be <200 pg ml^{-1}. This can be achieved by chemical separation of U from Pu, with a uranium decontamination factor of $>10^5$ (atoms of U in final solution/atoms of U in starting material), assuming soil or sediment samples contain 2 μg g^{-1} of uranium and 0.2 pg g^{-1} of plutonium [equivalent to 646 μBq g^{-1} $^{239+240}Pu$ and a $(U/Pu)_{activity}=79$, assuming $^{240}Pu/^{239}Pu = 0.18$].

Table 3 Levels of UH^+ at *m/z* 239 at three different uranium concentrations on different days. All signals are blank subtracted. Counts at *m/z* 239 are corrected for a ^{238}U tail of 200 ppb, which is reckoned as 0.32 times the counts measured at *m/z* 238.5. 1 V = 1×10^{-11} A ion current

Nominal U content/ng ml^{-1}	^{238}U signal/ V	239 signal/ counts s^{-1} (μV)	$^{238}UH^+/^{238}U^+$
2	0.72	262 (4.2)	5.80×10^{-6}
12	5.25	1707 (27.3)	5.00×10^{-6}
25	9.50	3177 (50.8)	5.15×10^{-6}

Table 4 Isotope ratios and concentration of the Southampton $^{236}U+^{233}U$ double spike (DSU1). Ratios calibrated by static Faraday measurement by TIMS against natural uranium and NIST SRM U500. Concentration measured by TIMS isotope dilution against international rock standards. Pu contaminants measured using MC-ICP-MS on a 38 ng ml^{-1} DSU1 solution

$^{238}U/^{236}U$	0.060 02	±0.000 09 2*s* *n* = 12
$^{235}U/^{236}U$	0.000 418	±0.000 002 2*s* *n* = 12
$^{234}U/^{236}U$	0.002 400	±0.000 007 2*s* *n* = 12
$^{236}U/^{233}U$	0.987 25	±0.000 24 2*s* *n* = 12
$^{239}Pu/^{236}U$	0.000 00183	±2% 2*s* *n* = 3
$^{240}Pu/^{236}U$	0.000 000098	±4% 2*s* *n* = 3
Concentration/μg g^{-1}	2.2306	±0.0008 2*s* *n* = 6

Measurement systematics

An equal atom $^{236}U/^{233}U$ double spike (SOC DSU1, Table 4) was added to the samples for two purposes: to correct for instrumental mass bias; and to correct for instrument drift between Daly peak-jumps.

The use of a $^{236}U/^{233}U$ double spike as a drift and bias monitor has the advantage of not introducing significant $^{238}UH^+$ interference on ^{239}Pu (DSU1 ~3% ^{238}U, Table 4), and, unlike the $^{238}U/^{235}U$ ratio, can be relied upon to have a consistent ratio in environmentally contaminated samples. Furthermore, since the $^{236}U/^{233}U$ is approximately 1 in the double spike, the ratio can be measured at optimum precision. The double spike contains small quantities of plutonium (Table 4) that can be corrected for using the in-run ^{236}U measurements.

Pu isotope measurements in this study were made using a combination of Daly and Faraday detectors in a peak-jump sequence. Pu isotope masses were measured with the Daly detector in the sequence $^{240}Pu\rightarrow^{239}Pu\rightarrow^{242}Pu$. Faraday collectors were positioned at 3, 4 and 6 mass units lighter than Pu to receive the uranium ion beams, as shown in Fig. 3. Each sequence was counted for 5 s, with a delay of 2 s before data acquisition after each mass jump. 50 cycles of the peak jump sequences were taken, each analysis lasting for about 18 min, during which about 1 ml of sample solution was aspirated.

In this detector array ^{236}U can be measured in a Faraday detector at the same time as ^{239}Pu, ^{240}Pu and ^{242}Pu. As the fluctuations in signal intensity caused by plasma instability or ion beam drift will affect uranium and plutonium to the same degree, normalisation of each plutonium isotope to a simultaneously measured ^{236}U ion beam effectively eliminates this source of error. Efficiencies of the Faraday detectors were found to differ by <0.02%, and are thus a negligible source of error. ^{238}U is measured in low 2 Faraday during sequence 2, which is then used to calculate UH^+ and ^{238}U tailing at *m/z* 239. During the second sequence ^{236}U is received in low 1 Faraday while low 3 detects ^{233}U. From this static measure-

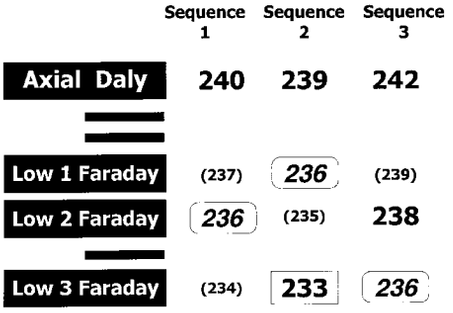

Fig. 3 Collector and peak jump array for measurement of plutonium and uranium isotopes. Circled 236 measurements are used for beam intensity normalisation and boxed 233 is used in conjunction with 236 in sequence 2 to calculate mass bias. 238 in sequence 3 is used to calculate UH^+ interference on ^{239}Pu.

ment an in-run $^{236}U/^{233}U$ value is determined to calculate instrumental mass bias. $^{240}Pu/^{239}Pu$ and $^{242}Pu/^{239}Pu$ are corrected for signal fluctuation and a linear mass bias using eqns. (1) and (2), where the subscript t = corrected ratio, $236_{S3} = {}^{236}U$ measured in sequence 3, *etc.*, and $0.98725 = {}^{236}U/{}^{233}U$ of the double spike.

$$\left(\frac{240}{239}\right)_t = \left[\frac{240_{S_1}}{239_{S_2}} \times \frac{236_{S_2}}{236_{S_1}}\right] \times \left[1 - \left[\left(\frac{0.98725 \times 233_{S_2}}{236_{S_2}} - 1\right)/3\right]\right] \quad (1)$$

$$\left(\frac{242}{239}\right)_t = \left[\frac{242_{S_3}}{239_{S_2}} \times \frac{236_{S_2}}{236_{S_3}}\right] \times \left[\frac{0.98725 \times 233_{S_2}}{236_{S_2}}\right] \quad (2)$$

Correction for mass bias using an exponential law was also made using eqns. (3) and (4):

$$\left(\frac{240}{239}\right)_t = \left[\left(\frac{240_{S_1}}{239_{S_2}}\right)_m \times \left(\frac{236_{S_2}}{236_{S_1}}\right)\right] / \left(\frac{240.054}{239.052}\right)^{\beta} \quad (3)$$

$$\left(\frac{242}{239}\right)_t = \left[\left(\frac{242_{S_3}}{239_{S_2}}\right)_m \times \left(\frac{236_{S_2}}{236_{S_1}}\right)\right] / \left(\frac{242.059}{239.052}\right)^{\beta} \quad (4)$$

where:

$$\beta = \frac{\ln\left[\frac{236_{S_2}/233_{S_2}}{0.98725}\right]}{\ln\left[\frac{236.046}{233.040}\right]}$$

The exponentially corrected results are higher by about 0.008% and are thus essentially identical to those corrected by linear law.

The validity of using uranium to correct for plutonium mass bias has been verified by static Faraday measurements of a mixture of a $^{242}Pu/^{239}Pu$ equal atom standard (UK-Pu-5, AEA Technology, Harwell, Oxfordshire, UK) with our $^{236}U/^{233}U$ double spike (Fig. 4). The results indicate that the mass bias factors for each element are within 0.01% u^{-1}, which should be the maximum error on the $^{240}Pu/^{239}Pu$ and equates to 0.03% error on $^{242}Pu/^{239}Pu$.

For samples with Pu >200 pg ml^{-1}, signal levels of the less abundant Pu isotopes could be reliably measured on Faraday collectors. Such solutions were analysed using six Faradays, simultaneously receiving masses 233, 235, 236, 238, 239, 240 and 242.

TIMS measurements were made using only the Daly detector

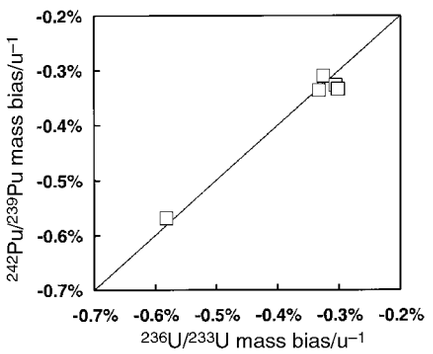

Fig. 4 Comparative fractionation of plutonium and uranium expressed as linear fractionation % u^{-1}. Mixture of equal-atom Pu standard ($^{242}Pu/^{239}Pu$) and equal-atom $^{236}U/^{233}U$ double spike measured on five separate days using static multicollector analysis. Internal errors (2 SE) on each measurement are smaller than symbols.

in a 240-239-240 peak jump sequence, counting for 2 s on each peak and measuring between 10 and 30 cycles.

Blank measurement

Blank measurements were made on 0.3 M HNO_3 on each of the peaks and for each of the collectors in an identical array to the dynamic sequence used for sample measurement. The analysis time for the blank was set to be 20% of the sample analysis time. Blank peak intensities were subtracted from the matching sample peak intensity array. Errors in the blank measurement were $<3\%$ 2 SE for ^{239}Pu at count levels similar to those in Table 2. The errors on the blank measurements indicate that the limit of detection (3 *s* error on the blank) for ^{239}Pu is <4 fg ml^{-1}, ^{240}Pu is <3 fg ml^{-1} and ^{242}Pu is <3 fg ml^{-1}.

Measurement solutions

To provide a plutonium solution with a similar matrix to environmental samples, Pu was purified from 30 g of a marine argillaceous sediment from the Irish Sea, UK (Site 112), by acid leaching followed by 5 stages of anion-exchange chromatography. This sample was chosen to test instrumental precision because it has a $^{240}Pu/^{239}Pu$ ratio of about 0.22, which is close to environmental ratios from weapons fallout (about 0.18) and spent reactor fuel (about 0.23). A 120 ml mother solution containing 70 ng of Pu was diluted with 0.3 M HNO_3 into fractions containing a range of plutonium concentrations between 100 fg ml^{-1} and the mother dilution of 580 pg ml^{-1}. The uranium double spike was added to each solution to provide a 1 ng ml^{-1} concentration of the ^{233}U and ^{236}U isotopes. Addition of the double spike at this level introduces about 60 pg ml^{-1} of ^{238}U.

Results and discussion

Plutonium isotope ratios for our test sample solution (Site 112), determined using the multicollector ICP-MS, are presented in Figs. 5 and 6. A summary of the precision and reproducibility of the measurements is given in Table 5. $^{240}Pu/^{239}Pu$ and $^{242}Pu/^{239}Pu$ are consistent across the range of concentrations (signal levels) with no systematic bias in the mean ratios for each concentration range (Table 5). Internal errors, shown as 2 SE error bars in Figs. 5 and 6, increase with decreasing signal.

To assess the accuracy of the method, an equal atom Pu standard (UK-Pu-5, AEA Technology, UK) was diluted to 10 pg ml^{-1} and spiked with $^{236}U/^{233}U$ at the same level as the Site 112 solutions. As this Pu standard contains ^{236}U ($^{236}U/^{239}Pu = 0.001\,870\,4$), a correction was made to the measured $^{236}U/^{233}U$ accordingly. Measurements were made using the same dynamic measurement sequence used for the Site 112 solutions. The results for UK-Pu-5 are presented in Table 6. Both the $^{240}Pu/^{239}Pu$ and $^{242}Pu/^{239}Pu$ ratios measured using the dynamic Daly routine and the static Faraday sequence are found to be within error of the recommended value. However, it is interesting to note that both the Daly and Faraday measurements resulted in fractionally lower value for $^{240}Pu/^{239}Pu$ (about 0.18%) than the recommended value. This could relate to the increased control on the mass bias resulting from the simultaneous uranium measurement in this study.

For comparison, Fig. 5(b) shows the TIMS analyses for the same Site 112 sample. The TIMS analyses were made using 1–2 ng of plutonium, which generated 10–15 peak jump ratio determinations. These data are uncorrected for mass fractionation, but this is expected to be $<0.12\%$ u^{-1}, and insignificant compared to the in-run errors on these measurements, which are about 0.5% 2 SE. $^{240}Pu/^{239}Pu$ measurements made by TIMS are all within the error range of the MC-ICP-MS data. In general, a disadvantage of TIMS is that, at low sample levels requiring peak-jump Daly detection, ion beam drift and signal

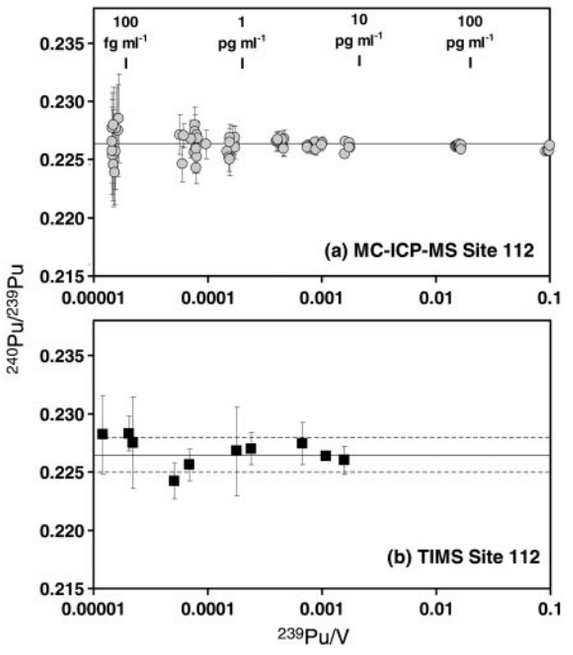

Fig. 5 (a) MC-ICP-MS $^{240}Pu/^{239}Pu$ measurements for Site 112 plutonium solution plotted against ion beam intensity (^{239}Pu, volts). Error bars are within run 2 SE on the 50 collected ratios. Horizontal line is the average of all data. Approximate Pu concentrations of solutions measured are shown at the top of the diagram, assuming normal instrument sensitivity. (b) TIMS $^{240}Pu/^{239}Pu$ measurements for Site 112 plutonium solution plotted against ion beam intensity (^{239}Pu, volts). Sample loads are about 1–2 ng Pu. Error bars are within-run 2 SE on the 10–25 collected ratios. Dashed lines define 95% of the MC-ICP-MS data, and solid line the mean MC-ICP-MS value.

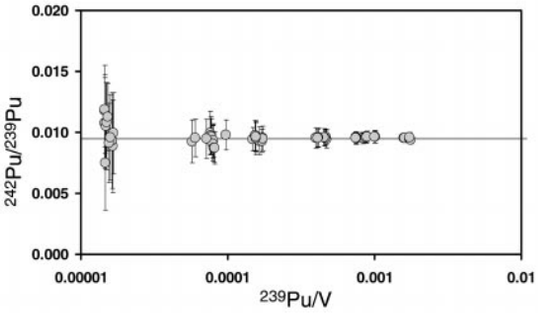

Fig. 6 MC-ICP-MS $^{242}Pu/^{239}Pu$ measurements for Site 112 plutonium solution plotted against ion beam intensity (^{239}Pu, volts). Error bars are within-run 2 SE on 50 ratios. Horizontal line is the average of all data.

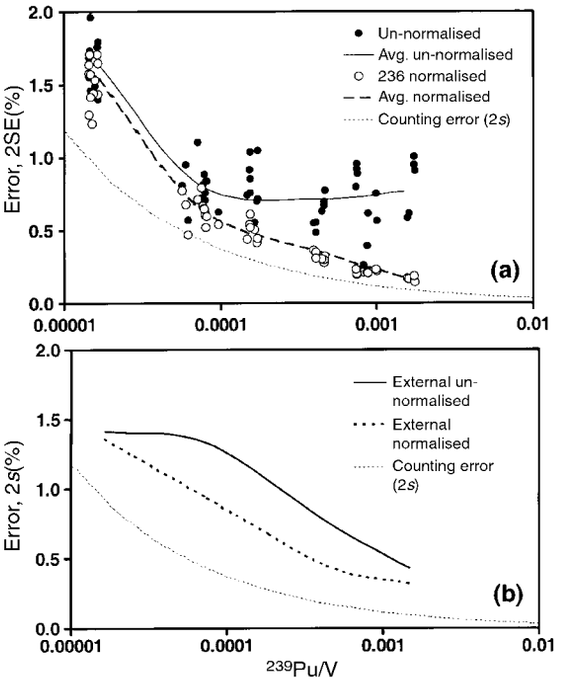

Fig. 7 (a) Internal (within run) error on $^{240}Pu/^{239}Pu$ plotted against ^{239}Pu signal level. Errors are 2 SE (%) for the 50 ratios measured. Data shown are both un-normalised and normalised to ^{236}U. Also shown are the calculated counting errors (2*s*) on $^{240}Pu/^{239}Pu$ with signal level. (b) External (reproducibility of runs) error on $^{240}Pu/^{239}Pu$ plotted against ^{239}Pu signal level. Errors are 2*s* (%) for the averages of the concentration groups outlined in Table 5 from the un-normalised and normalised data. Counting errors as for (a).

instabilities increase the error on the ratio measurement. This is compounded by the difficulty and inconsistency of the sample loading technique, namely mounting resin beads on a rhenium filament ribbon. Subtle variations in the loading characteristics are responsible for the variable efficiency of ionisation[6] and differences in amount of isotopic fractionation from sample to sample.

A plasma ion source provides a reproducible level of ionisation efficiency (0.2–1.0%) and consistent mass bias between samples. These characteristics provide the platform for precise isotope ratio measurement. In the presence of multiple collectors, precision can be further improved by eliminating signal fluctuation. The multicollector normalisation procedure described in this study provides a significant improvement in analytical precision. Fig. 7 shows the difference in the internal precision (within each analysis) between the un-normalised and double spike-normalised $^{240}Pu/^{239}Pu$ mea-

Table 5 $^{240}Pu/^{239}Pu$ and $^{242}Pu/^{239}Pu$ isotope ratios of Site 112 sediment at fg to pg ml^{-1} concentrations. External errors quoted as 2 standard deviations [2*s* (%)], average in-run errors (internal errors) are quoted as 2 standard errors (SE). Each in-run error is calculated from the 50 ratios measured during each analysis, except the TIMS analyses, which are from 10–20 ratios

Method and Pu concentration	$^{240}Pu/^{239}Pu$	+/-	2*s* (%)	*n*	Average in-run 2 SE (%)
Daly: 100 fg ml^{-1}	0.2265	0.0031	1.36	12	1.44
Daly: 500 fg ml^{-1}	0.2263	0.0021	0.94	13	0.66
Daly: 1–5 pg ml^{-1}	0.2262	0.0010	0.45	22	0.32
Daly: 5–10 pg ml^{-1}	0.2262	0.0007	0.32	7	0.18
Faraday: 100 pg ml^{-1}	0.2262	0.0003	0.11	10	0.12
Daly: TIMS 1–2 ng	0.2264	0.0024	1.04	10	0.50
Method and Pu concentration	$^{242}Pu/^{239}Pu$	+/-	2*s* (%)	*n*	Average in-run 2 SE (%)
Daly: 100 fg ml^{-1}	0.0101	0.0027	26.9	12	7.3
Daly: 500 fg ml^{-1}	0.0095	0.0008	8.3	13	2.0
Daly: 1–5 pg ml^{-1}	0.0095	0.0002	2.1	22	1.6
Daly: 5–10 pg ml^{-1}	0.0095	0.0002	1.7	7	0.7

Table 6 $^{240}Pu/^{239}Pu$ and $^{242}Pu/^{239}Pu$ isotope ratios of UK-Pu-5. Errors quoted as 2 standard deviations [2*s* (%)] for Daly measurements and as internal error [2 standard error (SE)] for the Faraday measurement

	$^{240}Pu/^{239}Pu$	+/-	2*s* (%)	*n*
Recommended value	0.9662	0.0011	0.11	
Daly (10 pg ml^{-1})	0.9645	0.0013	0.13	7
Faraday (1 ng ml^{-1})	0.9642	0.0001	0.01	1
	$^{242}Pu/^{239}Pu$	+/-	2*s* (%)	*n*
Recommended value	1.0253	0.0019	0.19	
Daly (10 pg ml^{-1})	1.0252	0.0034	0.34	7
Faraday (1 ng ml^{-1})	1.0250	0.0001	0.01	1

surements. At low signal levels (10–100 μV) the un-normalised and normalised errors are similar, the normalisation providing an improvement in precision to around 0.1–0.2%. At higher signal levels (>200 μV) the normalised data are 2–3 times more precise. Expected counting errors on $^{240}Pu/^{239}Pu$ are shown as a curve in Fig. 7. The normalised internal errors form a curve that approaches the level of the expected counting error, particularly at higher signal levels (>80 μV). The reproducibility of the $^{240}Pu/^{239}Pu$ (external error) before and after normalisation is also shown in Fig. 7. The un-normalised and normalised data have similar reproducibility at 10 μV ^{239}Pu, but the normalised data have a significantly smaller error for ^{239}Pu signals between 100–1000 μV (*e.g.*, 0.45% normalised, 0.76% un-normalised).

Conclusions

Plutonium isotope ratios can be precisely measured by multicollector sector-field ICP-MS in solutions of between 0.1 and 100 pg ml^{-1}. Reproducibility of $^{240}Pu/^{239}Pu$ in this concentration range is between 1.3% and 0.12% (2*s*). Limitations of peak-jump single collector analysis common to plasma ionisation instruments can be reduced by normalisation to a simultaneously measured reference peak, such as ^{236}U. Beneficially, uranium is found to have similar mass bias characteristics to plutonium, and hence in-run measurement of ^{236}U and ^{233}U added as a double spike can be used to correct for mass bias on plutonium. Accurate corrections can also be made during each analysis for UH^+ interference and ^{238}U tail at *m*/*z* 239. The sensitivity of the technique, low consumption of the analyte and the rapid sample throughput indicate that this technique is applicable to analysis of environmental samples.

Acknowledgements

The IsoProbe at the SOC was funded through the PRISMS project, EC contract SMT4-CT98-2220. The work was improved by discussions with Patrick Turner and Dave Churchman at Micromass.

References

1 M. Koide, K. K. Bertine, T. J. Chow and E. D. Goldberg, *Earth Planet. Sci. Lett.*, 1985, **72**, 1.
2 C. Gascó, M. P. Anton, A. Espinosa, A. Aragón, A. Alvarez, N. Navarro and E. García-Toraño, *J. Radioanal. Nucl. Chem.*, 1997, **222**, 81.
3 Y-f. Yu, H. H. E. Bjornstad and B. Salbu, *Analyst*, 1992, **117**, 439.
4 L. K. Fifield, A. P. Clacher, K. Morris, S. J. King, R. G. Cresswell, J. P. Day and F. R. Livens, *Nucl. Instrum. Meth. B*, 1996, **117**, 295.
5 R. S. Strebin Jr. and D. M. Robertson, *Anal. Chim. Acta*, 1977, **91**, 276.
6 D. H. Smith, D. C. Duckworth, D. T. Bostick, R. M. Coleman, R. L. McPherson and H. S. McKown, *Proceedings of the 42nd ASMS Conference on Mass Spectrometry and Allied Topics*, Chicago, IL, 1994, 839.
7 R. E. Perrin, G. W. Knobeloch, V. M. Armijo and D. W. Efurd, *Int. J. Mass Spectrom. Ion Processes*, 1985, **64**, 17.
8 J. D. Fassett and W. R. Kelly, *Anal. Chem.*, 1984, **56**, 550.
9 K. O. Buesseler and J. E. Halverson, *J. Environ. Radioactivity*, 1987, **5**, 425.
10 R. Fiedler, D. Donohue, G. Grabmueller and A. Kurosawa, *Int. J. Mass Spectrom. Ion Processes*, 1994, **132**, 207.
11 J. M. Kelley, L. A. Bond and T. M. Beasley, *Sci. Total Environ.*, 1999, **237/238**, 483.
12 J. S. Becker and H.-J Dietze, *Fresenius' J. Anal. Chem.*, 1999, **364**, 482.
13 Y. Muramatsu, S. Uchida, K. Tagami, S. Yoshida and T. Fujikawa, *J. Anal. At. Spectrom.*, 1999, **14**, 859.
14 S. Sturup, H. Dahlgaard and S. C. Nielsen, *J. Anal. At. Spectrom.*, 1998, **13**, 1321.
15 C.-S. Kim, C.-K. Kim, J-I. Lee and K. J. Lee, *J. Anal. At. Spectrom.*, 2000, **15**, 247.
16 A. J. Walder and P. A. Freeman, *J. Anal. At. Spectrom.*, 1992, **7**, 571.
17 T. Hirata, *Analyst*, 1996, **121**, 1407.
18 R. Chiappini, F. Pointurier, J. C. Millies-Lacroix, G. Lepetit and P. Hemet, *Sci. Total Environ.*, 1999, **237/238**, 269.
19 J. S. Becker, R. S. Soman, K. L. Sutton, J. A. Caruso and H.-J. Dietze, *J. Anal. At. Spectrom.*, 1999, **14**, 933.

Appendix 10

Manuscript:

The record of uranium and plutonium isotopes in nuclear fallout at northern temperate latitudes

Warneke T., Croudace I.W., Warwick P.E. and Taylor R.N.

The record of uranium and plutonium isotopes in nuclear fallout at northern temperate latitudes

Thorsten Warneke, Ian W. Croudace, Phillip E. Warwick & Rex N. Taylor

Southampton Oceanography Centre, Southampton SO14 3ZH, UK

Plutonium and uranium isotope ratios can be used to differentiate the sources of nuclear contamination from nuclear weapon establishments [1], weapons fallout [2-5], reprocessing plants, reactor or satellite accidents [6,7] and in addition they provide markers for post-1952 isotope geochronology. Using recently-developed mass spectrometric techniques [8] the first northern temperate latitude ground level record of $^{240}Pu/^{239}Pu$ and $^{238}U/^{235}U$ is presented. Grass samples taken from the IACR-Rothamsted herbage archive in England and an ice core from Mont Blanc glacier reveal hitherto unseen fluctuations in $^{238}U/^{235}U$ relating mostly to nuclear testing. Plutonium contamination originating from Nevada Desert atmospheric weapons tests in 1952 and 1953 is identified in England for the first time by its characteristic low $^{240}Pu/^{239}Pu$ isotope signature. Later samples (1954-68) show isotope ratios reflecting mostly stratospheric fallout from thermonuclear tests.

Atmospheric nuclear testing occurred at several locations (Figure P1) mostly in the Northern Hemisphere from 1945-1980. Until 1952 all nuclear tests were in the kiloton range, with radioactive debris only penetrating the troposphere, but the advent of sub-megaton and above thermonuclear weapons in late-1952 led to injection of contamination into the stratosphere. Radioactive debris from >500 kt (TNT equivalent) nuclear explosions partitioned into the troposphere and stratosphere according to particle size and the power of the explosion [9]. Latitude, total yield and season influenced the rate of fallout from these tests. Fine debris from small yield tests (< 100 kt) produced fallout that had a mean residence time of less than 70 days in the troposphere [10]. Fallout from large yield tests (> 500 kt), however, was almost wholly derived from material injected into the stratosphere and, though falling mostly in the hemisphere of injection, was distributed globally. The transfer of fallout from the stratosphere to the troposphere is seasonally-modulated and occurs mostly in the late winter and spring (the spring peak) [11].

Uranium and plutonium are both essential components of nuclear weapons although somewhat surprisingly there are no published accounts of $^{238}U/^{235}U$ in global weapons fallout. The two primordial isotopes of uranium are ^{235}U and ^{238}U with $^{238}U/^{235}U = 137.88$ [12] and this ratio has no significant variation in nature except in fossil natural reactors [13]. Deviations from this ratio in environmental materials can therefore only be explained by the addition of technologically-modified uranium (enriched and depleted uranium) [1]. Plutonium, unlike uranium, is virtually entirely anthropogenic [14] in origin and its main isotopes found in the environment, ^{238}Pu, ^{239}Pu, ^{240}Pu, ^{241}Pu and ^{242}Pu, are derived from civil and military sources. Approximately 6 tonnes of ^{239}Pu were introduced into the environment from 541 atmospheric weapon tests [14] having a total explosive yield of 440 megatons (TNT equivalent), with 25 tests accounting for two thirds of the yield. Fallout was distributed globally at a ~3:1 ratio between the Northern Hemisphere and Southern Hemispheres [14].

Techniques based on highly sensitive multi-collector ICP-mass spectrometer measurements enable precise determination of $^{240}Pu/^{239}Pu$ and $^{238}U/^{235}U$ in terrestrial samples at normally-encountered environmental concentrations. For the more demanding case of determining the $^{240}Pu/^{239}Pu$ isotope ratio, a precision of better than 1% (2s.d.) for sample sizes of 300 fg Pu is achievable. This is approximately equivalent to an activity of 1mBq for $^{240+239}Pu$ having a typical $^{240}Pu/^{239}Pu$ fallout ratio of 0.18. Annual samples of 1945-90 grass, including separate summer and autumn harvests where available (IACR-Rothamsted Archive, Hertfordshire, UK) were used to determine ^{137}Cs, plutonium (alpha), $^{240}Pu/^{239}Pu$ and $^{238}U/^{235}U$. The existence of samples from both harvests is important because they provide a means of identifying the source and timing of some nuclear tests due to the 'spring peak'. The first harvest samples should include stratospheric fallout (from the 'spring peak') while the second harvest should mostly include tropospheric fallout from summer tests or residual stratospheric fallout in the same year (Table P1). As confirmation of the Rothamsted grass record for temperate latitudes a 116-cm ice core from Dome du Gouter (4300m), Mont Blanc, France, shown by Vincent *et al* [15] to have a good fallout record, was also investigated.

The concentration results of the current study agree closely with records of device-testing [16,17] and radiochemical monitoring of fallout [18-20] that took place at the time (Figure 3). The main stratospheric events that dominate the ratios during 1952-1962 are the U.S. and UK tests on Bikini, Eniwetok and Christmas Island in 1954, 1956 and 1958 and 1962 and Soviet tests in the Arctic in 1958, 1961 and 1962. In November 1958 the Partial Test Ban

Treaty inhibited nuclear testing until the resumption of atmospheric testing first by the U.S.S.R. in September 1961 and then by the U.S. in April 1962. The U.S. and the U.S.S.R. finally ceased atmospheric testing in October 1962 and December 1962 following the ratification of the International Test Ban Treaty. Using a linear age-depth relation for the Mont Blanc ice core the $^{240}Pu/^{239}Pu$ profiles for the ice core and the Rothamsted grass are almost identical for the period 1955-1970. This good agreement indicates that the $^{240}Pu/^{239}Pu$ record is generally representative of northern temperate latitudes. This conclusion may not hold for areas influenced by relatively significant tropospheric fallout derived from a particular testing site. One of these is the Nevada Desert Test site NTS where eighty-four kiloton-range atmospheric nuclear tests were carried out between 1951-62 [16,17] (Table P1). A 1953 air sampling study of NTS-derived radioactive fallout showed northeasterly dispersal of the test plume toward W. Europe [9] (Figure P1). Hitherto the only record of this fallout in the UK was from measurements of beta/gamma activity in air carried out by UKAEA [21]. The current work shows that the 1952 Rothamsted grass (June-July harvest) has a $^{240}Pu/^{239}Pu$ of 0.06. This grass was harvested before the first ever thermonuclear test at Eniwetok Atoll (10.4 Mt 'Mike' shot; 31 October 1952) which had a $^{240}Pu/^{239}Pu$ greater than 0.30, as inferred from ice cores [18]. Similarly there were no USSR-tests in 1952 and therefore the 1952 Rothamsted ratio can only be due to fallout from one or more of the eight tests at the NTS between April-June 1952. The time-lag between a Nevada test and subsequent deposition in the UK could have been as short as 5 days if suitable weather conditions existed [21]. The 1952 second harvest (Sep-Nov) sample shows no measurable plutonium, which is consistent with the records of no summer testing at the NTS. It is notable that low ratios have been reported in North Atlantic, Gulf of Mexico and Mississippi Delta sediments [2-5] and attributed to NTS testing but they did not have the good time control of the grass samples. Additional evidence for tropospheric fallout is also seen for later samples. For example, $^{240}Pu/^{239}Pu$ in the 1953 grass is 0.154 for the first cut and 0.135 for the second cut. Since fallout from the 1952 “Mike”-Shot had a $^{240}Pu/^{239}Pu$ greater than 0.30 the lower 1953 ratios must represent mixtures of tropospheric fallout and stratospheric fallout. There were no NTS tests carried out between the two 1953 grass harvests and any stratospheric fallout $^{240}Pu/^{239}Pu$ would have remained close to 0.30 so there must have been another tropospheric input. This could be from the first Soviet thermonuclear test (Kazakhstan site) that occurred in August 1953 (440kt) and this could have contributed low $^{240}Pu/^{239}Pu$ material to the second 1953 harvest.

Chinese and French atmospheric thermonuclear tests were carried out between 1964-1980 and 1966-1974 respectively [16] and can also be related to the ratios seen in the grass. The small increase in the ratio during the late 1970s seen in N-stratosphere and Rothamsted data must be due to Chinese tests. There are no ice core $^{240}Pu/^{239}Pu$ data for this period although stratospheric aerosol measurements exist for 1975, 1977 and 1979. The Rothamsted isotope ratio data provide a useful alternative for this hiatus in the record.

Uranium isotope ratio data for atmospheric fallout from weapons testing have not been previously reported, perhaps because the small amounts of isotopically-altered uranium contamination are masked by the presence of natural uranium. The variation of the $^{238}U/^{235}U$ in the Rothamsted grass show three distinct negative inflections (enriched U ratio) at 1952, 1958 and 1963 and two small but significant positive inflections (depleted U ratio) at 1977/78 and 1983. The two negative inflections in the 1958 and 1963 grass data are also present in the ice record but no positive inflections are seen later in the ice core. The 1952 deviation in the Rothamsted grass, where Pu was also first detected, is likely to have been caused by tropospheric fallout from NTS. The 1953 deviation is likely to result from a mixture of tropospheric and stratospheric fallout, as also inferred from the Pu data, while the 1954 data can be attributed mostly to stratospheric fallout. The strongest deviations in $^{238}U/^{235}U$ in the grass record occur in 1958 and 1963 which coincide with the years of greatest atmospheric fallout from weapons testing by the U.S. and the U.S.S.R.. The measured ratios in both cases are about 0.55% lower than the natural ratio but the magnitude of the deviations for 1958 and 1963 are greater in the Mont Blanc ice. Enriched uranium isotopic ratios in the ice persist for the whole period of high yield atmospheric testing. It is likely that the reason for the differences between ice and grass is a higher content of natural uranium in the grass compared with the ice. The depleted $^{238}U/^{235}U$ in the grass in 1977, 1978 and 1983 is probably due to a local, but presently unidentified source, since no evidence of depleted ratios can be seen in the ice core. A possible though entirely speculative source for these very small perturbations could be from industrial uses of depleted uranium and/or the testing or fabrication of uranium-based weaponry [23].

Acknowlegements: We are grateful to IACR Rothamsted,particularly Dr Paul Poulton, for providing access to their valuable grass sample and we appreciate the help of Dr Pourchet from CNRS "Laboratoire de Glaciologie et Geophysique de l'Evironment" Grenoble for the ice core samples.

Table P1: Nuclear test data and $^{240}Pu/^{239}Pu$ for Rothamsted grass samples (1945-1957)*

	Stratos-pheric input	Potential tropospheric input		Jun-Jul Rothamsted harvest			Sep-Nov Rothamsted harvest		
Year	**Global fallout** $^{240}Pu/^{239}Pu$	**Kazakhstan Tests USSR (yield)**	**Nevada Desert Tests USA (yield)**	**Date of harvest**	$^{239,240}Pu$ **Bq/kg**	$^{240}Pu/^{239}Pu$	**Date of harvest**	$^{239,240}Pu$ **Bq/kg**	$^{240}Pu/^{239}Pu$
1945	-		16Jul (19kt)	n.r.+	-	-	n.r.+	-	-
1951	-	24Sep (38kt)	-	21 Jun	-	-	2 Oct	-	-
1952	-	-	1Apr-5Jun (104kt)	19 Jun	0.05	0.060	22 Sep	-	-
1953	0.33-0.34	12Aug-10Sep (440kt)	17Mar-4Jun (253kt)	21 Jul	0.04	0.154	19 Nov	0.08	0.135
1955	0.25-0.27	29Jul-5Aug (15kt)	18Feb-15May (163kt)	28 Jun	0.26	0.273	15 Sep	0.50	0.295
1957	0.19-0.22	8Mar-16Apr (1142kt) 22Aug-13Sep (526kt)	28May-7Oct (340kt)	18 Jun	0.19	0.165	24 Sep	0.44	0.113

* Only for the years where samples from both cuts were taken
** based on Arctic and Antarctic ice core measurements [6]
n.r. -· not recorded

Figures:

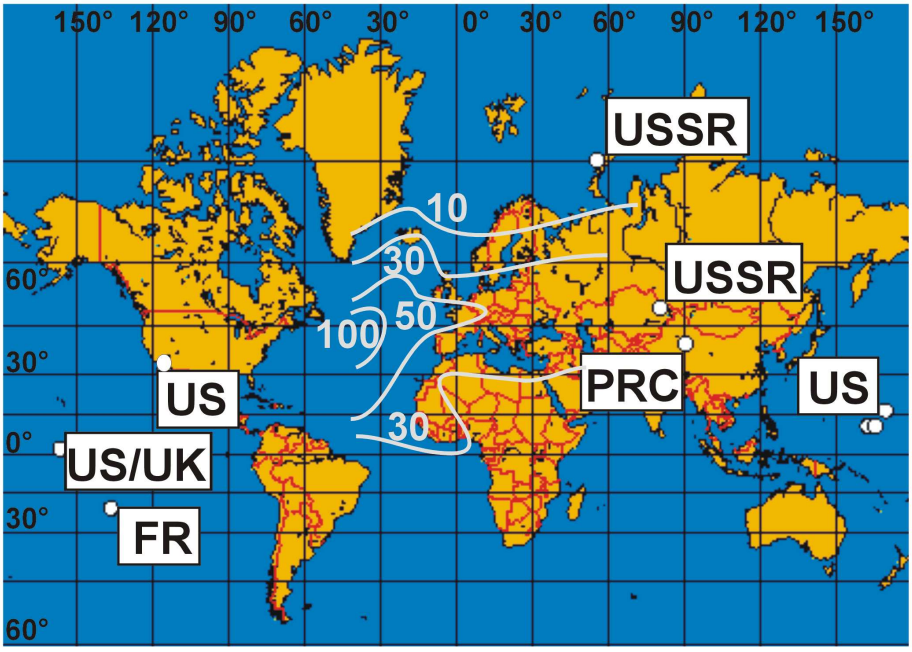

Figure P1. Locations of the main atmospheric test sites. The contour lines show the distribution of the Nevada Test Site fallout in 1953 in relative units [9].

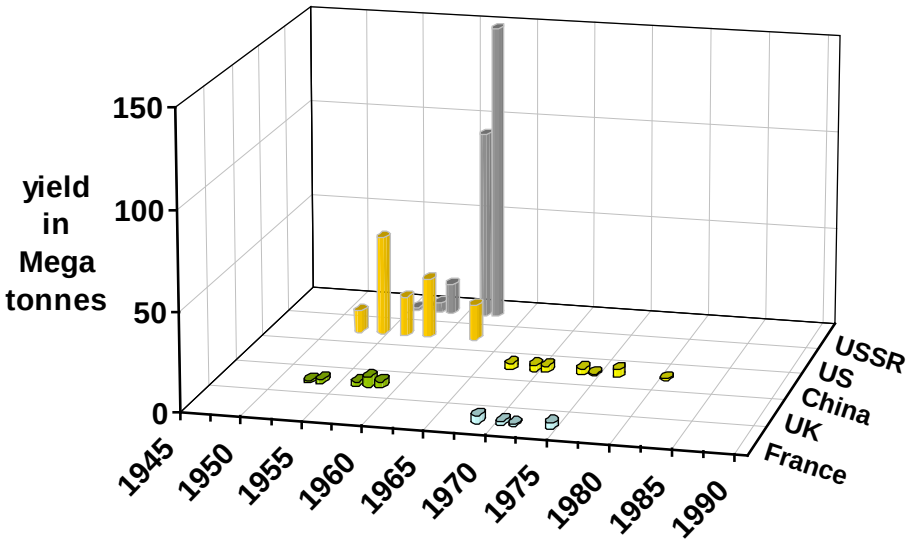

Figure P2. Yearly yields of atmospheric tests greater than 500 kt [16,17].

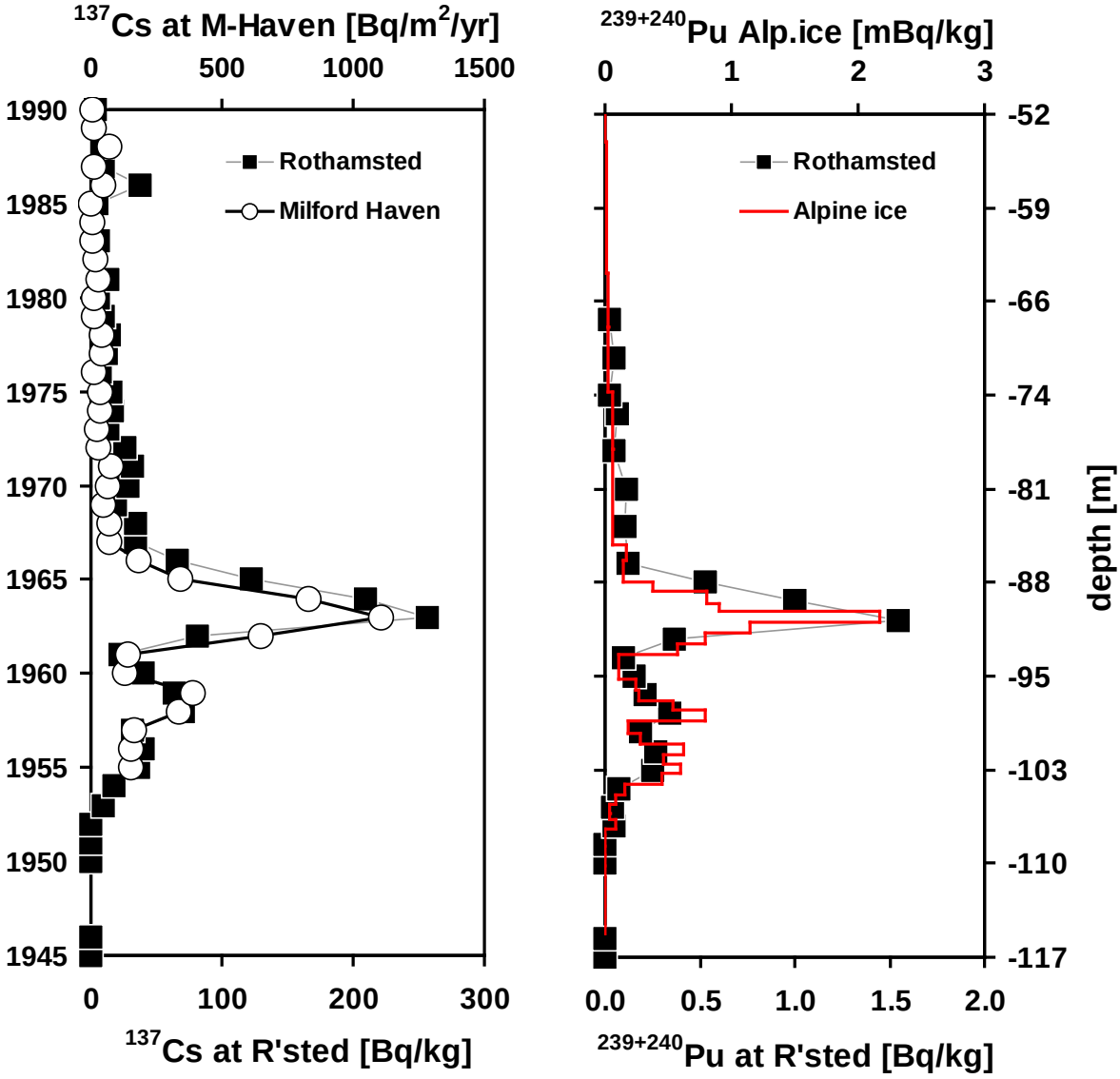

Figure P3a. ^{137}**Cs concentration in the Rothamsted grass (Bq/kg) and deposition flux at Milford Haven (Bq/m^2/yr) from AEA monitoring from 1957-1991[20].**

Figure P3b. ^{239,240}**Pu concentration in the Rothamsted grass and in Alpine ice.**

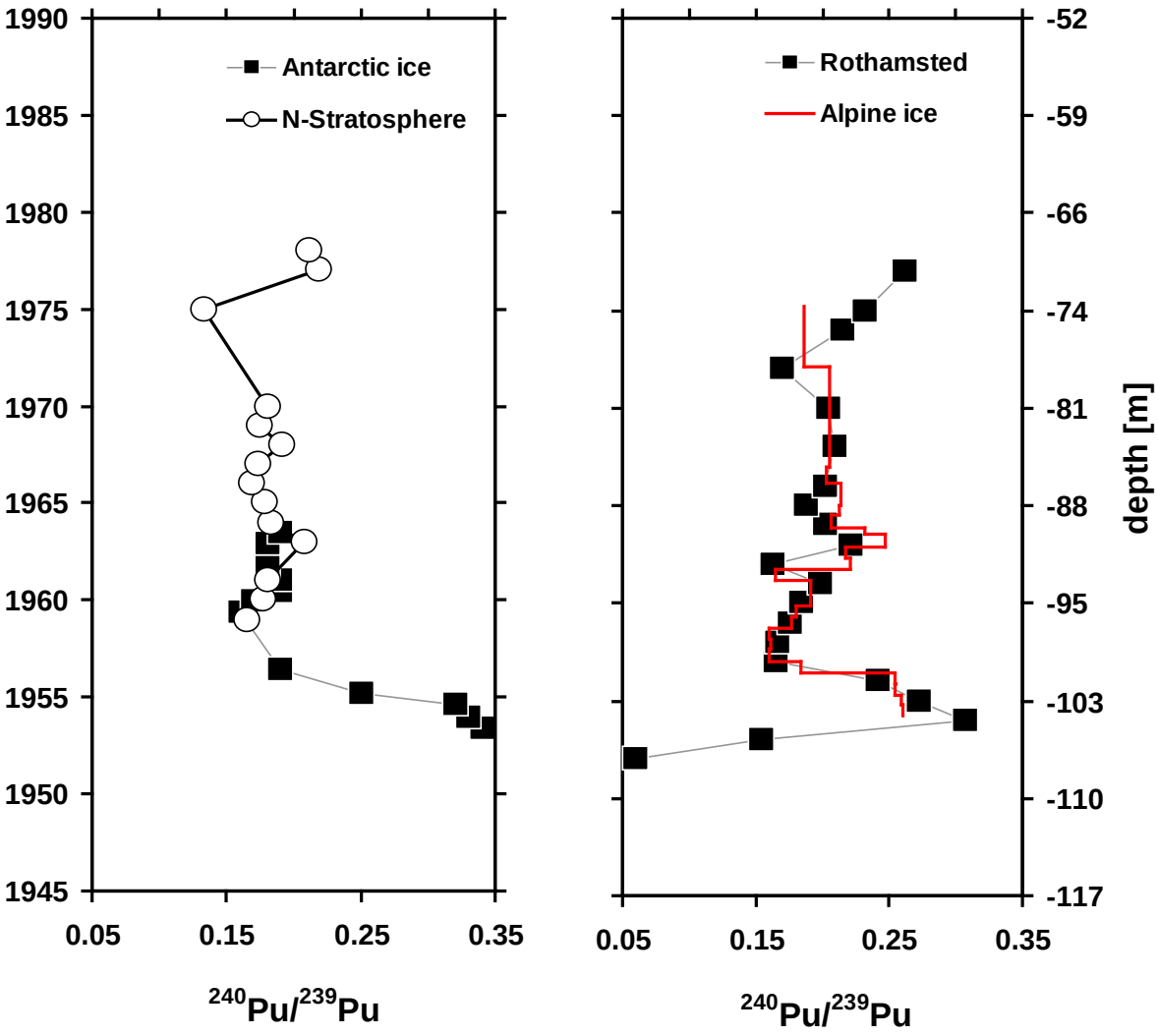

Figure P4a. $^{240}Pu/^{239}Pu$ atom ratio in an ice core from the J-9 Ross Ice Shelf, Antarctica [18] and in the northern Stratosphere [19].

Figure P4b. $^{240}Pu/^{239}Pu$ atom ratio in Rothamsted grass and Alpine ice. Full details of the mass spectrometer and the analytical procedures developed for uranium and plutonium are published elsewhere [8,22].

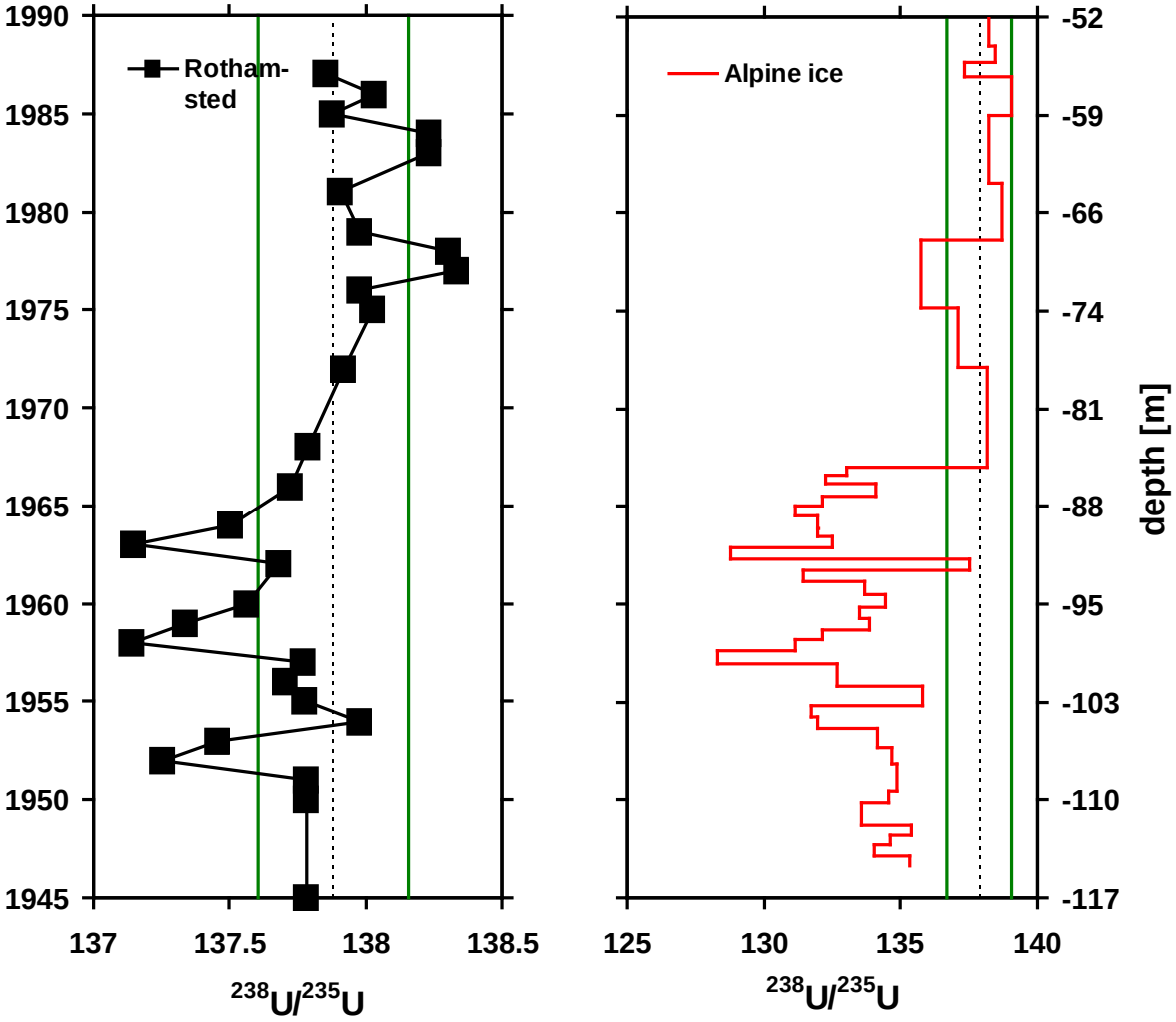

Figure P5a. $^{238}U/^{235}U$ in Rothamsted grass samples. The green lines represent the boundaries of the 3 s.d. analytical limit.

Figure P5b. $^{238}U/^{235}U$ in Alpine ice from Dome du Gouter (4300m), Mont Blanc, France

References

1. Croudace I.W., Warwick P.E., Taylor R.N. and Cundy A.B., Investigation of an alleged nuclear incident at Greenham Common airbase using TI-mass spectrometric measurements of uranium isotopes. *Env. Sci. Technol*. 34, 4496-4503 (2000).

2. Buesseler, K.O., Sholkovitz, E.R. The geochemistry of fallout plutonium in the north Atlantic: II. $^{240}/^{239}$Pu ratios and their significance, *Geochimica et Cosmochimica Acta* 51, 2623-2637 (1987).

3. Scott, M.R., Salter, P.F., Halverson, J.E. Transport and deposition of plutonium in the ocean: evidence from Gulf of Mexico sediments, *Earth and Planetary Science Letters* 63, 202-222 (1983).

4. Noshin, V.E., Gatrousis, C., Fallout ^{240}Pu and ^{239}Pu in Atlantic marine samples, *Earth and Planetary Science Letters*, 22, 111-117(1974).

5. Oktay, S.D., Santschi, P.H., Moran, J.E., Sharma, P. The ^{129}Iodine bomb pulse recorded in Mississippi River Delta sediments: Results from isotopes of I, Pu, Cs, Pb, and C, *Geochimica et Cosmochimica Acta* 64 (6), 989-996 (2000).

6. Krey, P.W., Leifert, R., Benson, W.K., Dietz, L.A., Hendrikson, H.C., Coluzza, J.L., Atmospheric burn-up of the Cosmos-954 reactor, *Science* 105, 583-585 (1979).

7. Leifert, R., Russel Juzdan, Z., Kelly, W.R., Fassett, J.D., Eberhardt, K.R., Detection of uranium from Cosmos-1402 in the stratosphere, *Science* 238, 512-514 (1987).

8. Taylor R.N., Warneke T., Milton J.A., Croudace I.W., Warwick P.E. and Nesbitt R.W. Plutonium isotope ratio analysis at femtogram to nanogram levels by multicollector ICP-MS. *J. Anal. At. Spectrom.*, 16, 279-284 (2001).

9. Eisenbud, M. and Gesell, T. Environmental Radioactivity 4th edition, Academic Press (1997).

10. Holloway, R.W., Hayes, D.W. Mean residence time of plutonium in the troposphere. *Environ. Sci. Technol.* 16, 127-129 (1982).

11. Reiter, E.R. Stratospheric-tropospheric exchange processes, *Reviews of Geophysics and Space Physics*, 4, 459(1975).

12. IUPAC *Pure and Applied Chemistry* 163, 991-1002 (1991).

13. Cowan G.A. A natural fission reactor. *Sci. Amer*., 36, 235-245 (1976).

14. Harley, J.H., Plutonium in the environment-a review, *J.Radiat. Res.* 21, 83-104 (1980).

15. Vincent, C., Vallon, M., Pinglot, J.F., Funk, M., Reynaud, L., Snow accumulation and ice flow at Dome du Gouter (4300m), Mont Blanc, French Alps, *Journal of Glaciology* 43, 513-521 (1997).

16. Lawson J.E., Nuclear Explosion Catalog, http://www.okgeosurvey1.gov/level2/nuke.cat. (1998).

17. Carter, M.W., Moghissi, A.A., Three decades of nuclear testing. *Health Physics* 33, 55-71(1977).

18. Koide, M., Bertine, K.K., Chow, T.J., Goldberg, E.D. The $^{240}Pu/^{239}Pu$ ratio, a potential geochronometer. *Earth and Planetary Science Letters* 72, 1-8 (1985).

19. EML (Department of Energy Environmental Measurements Laboratory) Stratospheric Radionuclide (RANDAB) Database. http://cdiac.esd.ornl.gov/by_new/bysubjec.html#atmospheric (2000).

20. AEA, 1957-1991, Annual Reports: Radioactivity in Air and Rainwater, United Kingdom Atomic Energy Authority, Harwell, Berkshire, UK

21. Stewart, N.G., Crooks, R.N., Fisher, E.M.R., The radiological dose to persons in the UK due to debris from nuclear test explosions prior to January 1956, AERE HP/R 2017, Harwell, Berkshire, UK (1957)

22. Delmas, R., Pourchet, M., Utilisation de filtres echangeurs d'ions pour l'etude de l'activite β globale d'un carottage glaciologique, International Association of Hydrological Sciences Publication 118, Symposium, Grenoble 1975 – Isotopes and Impurities in Snow and Ice, 159-163 (1977).

23. Barbante C., van de Velde K., Cozzi G., Capodaglio G., Cescon P., Planchon F., Hong S., Ferrari C. and Boutron C., Post-World war II uranium changes in dated Mont Blanc ice and snow. *Env, Sci Technol* 35, 4026-4030 (2001).